Metabolic control of EMT: The role of α-ketoglutarate and IDH1 in the regulation of Snail and tumor invasion

Inaugural Dissertation
submitted to the Faculty of Medicine
in partial fulfillment of the requirements
for the PhD-Degree
of the Faculties of Veterinary Medicine and Medicine
of the Justus Liebig University Giessen

By Alserw, Aya
From Cairo, Egypt

Giessen 2026

From the Institute of Neuropathology
Director: Prof. Dr. med. Till Acker
of the Faculty of Medicine of the Justus Liebig University Giessen

Supervisor and First Reviewer:
Prof. Dr. Till Acker
(Faculty of Medicine of the Justus-Liebig University)
Second Reviewer:
Prof. Dr. Elke Pogge von Strandmann
(Faculty of Medicine of Philipps University Marburg)
Committee Vice-Chair and Co-Supervisor:
Prof. Dr. Thorsten Stiewe
(Faculty of Medicine of Philipps University Marburg)
Committee Chair:
Prof. Dr. Ross Douglas
(Faculty of Veterinary Medicine of the JLU Giessen)

Date of Doctoral Defense: March 5, 2026

Ehrenwörtliche Erklärung

„Hiermit erkläre ich, dass ich die vorliegende Arbeit selbständig und ohne unzulässige Hilfe oder Benutzung anderer als der angegebenen Hilfsmittel angefertigt habe. Alle Textstellen, die wörtlich oder sinngemäß aus veröffentlichten oder nichtveröffentlichten Schriften entnommen sind, und alle Angaben, die auf mündlichen Auskünften beruhen, sind als solche kenntlich gemacht. Bei den von mir durchgeführten und in der Dissertation erwähnten Untersuchungen habe ich die Grundsätze guter wissenschaftlicher Praxis, wie sie in der Satzung der Justus-Liebig-Universität Gießen zur Sicherung guter wissenschaftlicher Praxis" niedergelegt sind, eingehalten sowie ethische, datenschutzrechtliche und tierschutzrechtliche Grundsätze befolgt. Ich versichere, dass Dritte von mir weder unmittelbar noch mittelbar geldwerte Leistungen für Arbeiten erhalten haben, die im Zusammenhang mit dem Inhalt der vorgelegten Dissertation stehen. Die vorgelegte Arbeit wurde weder im Inland noch im Ausland in gleicher oder ähnlicher Form einer anderen Prüfungsbehörde zum Zweck einer Promotion oder eines anderen Prüfungsverfahrens vorgelegt. Alles aus anderen Quellen und von anderen Personen übernommene Material, das in der Arbeit verwendet wurde oder auf welches direkt Bezug genommen wird, wurde als solches kenntlich gemacht. Insbesondere wurden alle Personen genannt, die direkt und indirekt an der Entstehung der vorliegenden Arbeit beteiligt waren. Mit der Überprüfung meiner Arbeit durch eine Plagiatserkennungssoftware bzw. ein internetbasiertes Softwareprogramm erkläre ich mich einverstanden.“

Unterschrift

Dedicated to my beloved Teita Thoraya, whose battle with breast cancer sparked my lifelong passion to understand this disease. To my younger self, I hope I've made you proud by staying true to our dream. To my life partner and love, Nour, who believed in me when I doubted myself, encouraged me to pursue a PhD, crossed continents to be by my side, and stood with me every single day through this journey.

Table of contents

Ehrenwörtliche Erklärung 4

1. Introduction 10

1.1. Cancer invasion and metastasis 11

1.1.1. EMT under physiological and pathological conditions 13

1.1.2. EMT/PMT inducers 16

1.1.1.1. TGFβ pathway 16

1.1.1.2. Hypoxia pathway 18

1.1.3. EMT TFs 21

1.1.1.3. SNAI family 21

1.1.1.3.1. Snail TF 21

1.1.1.3.2. Slug TF 25

1.1.1.4. TWIST family 25

1.1.1.5. ZEB family 26

1.2. Metabolic reprogramming 26

1.2.1. The pleiotropic functions of α-KG 27

1.2.1.1. α-KG production and metabolic function 27

1.2.1.2. Co-substrate function for α-KG dependent dioxygenases 30

1.2.1.2.1. The connection of α-KG to hypoxic response 32

1.2.1.2.2. The roles of α-KG in epigenetic modifications 35

1.2.1.2.3. The function of α-KG in collagen synthesis 36

1.2.1.3. α-KG-mediated inhibition of the ATP synthase-mTOR pathway 37

1.2.2. The ATP synthase-mTOR signaling pathway 37

1.2.2.1. ATP synthase 37

1.2.2.2. mTOR 39

1.2.2.2.1. mTORC1 upstream regulators 40

1.2.2.2.2. Major mTORC1 substrates 43

1.2.2.2.3. Other mTORC1 substrates 44

1.3. Aim of this study 46
2. Materials and methods 48
2.1. Materials 48
2.1.1. Chemicals 48
2.1.2. Antibodies 48
2.1.2.1. Primary antibodies 48
2.1.2.2. Secondary antibodies 50
2.1.3. Protein and DNA ladders 51
2.1.3.1. Protein ladders 51
2.1.3.2. DNA ladders 51
2.1.4. Antibiotics 51
2.1.5. Inhibitors 52
2.1.6. Primers 53
2.1.6.1. Reverse transcription quantitative polymerase chain reaction (RT-qPCR) primers 53
2.1.6.2. ChIP-qPCR primers 55
2.1.6.3. Cloning PCR primers 56
2.1.7. Plasmids 56
2.1.8. Short interfering RNAs (siRNAs) 57
2.1.9. Ribonucleoprotein (RNP) crRNAs components 58
2.1.10. Bacterial strains 58
2.1.11. Cell lines 58
2.1.11.1. Original cell lines 58
2.1.11.2. Cell lines generated in our laboratory 59
2.1.12. Restriction digestion enzymes 63
2.1.13. Growth factors 63
2.1.14. Buffers, media, and solutions 64
2.1.14.1. Bacterial culture 64

2.1.14.2. Cell culture 64
2.1.14.3. Nucleic acid isolation 66
2.1.14.4. Western blot 68
2.1.14.5. Immunofluorescence 69
2.1.14.6. Dual luciferase reagents 69
2.1.14.7. Animal experiments 70
2.2. Methods 70
2.2.1. Working with cell lines 70
2.2.1.1. Sub-culturing and passaging cells 70
2.2.1.2. Cryopreservation and thawing of cells 71
2.2.1.3. Determination of cell count and viability 71
2.2.1.4. Epithelial cells tumorsphere culture 71
2.2.1.5. Treatments 72
2.2.1.5.1. TGFβ and α-KG treatments 72
2.2.1.5.2. Hypoxia incubation 73
2.2.1.5.3. Inhibitor treatments 73
2.2.1.5.4. IDH1 overexpression 74
2.2.1.6. Transfection and transduction 75
2.2.1.6.1. Virus production and concentration 75
2.2.1.6.2. Virus titration 76
2.2.1.6.3. Stable lentiviral transduction 76
2.2.1.6.4. Transient transfection for RNP-mediated gene knockout 77
2.2.1.6.5. Transient transfection for dual luciferase reporter assay 77
2.2.1.6.6. Transient transfection for siRNA-mediated gene knockdown 79
2.2.1.7. Collagen invasion assay 81
2.2.1.8. Modified Boyden chamber assay 81
2.2.1.9. Proliferation assay 84
2.2.1.10. Measurement of the cellular ATP/ADP ratio 85

2.2.1.11. Measurement of the cellular ATP levels 85
2.2.2. Working with RNA 86
2.2.2.1. RNA extraction 86
2.2.2.2. cDNA synthesis 86
2.2.2.3. RT-qPCR 87
2.2.2.4. Bulk RNA-seq 88
2.2.3. Working with proteins - western blotting 89
2.2.3.1. Cell lysis and protein extraction 89
2.2.3.2. Determination of protein concentration 90
2.2.3.3. Sample preparation 90
2.2.3.4. Western Blot and Sodium-Dodecyl-Sulfate-PolyAcrylamide Gel Electrophoresis (SDS-PAGE) 90
2.2.3.5. Stripping of western blot membranes 91
2.2.4. Working with proteins - immunofluorescence 91
2.2.4.1. Immunofluorescence analysis of Snail protein 91
2.2.4.2. Immunofluorescence analysis of Vimentin protein 92
2.2.4.3. Immunofluorescence analysis of E-cadherin protein 93
2.2.5. Flow cytometry 94
2.2.6. Working with bacteria 95
2.2.6.1. Preparation of LB medium and LB agar plates 95
2.2.6.2. Bacterial transformation 95
2.2.6.3. Inoculation of liquid culture 95
2.2.6.4. Preparation of glycerol stocks 95
2.2.7. Working with DNA 96
2.2.7.1. Chromatin immunoprecipitation (ChIP) 96
2.2.7.2. Genomic DNA isolation 98
2.2.7.3. Plasmid DNA isolation 98
2.2.7.4. Plasmid DNA sequencing 98

2.2.7.5. PCR cloning 98
2.2.7.6. Restriction digestion 99
2.2.7.7. Agarose gel electrophoresis 99
2.2.7.8. Gel extraction of DNA fragments from agarose gels 100
2.2.7.9. Determination of DNA concentration 100
2.2.7.10. Ligation 100
2.2.8. Animal experiments 100
2.2.8.1. Subcutaneous models 100
2.2.8.2. Tumor growth measurement 100
2.2.8.3. Intravenous models 101
2.2.8.4. *In vivo* bioluminescence imaging 101
2.2.8.5. Tissue dissociation and sample preparation 101
2.2.9. Bioinformatic analysis 102
2.2.10. Visualization of sequencing data 102
2.2.11. Statistical analysis 103
3. Results 104
3.1. Snail is the sole EMT transcription factor consistently and highly upregulated by TGFβ across brain, breast and lung tumor cell lines 104
3.2. TGFβ-induced Snail is suppressed by α-KG addition 106
3.3. α-KG inhibits TGFβ-mediated EMT activation 108
3.4. α-KG suppresses TGFβ-induced cellular invasion 110
3.5. IDH1 regulates EMT and invasion 114
3.6. Snail as a critical mediator of IDH1 depletion-driven invasiveness 116
3.7. α-KG negatively regulates Snail expression partially through the ATP synthase-mTORC1-c-Myc axis 119
3.8. α-KG negatively regulates Snail expression synergistically through PHD-HIF and ATP synthase-mTORC1-c-Myc pathways 123
3.9. IDH1 depletion-mediated Snail regulation occurs at the transcriptional level 124

3.10. α-KG producing and consuming enzymes are regulated by TGFβ treatment 130
3.11. Reduced IDH1 levels correlate with poor patient prognosis 131
3.12. Testing growth and invasion capacity of LLC1 cells grown as spheres 133
3.13. Testing growth of LLC1 *in vivo* 134
3.14. Successive viral transductions render cells immunogenic 137
4. Discussion 138
4.1. The TGFβ–Snail axis is a shared driver of EMT in the investigated brain, lung and breast cancer models 138
4.2. α-KG-mediated suppression of EMT and invasion 140
4.3. α-KG as a therapeutic agent in cancer and beyond 143
4.4. IDH1 depletion regulates EMT induction and invasive behavior 146
4.5. α-KG homeostasis regulation under TGFβ signaling 150
4.6. Snail as a central mediator of EMT and invasion in IDH1-deficient cells 152
4.7. Snail regulation is exerted via multiple signaling pathways in IDH1-depleted cells 154
4.8. α-KG activates signaling pathways that converge on SNAI1 158
4.9. α-KG could modulate Snail levels via intricate transcriptional and post-transcriptional mechanisms 160
4.10. Conclusion and outlook 162
5. Summary 164
6. Zusammenfassung 166
Abbreviations list 168
Index of figures and tables 175
Figure Index 175
List of Tables 177
References 178
Acknowledgments 225

1. Introduction

The hallmarks of cancer (Fig. 1.1), are defined as a set of molecular, biochemical, and cellular traits acquired by the cancer cells during the multistep development of human tumors. These functional capabilities are shared by almost all types of human malignancies, although they are not necessarily acquired through similar mechanisms or at the same time. The concept of cancer hallmarks was introduced in 2000 (Hanahan and Weinberg 2000). This conceptual framework aids in rationalizing the complexity of tumorigenesis, and is continuously revisited. Eight core capabilities have been described, including sustaining proliferative signaling, evading growth suppressors, resisting programmed-cell death, inducing angiogenesis, enabling replicative immortality, activating invasion and metastasis, evading immune destruction, and reprogramming of energy metabolism (Hanahan and Weinberg 2000, 2011). Throughout the past two decades, more acquired features have been introduced, such as unlocking phenotypic plasticity, and undergoing epigenetic modifications (Hanahan 2022). Emerging evidence indicates a complex interplay between different hallmarks. Our interest is focused on the crosstalk between metabolic rewiring and tumor invasion and metastasis.

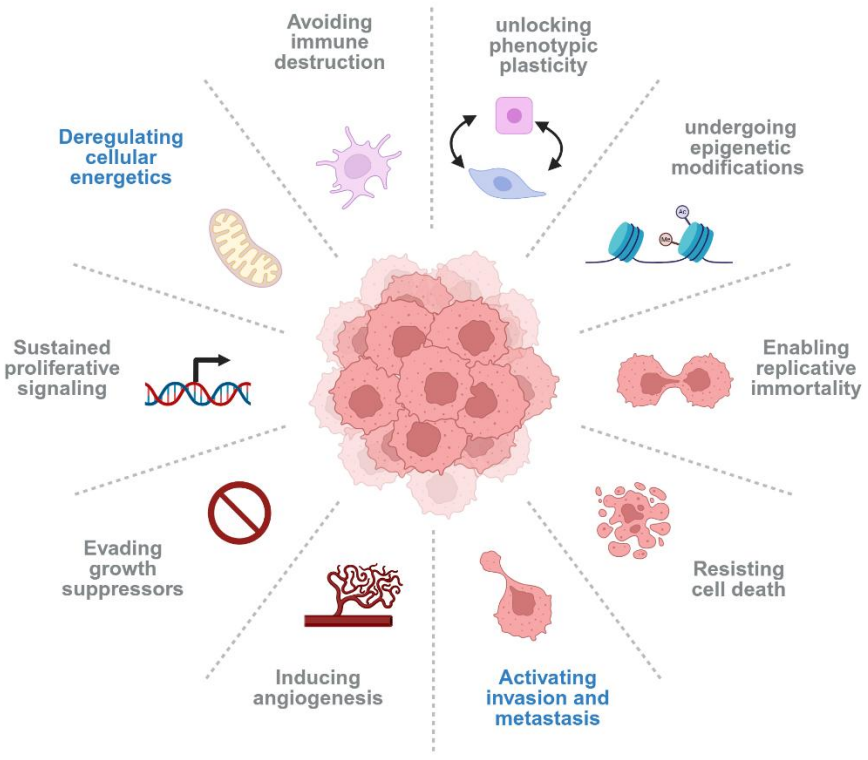

Figure 1.1. Schematic illustration of the hallmarks of cancer. The hallmarks defined by Hanahan and Weinberg are shown, with an emphasis on activating invasion and metastasis, and deregulating cellular energetics. Adapted from (Hanahan 2022; Hanahan and Weinberg 2000, 2011). Created with BioRender.com

1.1. Cancer invasion and metastasis

Metastasis, the spread of cancer cells from the primary tumor to distant sites, is the terminal and most lethal manifestation of cancer. The majority of cancer-related deaths result from metastatic disease rather than the primary tumors (Mani et al. 2024). Although the precise proportion of metastasis-related mortality cannot be accurately calculated (Dillekås, Rogers, and Straume 2019), its devastating clinical impact is indisputable, underscoring the need to target this process at its earliest stages. In particular, brain metastases, which occur in 20-40% of systemic cancer patients, are associated with poor quality of life, and limited overall survival (Achrol et al. 2019; Suh et al. 2020). The true incidence rates are thought to be higher than the reported numbers, as improved primary tumor treatments and extended survival durations of patients have increased the risk of metastatic spread to the brain (Brenner and Patel 2022; Suh et al. 2020). Moreover, many patients with extracranial cancer do not undergo routine brain MRI screening, and do not display neurological symptoms, hindering their diagnosis. Almost every cancer type can metastasize to the brain, but the majority of brain metastases develop from lung, breast, and skin cancers (Achrol et al. 2019; Brenner and Patel 2022; Suh et al. 2020). Notably, the primary tumor type or the molecular subtype can further dictate the risk of developing brain metastases. Lung carcinoma patients are more likely to develop secondary brain tumors more often than patients with other tumors, with small cell and non-small cell lung cancers (NSCLC) showing the highest incidence among lung cancer subtypes. Moreover, breast cancer patients of human epidermal growth factor receptor 2 (HER2)-positive or triple negative (TNBC) subtypes have a significantly higher risk of developing brain metastases compared to those who have estrogen-positive and/or progesterone-positive breast cancer (Achrol et al. 2019; Aizer et al. 2022; Suh et al. 2020). According to brain tumor statistics, brain metastases account for the majority of brain neoplasms and exceed the number of benign and malignant primary brain tumors combined (Brenner and Patel 2022; Khan and Steeg 2022; McFaline-Figueroa and Lee 2018), while the most prevalent and aggressive primary brain malignancy is isocitrate dehydrogenase-wild-type glioblastoma (IDH WT GBM) (Lapointe, Perry, and Butowski 2018; McKinnon et al. 2021; Schaff and Mellinghoff 2023). Despite the rare incidence of extracranial GBM metastasis, GBM cells display highly diffuse infiltration and aggressive invasion into the surrounding brain parenchyma, leading to a high rate of recurrence following therapeutic interventions (Pouyan et al. 2025; Seker-Polat et al. 2022). Consequently, the current treatment modalities, including surgical resection, followed by concomitant radiotherapy and chemotherapy, and subsequent adjuvant chemotherapy, only slightly improve

patients outcome (Pouyan et al. 2025; Seker-Polat et al. 2022). The development of novel therapies for invasive GBM poses enormous challenges similar to those for brain metastases.

Metastasis is a multistep process. The metastatic cascade (Fig. 1.2), comprehensively described by Dr. Isaiah J. Fidler (Fidler 1990, 2003), begins with molecular and phenotypical changes in cancer cells. These changes are collectively known as the epithelial-to-mesenchymal transition (EMT) (Brabletz et al. 2021; Dongre and Weinberg 2019; Nieto et al. 2016; Thiery 2002). Acquired mesenchymal traits facilitate cells detachment from neighboring cells, and degradation of the extracellular matrix (ECM), followed by increased migration and invasion into the surrounding tissue (Fidler 1990, 2003). Metastasis-initiating cells subsequently enter nearby blood and lymphatic vessels through a process termed intravasation, allowing them to disseminate via the circulatory system. Upon reaching distant sites, they exit the vasculature through extravasation and infiltrate the parenchyma of secondary organs, where they establish small nodules of micrometastases. These disseminated tumor cells can often remain in a dormant state. Eventually, they evade immune surveillance, adapt to the new microenvironment, and resume proliferation and colonization of the tissue to develop into macroscopic lesions (Fares et al. 2020; Hanahan and Weinberg 2000; Pérez-González, Bévant, and Blanpain 2023).

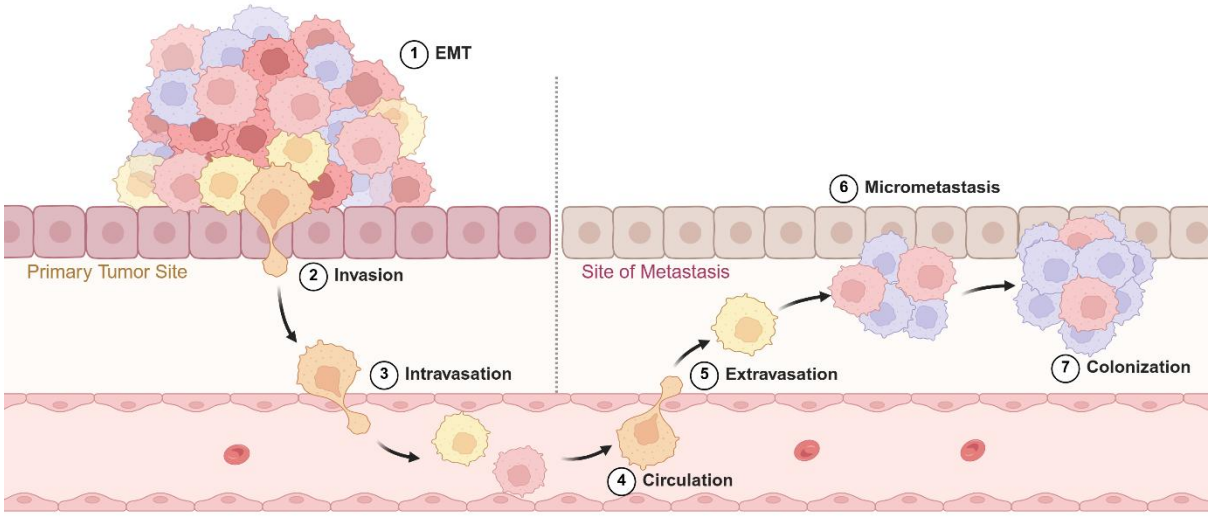

Figure 1.2. Overview of the metastatic cascade. Schematic showing the essential steps of metastasis. (1) Malignant cells activate the EMT program, (2) migrate and invade their surrounding tissue and break through the basement membrane. (3) They intravasate into nearby vessels, (4) where they travel through and survive in the circulation. (5) Once they reach their secondary sites, they extravasate and cross the endothelial barrier. (6) They form dormant micrometastasis, which upon microenvironmental cues, (7) colonize the tissue and form clinically detectable macrometastasis. Adapted from (Drapela and Gomes 2021; Fares et al. 2020). Created with BioRender.com

1.1.1. EMT under physiological and pathological conditions

EMT is a reversible cellular program that enables polarized epithelial cells to partially or fully transition towards a mesenchymal phenotype, characterized by high motility (Fig. 1.3). During embryogenesis, EMT plays a critical role in key developmental processes such as gastrulation, tissue morphogenesis, and neural crest delamination (Dongre and Weinberg 2019; Lu and Kang 2019; Youssef and Nieto 2024). In adult tissues, EMT is transiently activated during physiological wound healing and tissue repair (Youssef and Nieto 2024), but can be pathologically reactivated in conditions such as fibrosis and cancer (Babaei, Aziz, and Jaghi 2021; Pérez-González et al. 2023; Yang et al. 2020). EMT was long considered as a binary switch, however, recent studies have suggested that EMT is a dynamic process, where cells could exist within a continuum of intermediate or hybrid states, which simultaneously exhibit both epithelial and mesenchymal (E/M) properties. These hybrid states, also referred to as quasi-mesenchymal cell states, confer high plasticity, allowing cells to reversibly transition between states depending on environmental cues, a phenomenon termed epithelial-to-mesenchymal plasticity (EMP) (Chaffer et al. 2016; Dongre and Weinberg 2019; Nieto et al. 2016; Thompson et al. 2025; Yang et al. 2020).

In the context of tumor progression, carcinoma cells in E/M states are endowed with features like enhanced invasion and metastasis, cancer stem cell properties, increased inflammation, therapy resistance, immune evasion, and the ability to resist anoikis, the detachment-induced apoptosis, during dissemination and circulation (Brabletz et al. 2021; Dongre and Weinberg 2019; Lu and Kang 2019; Thompson et al. 2025; Youssef et al. 2024). Although mesenchymal features facilitate early steps of metastasis, secondary tumors often exhibit similar histological characteristics as their epithelial-like primary counterparts. This observation highlights the necessity of a reverse process, known as mesenchymal-to-epithelial transition (MET), during which metastasizing cells lose their mesenchymal features and revert back to an epithelial state with high proliferative capacities (Brabletz et al. 2001; Lu and Kang 2019). While EMT/MET are considered accountable for successful invasion and colonization in distant locations, a more comprehensive understanding of possible alternative mechanisms is also desired (Huang, Hong, and Wei 2022; Jolly et al. 2017; Nieto et al. 2016).

Prior to the onset of EMT, epithelial cancer cells display a well-defined apical-basal polarity and maintain close cell-cell adhesion through various intercellular junctions, including tight junctions, gap junctions, desmosomes, and adherens junctions, mainly mediated by epithelial cadherin (E-cadherin). Epithelial cells are also anchored to the basement membrane via hemidesmosomes (Fig. 1.3) (Lamouille, Xu, and Derynck 2014; Lu and Kang 2019; Yang

et al. 2020). This organization maintains their structural and functional integrity (Lamouille et al. 2014; Springer et al. 2025). During EMT, these different junctions are deconstructed, E-cadherin at the plasma membrane is cleaved and subsequently degraded, and actin cytoskeletal architecture is reorganized. This is accompanied by a loss of apical-basal polarity and the acquisition of front-rear polarity, resulting in a morphological change from a polygonal to spindle-like shaped mesenchymal cells, with increased cell motility and protrusions, facilitating degradation of the ECM and invasion into surrounding tissues (Fig. 1.2, Fig. 1.3) (Lamouille et al. 2014; Lu and Kang 2019; Yang et al. 2020).

At the molecular level, these phenotypic changes are driven by a reprogramming of gene expression (Fig. 1.3). Epithelial markers such as E-cadherin, Claudins, Occludins, and Cytokeratins are downregulated or transcriptionally repressed. Concurrently, mesenchymal markers are upregulated, including neural cadherin (N-cadherin), an adhesion molecule that promotes interactions and attachment with neighboring mesenchymal cells, and Vimentin, an intermediate filament protein that interacts with motor proteins and contributes to cytoskeletal plasticity and motility (Yang et al. 2020). In addition, EMT confers the capacity to traverse the basement membrane through the upregulation of matrix metalloproteinases (MMPs), a family of proteases that degrade the ECM components, thereby facilitating local invasion and intravasation (Dongre and Weinberg 2019).

A similar transcriptional and phenotypic reprogramming process has also been described in GBM, commonly referred to as proneural-to-mesenchymal transition (PMT), glial-to-mesenchymal transition (GMT), or more generally as an EMT-like process. Gene expression profiling led to the classification of GBM into three or four distinct molecular subgroups with different clinical implications, including proneural, (neural,) classical, and mesenchymal. The latter is strongly associated with higher infiltration and poorer prognosis compared to the other subgroups (Fedele et al. 2019; Majc et al. 2020). Single-cell transcriptome analyses revealed that although the names of the subgroups represent the predominant cell subtype, other cell subtypes are also present in the same tumor due to the intrinsic intratumoral heterogeneity of GBM (Verhaak et al. 2010; Wang et al. 2017; Xu et al. 2025). During PMT, GBM cells transition from the proneural to the mesenchymal subtype, particularly at recurrence following radiation and chemotherapy (Fedele et al. 2019; Iwadate 2016; Mahabir et al. 2014; Seker-Polat et al. 2022; Xu et al. 2024). Several studies suggest that the molecular events and microenvironmental factors that trigger this mesenchymal shift and contribute to the increased diffuse infiltration of GBM cells into the brain parenchyma are similar to those governing EMT

in carcinoma cells (Depner et al. 2016; Fedele et al. 2019; Iwadate 2016; Mahabir et al. 2014; Majc et al. 2020; Pouyan et al. 2025; Seker-Polat et al. 2022).

EMT is a complex process, during which the changes in EMT-associated gene expression profiles and phenotypes depend on the cellular context and the microenvironmental cues, as discussed below. The gene expression changes are mainly orchestrated by a group of transcription factors (TFs), with Snail (SNAI1), Slug (SNAI2), TWIST1, TWIST2, ZEB1, and ZEB2 being considered as core EMT regulators (Lamouille et al. 2014; Yang et al. 2020). They regulate the repression of epithelial markers, and the activation of the mesenchymal genes (Fig. 1.3) (Haerinck, Goossens, and Berx 2023), as detailed later.

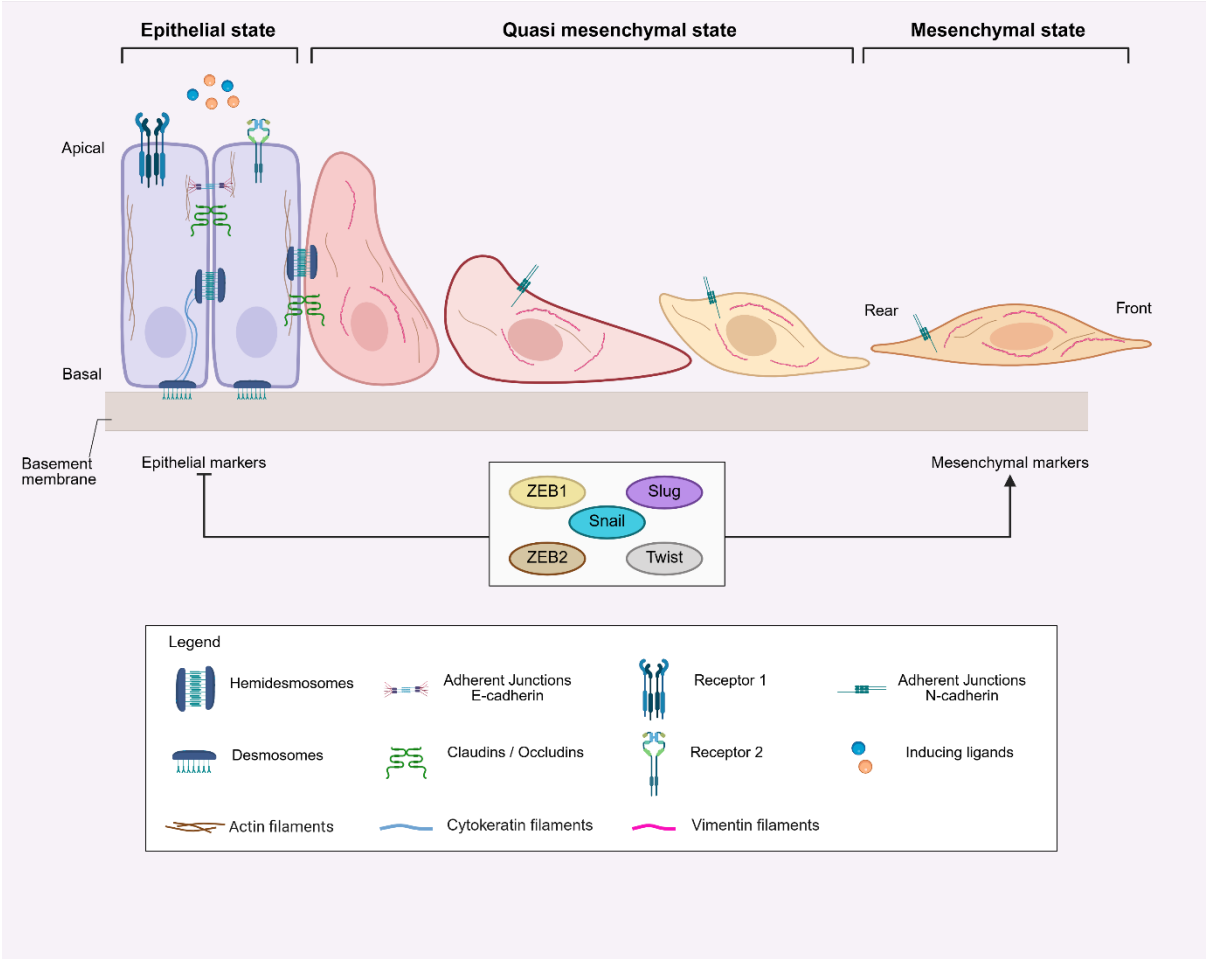

Figure 1.3. Overview of molecular and phenotypic changes during EMT. Upon the induction by microenvironmental stimuli, such as binding of inducing ligands to their receptors, EMP program is activated, and molecular and morphological changes occur in epithelial cells, which lose their apical-basal polarity, by shedding their epithelial cell-cell junctions, passing by intermediate states where cells have both E/M characteristics. At the end of the spectrum, cells gain a full mesenchymal phenotype, with front-rear polarity, and an increased invasive capacity. This is concurrent with changes in intracellular adherent junctions and cytoskeleton filaments. EMT is orchestrated by core TFs which repress the expression of epithelial markers and activate the expression of mesenchymal markers. Adapted from (Dongre and Weinberg 2019; Yang et al. 2020). Created with BioRender.com.

1.1.2. EMT/PMT inducers

Both EMT and PMT, hereafter collectively referred to as EMT, can be triggered by various microenvironmental stimuli. Ligands secreted by neighboring stromal cells, such as cytokines and growth factors, bind to their respective receptors on cancer cells, initiating intracellular signaling cascades that ultimately activate the EMT process (Dongre and Weinberg 2019; Pérez-González et al. 2023). Key signaling pathways activating EMT include transforming growth factor beta (TGFβ), receptor tyrosine kinases (RTKs), Wnt/β-catenin, tumor necrosis factor alpha (TNFα), and Notch. RTK signaling initiates EMT-associated events through several downstream effectors, notably the phosphatidylinositol 3-kinase (PI3K)-AKT, mitogen-activated protein kinase (MAPK), and JAK-STAT pathways (Majc et al. 2020). Additionally, other microenvironmental conditions, including oxygen level, nutrient availability and ECM stiffness are sensed by cancer cells. Along with intrinsic alterations such as metabolic reprogramming, they are integrated into EMT regulatory networks that control the expression, stability, and activity of EMT TFs and ultimately their target genes (Babaei et al. 2021; Haerinck et al. 2023; Majc et al. 2020; Williams et al. 2019).

1.1.1.1. TGFβ pathway

The TGFβ family of cytokines stands out as the most potent and pleiotropic of the aforementioned signals. What distinguishes TGFβ from other EMT-inducing signals is its dual role in tumorigenesis, whereby it can exert both tumor-suppressive and tumor-promoting functions. Its functions vary from enforcing homeostasis in healthy epithelium, to having anti-proliferative effects and inducing apoptosis in pre-malignant cells, and finally promoting EMT, invasion, and metastasis in advanced carcinoma and glioblastoma cells (Hao, Baker, and Ten Dijke 2019; Iser et al. 2017; Lebrun 2012; Massagué and Sheppard 2023; Seoane and Gomis 2017). The TGFβ family includes numerous cytokines, of which the most relevant members in the context of EMT and tumor progression are TGFβ1, TGFβ2, and TGFβ3 members. These isoforms are secreted by various cell types within the tumor microenvironment, including cancer-associated fibroblasts, cancer-associated macrophages, or the cancer cells themselves (Majc et al. 2020). Compared to EMT processes initiated by other factors, TGFβ-induced EMT has been extensively characterized, both in terms of its signaling pathways and transcriptional regulatory networks (Derynck, Muthusamy, and Saeteurn 2014). TGFβ mediates EMT through both canonical (Smad-dependent) and non-canonical (Smad-independent) signaling pathways (Fig. 1.4) (Deng et al. 2024; Lamouille et al. 2014; Majc et al. 2020; Massagué and Sheppard 2023). In the canonical pathway, active TGFβ homodimers bind to a receptor complex composed of type II (TGFBR2) and type I (TGFBR1) serine/threonine kinase receptors. Ligand

engagement induces phosphorylation of TGFBR1 by TGFBR2, enabling TGFBR1 to phosphorylate its substrates Smad2 and Smad3 TFs. These activated Smads then form complexes with Smad4, translocate to the nucleus, where they regulate gene expression of multiple genes, implicated in cell growth, proliferation, motility, and invasion (Dongre and Weinberg 2019; Massagué and Sheppard 2023). Smad complexes also induce the expression of EMT TFs, including SNAI1/2, ZEB1, and TWIST1, as well as mesenchymal genes, such as Vimentin and Fibronectin (Dongre and Weinberg 2019). These EMT TFs upregulate TGFβ ligand expression establishing a positive feedback loop that reinforces and sustains EMT (Brabletz et al. 2021; Dongre and Weinberg 2019).

Interestingly, TGFβ signaling can act on other signaling pathways (Fig. 1.4), such as PI3K-AKT, MAPK, JAK-STAT, and RHO-like GTPases, in a Smad-independent, non-canonical mechanism (Deng et al. 2024; Dongre and Weinberg 2019; Lamouille et al. 2014; Massagué and Sheppard 2023; Xia 2025). These non-canonical pathways contribute to the complexity and versatility of TGFβ signaling in promoting EMT and tumor progression. The PI3K-AKT pathway, in particular, is frequently hyperactivated in a variety of malignancies, including lung cancer and glioblastoma (Langhans et al. 2017; Lin et al. 2014). Inhibition of this pathway has been shown to impair EMT induction, and reduce invasive potential in multiple tumor types (Lamouille et al. 2014; Lin et al. 2014; Moghbeli 2024; Xia 2025). TGFβ ligands also activate multiple MAPK signaling axes, including extracellular signal-regulated kinase (ERK1/2), p38, and JNK, although to a lesser extent compared to growth factor-activated RTKs (Deng et al. 2024; Lamouille et al. 2014; Massagué and Sheppard 2023). Notably, pharmacological inhibition of ERK has been shown to reverse TGFβ-induced EMT, restore E-cadherin expression, and suppress MMPs expression (Lamouille et al. 2014).

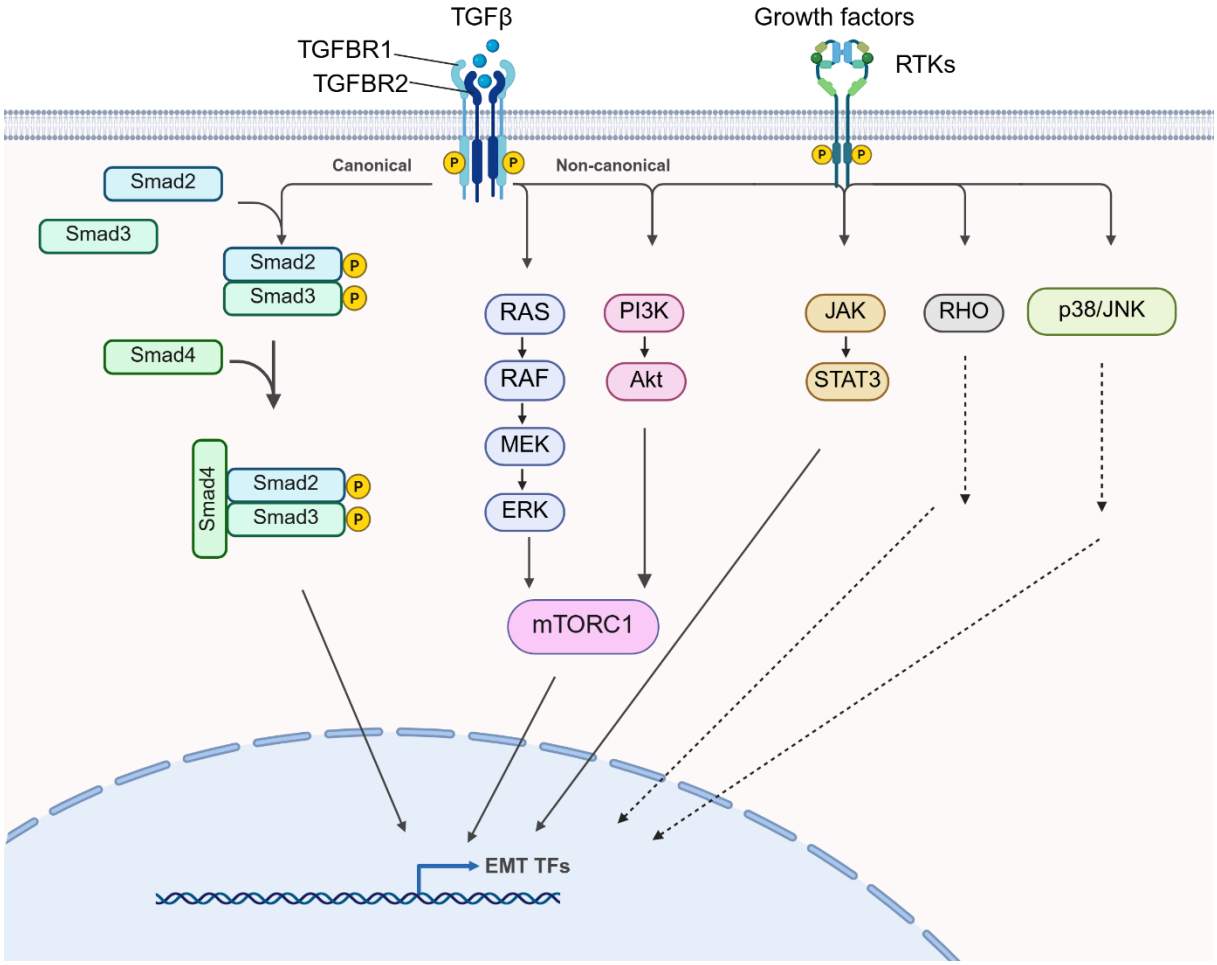

Figure 1.4. Overview of the TGFβ canonical and non-canonical signaling pathways regulating EMT core TFs. Canonical TGFβ signaling includes Smad-dependent pathways, whereas non-canonical signaling includes PI3K-AKT, RAS-RAF-MEK-ERK, JAK-STAT, RHO-GTPases, p38, and JNK pathways. Adapted from (Dongre and Weinberg 2019; Huang et al. 2022; Iser et al. 2017; Majc et al. 2020). Created with BioRender.com

1.1.1.2. Hypoxia pathway

Hypoxia, or low oxygen (O_2) level, is a common environmental stress, and a characteristic of solid aggressive tumors, including GBM, breast, and lung carcinomas (Huang, Lin, and Taniguchi 2017; Iser et al. 2017). This condition arises when the rapid and uncontrolled proliferation of cancer cells within tumor tissue outpaces the oxygen supply provided by the existing vasculature and the newly formed, yet often dysfunctional, blood vessels (Chen et al. 2023; Hapke and Haake 2020; Muz et al. 2015; Shen et al. 2024). This generates a hypoxic tumor microenvironment, with oxygen concentrations reaching as low as 0.1% (Losman, Koivunen, and Kaelin 2020). In response, cancer cells activate a range of adaptive mechanisms to thrive in this microenvironment (Iser et al. 2017). Adaptation to hypoxia-induced microenvironmental change is mediated by the hypoxia-inducible factors (HIFs). These TFs regulate the expression of hundreds of target genes, including those involved in glucose

metabolism, enabling a metabolic shift towards aerobic glycolysis, angiogenesis, increasing oxygen and nutrients supply to hypoxic niches, mitogenesis, and EMT and invasion, supporting cancer cells growth, survival, and metastasis (Fan et al. 2023; Hapke and Haake 2020; Huang et al. 2017; Saxena, Jolly, and Balamurugan 2020).

Transcriptional regulation by HIF proteins is coordinated by a heterodimeric HIF complex, compromising of two subunits, an oxygen-sensitive HIF-α subunit, and a constitutively expressed oxygen-independent HIF-β subunit, also known as aryl hydrocarbon nuclear translocator (ARNT). Both HIF-α and β contain Per-Arnt-Sim (PAS) domains that facilitate protein-protein interactions and are essential for the dimerization of the two subunits, as well as a basic helix-loop-helix (bHLH) domain, which mediates DNA binding of the dimers (Dengler, Galbraith, and Espinosa 2014; Springer et al. 2025). There are three isoforms of HIF-α subunit, HIF-1α, HIF-2α, and HIF-3α, each exhibiting distinct tissue- and context-specific functions (Abla et al. 2020). All HIF-α isoforms contain oxygen-dependent degradation domains (ODDDs), which serve as targets for their oxygen-mediated hydroxylation by prolyl hydroxylase domain-containing proteins (PHDs) (Abla et al. 2020). Both HIF-1α and HIF-2α harbor two ODDDs in their N-terminal and C-terminal transactivating domains (NTAD and CTAD) (Fiorini and Schofield 2024). CTAD of these isoforms also contains a conserved asparagine residue, which is critical for the recruitment of transcriptional co-activators CREB-binding protein (CBP) and histone acetyltransferase p300. In contrast, HIF-3α only possesses a single ODDD and lacks a CTAD, suggesting a structurally and functionally distinct role (Dengler et al. 2014).

Under normoxic conditions, PHDs hydroxylate two conserved proline residues in the ODDDs in HIF-α proteins; Pro402 and Pro564 in HIF-1α, and Pro405 and Pro531 in HIF-2α, triggering the recognition and binding of von Hippel-Lindau protein (pVHL), a subunit of the E3 ubiquitin ligase complex, which induces HIF-α ubiquitination and subsequent proteasomal degradation by the 26S proteosome (Fig. 1.5) (Abla et al. 2020; Huang et al. 2017). However, under hypoxia, PHDs are inactive due to the lack of oxygen. This prevents HIF-α hydroxylation and subsequent degradation, allowing HIF-α stabilization, nuclear translocation, and dimerization with HIF-1β. The heterodimer recognizes and binds to the core consensus sequence 5'-(A/G)CGTG-3' within hypoxia-response elements (HREs) in the promoter of target genes (Dengler et al. 2014; Huang et al. 2017; Saxena et al. 2020). The complex subsequently recruits CBP/p300, thereby initiating and sustaining transcriptional activity (Fig. 1.5) (Dengler et al. 2014; Springer et al. 2025).

A functional link between invasion and hypoxia, as cancer hallmarks of metastasis and angiogenesis, has been established (Hapke and Haake 2020; Saxena et al. 2020; Shen et al. 2024). While hypoxic regions are typically present within the tumor core, studies have shown that the invasive tumor edge, often enriched in cells with a pronounced mesenchymal phenotype, also contains HIF-1α-positive cells (Saxena et al. 2020). Indeed, HIFs can promote EMT and invasion via multiple mechanisms, including the modulation of EMT signaling pathways, and direct transcriptional regulation of EMT TFs (Hapke and Haake 2020; Shen et al. 2024). For instance, in gliomas, hypoxia promotes the recruitment of resident or infiltrating myeloid cells. These immune cells release cytokines and growth factors, such as TGFβ, which in turn initiate EMT and upregulate core EMT TFs (Iwadate 2016). Notably, both HIF-1α and TGFβ have been shown to reciprocally enhance each other's activation in cancer cells (Hapke and Haake 2020). Hypoxia not only activates signaling cascades that drive EMT TFs expression but also directly induces their transcription. The promoter regions of key EMT TFs, including SNAI1, ZEB1/2, and TWIST1, harbor conserved HREs, which are recognized and directly bound by HIF-1, thereby initiating EMT program, and promoting cancer cells invasion (Hapke and Haake 2020; Majc et al. 2020; Saxena et al. 2020; Shen et al. 2024).

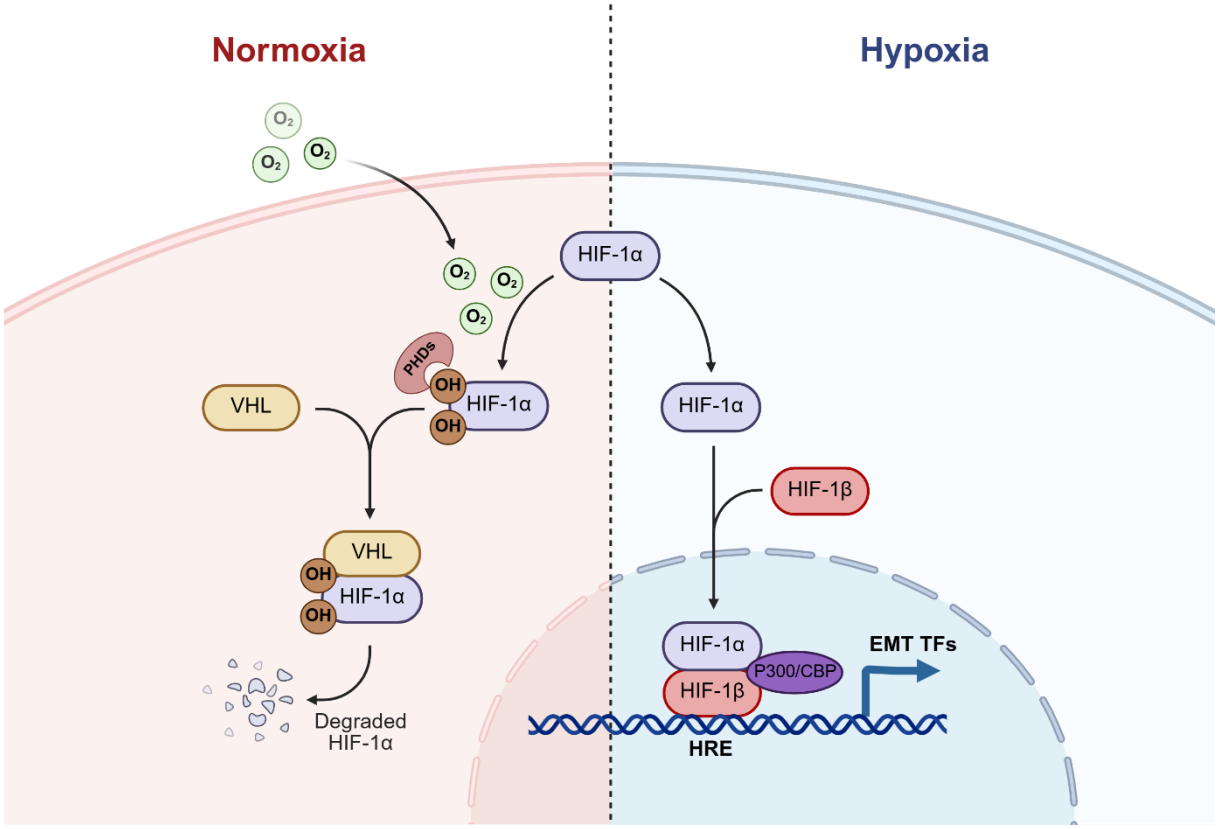

Figure 1.5. Overview of the HIF signaling pathway. HIF-1α is hydroxylated by PHDs enzymes under normoxia, which activates its pVHL-mediated ubiquitination followed by proteasomal degradation. Under hypoxia, PHDs become inactive, HIF-1α is stabilized, translocates to the nucleus, binds to HIF-

1β, and together with their transcriptional co-activators regulate target genes, such as EMT TF genes. Modified from BioRender.com

1.1.3. EMT TFs

The molecular and phenotypic changes associated with EMT are governed by core EMT TFs, namely SNAI1/2, ZEB1/2 and TWIST1/2 (Fig. 1.3). Their levels are tightly controlled through transcriptional, post-transcriptional, post-translational, epigenetic, and metabolic mechanisms. The level and activity of EMT TFs in turn determine the cell state along the EMP spectrum and influence the extent and reversibility of the EMT phenotype (Haerinck et al. 2023). These TFs can also regulate one another and often share and cooperate at some sets of target genes, however, the inhibition of a single TF has been shown to be sufficient to block EMT *in vitro* (Gonzalez and Medici 2014; Yang et al. 2020). Moreover, the same TF can function as both transcriptional repressor and activator, depending on its binding partners and the chromatin-modifying enzymes recruited to the target genes (Haerinck et al. 2023). In addition to the well-characterized core EMT TFs, a growing number of additional regulators have been identified that contribute to EMT induction and the acquisition of invasive and migratory capabilities, although their detailed functions are not well elucidated (Saitoh 2023; Youssef et al. 2024). These include forkhead box C1 (FOXC1), paired-related homebox 1 (PRRX1), YAP/TAZ, TCF3, among others, many of which function within broader developmental or oncogenic signaling pathways (Haerinck et al. 2023; Lambert and Weinberg 2021; Lu and Kang 2019; Yang et al. 2020). In GBM, other key regulators of mesenchymal transition have been recognized, including STAT3, nuclear factor kappa-light chain-enhancer of activated B cells (NF-κB), BCL2L2, and WWTR1 (Karsy et al. 2016; Kubelt et al. 2015), further highlighting the complexity and tumor-specific modulation of the EMT program.

1.1.1.3. SNAI family

Snail proteins are a family of zinc-finger transcription factors, compromising of three members, SNAI1 (Snail), SNAI2 (Slug), and SNAI3 (Smuc). Among them, Snail's role in EMT is the most studied in various developmental and pathological contexts, including tumorigenesis, and it is the primary focus of this study.

1.1.1.3.1. Snail TF

The Snail protein has a rapid turnover with a reported half-life of approximately 25 minutes, and its levels are tightly regulated both transcriptionally, post-transcriptionally, and post-translationally. Its expression is upregulated by several TFs, such as Smads, NF-κB, HIF-1α, or Glioma-associated oncogene homolog 1 (GLI1), among others, following TGFβ, WNT, and other ligands binding to their receptors, or upon hypoxic conditions (Babaei et al. 2021;

Saitoh 2023; Youssef et al. 2024). Moreover, Snail expression could be modulated at post-transcriptional levels, via miRNAs (Cano and Nieto 2016), or via chemical modifications of bases in the RNA sequence (M. Sun et al. 2022), resulting in its degradation, instability, or translation inhibition (Dong and Wu 2021). At the post-translational level, glycogen synthase kinase 3 beta (GSK-3β) functions as a negative regulator of Snail stability and activity. Activated GSK-3β phosphorylates Snail at two phosphorylation motifs, the first targets Snail for cytoplasmic translocation, while the second promotes its ubiquitination and proteasomal degradation (Dong and Wu 2021; Huang et al. 2022; Lu and Kang 2019; Zhou et al. 2004). In contrast, upstream kinases ERK and AKT, activated by RTKs and TGFβ (discussed in detail in section 1.2.2.2.1), phosphorylate GSK-3β at Ser9, leading to its inactivation (Lamouille et al. 2014). This results in Snail stabilization, nuclear retention, and EMT induction.

Snail is upregulated in breast, lung, and GBM tumors, among other cancer entities. Its upregulation is associated with EMT induction, elevated mesenchymal marker levels and increased invasive and metastatic potential (Iser et al. 2017; Jeschke et al. 2021; Saitoh 2023; Smith et al. 2014).

1.1.3.1.1.1. Snail target genes

Functionally, Snail as a master regulator, can both repress and activate gene transcription (Fig. 1.6). It recognizes and binds to the multiple conserved E-box motifs in the promoter of CDH1 (E-cadherin), and recruits complexes such as the Polycomb repressive complex 2 (PRC2), which coordinate CDH1 transcriptional silencing (Dongre and Weinberg 2019; Lamouille et al. 2014; Villarejo et al. 2014). It also represses other epithelial genes including Claudins (CLDNs), Occludin (OCLN), Cytokeratins, and Mucins, which are involved in tight junction integrity and apical-basal polarity. (Babaei et al. 2021; Iwadate 2016; Lamouille et al. 2014; Lu and Kang 2019). Conversely, Snail directly activates other EMT TFs such as SNAI2, TWIST, ZEB1/2, and PRRX1, as well as mesenchymal markers, such as Vimentin (Lamouille et al. 2014; Saitoh 2023; Youssef et al. 2024), it can also control its own expression (Peiró et al. 2006). Moreover, it induces the expression of genes involved in ECM remodeling, invasion, survival, and stemness, namely, MMPs, collagens, PI3K, and CD44, respectively (Cano and Nieto 2016; Nieto 2002).

MMPs belong to a family of zinc-dependent endopeptidases, which encompasses 23 members. The dysregulation of their activity has been heavily implicated in tumor progression (Cabral-Pacheco et al. 2020; Cox 2021; Khalili-Tanha et al. 2025; M. Li et al. 2023; Niland, Riscanevo, and Eble 2021). They can exert both pro-tumorigenic and anti-tumorigenic functions. Among other functions, they promote EMT by cleaving E-cadherin, enhance cell

invasion and infiltration by disintegrating the ECM components and the basement membrane collagen, promote angiogenesis, and selectively release and thus render specific cytokines and growth factors available, which reinforces and maintains EMT induction (Cabral-Pacheco et al. 2020; Cox 2021; Khalili-Tanha et al. 2025; M. Li et al. 2023; Niland et al. 2021). MMPs are also classified based on their substrate preference (Cabral-Pacheco et al. 2020; Khalili-Tanha et al. 2025; M. Li et al. 2023; Niland et al. 2021). For instance, MMP7 belongs to the Matrilysins, which digest variable ECM components, including Fibronectin, laminin, and proteoglycans. MMP13 is a collagenase, which degrades triple-helical fibrillar collagen, while MMP15 is part of Membrane-type MMPs (MT-MMPs), which have collagenolytic activity, but also target different ECM components (Cabral-Pacheco et al. 2020).

Notably, MMP7 has been extensively associated with EMT induction, Snail upregulation, invasion, and metastasis, irrespective of the upstream stimuli or signaling pathways involved (Cheng 2022; Ma et al. 2018; Sizemore and Keri 2012; Z. Sun et al. 2022; Y. Wu et al. 2019; Zhang et al. 2017). Its knockdown via gene silencing markedly reduces EMT features, migratory and invasive behavior, and metastatic potential in colorectal, prostate, lung and breast cancer models (Blaheta et al. 2025; Sizemore and Keri 2012; Zhang et al. 2014, 2017). Likewise, the upregulation of MMP13, which is one of the few MMPs primarily expressed by tumor rather than stromal cells (Ala-Aho et al. 2002), has been correlated with EMT induction, and invasion across various cancer models, including osteosarcoma (Huang et al. 2020; Ren, Minami, and Nishita 2011), head and neck carcinoma (Ho et al. 2023), GBM (Inoue et al. 2010), fibrosarcoma (Ala-Aho et al. 2002), lung cancer (Chang et al. 2021), as well as breast cancer (Aftab and Shakoori 2022). MMP13 expression has been shown to be upregulated in glioma samples compared to normal counterparts. Its expression increases with grade, and is associated with worse overall survival (Wang et al. 2012). Similar observations are found in melanoma, where MMP13 expression is associated with metastasis and poor survival (X. Zhao et al. 2015). MMP13 depletion suppresses the migration and invasion of GBM stem cells (Inoue et al. 2010), and reduces migration and lung metastasis in thyroid carcinoma cells, whereas its overexpression promotes invasion in various tumor models (J.-R. Wang et al. 2013; X. Zhao et al. 2015). Few reports have shown that MMP15 is highly expressed in primary and metastatic cervical cancer and hepatocellular carcinoma (HCC) samples compared to normal tissues (M.-H. Wu et al. 2020; Zheng et al. 2019). Its knockdown results in reduced proliferation and EMT, by suppressing Ki67, Vimentin, N-cadherin and ZEB1 levels, it also decreases migration and invasion (Lin et al. 2013; Zheng et al. 2019; Zuo et al. 2020). Interestingly, MMP15 has been frequently reported to be regulated by long-non-

coding RNAs and miRNAs in cancer (Jia et al. 2019; H. Li et al. 2019; Wang et al. 2020; Y. Wu et al. 2019; Zuo et al. 2020).

Other interesting downstream targets of Snail are collagens. ECM remodeling is an essential event during the initial steps of the metastatic cascade. It is not only characterized by degradation of ECM components by MMPs, but also re-depositing, cross-linking, and stiffening of collagens (Fang et al. 2014). Depositing of collagen destabilizes cell-polarity and cell-to-cell adhesion, accompanying EMT process, enabling cancer cells migration, whereas ECM degradation enables cells invasion. Both reciprocal events are required for tumor progression (Fang et al. 2014; Gonzalez and Medici 2014; Lo Buglio et al. 2024; Winkler et al. 2020).

COL3A1 expression has been increased with glioma grade, as well as in esophageal squamous cell carcinoma, cisplatin-resistant NSCLC, and irradiated breast cancer. Indeed COL3A1 has been shown to be an independent poor prognostic factor for overall survival in these cancer models (Gao et al. 2016, 2018; Lihuai Wang et al. 2022; Yao et al. 2022; Zhang, Zhang, and Wang 2020; Zhou et al. 2022). In addition, COL8A2 is overexpressed in GBM samples compared to normal counterparts, and it has been associated with shorter overall survival (Cheng et al. 2021). Both COL3A1 and COL8A2 expressions have been associated with increased migration and invasion in multiple tumor models (Cheng et al. 2021; Choi, Kim, and You 2025; Gao et al. 2018; Ren, Zhao, and Lai 2024; W. Wang et al. 2013; F. Yang et al. 2022; Yang et al. 2025; Yin et al. 2021; Zhou et al. 2022). In the contrary, the expression and role of COL14A1 in cancer is not well understood, and there is lack of relevant studies on the prognostic effect of COL14A1. On one hand, it was found to be downregulated in renal cell cancer (Morris et al. 2010), breast cancer (Uddin and Wang 2022), and others (Fu et al. 2023). On the other hand, only one study shows that its upregulation promoted gastric cancer cell proliferation (Jiang et al. 2022).

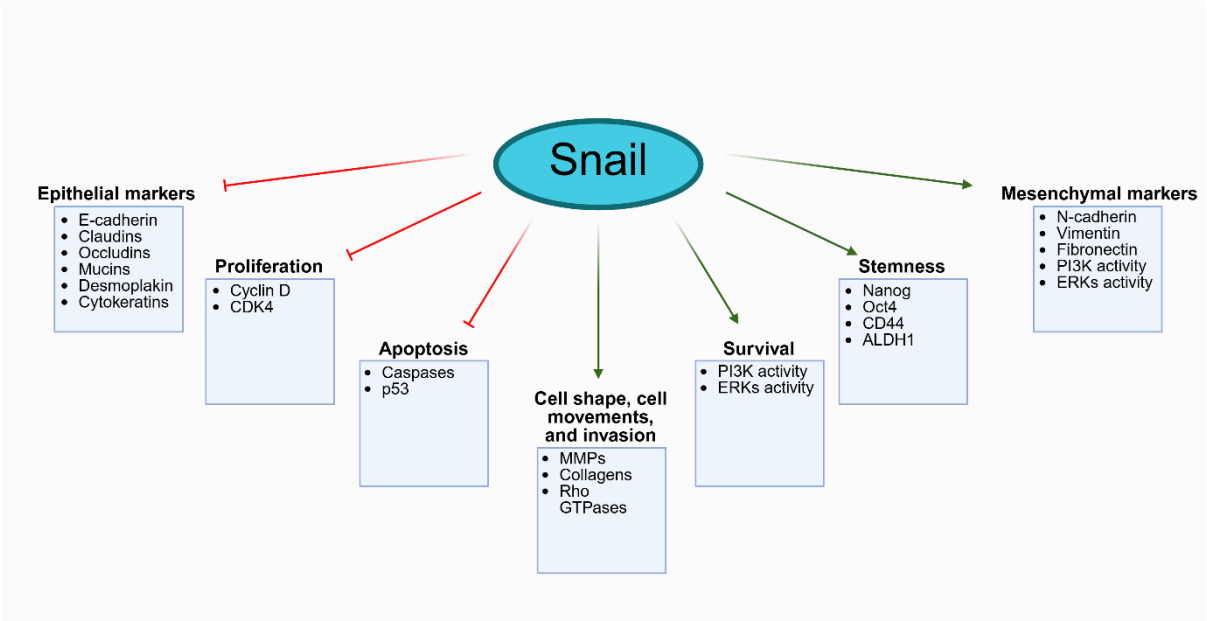

Figure 1.6. Overview of Snail target genes. Snail induces EMT through the downregulation of epithelial markers, proliferation and apoptosis genes, concomitant with upregulation of mesenchymal markers, and genes involved in invasion, ECM remodeling, survival, and dedifferentiation. Adapted from (Cano and Nieto 2016; Nieto 2002). Created by Biorender.com

1.1.1.3.2. Slug TF

SNAI2 (Slug), another member of the SNAIL family, also represses CDH1 by directly binding to the E-box sequence (CAGGTG/CACCTG) in the CDH1 promoter (Lamouille et al. 2014; Saitoh 2023; Villarejo et al. 2014). However, while Snail is often upregulated by TGFβ in various tumors, TGFβ-induced Slug expression seems to be less typical (Saitoh 2023). Still, Slug has been implicated in various tumors, associating with invasion, and metastasis (Iwadate 2016). For example, Slug overexpression promotes GBM cells proliferation and invasion *in vitro*, and enhances angiogenesis and growth *in vivo* (Yang et al. 2010).

1.1.1.4. TWIST family

TWIST1 and TWIST2 are highly conserved transcription factors belonging to the TWIST subfamily of the bHLH family of TFs. Their expression is usually induced following TGFβ non-canonical signaling activation (Saitoh 2023). In addition, hypoxia or HIF-1α overexpression can induce TWIST transcription through direct binding of HIF-1α to HREs in the proximal promoter regions of TWIST1/2, thereby activating the EMT program (Iser et al. 2017; Saitoh 2023). TWIST1/2 also repress CDH1 expression, in addition to directly activating CDH2 (N-cadherin) gene, Fibronectin, and SNAI2 (Iwadate 2016; Saitoh 2023). TWIST1 expression is positively correlated with breast carcinoma progression, where it enhances EMT, invasiveness and dissemination (Saitoh 2023). Additionally, elevated TWIST1 levels are also observed in gliomas, where it promotes PMT process, as well as invasion and parenchymal infiltration (Iser et al. 2017; Iwadate 2016). Furthermore, HGF-mediated TWIST1 induces

EMT onset and acquired tyrosine kinase inhibitors resistance in NSCLC (Kumar et al. 2024), and TWIST1 has also been associated with poor prognosis in lung cancer (Zeng et al. 2015).

1.1.1.5. ZEB family

ZEB1 and ZEB2 are zinc-finger E-box-binding homeobox TFs. They are induced by several external cues, including TGFβ, WNT signaling, and hypoxia, and could regulate or be regulated by Snail and Twist (Iser et al. 2017; Majc et al. 2020; Saitoh 2023). ZEB1/2 exert their repressive function by binding to the spaced E-box consensus sequence 5'-CANNTG-3' on the CDH1 promoter (Debnath et al. 2022; Majc et al. 2020; Saitoh 2023). Their transcriptional repression of CDH1 and other epithelial markers is mediated by the recruitment of various co-repressor complexes, histone deacetylases, and histone methyltransferases, which collectively establish a repressive chromatin environment at epithelial gene loci (Majc et al. 2020). They activate plenty of mesenchymal genes, such as Vimentin, and collagens, thereby increasing motility and invasion of aggressive cancer cells, such as GBM cells (Iser et al. 2017; Iwadate 2016). Canonical TGFβ-induced ZEB2 expression also promotes Fibronectin and COL5A1 expression, which further enhances GBM cell invasion (Majc et al. 2020). Conversely, ZEB1 knockdown dramatically reduces GBM cells tumorigenicity and invasiveness (Iwadate 2016). Moreover, elevated ZEB1/2 expression has been observed in TNBC, often in parallel with ERK and NF-κB pathway activation (Saitoh 2023).

1.2. Metabolic reprogramming

During the course of tumor progression, cancer cells tend to rewire their metabolism to meet the increasing demands of cell growth and proliferation, and to withstand the adverse conditions within the tumor microenvironment, such as nutrient deprivation, and hypoxia (Brunner and Finley 2023; Drapela and Gomes 2021; Pérez-González et al. 2023; Xiang et al. 2024). Reprogramming of the key metabolic pathways such as glycolysis, the tricarboxylic acid (TCA) cycle and glutaminolysis, is a hallmark of cancer (Jiang, Fang, and Tian 2025; Kodama et al. 2020; Pavlova, Zhu, and Thompson 2022; Trejo-Solis et al. 2023). Glucose and glutamine, which serve as the primary carbon and nitrogen sources, are heavily consumed by cancer cells. Notably, increased glucose influx sustains aerobic glycolysis, while glutamine addiction replenishes TCA cycle intermediates, and fuel biosynthetic and bioenergetic pathways (Han et al. 2013).

Importantly, such metabolic reprogramming not only support cellular proliferation and growth, but metastasizing cancer cells have been shown to further alter their metabolism throughout the metastatic cascade in order to invade, adapt and survive during circulation, and colonize secondary sites (Bergers and Fendt 2021; Han et al. 2013; Jia et al. 2021; Jiang et al.

2025; Pérez-González et al. 2023; Schwager et al. 2022). For instance, metastasis-initiating cancer cells often increase aerobic glycolysis, commonly known as the Warburg effect (Fendt 2024), concurrent with a downregulation of oxidative phosphorylation (OXPHOS) (Drapela and Gomes 2021; Jiang et al. 2025; M. Li et al. 2019; Liaghat et al. 2024). Moreover, highly migratory, mesenchymal-like breast cancer cells exhibit elevated glycolytic activity, in contrast to their slower, more epithelial-like counterparts, which rely more heavily on OXPHOS (Schwager et al. 2022).

Accumulating evidence underscores a strong reciprocal crosstalk between metabolic rewiring and EMT and invasion (Bergers and Fendt 2021; Jiang et al. 2025; Pérez-González et al. 2023). On one hand, cells undergoing EMT acquire mesenchymal and motile traits that demand metabolic flexibility, orchestrated by EMT-inducing signals and transcription factors, to facilitate adaptation and survival. On the other hand, beyond their canonical roles as intermediates in energy metabolism, numerous metabolites have emerged as key active drivers of EMT via nonmetabolic mechanisms, through acting as signaling molecules or cofactors for enzymes implicated in the EMT process (Jia et al. 2021; Krieg et al. 2024). For instance, pyruvate uptake by breast cancer cells promotes their metastatic colonization of the lungs through indirectly upregulating the activity of enzymes that mediate collagen biosynthesis and ECM deposition (Elia et al. 2019), highlighting the crosstalk between metabolism, EMT and metastasis. These interconnections are dynamic and context-dependent, shaped by microenvironmental cues, transcriptional, post-translational, and epigenetic programs. This complexity presents a significant challenge but also a promising opportunity for development of targeted combinatorial therapies that exploit metabolic vulnerabilities in metastasizing cancer cells (Han et al. 2013; Jia et al. 2021).

1.2.1. The pleiotropic functions of α-KG

α-Ketoglutarate (α-KG), also known as 2-oxoglutarate (2-OG), is considered a rate-determining intermediate metabolite in the TCA cycle. It is generated and regulated in human cells by various enzymes and distributed across cellular compartments by different transporters as shown in Fig. 1.7. Beyond its central role in energy metabolism, α-KG participates in a wide spectrum of metabolic and signaling pathways. Its diverse, pleiotropic functions are highlighted in Fig. 1.8.

1.2.1.1. α-KG production and metabolic function

α-KG is generated through the oxidative decarboxylation of isocitrate, catalyzed by IDH enzymes. This reaction is reversible in the case of $NADP^+$-dependent IDH isoforms, IDH1 and IDH2, both function as homodimers, localized in the cytoplasm and the

mitochondria/peroxisomes, respectively. Isocitrate conversion in the TCA cycle by the mitochondrial NAD^+-dependent IDH3 isoform, which consists of three subunits (α, β and γ) and functions as a heterooctamer, also produces α-KG (Abla et al. 2020; Chen et al. 2022; Sun et al. 2020), which undergoes irreversible oxidative decarboxylation to succinyl-CoA and CO_2 by α-KG dehydrogenase (α-KGDH), also known as 2-oxoglutarate dehydrogenase (2-OGDH) (Wu et al. 2016).

α-KG is not exclusively produced within the TCA cycle, in fact, its intracellular levels and homeostasis are dynamically regulated by several interconnected metabolic pathways. The α-KG pool is also regulated by glutaminolysis (Fig. 1.7), in which glutamine is first deaminated by glutaminase (GLS) to yield glutamate, which is subsequently converted to α-KG and ammonia by glutamate dehydrogenase 1 and 2 (GLUD1/2, also known as GDH1/2) (Abla et al. 2020; Legendre et al. 2020; Zdzisińska, Żurek, and Kandefer-Szerszeń 2017). Additionally, glutamine can be transaminated to α-ketoglutaramate (KGM), an intermediate ketoacid, which is further hydrolyzed by ω-amidase to generate α-KG and ammonia (Abla et al. 2020; Guo et al. 2022). Moreover, glutamate pyruvate transaminases (GPT1/2) and glutamate oxaloacetate transaminases (GOT1/2) generate α-KG in addition to pyruvate or oxaloacetate following reversible transamination reactions of glutamate, respectively (Abla et al. 2020; Zdzisińska et al. 2017). Glutamate could also be converted into α-KG by branched-chain aminotransferases (BCAT1/2), which catalyze reversible transamination of branched-chain α-keto acids (BCKAs) to branched-chain amino acids (BCAAs), although the reverse reaction is more predominant in cells (Islam et al. 2010). Furthermore, the phosphoserine aminotransferase (PSAT1), a key enzyme in the serine biosynthesis pathway, can also participate in α-KG homeostatic levels, through catalyzing the conversion of 3-phosphohydroxypyruvate and glutamate into 3-phosphoserine and α-KG (Li, Copeland, and Le 2021; Shu, Liu, and Wang 2025). Glutamine-derived α-KG then feeds into the TCA cycle to sustain energy production, or to produce biosynthetic molecules through anaplerotic reactions (Fig. 1.7) (Abla et al. 2020; Conza, Tsai, and Ho 2019). Once generated, α-KG can be transported between cellular compartments, to meet diverse metabolic demands. In particular, α-KG traverses the outer mitochondrial membrane through passive diffusion via voltage-dependent anion channels (VDAC), and crosses the inner mitochondrial membrane through the oxoglutarate carrier (OGC), also known as α-KG / malate antiporter (Abla et al. 2020; Zdzisińska et al. 2017).

Due to the existence of various metabolic reactions responsible for α-KG synthesis and consumption, it places this unique metabolite in the center of diverse metabolic processes (Fig. 1.7). As a key TCA cycle intermediate, α-KG plays a fundamental role in cellular energy

metabolism by generating NADH and $FADH_2$, both of which are essential electron donors for the mitochondrial electron transport chain, ultimately driving OXPHOS, and adenosine triphosphate (ATP) production. Beyond its role in bioenergetics, α-KG serves as a critical precursor for amino acid synthesis (Fig. 1.7), particularly for glutamate, which in turn is converted into glutamine, proline, and arginine (Abla et al. 2020; Legendre et al. 2020). It is worthy to highlight that glutamine is an essential energy source for most proliferating cells, compromising over 60% of the total amino acid pool, emphasizing the importance of α-KG as a precursor of glutamine and amino acids (Wu et al. 2016). Glutamine is indispensable for aggressive glioma tumors, particularly under hypoxic conditions where cells mainly rely on aerobic glycolysis, as well as glutamine metabolism, to ensure their survival and proliferation (Oizel et al. 2017). In addition, α-KG contributes significantly to lipid metabolism (Fig. 1.7) when glucose catabolism is impaired, and pyruvate import into the mitochondria is impeded. Under such metabolic stress, glutamine-produced α-KG is converted via reductive carboxylation into acetyl-CoA, a key substrate for fatty acid and lipid biosynthesis (Abla et al. 2020). This ability to fuel both reductive and oxidative pathways of the TCA cycle highlights the pivotal role of α-KG in supporting the bioenergetic and biosynthetic needs of proliferating cells (Abla et al. 2020).

A byproduct of aerobic cellular respiration and OXPHOS is the accumulation of reactive oxygen species (ROS) and reactive nitrogen species (RNS), which, when uncontrolled, induce oxidative stress that can be detrimental for the cells. To mitigate oxidative stress, cells employ several anti-oxidative defense strategies and there is growing evidence for the function of α-KG as an antioxidant molecule. Owing to its ketone group, α-KG directly scavenges reactive species such as hydrogen peroxide and superoxide by undergoing non-enzymatic oxidative decarboxylation, yielding succinate, carbon dioxide, and water (Abla et al. 2020; Legendre et al. 2020). In addition, α-KG neutralizes cyanide toxicity through formation of α-ketoglutarate-cyanohydrin, a less toxic intermediate. Furthermore, α-KG enhances the enzymatic activity of antioxidant enzymes though the precise molecular pathways remain under investigation (Abla et al. 2020; Legendre et al. 2020; S. Liu, He, and Yao 2018; Zdzisińska et al. 2017). However, several reports have been shown that α-KG could indirectly promote ROS accumulation in cancer cells, likely through its incorporation into the TCA cycle and the subsequent OXPHOS and electron transport chain. In particular, electron leakage at complexes I and III contributes to excessive ROS generation (Choi et al. 2025; Murphy 2009; Tretter and Adam-Vizi 2004; Wu et al. 2023; Zhao et al. 2019).

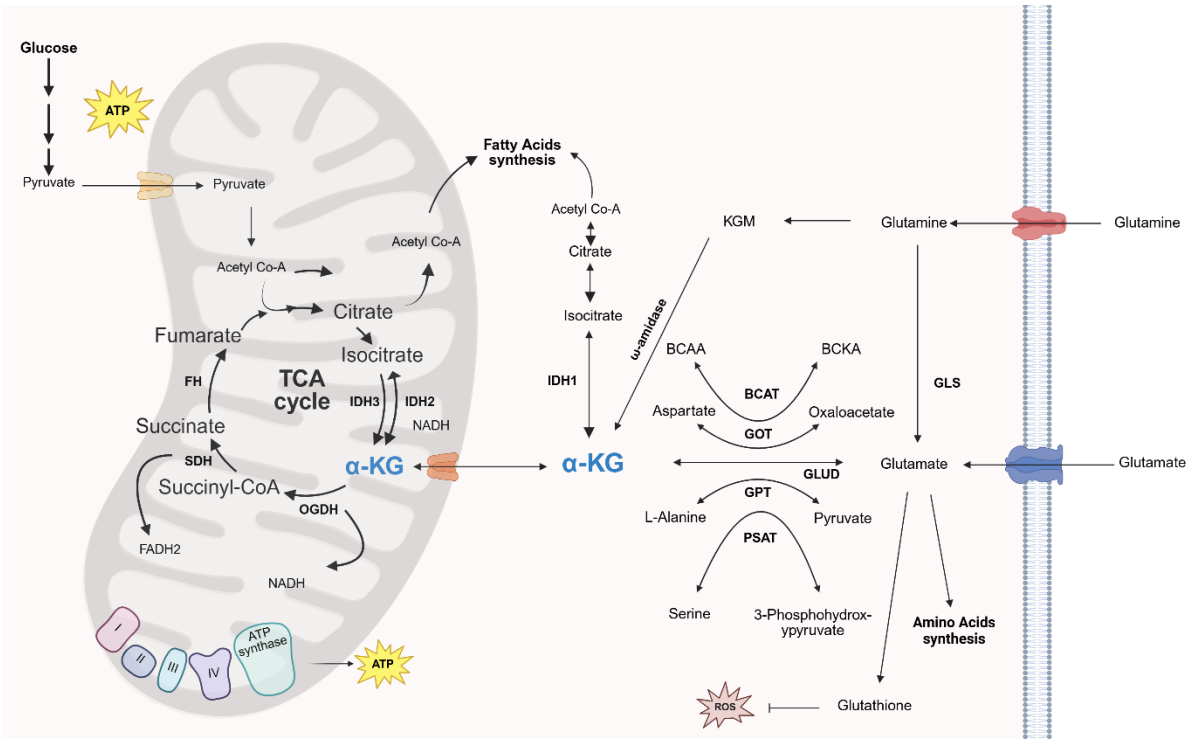

Figure 1.7. Overview of the enzymes and transporters governing α-KG homeostasis. α-KG cellular levels are regulated either by cytoplasmic or mitochondrial enzymes, via glutaminolysis, or TCA cycle, which either produce or consume α-KG. This metabolic control is required for ATP production, fatty acids and amino acids synthesis, and ROS regulation. α-KG levels are also controlled subcellularly via transporters that shuttle it between the mitochondria and the cytosol. Adapted from (Abla et al. 2020; Bögürcü-Seidel 2018; Zdzisińska et al. 2017). Created with BioRender.com

1.2.1.2. Co-substrate function for α-KG dependent dioxygenases

In addition to its metabolic functions, α-KG serves as a co-substrate for a superfamily of enzymes known as α-ketoglutarate dependent dioxygenases (α-KGDDs), also referred to as 2-oxoglutarate-dependent dioxygenases (2-OGDDs). This protein family comprises over 60 members, all of which catalyze similar hydroxylation reactions, yet regulate a wide range of biological functions by acting on a broad spectrum of substrates including histones, DNA, RNA, proteins, and lipids (Losman et al. 2020). Through these diverse targets, α-KGDDs regulate the fate of normal and cancer cells. These enzymes require oxygen, ferrous (Fe^{2+}) iron, and ascorbate (Vitamin C) in addition to α-KG, for catalytic activity, positioning them as cellular sensors for changes in oxygen levels, metabolic homeostasis, and Fe^{2+} redox status (Salminen, Kauppinen, and Kaarniranta 2015). While sharing common co-substrates, different α-KGDDs exhibit varying affinities for each substrate, offering a regulatory mechanism for controlling subsets of α-KGDDs based on the availability of co-substrates (Losman et al. 2020). The catalytic domain and hydroxylation activity of α-KGDDs are highly conserved across substrates (Losman et al. 2020). Although ascorbate is not a direct participant in the catalytic reaction, it is essential for reducing oxidized Fe^{4+} and Fe^{3+} back to Fe^{2+} following the release of

the hydroxylated substrate, and restoring the activity of the α-KGDDs (Kuiper and Vissers 2014; Smith-Díaz et al. 2025). The hydroxylated product can then undergo further non-enzymatic modifications such as demethylation (Kuiper and Vissers 2014; Losman et al. 2020; Zdzisińska et al. 2017).

There is mounting evidence that α-KGDDs are heavily implicated in various cancer hallmarks. In this context, our focus is to highlight the link between α-KG and EMT, invasion, and metastasis, via the activity of α-KGDDs. The dysregulation of α-KGDD function in cancer could arise through genetic alterations, including mutations, amplifications, or deletions of their encoding genes. Their activity could also be perturbed by mutations in α-KG-producing or -consuming enzymes, or by fluctuations in cofactor availability. In particular, loss-of-function mutations in genes encoding succinate dehydrogenase (SDH), and fumarate hydratase (FH), lead to excessive buildup of succinate and fumarate, respectively. Neomorphic mutations in IDH1/2, which frequently arise in diffuse astrocytomas, oligodendrogliomas, and leukemias, convert α-KG into the oncometabolite D-2-hydroxyglutarate (D-2-HG). Hypoxia can also induce the production of L-2-hydroxyglutarate (L-2-HG), primarily through LDHA (Intlekofer et al. 2015; Struys 2013). These aberrantly accumulated oncometabolites inhibit α-KGDD activity by competing with α-KG binding (Intlekofer et al. 2015; Kuiper and Vissers 2014; Losman et al. 2020; Salminen et al. 2015; Struys 2013). Furthermore, ROS impair α-KGDDs activity, partly by oxidizing Fe^{2+} to Fe^{3+}, disrupting the enzymes' catalytic function (Kuiper and Vissers 2014; Salminen et al. 2015, 2015).

Notably, the α-KGDDs family comprises several evolutionary conserved subfamilies, which are classified based on sequence similarity and/or function. Here, they are grouped based on the cellular pathways they regulate, including hypoxic response, epigenetic modifications on various levels, and collagen synthesis (Fig. 1.8) (Zdzisińska et al. 2017). By influencing these processes, α-KGDDs serve as critical links between cellular metabolism and the transcriptional, epigenetic, and structural adaptations that underlie tumor progression and dissemination.

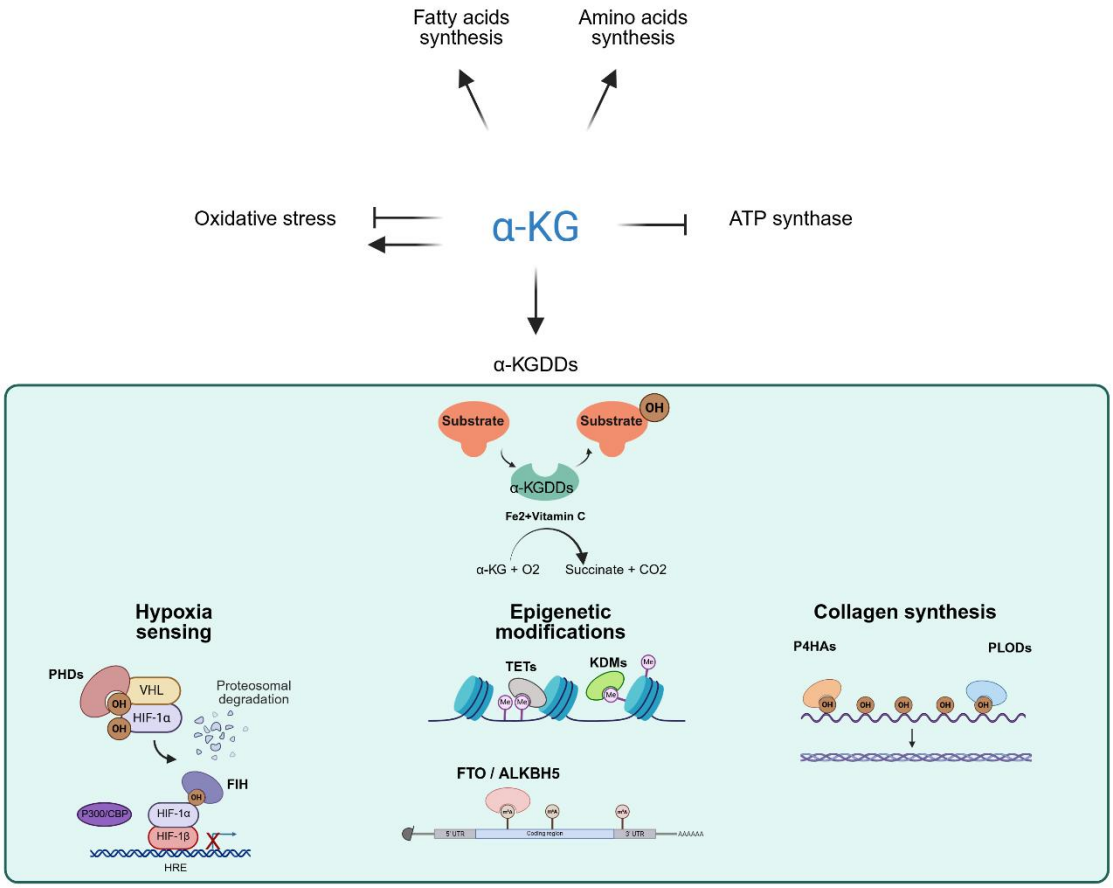

Figure 1.8. Overview of α-KG pleiotropic activities and a schematic of α-KGDDs reactions and subfamilies. α-KG is involved in fatty acid and amino acid synthesis, oxidative stress suppression and induction, inhibition of ATP synthase, as well as the activation of α-KGDDS. The reaction of α-KGDDs is presented along with the three subfamilies, classified based on their cellular functions. Based on (Baksh and Finley 2021; Losman et al. 2020). Created with BioRender.com

1.2.1.2.1. The connection of α-KG to hypoxic response

As described in Section 1.1.2.2., the HIF pathway is central to tumor progression and metastasis. Importantly, the PHD subfamily of α-KGDDs plays a fundamental role in sensing and responding to oxygen deficiency. Three genes encoding for PHD enzymes (PHD1-3) are also known as *egg laying defective nine* (*EGLN1-3*) genes after the *C. elegans* orthologues. However, it is important to highlight that the gene numbering do not match in both gene nomenclature systems (Huang et al. 2017). PHD2 is encoded by the *EGLN1* gene, while PHD1 by *EGLN2*. PHDs are considered as oxygen sensors, as they have low affinity for oxygen, meaning that slight changes in oxygen levels, dramatically affect PHDs activity (Losman et al. 2020). Their inhibition prevents HIF-α hydroxylation and subsequent degradation, allowing HIF-α stabilization, nuclear translocation, dimerization with HIF-1β, and transcriptional activation of target genes (Fig. 1.5) (Abla et al. 2020; Gaete et al. 2021; Huang et al. 2017; Losman et al. 2020; Yu et al. 2021; Zdzisińska et al. 2017).

Although HIFs are the primary substrates of PHDs, several HIF-independent functions of PHDs have been identified. For instance, PHD1 has been linked to inflammation, as it was established that it could hamper NF-κB signaling pathway. Hyperactive NF-κB signaling promotes tumor invasion in various tumors, including GBM (Pouyan et al. 2025). In the inactive state, the NF-κB subunits p65 and p50 are sequestered in the cytoplasm by inhibitor of κB (IκB) proteins. Upon TNF-α stimulation, the IκB kinase (IKK) complex phosphorylates IκB proteins on specific serine residues, marking them for ubiquitination and degradation. This releases the NF-κB subunits to freely translocate to the nucleus and activate the transcription of target genes involved in inflammation, immune responses, cell survival and EMT. Interestingly, IKKβ harbors a conserved LXXLAP motif, which resembles the prolyl hydroxylation sites in HIF-α, suggesting that PHD1 could inhibit the kinase activity of the IKK complex through hydroxylation of IKKβ at proline 191, although this remains to be confirmed biochemically (Cockman et al. 2019; Cummins et al. 2006; Oliver, Taylor, and Cummins 2009; Scholz and Taylor 2013).

Another α-KGDDs enzyme involved in HIF-α regulation is factor inhibiting HIF-1 (FIH1), an asparaginyl hydroxylase. FIH1 hydroxylates Asn803 in the CTAD of HIF-α, preventing its interaction with the transcriptional co-activators CBP and p300, consequently suppressing HIF-mediated transcription (Losman et al. 2020). It is worth noting that FIH1 has an intermediate affinity to oxygen, allowing it to remain active under moderately hypoxic conditions, which are detrimental for PHD activity, but becomes inactive under more severe oxygen deprivation (Losman et al. 2020).

Previous work from our laboratory had focused on IDH1 WT GBM, lung and breast cancer cells and investigated the impact of IDH1 depletion on invasion and metastasis, upon hypoxic incubation or TGFβ stimulation (Fig. 1.9) (Bögürcü-Seidel 2018). It was demonstrated that IDH1 depletion in U87MG GBM cells significantly reduces intracellular α-KG levels. To assess the functional consequences of IDH1 loss, tumor growth and invasiveness were assessed *in vivo*. Intracranial injection of control and IDH1-silenced G55 human GBM cells revealed that IDH1 depletion promotes local tumor invasiveness and subsequently brain tumor growth. Moreover, orthotopic transplantation of IDH1-deficient MDA-MB-231 breast cancer cells into the mammary fat pad of immunocompromised mice had no effect on primary tumor growth, but significantly increased lung metastatic nodules, compared to control cells. Furthermore, IDH1 knockdown significantly enhanced GBM cells invasiveness *in vitro*. Mechanistically, IDH1 loss results in elevated levels of HIF-1α and HIF-2α following hypoxic exposure, across GBM, lung, and breast cancer cell lines. Similarly, Snail protein levels are strongly induced

upon IDH1 knockdown and TGFβ stimulation. Interestingly, α-KG supplementation attenuates HIF-1α and HIF-2α levels and activity, as evidenced by reduced HIF-α protein levels, as well as the expression of their downstream targets, highlighting the suppressive role of α-KG in modulating hypoxic responses. Importantly, IDH1 regulates HIF-α in a PHD-dependent manner, as IDH1 knockdown-induced HIF-α expression is abrogated upon overexpressing an undegradable mutant form of HIF-1α, which carries point mutations at the PHD hydroxylation sites (mPPN[39]), preventing its hydroxylation by PHDs. Given that PHDs can also inhibit NF-κB signaling pathway, NF-κB activity was investigated upon IDH1 knockdown. Indeed, NF-κB activity was enhanced in IDH1-silenced cells, as demonstrated by nuclear accumulation of the p65 (RelA) subunit, and increased expression of NF-κB target genes. Interestingly, knockdown of HIF-1/2α, but not of the p65 subunit, partially suppresses both Snail protein and mRNA levels. These findings suggested that α-KG regulates Snail expression at least in part via the PHD–HIF axis, while also implicating the involvement of other signaling pathways in this regulatory network.

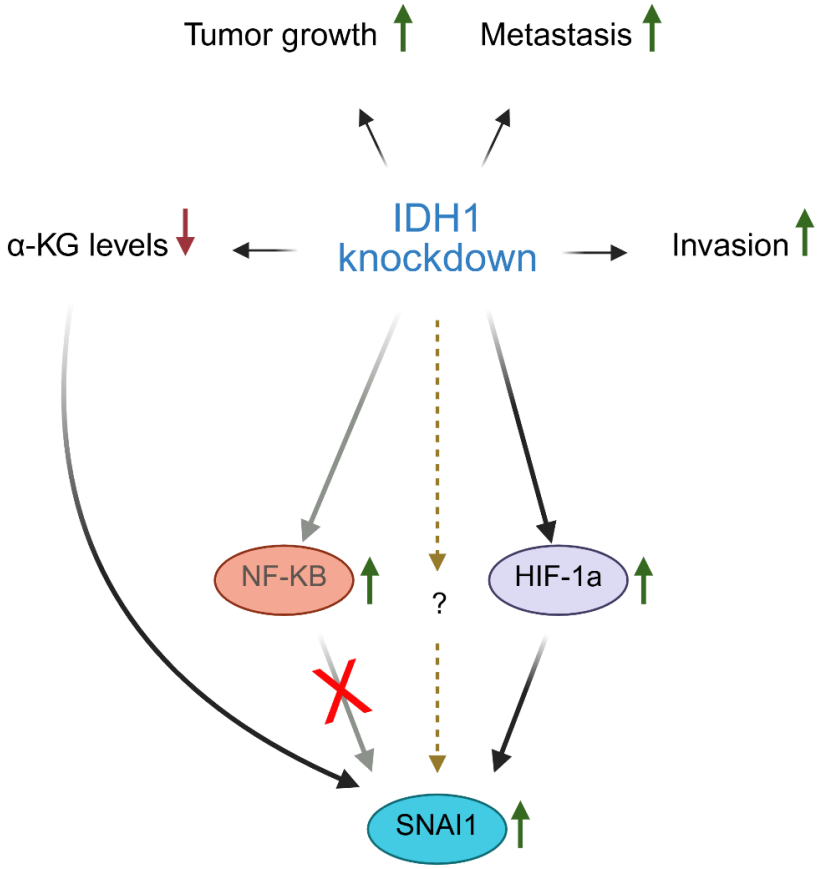

Figure 1.9. The impact of IDH1 knockdown on EMT, invasion, tumor growth, and metastasis. IDH1 depletion reduces α-KG levels, and enhances tumor growth and metastasis, as well as EMT and cellular invasion. IDH1 knockdown induces Snail expression partially through PHD-HIF but not NF-κB signaling pathway (Bögürcü-Seidel 2018). Created with BioRender.com

1.2.1.2.2. The roles of α-KG in epigenetic modifications

Histone, DNA and RNA modifications are critical determinants of gene expression and cancer progression. The addition or removal of chemical groups on histone residues, such as methylation, phosphorylation, acetylation, ubiquitination, and succinylation, is a dynamic process that modulates chromatin structure and DNA accessibility, thereby influencing transcription and replication. Importantly, this process is mediated by enzymes whose activity depends on cellular levels of metabolic intermediates as cofactors.

Maintenance of histone lysine methylation is regulated by two classes of enzymes, histone methyltransferases and lysine demethylases (KDMs). Nearly 30 KDMs have been identified and are classified into two families based on their mechanism of action, and into eight subfamilies according to their sequence homology, domain types, mode of activation, and substrate specificity (Eckschlager, Vicha, and Frolikova 2025; Gray et al. 2025; Zdzisińska et al. 2017). Importantly, KDM2-8 family members that contain a Jumonji C (JmjC) domain are α-KGDDs. They can remove mono-, di-, and tri-methyl groups from lysine residues. In contrast, KDM1 family members are flavin adenine dinucleotide (FAD)-dependent enzymes and limited to demethylating mono- and di-methylated lysines.

Perturbation of DNA methylation is a key feature of cancer cells. Tumors commonly exhibit global DNA hypomethylation, which contributes to oncogene activation and genomic instability, alongside focal hypermethylation at specific promoters, leading to silencing of tumor suppressor genes (Bray et al. 2021; Casalino and Verde 2020). DNA methylation typically occurs at cytosine residues within CpG islands, often found in gene promoters (Casalino and Verde 2020; Zacapala-Gómez et al. 2024). The addition of a methyl group at the 5-position of cytosine (5mC) is associated with transcriptional repression. α-KG-dependent Ten-Eleven Translocation (TET) enzymes oxidize 5mC in the genes' promoters and enhancers to 5-hydroxymethylcytosine (5hmC), and further to 5-formylcytosine (5fC) and 5-carboxylcytosine (5caC) (Bray et al. 2021; Zacapala-Gómez et al. 2024). 5fC and 5caC are excised by thymine-DNA glycosylase (TDG), which hydrolyzes the bond between the base and deoxyribose ring generating abasic sites. These sites are then replaced by unmodified cytosines via the Base-Excision Repair (BER) pathway (Zacapala-Gómez et al. 2024).

Epigenetic regulation also extends to the post-transcriptional level. N6-methyladenosine (m6A) is the most abundant internal mRNA modification, influencing RNA splicing, stability, translation, and nuclear export (Qu et al. 2022; Zaccara, Ries, and Jaffrey 2019). This modification is dynamically regulated by methyltransferases, readers and binding proteins, and

removed by α-KG-dependent demethylases, such as fat mass and obesity-associated protein (FTO) and alkB homolog 5 (ALKBH5).

Several studies have indicated that the expression and activity of these α-KGDDs are deregulated in various cancer types, including brain, breast, and lung cancers. They exhibit dual roles, as they can function as either suppressors or oncogenes, depending on their interacting binding partners, as well as their target gene, and cellular environment (Bray et al. 2021; Hua et al. 2021; Li et al. 2022; Qu et al. 2022; Yang et al. 2021). Importantly, they have been heavily implicated in EMT regulation, invasion, and metastasis, highlighting another route of how metabolic reprogramming can dictate tumor progression (Bray et al. 2021; Enkhbaatar et al. 2013; Jeschke et al. 2021; Li et al. 2022).

1.2.1.2.3. The function of α-KG in collagen synthesis

Collagen forms the ECM together with other structural proteins such as fibronectins, laminins and elastins. It is the most abundant component, comprising 90% of the ECM (Gilkes, Semenza, and Wirtz 2014; Huang et al. 2021). ECM remodeling, particularly increased collagen deposition, has been implicated in cancer progression, EMT induction, migration, and invasion (Gilkes et al. 2014; Huang et al. 2021). Collagen synthesis and stabilization are initiated in the endoplasmic reticulum (ER) through the activity of the α-KG-dependent collagen prolyl 4-hydroxylases alpha subunits (P4HA1-3), which associate with the beta subunit P4HB to form a functional tetramer composed of two alpha and two beta subunits. P4H tetramers catalyze hydroxylation of proline residues within the repeating X-Pro-Gly motif on each collagen strand, where X represents any amino acid. This produces 4-hydroxyproline, a modification crucial for collagen triple helix formation. Improper hydroxylation results in incomplete and irregular folding of the triple helices, leading to ER retention and subsequent degradation of incorrectly folded procollagen (Gilkes et al. 2014; Wu et al. 2016). α-KG availability is critical for P4HA activity, and its replenishment via enhanced pyruvate uptake, has been shown to promote ECM deposition, tumor growth, and lung metastasis in breast cancer models (Elia et al. 2019).

Additional α-KGDDs involved in collagen synthesis include the procollagen-lysine 2-oxyglutarate 5-dioxygenases (PLOD1-3), which hydroxylate lysine rather than proline residues. These enzymes possess glucosyltransferase and galactosyltransferase domains, which mediate the glycosylation of the collagen fibrils, required for proper basement membrane formation (Salminen et al. 2015).

1.2.1.3. α-KG-mediated inhibition of the ATP synthase-mTOR pathway

A study by Chin et al., (2014) identified the ATP synthase subunit β as a novel direct binding partner of α-KG. This binding inhibits ATP synthase activity, resulting in marked reduction in ATP levels, ATP/ADP ratio, as well as oxygen consumption. The authors proposed that α-KG-mediated inhibition of ATP synthase suppresses mechanistic target of rapamycin (mTOR), also known as mammalian target of rapamycin, a cellular energy and nutrient sensor. Consistent with this, α-KG treatment results in reduced TOR activity, as evidenced by decreased phosphorylation of its downstream targets, P70S6K and 4EBP1 (Chin et al. 2014; Fu et al. 2015). Similarly, oligomycin treatment, or ATP5B knockdown decreases ATP levels and TOR activity (Chin et al. 2014; Fu et al. 2015). ATP synthase is an evolutionary conserved enzyme, as further discussed in section 1.2.2.1, suggesting that α-KG inhibition of this enzyme is likely a universal mechanism. Similarly, perturbations in α-KG levels, via accumulation of the oncometabolite D-2-HG, similarly inhibited ATP synthase, lowered ATP levels, and mTOR activity, and reduced cell viability (Fu et al. 2015).

These findings highlight the pleiotropic functions of α-KG, extending beyond its classical role in intermediary metabolism and cellular signaling, by exerting a counterintuitive inhibitory effect on the ATP synthase–mTORC1 signaling axis. These observations led us to investigate if α-KG may regulate Snail expression, the EMT phenotype, and invasiveness, through modulating this pathway.

1.2.2. The ATP synthase-mTOR signaling pathway

1.2.2.1. ATP synthase

ATP synthase, also known as F1F0-ATPase or complex V of the mitochondrial electron transport chain (ETC), is the enzyme complex catalyzing the last step of OXPHOS under aerobic respiration, by generating ATP. It also possesses ATP hydrolytic activity (Vlasov et al. 2022). As ATP serves as the universal cellular energy currency, this rotatory enzyme embedded in the inner mitochondrial membrane (IMM) is considered the “enzyme of life” (Nesci et al. 2019; Vlasov et al. 2022). During OXPHOS, high-energy electron carriers generated during glycolysis and the citric acid cycle, donate electrons to the ETC complexes (I–IV). Through the series of redox reactions, the released energy creates a proton gradient by pumping hydrogen ions (H^+) from the mitochondrial matrix to the intermembrane space. This produces an electrical potential difference with a positive charge due to protons in the IMM, and a negative charge in the matrix. In the final step of OXPHOS, ATP synthase harnesses energy from the proton

gradient to generate ATP from ADP and inorganic phosphate (P) by rotational motor system (Nesci et al. 2019).

Due to its vital role, ATP synthase is ubiquitously expressed and evolutionarily conserved with some variations in subunit composition and assembly across species. The recently resolved human homolog comprises two main domains, the membrane-embedded hydrophobic F0 domain, and the matrix-facing hydrophilic F1 domain (Fig. 1.10). The F0 domain is composed of several subunits; a barrel-like c8-rotor ring, ATP6 or a, ATP8 or A6L, subunits e, f, g, diabetes-associated protein in insulin-sensitive tissue (DAPIT), and 6.8-kDa proteolipid (6.8PL), which collectively facilitate proton translocation across the IMM. The F1 domain consists of α3β3 subunits and governs ATP synthesis. These two domains are connected by central stalk made of subunits γ, δ, and ε, rotating with the c-ring during proton translocation, and a stationary peripheral stalk, composed of F6, b, d, and oligomycin sensitivity-conferring protein (OSCP) (Lai et al. 2023; Vlasov et al. 2022). Flowing of protons through F0 along the electrochemical potential gradient drives the rotation of the c8 ring, along with the central stock, which acts as a rotor shaft inside of the F1 domain, triggering its rotation and conformational changes catalyzing ATP synthesis (Lai et al. 2023; Saita et al. 2015; Vlasov et al. 2022). Despite the name OSCP, this protein is not targeted by oligomycin. However, as part of the peripheral stalk that connects both domains of ATP synthase, it mediates oligomycin inhibitory effect to the whole enzyme. In fact, oligomycin binds to and inhibits the c8 ring as well as the ATP6 subunit of the F0 domain, preventing the flow of protons, whereas α-KG binds to the beta subunit of F1, reducing ATP production (Fig. 1.10) (Antoniel et al. 2014; Chin et al. 2014; Hearne et al. 2020; Symersky et al. 2012). Interestingly, ATP synthase exists predominantly as a dimer in mammalian mitochondria, which enhances its functionality (Lai et al. 2023).

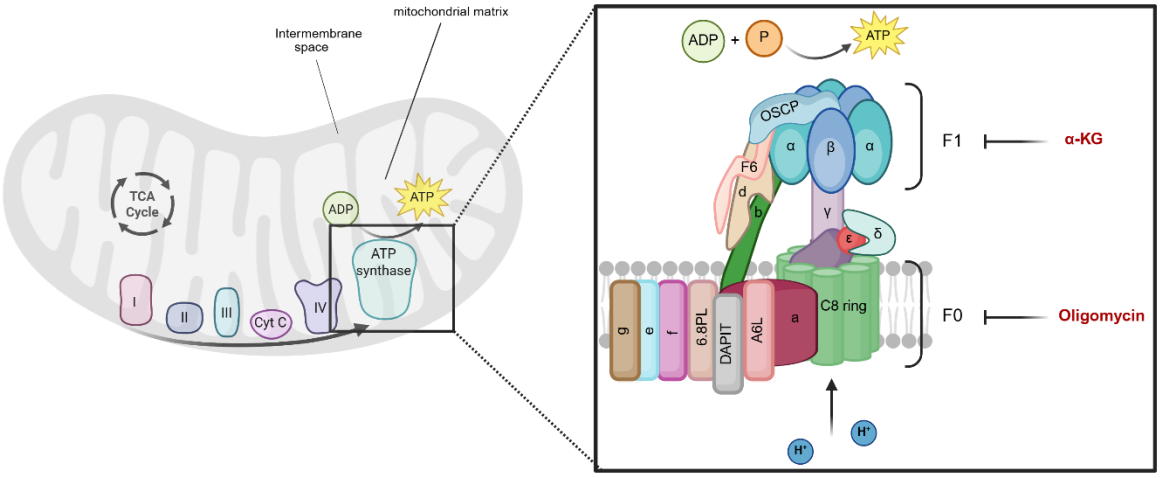

Figure 1.10. Overview of ATP synthase structure and α-KG and oligomycin target sites. OXPHOS and ETC flow are shown on the left, whereas the structure and the components of human ATP synthase domains F1 and F0 are shown on the right. α-KG binds to the beta subunit of F1 domain, while oligomycin to the c8 ring and the ATP6 subunit of the F0 domain. Created with BioRender.com

1.2.2.2. mTOR

mTOR is an evolutionarily conserved serine/threonine kinase belonging to the phosphoinositide 3-kinase related kinase (PIKK) family. It acts as a master regulator of cell growth, metabolism, proliferation, and survival. By integrating both intracellular and extracellular signals, mTOR promotes anabolic processes, including protein, nucleotide, and lipid synthesis, as well as ribosome biogenesis, while suppressing catabolic reactions such as autophagy. Given its pivotal role in maintaining cellular homeostasis, its dysregulation has been linked to a wide range of diseases, namely, cancer, diabetes, and aging (Laplante and Sabatini 2013). mTOR is the catalytic core of two structurally and functionally distinct multi-protein complexes (Fig. 1.11), named mTOR complex 1 (mTORC1), and mTOR complex 2 (mTORC2). mTORC1 consists of mTOR, regulatory-associated protein of mTOR (RAPTOR), mammalian lethal with sec-13 protein 8 (mLST8), proline-rich AKT substrate 40 kDa (PRAS40), and DEP-domain-containing mTOR-interacting protein (DEPTOR) (Liu and Sabatini 2020; Panwar et al. 2023). RAPTOR is indispensable for mTORC1 function, such that its dissociation from mTOR effectively suppresses mTORC1 activity. Moreover, it is also responsible for targeting mTOR to the surface of the lysosomes for proper functioning (Liu and Sabatini 2020; Panwar et al. 2023). In contrast, mTORC2 contains mTOR, rapamycin-insensitive companion of mTOR (RICTOR), mammalian stress-activated MAPK-interacting protein 1 (mSIN1), protein observed with Rictor-1 (PROTOR-1), as well as mLST8, and DEPTOR, both of which are shared components between mTORC1 and mTORC2, acting as

positive and negative regulators, respectively (Liu and Sabatini 2020; Panwar et al. 2023; Zoncu, Efeyan, and Sabatini 2011).

mTORC1 is sensitive to rapamycin inhibition. Upon administration, rapamycin binds to FK506-binding protein 12 (FKBP12) and, in turn, this complex recognizes and binds to the FKBP12-rapamycin binding (FRB) domain of mTOR, allosterically preventing substrate access and suppressing mTORC1 activity. mTORC2 is insensitive to acute rapamycin treatment, as RICTOR partially masks the FRB domain of mTOR, blocking FKBP-rapamycin binding. However its response to rapamycin is context- and time-dependent, as prolonged treatment with rapamycin can indeed inhibit mTORC2 in a subset of tissues and cell lines (Mossmann, Park, and Hall 2018). This is sought to be a result of indirect inhibition, likely by binding of FKBP-rapamycin complex to free mTOR and preventing complex formation (Battaglioni et al. 2022; Zoncu et al. 2011).

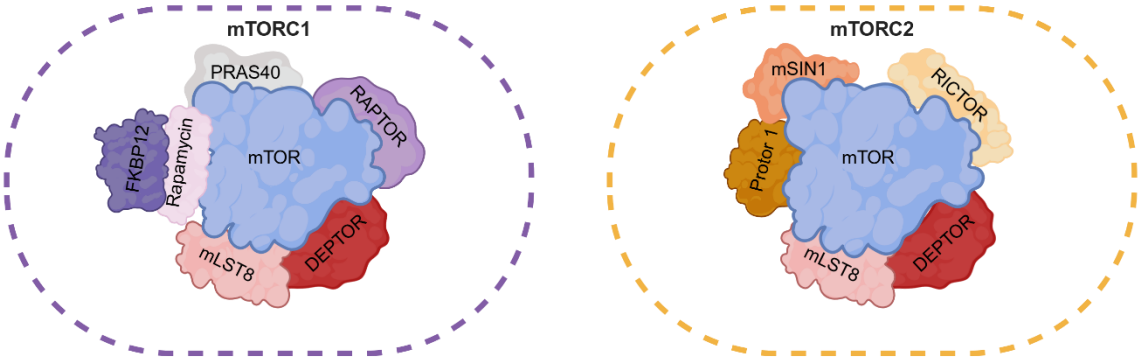

Figure 1.11. Overview of mTORC1 and mTORC2 structure. The shared subunits include the catalytic subunit mTOR, the positive regulator mLST8, and the negative regulator DEPTOR. Specific mTORC1-subunits are RAPTOR and PRAS40, whereas RICTOR, mSIN1 and PROTOR1 are specific for mTORC2. Adapted from (Panwar et al. 2023). Created with BioRender.com

1.2.2.2.1. mTORC1 upstream regulators

The activation of mTORC1 is orchestrated through a complex integration of growth factor signals, nutrient availability, and cellular energy levels (Fig. 1.12). Growth factors, such as insulin or insulin-like growth factors (IGFs) activate RTKs, which initiate the PI3K-AKT signaling cascade. PI3K catalyzes the conversion of phosphatidylinositol-4,5-bisphosphate (PIP2) into phosphatidylinositol-3,4,5-triphosphate (PIP3). PIP3 recruits phosphoinositide-dependent kinase 1 (PDK1) to the plasma membrane, where PDK1 phosphorylates AKT. Active AKT promotes mTORC1 by mainly phosphorylating and inactivating the tuberous sclerosis complex (TSC), a protein complex composed of TSC1, TSC2 (also known as tuberin)

and TBC1 domain family member 7 (TBC1D7). The TSC complex functions as a GTPase-activating protein (GAP) for Rheb GTPase. The GTP-bound form of Rheb directly interacts with mTORC1 and strongly induces its kinase activity. As a Rheb GAP, the TSC complex impairs mTORC1 activity by converting Rheb into its inactive GDP-bound state. Thus, the PI3K-AKT-TSC pathway activates mTORC1 by locking Rheb in its active GTP-bound state, through TSC inhibition. Interestingly, mTORC2 also phosphorylates AKT, which in turn stimulates mTORC1 function (Panwar et al. 2023; Saxton and Sabatini 2017). mTORC1 activity is also modulated by other upstream signals. The Ras-MAPK pathway, through ERK1/2 and p90 ribosomal S6 kinase (RSK1) activation, downstream of RTKs, also targets TSC2, phosphorylating it at distinct sites to those targeted by AKT (Laplante and Sabatini 2013; Mendoza, Er, and Blenis 2011). This similarly suppresses TSC2 GAP activity, enhancing mTORC1 activation. ERK and RSK additionally phosphorylate RAPTOR, enhancing mTORC1's ability to phosphorylate downstream targets like 4E-BP1, contributing to oncogenic growth (Mendoza et al. 2011). Amino acids, notably leucine, arginine and glutamine, as well as glucose induce mTORC1 activation, via the RAS-related GTP-binding proteins (RAGs). Activated RAGs interact with RAPTOR, driving mTORC1 translocation to the lysosome, where the endogenous mTOR activator Rheb resides and promotes mTORC1 activation (Laplante and Sabatini 2013; Mendoza et al. 2011; Panwar et al. 2023).

mTORC1 activity is also sensitive to changes in energy levels. Energy stress, such as limited glucose availability, and reduced ATP production lead to an increased intracellular AMP/ATP and ADP/ATP ratio. This energetic imbalance allosterically activates AMP-activated protein kinase (AMPK), a central energy sensor and metabolic regulator. Activated AMPK inhibits mTORC1 through multiple mechanisms. First it phosphorylates TSC2 at Thr1271 and Ser1387, enhancing the GAP activity of the TSC complex, which in turn promotes the conversion of Rheb to its inactive GDP-bound state, thereby inhibiting mTORC1 activity. Second, AMPK directly phosphorylates RAPTOR on Ser722 and Ser792 (Battaglioni et al. 2022). This phosphorylation disrupts the interaction between RAPTOR and mTOR, further reducing mTORC1 activity (Battaglioni et al. 2022). Interestingly, ATP itself has been shown to act as a direct activator of mTOR, independent of AMPK and TSC2 signaling, by interacting with the ATP-binding pocket in the catalytic site of mTOR kinase domain. This has important pharmacological implications, as ATP-competitive mTOR inhibitors have shown a greater reduction in cell proliferation and migration in glioblastoma, compared to rapamycin treatment (Amin et al. 2021). In addition, they showed potent selective inhibition of both mTORC1 and mTORC2, as opposed to the allosteric inhibition of rapamycin, which exerts a partial and

selective inhibition of mTORC1 and has minimal impact on mTORC2 (Ali et al. 2022; Amin et al. 2021).

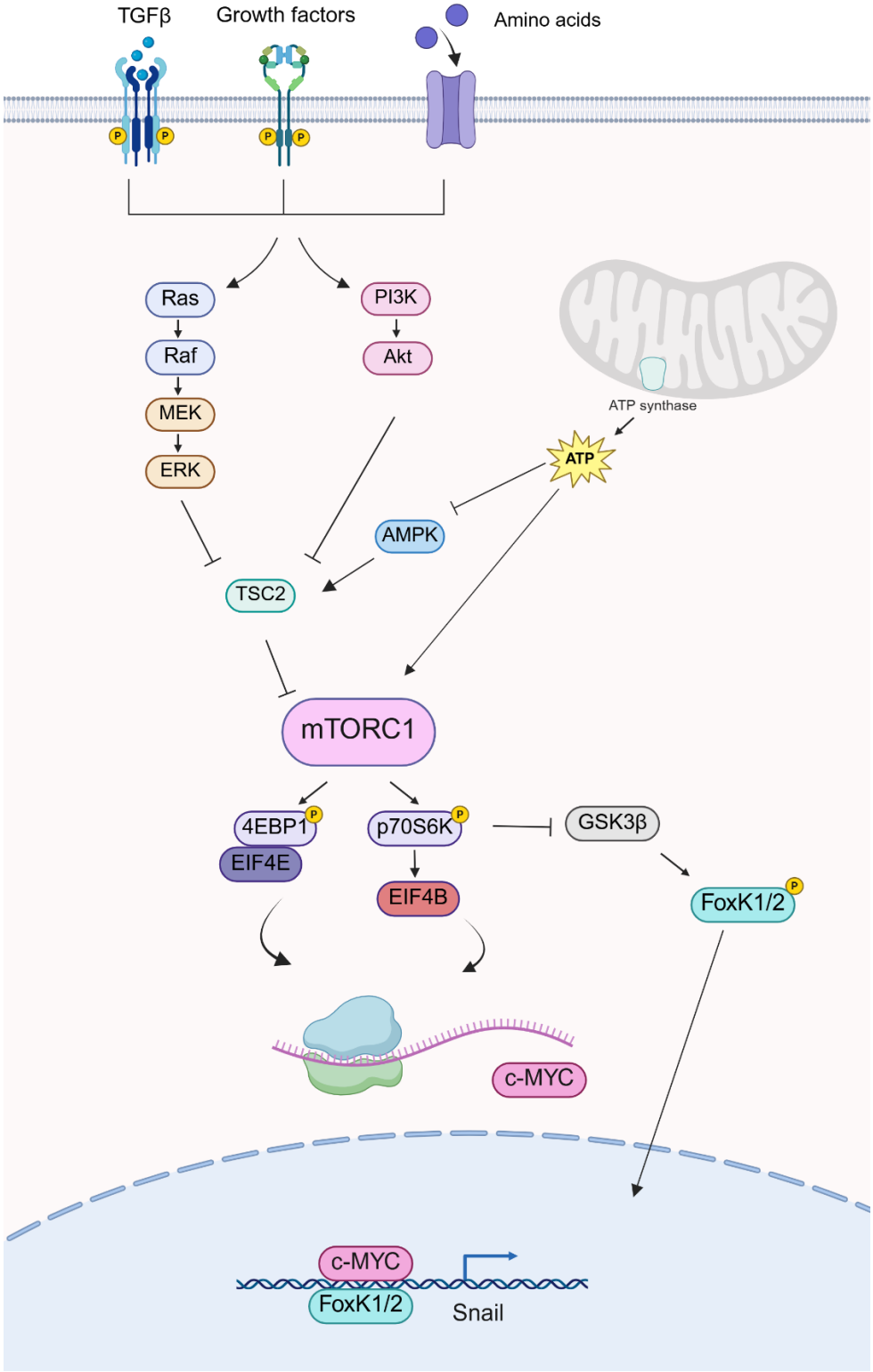

Figure 1.12. Overview of mTORC1 upstream and downstream signaling pathways from TGFβ receptors and RTKs to Snail gene regulation. mTORC1 is regulated downstream of TGFβ, RTKs, amino acids, and ATP synthase-AMPK through RAS-RAF-MEK-ERK and PI3K-AKT. mTORC1 controls c-Myc translation via P70S6K and 4EBP1, which regulate mRNA translation. mTORC1

regulates FoxK1 and FoxK2 through the inhibition of GSK3β, reducing FoxK1/2 phosphorylation and enabling their nuclear translocation. Created with BioRender.com

1.2.2.2.2. Major mTORC1 substrates

mTORC1 and mTORC2 exert their functions either through direct phosphorylation of their targets, or indirectly through downstream signaling effectors. The best characterized mTORC1 substrates are ribosomal protein S6 kinase 1 (S6K1), also known as P70S6K, and eIF4E binding protein 1 (4EBP1) (Fig. 1.12), both of which are important regulators of protein translation. They are also widely used as readouts of mTORC1 activity, due to the availability of antibodies that specifically recognize the phosphorylated forms of these two proteins.

P70S6K is phosphorylated by mTORC1 at the Thr389 residue, leading to its subsequent phosphorylation at Ser229 and activation by PDK1. Phosphorylation of both sites is required for full S6K1 activation (Battaglioni et al. 2022). Once activated, P70S6K regulates many cellular processes through phosphorylating diverse array of substrates. However, it mainly promotes mRNA translation initiation and elongation, which is achieved through the action of the eukaryotic translation initiation factor 4F (eIF4F), a protein complex comprising of eIF4E, eIF4A, and the scaffold protein eIF4G. This complex recruits the small ribosomal subunit 40S to mRNA to start cap-dependent translation initiation. P70S6K promotes the activity of eIF4A, an RNA helicase required for unwinding the secondary structures in 5′ untranslated regions (UTRs) of many mRNAs. This is achieved via phosphorylation-dependent degradation of programmed cell death 4 (PDCD4), an inhibitor of eIF4A, as well as phosphorylation-dependent activation and recruitment of elF4B to eIF4A, enhancing its helicase activity (Liu and Sabatini 2020; Panwar et al. 2023; M. Yang et al. 2022; Zoncu et al. 2011). Importantly, P70S6K also enhances translation initiation and ribosome biogenesis through direct phosphorylation and activation of ribosomal protein S6 (rpS6), a structural component of the 40S ribosomal subunit, thereby promoting translation initiation and ribosome biogenesis (M. Yang et al. 2022).

The second major mTORC1 substrate, 4EBP1, also plays a pivotal role in translation. When it is unphosphorylated, 4EBP1 binds to eukaryotic mRNA cap-binding protein/ translation initiation factor 4E (eIF4E), blocking the binding of eIF4G, and preventing the formation of translation initiation complex eIF4F, thereby suppressing translation initiation. In contrast, upon mTORC1 activation, 4EBP1 undergoes sequential phosphorylation, initially at Thr37/Thr46, followed by Ser65/Thr70, which induces its dissociation from elF4E. This allows eIF4E to associate with the scaffold protein eIF4G at the 5′ cap of target mRNAs (M. Yang et al. 2022). Intriguingly, while the initial phosphorylation of 4EBP1 at Thr37/Thr46 can still occur in the presence of FKBP–rapamycin-bound mTOR, phosphorylation at Ser65/Thr70 is

rapamycin sensitive. Structural studies suggest that 4EBP conformational changes following the first phosphorylation step prevent access of Ser65/Thr70 to the catalytic site in rapamycin-inhibited mTORC1, which explains the incomplete inhibitory effect of rapamycin on 4EBP1 function (Battaglioni et al. 2022).

1.2.2.2.3. Other mTORC1 substrates

Given mTORC1's critical role in coordinating protein synthesis, its dysregulation is closely linked to tumor growth, proliferation, invasion, and metastasis, often through upregulation of translation of specific mRNAs encoding oncogenic TFs, invasion-related proteins, and EMT regulators (Mossmann et al. 2018; Saxton and Sabatini 2017). Among them c-Myc and forkhead box K1/2 (FoxK1/2) have been shown to directly regulate SNAI1 gene expression, thereby controlling a mesenchymal phenotype and tumor progression (Chen et al. 2017; Smith et al. 2009; H. Xu et al. 2018).

1.2.2.2.3.1. The mTORC1-MYC-SNAI1 axis

c-Myc (MYC) is a well-characterized proto-oncogene that is frequently activated in different cancer types. c-Myc functions as a heterodimeric TF, as it binds to Max TF, through its basic-region/helix-loop-helix/leucine-zipper (BR/HLH/LZ) motif (Chen, Liu, and Qing 2018). They regulate the expression of thousands of genes, by binding to the conserved E-box DNA sequence (5'-CACGTG-3') located in the target genes regulatory regions (Chen et al. 2018; Dhanasekaran et al. 2022). c-Myc activation contributes to many hallmarks of cancer, including metabolism, and invasiveness (Dhanasekaran et al. 2022). c-Myc is regulated at genetic, epigenetic, post-transcriptional, and post-translational levels. Indeed, it has been established that MYC mRNA translation is regulated by PI3K-AKT-mTORC1 pathway (Fig. 1.12) (Chen et al. 2018). Its levels are upregulated following insulin stimulation (West, Stoneley, and Willis 1998), whereas they are dramatically reduced with knockdown or pharmacological inhibition of the PI3K-AKT-mTORC1 pathway (Stengel et al. 2022). In particular, the translation of MYC mRNA, as it contains complex secondary structures, requires translation initiation complexes downstream of activated 4EBP1 and P70S6K (Chen et al. 2018; West et al. 1998; Yun et al. 2016). c-Myc is also regulated at post-translational levels. Notably, mTORC2 and its downstream activated AKT kinase prevent c-Myc protein degradation by inhibiting GSK-3β-mediated c-Myc-T58 phosphorylation (Stengel et al. 2022).

c-Myc has been reported to directly bind to consensus E-box elements in the promoter of the SNAI1 gene, as well as its TSS, as determined by ChIP-qPCR in breast cancer cells (Smith et al. 2009). This binding occurs prior to TGFβ stimulation, but is required for rapid SNAI1 activation upon Smads binding (Smith et al. 2009), highlighting the cooperative action

of c-Myc and Smads. Consistent with this, c-Myc has been implicated in the regulation of Snail expression, and subsequent N-cadherin and vimentin upregulation, as well as E-cadherin suppression, promoting migration and invasion, in various cancer types (X. Lin et al. 2017; Runze Wang et al. 2022; Zhai et al. 2018). Interestingly, c-Myc can also regulate Snail expression and stability indirectly at post-translational level. Namely, c-Myc activates the ERK1/2 signaling pathway, which in turn phosphorylates GSK-3β, a direct negative regulator of Snail, preventing the subsequent phosphorylation and degradation of the Snail protein (Huang et al. 2015).

1.2.2.2.3.2. The mTORC1-FOXK-SNAI1 axis

Other recently identified mTORC1 targets are the FoxK TFs, through which mTORC1 regulates cellular metabolism and other key processes. FoxK1 and FoxK2 belong to a conserved superfamily of transcription factors, comprising over 50 members, all characterized by forkhead and winged-helix DNA binding domains. FoxK1 and FoxK2 share the DNA binding Fox domain, which recognizes and binds to the highly conserved DNA motif 5′-GTAACA-3′, and the forkhead-associated domain (FHA), which enables phospho-dependent protein–protein interactions (Yu et al. 2022).

Notably, FoxK1 is an unusual target of mTORC1, as it has been demonstrated that mTORC1 suppresses FoxK1 phosphorylation rather than stimulating it (He et al. 2018; Nakatsumi, Matsumoto, and Nakayama 2017). Mechanistically, when mTORC1 is inactive, FoxK1 is phosphorylated by GSK-3β at several serine sites, including S402/S406. This phosphorylation facilitates 14-3-3 scaffold proteins recognition and binding, which masks its nuclear localization signal (NLS), resulting in nuclear exclusion of FoxK (He et al. 2018). In addition, increased phosphorylation of FoxK1 impedes its DNA-binding affinity (He et al. 2018; Sakaguchi et al. 2019). Upon mTORC1 activation, GSK-3β is inhibited through P70S6K phosphorylation (Zhang et al. 2006), FoxK1 phosphorylation is suppressed, enhancing its nuclear translocation and its increased transcriptional activity (Fig. 1.12) (He et al. 2018). Importantly, FoxK1 translocation to the nucleus is dependent on the activation of AKT-mTORC1 rather than the ERK-mTORC1 pathway, following insulin, or growth factors stimulation (Sakaguchi et al. 2019). In contrast, although FoxK2 is also phosphorylated by GSK-3β and dephosphorylated by mTORC1 at S415/S419, it predominantly localizes to the nucleus, even in the absence of stimulation, and its precise regulation by mTORC1 remains less well understood and warrants further investigation (He et al. 2018; Sakaguchi et al. 2019).

FoxK deregulation has been associated with various tumor aspects, including, cell cycle progression, proliferation, differentiation, apoptosis (Sakaguchi et al. 2019), autophagy

(Bowman, Ayer, and Dynlacht 2014; Chen et al. 2020), angiogenesis and inflammation (Nakatsumi et al. 2017), and metastasis (Peng et al. 2016; Zhang et al. 2019). FoxK1 mainly acts as an oncogene in numerous tumor types, and its expression correlates with increased tumor size, stage, grade, and metastasis (Wencong et al. 2020; H. Xu et al. 2018). Its overexpression enhances glioblastoma cell invasion and migration by directly binding and upregulating the expression of SNAI1 (H. Xu et al. 2018). In triple-negative breast cancer, FoxK1 promotes lymphangiogenesis and lymph node metastasis. It also enhances invasive capacity and induces EMT, shown by downregulation of the epithelial marker E-cadherin and upregulation of the mesenchymal markers N-cadherin and Vimentin (Zheng et al. 2020). Similar findings have been reported in gastric cancer, where its overexpression results in EMT induction and enhanced migration and invasion (Peng et al. 2016).

While FoxK1 generally promotes tumor progression, various reports suggest that FoxK2 mainly functions as a tumor suppressor (Nestal de Moraes et al. 2019; Wang et al. 2018; Zhaojun Wang et al. 2022; Yu et al. 2022). For instance, FoxK2 expression is significantly downregulated in high grade glioma, breast, lung, and gastric cancers. Its higher expression is correlated with improved overall survival (Chen et al. 2017; X. Liu et al. 2018; Shan et al. 2016; Wang et al. 2018). Moreover, FoxK2 overexpression directly represses Snail and N-cadherin, inhibiting EMT and invasiveness in NSCLC (Chen et al. 2017). Additionally, FoxK2 depletion enhances, while its overexpression inhibits glioma and gastric cancer cells proliferation, EMT induction, invasion, and migration (X. Liu et al. 2018; Wang et al. 2018). Furthermore, FoxK2 knockdown significantly enhances primary and secondary tumor growth in an orthotopic breast cancer mouse model (Shan et al. 2016). Conversely, FoxK2 is significantly overexpressed in human colorectal cancer (CRC) and HCC tissues, and is further upregulated in metastatic tissues compared with primary tissues (Du et al. 2019). Its high expression is correlated with worse prognosis, advanced stage, and tumor vascular invasion (Du et al. 2019; M.-F. Lin et al. 2017). Notably, FoxK2 transcriptionally activates ZEB1, promoting EMT, and hepato-lung metastasis in CRC. Likewise, FoxK2 induces cell migration, and invasion by upregulating the expression of Snail, and c-Myc (Kong et al. 2020; M.-F. Lin et al. 2017).

1.3. Aim of this study

Glioblastoma and brain metastases originating from lung and breast cancers represent the most prevalent and aggressive forms of malignant brain tumors in adults. Despite advances in multimodal treatments, encompassing surgical resection, chemotherapy, and radiotherapy, these primary and secondary brain neoplasms remain incurable, often associated with poor prognosis and limited survival (van den Bent et al. 2023; Schaff and Mellinghoff 2023).

Although brain metastases have shown evidence of responsiveness to targeted therapies and immunotherapies in selected settings, the use of these treatment modalities for brain metastases has not yet reached clinical approval, and is often extrapolated from systemic disease approvals (Schaff and Mellinghoff 2023; Suh et al. 2020). EMT and invasiveness are key characteristics of these tumors and great contributors to the initial step of brain metastasis (Liaghat et al. 2024; Liang et al. 2025; Lu et al. 2025; Lu and Kang 2019; Margarido et al. 2022), as well as to poor GBM clinical outcome and therapy failure (Fedele et al. 2019; Iser et al. 2017; Iwadate 2016; Seker-Polat et al. 2022; Xia 2025). EMT is a dynamic and reversible process regulated by diverse signaling pathways that collectively dictate the molecular and phenotypic changes of the tumor cells. Equally important, metabolic reprogramming, another hallmark of cancer, has been implicated in both negatively and positively regulating EMT, and tumor invasiveness. In particular, we have previously demonstrated that the modulation of cellular α-KG levels by IDH1 depletion enhances cellular invasion, migration, and metastasis, in addition to upregulation of Snail expression at both the transcript and protein levels (Bögürcü-Seidel 2018). These observations have been primarily observed under hypoxic condition, as well as following TGFβ stimulation, both well-established EMT inducers.

The research presented in this thesis aimed first to gain a deeper understanding of the reciprocal crosstalk of EMT and metabolism. First, by defining the TGFβ-mediated EMT induction and metabolic changes, and secondly, by examining the function α-KG in the regulation of Snail expression, EMT/PMT induction, and invasion in brain, breast, and lung cancer models. A key objective was also to identify Snail-regulated targets through which α-KG exerts its effects. Moreover, we expanded our investigations on IDH1-dependent EMT modulation in various tumor models *in vitro*, and in lung cancer *in vivo*. Another major goal was to determine whether and how the ATP synthase-mTORC1 axis could act as an α-KG-dependent Snail regulatory pathway through c-Myc, FoxK1, or FoxK2, possibly in concert with the PHD-HIF signaling axis. Finally, we aimed to evaluate the clinical relevance of IDH1 and Snail expression levels across the three cancer types studied, thereby integrating mechanistic insights with translational perspectives.

2. Materials and methods

2.1. Materials

2.1.1. Chemicals

Solvents and standard chemicals were purchased from Sigma-Aldrich, Carl Roth, Merck, or AppliChem, unless otherwise stated.

2.1.2. Antibodies

2.1.2.1. Primary antibodies

Table 2.1. Primary antibodies (WB: Western blotting, IF: Immunofluorescence, ChIP: Chromatin immunoprecipitation)

Antigen	Species	Company	Order number	Dilution
Snail	Rat (monoclonal)	Cell Signaling Technology	4719	WB: 1:250 IF: 1:100
Snail (C15D3)	Rabbit (monoclonal)	Cell Signaling Technology	3879	WB: 1:500
Slug (C19G7)	Rabbit (monoclonal)	Cell Signaling Technology	9585	WB: 1:1000
Vimentin	Mouse (monoclonal)	Dako	M0725	WB: 1:2000 IF: 1:500
E-cadherin	Mouse (monoclonal)	BD Biosciences	610181	WB: 1:1000 IF: 1:50
N-cadherin	Mouse (monoclonal)	BD Biosciences	610920	WB: 1:1000
IDH1	Goat (Polyclonal)	Santa Cruz Biotechnology	sc-49996	WB: 1:1000
IDH1	Rat (monoclonal)	Dianova	Dia-W09	WB: 1:500
HIF-1α	Rabbit (Polyclonal)	Cayman Chemical	10006421	WB: 1:5000
HIF-1α	Mouse (monoclonal)	Novus Bio	NB100-105	ChIP: 1:100
HIF-2α	Rabbit (Polyclonal)	Novus Bio	NB 100-122	WB: 1:500

HIF-1β	Rabbit (Polyclonal)	Novus Bio	NB100-110	ChIP: 1:100
c-Myc	Mouse (monoclonal)	Santa Cruz Biotechnology	sc-42	WB: 1:500
c-Myc	Mouse (monoclonal)	Abcam	ab56	ChIP: 1:100
c-Myc	Rabbit (Polyclonal)	Cell Signaling Technology	9402	ChIP: 1:100
c-Myc	Mouse (monoclonal)	Santa Cruz Biotechnology	sc-40 X	ChIP: 1:100
P70 S6 Kinase	Rabbit (polyclonal)	Cell Signaling Technology	9202	WB: 1:1000
Phospho-p70 S6 Kinase (Thr389)	Rabbit (polyclonal)	Cell Signaling Technology	9205	WB: 1:1000
4EBP1 (53H11)	Rabbit (monoclonal)	Cell Signaling Technology	9644	WB: 1:10000
P-4EBP1 (Th37/46) (236B4)	Rabbit (monoclonal)	Cell Signaling Technology	2855	WB: 1:5000
P-4EBP1 (Ser65)	Rabbit (Polyclonal)	Cell Signaling Technology	9451	WB: 1:5000
AMPKα	Rabbit (monoclonal)	Cell Signaling Technology	2603	WB: 1:1000
P- AMPKα	Rabbit (monoclonal)	Cell Signaling Technology	2535	WB: 1:1000
P-AMPK substrate motif	Rabbit (monoclonal)	Cell Signaling Technology	5759	WB: 1:1000
FoxK1	Rabbit (polyclonal)	Abcam	ab18196	WB: 1:2000
FoxK2	Goat (Polyclonal)	Abcam	ab5298	WB: 1:2000
AKT	Rabbit (polyclonal)	Cell Signaling Technology	9272	WB: 1:2000

Phospho-AKT (Ser473)	Rabbit (polyclonal)	Cell Signaling Technology	9271	WB: 1:1000
ERK2 (c-14)	Rabbit (polyclonal)	Santa Cruz Biotechnology	sc-154	WB: 1:1000
pERK1/2 (E-4)	Mouse (monoclonal)	Santa Cruz Biotechnology	sc-7383	WB: 1:1000
Phospho-Tuberin / TSC2 (Ser1387)	Rabbit (Polyclonal)	Cell Signaling Technology	5584	WB: 1:1000
Phospho-Raptor (Ser792)	Rabbit (Polyclonal)	Cell Signaling Technology	2083	WB: 1:1000
Raptor	Rabbit (Monoclonal)	Cell Signaling Technology	2280	WB: 1:1000
Histone 3 (D1H2) XP	Rabbit (monoclonal)	Cell Signaling Technology	4499	WB: 1:10000
Tri-methyl-Histone H3 Lys27 (C36B11)	Rabbit (monoclonal)	Cell Signaling Technology	9733	WB: 1:2000 ChIP: 1:500
Tri-methyl-Histone H3 Lys36 (D5A7) XP	Rabbit (monoclonal)	Cell Signaling Technology	4909	WB: 1:2000
Tri-methyl-Histone H3 Lys4 (C42D8)	Rabbit (monoclonal)	Cell Signaling Technology	9751	WB: 1:2000 ChIP: 1:100
Histone3Lysine27ac	Rabbit (polyclonal)	Abcam	ab4729	ChIP: 1:500
α-Tubulin (DM1A)	Mouse (monoclonal)	Dianova	DLN09992	WB: 1:10,000
α-Tubulin (DM1A)	Mouse (monoclonal)	Santa Cruz Biotechnology	sc-32293 HRP	WB: 1:5000
IgG	Rabbit (Polyclonal)	Cell Signaling Technology	2729	ChIP: 1:500

2.1.2.2. Secondary antibodies

Table 2.2. Secondary antibodies (WB: Western blotting, IF: Immunofluorescence)

Antibody	Company	Order number	Dilution
Goat anti-Rabbit IgG (H+L)-HRPO conjugated	Dianova	111-035-144	WB: 1:5000
Goat IgG anti-Mouse IgG+IgM (H+L)-HRPO conjugated	Dianova	115-035-146	WB: 1:5000
F(ab')2 Rat IgG (H&L) Antibody Peroxidase Conjugated Pre-Adsorbed	Rockland	712-1333	WB: 1:5000
Goat anti rat IgG, Alexa Fluor 488	Invitrogen	A-11006	IF: 1:200
Goat anti mouse IgG, Alexa Fluor 488	Invitrogen	A-11029	IF: 1:200
Goat anti mouse IgG, Alexa Fluor 568	Invitrogen	A-11031	IF: 1:250

2.1.3. Protein and DNA ladders

2.1.3.1. Protein ladders

Spectra Multicolor High Range Protein Ladder, Thermo Scientific, #26616.

PageRuler Prestained Protein Ladder, Thermo Scientific, #26625.

2.1.3.2. DNA ladders

100 bp DNA Ladder, Invitrogen, #15628-018.

GeneRuler 1 kb Plus DNA Ladder, Thermo Scientific, #SM1333.

2.1.4. Antibiotics

All the stock solutions were sterile filtered before use (0.22 µm, Sarstedt, #83.1826.001).

Table 2.3. Antibiotics used for selection of bacterial cells

Antibiotic	company	Catalog number	Stock solution	Final concentration
Ampicillin	Sigma-Aldrich	A9518	100 mg/mL in distilled water	100 µg/mL

Table 2.4. Antibiotics used for selection of mammalian cells

Antibiotic	Company	Catalog number	Stock Solution	Final Concentration	
				Cells	Concentration
Puromycin	InvivoGen	Ant-pr-1	10 mg/mL in HEPES buffer	U87MG	500 ng/mL
				MDA-MB-231-POR	500 ng/mL
				MDA-MB-231 VIM-RFP	500 ng/mL
				LLC1	6 µg/mL
Hygromycin B	Invitrogen	10687-010	50 mg/mL in PBS	U87MG	10 µg/mL

Blasticidin S HCl	Invitrogen	R210-01	6 mg/mL in distilled water	MDA-MB-231-POR	6 µg/mL
				MDA-MB-231-VIM-RFP	6 µg/mL
				A549-VIM-RFP	6 µg/mL
Plasmocin	InvivoGen	ant-mpt-1	25 mg/mL	U87MG	12.5 to 37.5 µg/mL
Plasmocure	InvivoGen	ant-pc	100 mg/mL	MDA-MB-231-POR	50 µg/mL
Amphotericin B	Sigma-Aldrich	A2942	250 µg/mL	GBM cells in Tumorsphere medium	500 ng/mL
Gentamicin	Gibco	15750-045	50 mg/mL	GBM cells in Tumorsphere medium	50 µg/mL

2.1.5. Inhibitors

Table 2.5. Inhibitors used and their targets

Inhibitor	**Target**	**Company**	**Catalog number**	**Stock concentration**	**Final working concentration (µM)**
Rapamycin	mTOR	LC laboratories	R-5000	10 mM in DMSO	10
U0126	MEK	InvivoGen	tlrl-u0126	20 mM in DMSO	10
LY294002	PI3K	InvivoGen	tlrl-ly29	20 mM in DMSO	20
SB431542	TGFB	Tocris	1614	10 mM in DMSO	10
Oligomycin	ATP synthase	sigma	4876	2.5 mM in DMSO	5
Dorsomorphin	AKT and AMPK	Cayman Chemical	11967	5 mM in DMSO	5

2.1.6. Primers

2.1.6.1. Reverse transcription quantitative polymerase chain reaction (RT-qPCR) primers

Table 2.6. List of RT-qPCR primers used in this study (for: forward, rev: reverse)

Primer	Sequence (5´- 3´)	Gene function/ group
IDH1 for	AGAAGCATAATGTTGGCGTCA	Human α-KG producing enzymes
IDH1 rev	CGTATGGTGCCATTTGGTGATT	
IDH2 for	ACACGTGGCCTGGAGCACCG	
IDH2 rev	CACATTGCTGAGGCCGTGAATGC	
IDH3A for	ACTGGTGGTGTTCAGACAGT	
IDH3A rev	TGAATGGCAGTGACGTTCCG	
GOT1 for	GTCCAGTACCACCAAAGTAGTTCTC	
GOT1 rev	GGCTCTAATCCCAGTCTCCAAA	
GOT2 for	GTGGATGGTGGTGAGTGGAT	
GOT2 rev	TCTGAGAAACATTCAAATGCTGA	
GPT for	GTGCGGAGAGTGGAGTACG	
GPT rev	GATGACCTCGGTGAAAGGCT	
GLUD1 for	AGGAAAGGGAATGACCTGCC	
GLUD1 rev	GCACATCAACCACTGCACAC	
BCAT1 for	CAACTATGGAGAATGGTCCTA	
BCAT1 rev	TGTCCAGTCGCTCTCTTCTCT	
BCAT2 for	GCTCAACATGGACCGGATG	
BCAT2 rev	CCGCACATAGAGGCTGGTG	
PSAT1 for	TCCTCAAACTTCCTGTCCAAGC	
PSAT1 rev	CAGCAGGTCATCACGGACAATC	
OGDH for	GGAATCAGCACTTCCTCTGC	
OGDH rev	ACGTAGTCCACGCCATTCTC	
SNAI1 (SNAIL) for	CTTCCAGCAGCCCTACGAC	Human EMT transcription factors
SNAI1 (SNAIL) rev	CGGTGGGGTTGAGGATCT	
SNAI2 (SLUG) for	CGGACCCACACATTACCTTG	
SNAI2 (SLUG) rev	CAAATGCTCTGTTGCAGTGAG	
ZEB1 for	CCTGAAGAGGACCAGAGG	

ZEB1 rev	TATCACAATATGGACAGGTGAG	
ZEB2 for	AACAAGCCAATCCCAGGAG	
ZEB2 rev	ACCGTCATCCTCAGCAATATG	
TWIST1 for	CTACGCCTTCTCGGTCTGG	
TWIST1 rev	CTCCTTCTCTGGAAACAATGAC	
TWIST2 for	AGCAAGATCCAGACGCTCAAG	
TWIST2 rev	GGAGAAGGCGTAGCTGAGG	
CDH1 (E-CADHERIN) for	ATTTTTCCCTCGACACCCGAT	Human EMT markers
CDH1 (E-CADHERIN) rev	TCCCAGGCGTAGACCAAGA	
CDH2 (N-CADHERIN) for	GGTGGAGGAGAAGAAGACCAG	
CDH2 (N-CADHERIN) rev	GGCATCAGGCTCCACAGT	
FOXK1 for	CTTCCAGGAGCCGCACTTCTA	Human Snail upstream regulators
FOXK1 rev	AACTGGATCTTGATGGCCGTG	
FOXK2 for	CGCCCCTGACCATCAACATT	
FOXK2 rev	CTTGTACCCTGAAGACCCCG	
C-MYC for	CTTGTTGCGGAAACGACGAG	
C-MYC rev	ACTCAGCCAAGGTTGTGAGG	
MMP7 for	TGTATGGGGAACTGCTGACA	Human Snail downstream targets
MMP7 rev	GCGTTCATCCTCATCGAAGT	
COL14A1 for	AGCATGGGACCGCAAGGC	
COL14A1 rev	GACGCGCCACTGATCTCACC	
MMP15 for	CAAGCCCATCAGTGTCTGG	
MMP15 rev	TGGTGCCCTTGTAGAAGTAGG	
HPRT1 for	TATGGCGACCCGCAGCCC	Human housekeeping genes
HPRT1 rev	GCAAGACGTTCAGTCCTGTCCAT	
ACTB for	AGAAAATCTGGCACCACACC	
ACTB rev	AGAGGCGTACAGGGATAGCA	

m-idh1- for	CCAGTCGCTGTTACCGTATGT	Mouse α-KG producing enzyme
m-idh1-rev	TCCACCACAGAACCTCCTTG	
mSnai1- for	CTGCTTCGAGCCATAGAACTAAAG	Mouse EMT transcription factors
mSnai1-rev	GAGGGGAACTATTGCATAGTCTGT	
mSnai2- for	CCTCCAAGAAGCCCAACTAC	
mSnai2-rev	GGGTAAAGGAGAGTGGAGTG	
mZeb1- for	CTTACGGATTCACAGTGGAGAG	
mZeb1-rev	GTGAGCTATAGGAGCCAGAATG	
mZeb2- for	CTCATTCTGGGTCCTACAGTTC	
mZeb2-rev	GGGAAGAACCCGTCTTGATATT	
mEcad-for	TTGGTGTGGGTCAGGAAATC	Mouse EMT markers
mEcad-rev	GTGTCCCTCCAAATCCGATAC	
mNcad-For	AGTGGCAGGTAGCTGTAAAC	
mNcad-rev	TGGCAAGTTGTCTAGGGAATAC	
mVimentin- for	CCCTGAACCTGAGAGAAACTAAC	
mVimentin-rev	CTCTGGTCTCAACCGTCTTAATC	
m-Actb-for	GGCTGTATTCCCCTCCATCG	Mouse housekeeping gene
m-Actb-rev	CCAGTTGGTAACAATGCCATGT	

2.1.6.2. ChIP-qPCR primers

Table 2.7. ChIP-qPCR primers list used in this study (for: forward, rev: reverse)

Primer	**Sequence (5´- 3´)**
SNAI1-33/+58 for*	GTACTTAAGGGAGTTGGCGG
SNAI1-33/+58 rev*	CCGATTCGCGCAGCAGTA
SNAI1+27/+122 for*	GGTTCTTCTGCGCTACTGCT
SNAI1+27/+122 rev*	ATTGGGGTCGGAGGGCTT
SNAI1 -556/-496 for	CTCTGAGTGTTCTGTCCGGG
SNAI1 -556/-496 rev	GCACCCGTTCCTTCCCTTAT
SNAI1 +120/+205 for	ATCGGAAGCCTAACTACAGCG
SNAI1 +120/+205 rev	GTCTCCCCCAAACCTCCTGG

* Selected from Choi et al. 2015

2.1.6.3. Cloning PCR primers

Table 2.8. PCR primers used to amplify and clone part of the human SNAI1 promoter
Green: flanking sequence, blue: restriction enzyme site, black: SNAI1 promoter sequence.

Primer	Sequence (5´- 3´)
Snail Pro#2 for	TAAGCAACGCGTAATCCTTCGGTGGCTCC
Snail Pro#2 rev	TGCTTACTCGAGGCAGAAGAACCACTCGCTA

2.1.7. Plasmids

The IDs of the laboratory's plasmid library are given in parentheses after the plasmid names.

pCI-VSVG (A0097): Lentiviral packaging plasmid (2nd generation), expresses the envelope vesicular stomatitis virus glycoprotein G (Addgene, #1733, Garry Nolan's lab).

psPAX2 (A0098): Lentiviral packaging plasmid (2nd generation) coding the Gag and Pol genes (Addgene, #12260, Didier Trono's lab).

pGIPZ non silencing control (A0055): Lentiviral expression vector (non-targeting hairpin), the non-silencing shRNA is a negative control for any transduction experiment performed using GIPZ shRNA constructs in human and mouse cell lines. Sequence should not match any known mammalian genes, however sequence is not available (Open biosystems, #RHS4346).

pGIPZ-shIDH1 (A0365): Short hairpin RNA against human IDH1 in pGIPZ lentiviral vector, (Open biosystems, #V3LHS_320103).

Mature antisense: TGTTATCAAGCTTTGCTCT

pGIPZ-shidh1 #1 (A0919): Short hairpin RNA against mouse Idh1 (sequence 1) in pGIPZ lentiviral vector, (Open biosystems, #V2LMM_216812), targeting open reading frame (ORF).

Mature antisense: TTCTTTATAGCCTCTGCAG

pGIPZ-shidh1 #2 (A0920): Short hairpin RNA against mouse Idh1 (sequence 2) in pGIPZ lentiviral vector, (Open biosystems, #V3LMM_522512), targeting 3'-untranslated region (3'-UTR). (used in preliminary knockdown efficiency experiments, but not shown).

Mature antisense: TTTTAGCTACACACATCCT

pGIPZ-shidh1 #3 (A0921): Short hairpin RNA against mouse Idh1 (sequence 3) in pGIPZ lentiviral vector, (Open biosystems, #V3LMM_522513), targeting 3'-untranslated region (3'-UTR).

Mature antisense: AGCTACACACATCCTATCT

pGIPZ-shidh1 #4 (A0922): Short hairpin RNA against mouse Idh1 (sequence 4) in pGIPZ lentiviral vector, (Open biosystems, #V3LMM_425008), targeting ORF. (used in preliminary knockdown efficiency experiments, but not shown).

Mature antisense: TTCTTGTCATAGATCTCCT

pGIPZ-shSnail (A0260): Short hairpin RNA against human SNAI1 in pGIPZ lentiviral vector, (Open Biosystems, #V2LHS_199873).

Mature antisense: ATATAAATACCAGTGTACC

pRL-SV40 (A0250): Renilla luciferase internal control reporter, contains SV40 enhancer and early promoter elements, which has high Renilla luciferase signal (purchased from Promega)

Snail_pGL2 (A0954): Mammalian expression vector, contains Snail promoter (-1045 to -56) sequence upstream of firefly luciferase, (purchased from Addgene, #31694) (Fujita et al. 2003).

pGL3-control vector (A0267): Contains SV40 promoter and enhancer sequences, used as an internal standard control (purchased from Promega, #E1741).

pGL3-Basic vector (A0618): Lacks promoter and enhancer sequences, allowing cloning putative regulatory sequences and promoter sequences of interest. The expression of luciferase activity depends on proper insertion and orientation of a functional promoter upstream from *luc*+ gene (purchased from Promega, #E1751).

Snail_pGL3#1 (A0956): created by cloning Snail promoter sequence from Snail_pGL2 (Addgene, #31694) into pGL3-basic vector using KpnI and HindIII restriction digestion enzymes.

Snail_pGL3#2 (A0975): created by cloning Snail promoter sequence amplified from human genomic DNA, into pGL3-basic vector using MluI and XhoI restriction digestion enzymes.

pSLIK-GFP (A0712): Mammalian expression vector, containing Tet-inducible expression of green fluorescent protein (GFP), with mammalian selection via Hygromycin, used as a control in overexpression experiments (Addgene, #66844) (Lewis et al. 2014).

pSLIK-IDH1-FLAG (A0713): Mammalian expression vector, containing Tet-inducible expression of IDH1, with mammalian selection via Hygromycin (Addgene, #66802).

2.1.8. Short interfering RNAs (siRNAs)

siControl: SMARTPool ON-Targetplus Non-targeting Control siRNAs (Dharmacon, 001810-10-05).

siHIF-1α: SMARTPool ON-Targetplus siRNA against human HIF-1α (Dharmacon, NM_181054).

siHIF-2α: SMARTPool ON-Targetplus siRNA against human HIF-2α (Dharmacon, NM_001430).

siSnail: SMARTPool ON-Targetplus siRNA against human Snail (Dharmacon, NM_005985.3).

siRNA c-Myc: SMARTPool ON-Targetplus siRNA against human c-Myc (Dharmacon, NM_002467).

siRNA FOXK1: SMARTPool ON-Targetplus siRNA against human FOXK1 (Dharmacon, NM_001037165).

siRNA FOXK2: SMARTPool ON-Targetplus siRNA against human FOXK2 (Dharmacon, NM_004514).

2.1.9. Ribonucleoprotein (RNP) crRNAs components

Table 2.9. Crispr RNAs (crRNAs) and guide RNAs (gRNAs) purchased from IDT

crRNA/gRNAs	Sequence
Hs.Cas9.SNAI1.1.AA	GCTGTAGTTAGGCTTCCGAT
Hs.Cas9.SNAI1.1.AC	TCGGCTCCAGGAGAGTCCCA

Table 2.10. Commercial components from IDT

Reagent	Catalog number
Alt-R CRISPR-Cas9 tracrRNA-ATTO550	1077024
Alt-R S.p. HiFi Cas9 Nuclease V3	1081061
Nuclease-Free Duplex Buffer	1072570
Alt-R CRISPR-Cas9 HPRT Positive Control crRNA	1079132
Alt-R CRISPR-Cas9 Negative Control crRNA #1	1079138

2.1.10. Bacterial strains

One Shot® Stbl3™ chemically competent *E. coli*: This strain was used for cloning into lentiviral vectors or luciferase vectors (Thermo Fisher Scientific, #C737303).

2.1.11. Cell lines

2.1.11.1. Original cell lines

HEK293T: established cell line derived from the embryonic human kidney line HEK293 by stable transfection of the large T antigen (ATCC, #CRL-3216).

U87MG: established human glioblastoma cell line (ATCC, #HTB-14).

G55: established human glioblastoma cell line, kindly provided by M. Westphal and K. Lamszus (Hamburg, Germany) (Hamel, Westphal, and Shepard 1993).

A549: established human lung carcinoma cells (ATCC, #CCL-185).

A549 VIM-RFP: established reporter human lung carcinoma cells (ATCC, #CCL-185EMT), used as an EMT model, which harbors through CRISPR/Cas9 gene editing a C-terminal red fluorescent protein (RFP) tag on the vimentin gene, enabling tracking of EMT status *in vitro* by monitoring RFP expression.

MDA-MB-231: established human breast adenocarcinoma line (ATCC, # HTB-26).

MDA-MB-231 VIM-RFP: established reporter human breast adenocarcinoma cell line (ATCC, #HTB-26MET), used as a MET model, which harbors through CRISPR/Cas9 gene editing a C-terminal RFP tag on the vimentin gene, enabling tracking of EMT and MET status *in vitro* by monitoring RFP expression.

LLC1: established mouse Lewis lung carcinoma cell line (ATCC, # CRL-1642).

H2030: established human lung adenocarcinoma cells (ATCC, #CRL-5914)

2.1.11.2. Cell lines generated in our laboratory

MDA-MB-231 i10 (invasive 10 times): MDA-MB-231 cells that invaded into the lower compartment of Boyden chamber assay were collected and re-seeded again from which the invading cells were collected. After 10 rounds of selection of the most invasive cells, MDA-MB-231 i10 cells were isolated and sub-cultured.

MDA-MB-231 ni (non-invasive): MDA-MB-231 cells that did not invade after being seeded in standard Matrigel for 48 hours and were isolated from the upper chamber of Boyden chamber wells, and sub-cultured.

MDA-MB-231-POR (pLenti6-ODD-RLuc): Human breast carcinoma cell line (ATCC, # HTB-26) transduced with a **p**Lenti6 construct consisting of firefly luciferase under control of HIF-2α-**O**DDD (Safran et al. 2006), and constitutively active **R**enilla luciferase. Single cell clone was created by Omelyan Trompak.

LLC1 pCDH B3: established mouse Lewis lung carcinoma cell line transduced three times with the pCDH-EF1a-eFFly-eGFP lentiviral construct (Addgene, #104834), allowing enhanced green fluorescent protein (EGFP) detection *in vitro*, and luciferase detection for *in vivo* studies (Sandhöfer et al. 2015), created by Nazli Salik.

LLC1 pCDH B3 / sLP-mCherry B2: LLC1 pCDH B3 transduced two times with the lentiviral construct of pcPPT-mPGK-attR-sLPmCherry-WPRE lentiviral construct, which secrets a soluble form of mCherry, that is taken up by surrounding cells. This allows tracing of tumor microenvironment cells in *in vivo* studies (Ombrato et al. 2019), created by Nazli Salik.

LLC1 pCDH B3 / sLP-mCherry B3: LLC1 pCDH B3 transduced three times with the lentiviral construct pcPPT-mPGK-attR-sLPmCherry-WPRE, which secrets a soluble form of

mCherry, that is taken up by surrounding cells. This allows tracing of tumor microenvironment cells in *in vivo* studies (Ombrato et al. 2019), created by Nazli Salik.

LLC1 sLP-mCherry B3: established mouse Lewis lung carcinoma cell line transduced three times with the lentiviral construct pcPPT-mPGK-attR-sLPmCherry-WPRE (Ombrato et al. 2019), created by Nazli Salik.

H3030 pCDH B3: H2030 cells transduced three times with the pCDH-EF1a-eFFly-eGFP lentiviral construct (Addgene, #104834), allowing EGFP detection *in vitro*, and luciferase detection for *in vivo* studies (Sandhöfer et al. 2015), created by Nazli Salik.

Cell lines with stable knockdown, knockout, or overexpression, are listed below. Unless otherwise indicated, the cell lines were generated by the author of the thesis.

Table 2.11. Stable knockdown (KD) through shRNAs, knockout (KO) using RNP system, or overexpression (OE) cell lines generated by lentivirus transduction or transfection and subsequent selection

Line name	Construct	Genetic modification (transient/stable, MOI, KD/KO/OE)	comments
U87MG co	pGIPZ non silencing control	Moi 40, KD	Created by Nuray Bögürcü-Seidel
U87MG shIDH1	pGIPZ shIDH1#3		
MDA-MB-231-POR co	pGIPZ non silencing control	Moi 50, KD	Created by Nuray Bögürcü-Seidel
MDA-MB-231-POR shIDH1	pGIPZ shIDH1#3		
LLC1 pCDH-EF1a-eFFly-eGFP B3/ co B3	pGIPZ non silencing control	Moi100/200, KD	pGIPZ transduction was done on 3 rounds
LLC1 pCDH-EF1a-eFFly-eGFP B3/ shIDH1#1 B3	pGIPZ shIdh1#1		
LLC1 pCDH-EF1a-eFFly-eGFP B3/ shIDH1#2 B3	pGIPZ shIdh1#2		

LLC1 pCDH-EF1a-eFFly-eGFP B3/ shIDH1#3 B3	pGIPZ shIdh1#3		
LLC1 pCDH-EF1a-eFFly-eGFP B3/ shIDH1#4 B3	pGIPZ shIdh1#4		
LLC1 pCDH-EF1a-eFFly-eGFP B3/ co B2	pGIPZ non silencing control	Moi100/200, KD	pGIPZ transduction was done on 2 rounds
LLC1 pCDH-EF1a-eFFly-eGFP B3/ shIDH1#1 B2	pGIPZ shIdh1#1		
LLC1 pCDH-EF1a-eFFly-eGFP B3/ shIDH1#2 B2	pGIPZ shIdh1#2		
LLC1 pCDH-EF1a-eFFly-eGFP B3/ shIDH1#3 B2	pGIPZ shIdh1#3		
LLC1 pCDH-EF1a-eFFly-eGFP B3/ shIDH1#4 B2	pGIPZ shIdh1#4		
LLC1 pCDH-EF1a-eFFly-eGFP B3/ co B1	pGIPZ non silencing control	Moi100/200, KD	pGIPZ transduction was done on 1 round
LLC1 pCDH-EF1a-eFFly-eGFP B3/ shIDH1#1 B1	pGIPZ shIdh1#1		
LLC1 pCDH-EF1a-eFFly-eGFP B3/ shIDH1#2 B1	pGIPZ shIdh1#2		
LLC1 pCDH-EF1a-eFFly-eGFP B3/ shIDH1#3 B1	pGIPZ shIdh1#3		
LLC1 pCDH-EF1a-eFFly-eGFP B3/ shIDH1#4 B1	pGIPZ shIdh1#4		
LLC1 pCDH-EF1a-eFFly-eGFP B3/ sLP-mCherry B2/ co B1	pGIPZ non silencing control	Moi100, KD	pGIPZ transduction was done only once
LLC1 pCDH-EF1a-eFFly-eGFP / sLP-mCherry/ shIDH1 #3 B1	pGIPZ shIdh1#3		
MDA-MB-231-VIM-RFP co	pGIPZ non silencing control	Moi 50, KD	
MDA-MB-231-VIM-RFP shIDH1	pGIPZ shIDH1#3		

H2030 pCDH-EF1a-eFFly-eGFP B3/ co	pGIPZ non silencing control	Moi 50, KD	
H2030 pCDH-EF1a-eFFly-eGFP B3/ shIDH1	pGIPZ shIDH1#3		
U87MG co/co	pGIPZ non silencing control	Moi 40+40	U87MG co and shIDH1 cells were later transduced with shSnail, created by Nuray Bögürcü-Seidel
U87MG co/shSnail	pGIPZ shSnail		
U87MG shIDH1/co	pGIPZ non silencing control		
U87MG shIDH1/shSnail	pGIPZ shSnail		
MDA-MB-231-POR co/co	pGIPZ non silencing control	Moi 50+50	MDA-MB-231-POR co and shIDH1 cells were later transduced with shSnail, created by Nuray Bögürcü-Seidel
MDA-MB-231-POR co/shSnail	pGIPZ shSnail		
MDA-MB-231-POR shIDH1/co	pGIPZ non silencing control		
MDA-MB-231-POR shIDH1/shSnail	pGIPZ shSnail		
U87MG pSLIK GFP (control)	pSLIK-GFP	Moi 10	Created by Nuray Bögürcü-Seidel
U87MG pSLIK IDH1	pSLIK-IDH1-FLAG	Moi 10	
U87MG co negative control (NC#1)	Indicated crRNA using RNP system	KO, 15 nM	Created by Nuray

U87MG co HPRT			Bögürcü-Seidel
U87MG shIDH1 negative control (NC#1)			
U87MG shIDH1 SNAI1 1.AA			
U87MG shIDH1 SNAI1 1.AC			
U87MG shIDH1 HPRT			
MDA-MB-231-POR co negative control (NC#1)	Indicated crRNA using RNP system	KO, 15 nM	
MDA-MB-231-POR co HPRT			
MDA-MB-231-POR shIDH1 negative control (NC#1)			
MDA-MB-231-POR shIDH1 SNAI1 1.AA			
MDA-MB-231-POR shIDH1 SNAI1 1.AC			
MDA-MB-231-POR shIDH1 HPRT			

2.1.12. Restriction digestion enzymes

Table 2.12. Restriction digestion enzymes used for molecular cloning

Enzyme	Company	Order number
FastDigest MluI	Thermo Fischer Scientific	FD0564
FastDigest XhoI	Thermo Fischer Scientific	FD0694
HindIII (10 U/µL)	Thermo Fischer Scientific	ER0501
KpnI (10 U/µL)	Thermo Fischer Scientific	ER0522

2.1.13. Growth factors

Table 2.13. Growth factors used in cell culture

Growth factors Reagent	Company	Order number	Stock concentration	Final concentration
Animal-Free recombinant human EGF (epidermal growth factor)	Peprotech	AF-100-15	200 µg/mL	20 ng/mL
Recombinant human FGF-basic (fibroblast growth factor)	Peprotech	100-18B	200 µg/mL	20 ng/mL

TGFβ1	Peprotech	100-21C	10 mg/mL	5 ng/mL

2.1.14. Buffers, media, and solutions

2.1.14.1. Bacterial culture

LB-Agar (Luria-Bertani-Agar): 32 g LB-Agar powder (Carl Roth, #X965.2) were dissolved in 1 liter of ultrapure water. The solution was autoclaved at 121 °C for 15 minutes, cooled down to 40 °C, the appropriate amount of antibiotics added, swirled to mix and poured in 10 cm petri dishes in a horizontal flow hood. The plates were stored at 4 °C.

LB-broth medium: 20 g LB powder (Carl Roth, #X964.1) were dissolved in 1 liter of ultrapure water and autoclaved at 121 °C for 15 minutes. The medium was stored at 4 °C.

2.1.14.2. Cell culture

Table 2.14. Medium, buffers, and reagents purchased ready-to-use

Solution	Company	Catalog number
1x Dulbecco's Modified Eagle Medium (DMEM) high glucose, pyruvate	Gibco	11995065
DMEM, high glucose, sodium pyruvate	Capricorn Scientific	DMEM-HPA
Roswell Park Memorial Institute (RPMI) 1640	Gibco	11875-093
1x Dulbecco's Modified Eagle Medium/Nutrient Blend F-12 (DMEM/F12)	Gibco	11320033
Trypsin/EDTA	Gibco	25300-62
Fetal Bovine Serum (FBS)	Merck	S0115
Fetal Bovine Serum (FBS)	Sigma-Aldrich	F7524
B-27 supplement without vitamin A	Gibco	12587-010
1x PBS (pH 7.4)	Gibco	10010-056
1x Dulbecco's PBS without Ca^{2+}, Mg^{2+}, and phenol red	Capricorn Scientific	PBS-1A
0.05 % Trypsin-EDTA	Gibco	25300054
Accutase	Gibco	A11105-01
Opti-MEM Reduced Serum Medium	Gibco	31985047
DMSO	Carl Roth	A994.1
CASY ton solution	OMNI Life Sciences	5651808

CASY clean	OMNI Life Sciences	5651787
Crystal violet	Fluka	61135
Matrigel basement membrane matrix, LDEV-free	Corning	354234
Doxycycline hyclate	Sigma-Aldrich	D9892
HEPES	Gibco	1563-056
Dm-α-KG	Sigma-Aldrich	349631
Chloroquine	Sigma-Aldrich	C6628-25G
Polybrene	Sigma-Aldrich	H9268-5G
Polyethylenimine (PEI 25K)	Polysciences	23966-1
PureCol Type I Collagen	Advanced Biomatrix	5005
Poly-2-hydroxyethyl methacrylate (p-Hema)	Sigma-Aldrich	P3932-25G
Laminin (1 mg)	Sigma-Aldrich	L2020-1MG
Deoxyribonuclease I (DNase I) from bovine pancreas	Sigma-Aldrich	D4263
Hydrochloric acid (HCl) solution 1 N	Sigma-Aldrich	H9892-100
Sodium hydroxide (NaOH) solution 1N	Sigma-Aldrich	S2770-100

Complete medium for culturing adherent cells: 500 mL of DMEM or DMEM/F12 with 10% FBS. In case of starvation for TGFβ and/or α-KG experiments, 1-5% FBS was used.

Complete medium for culturing glioblastoma and carcinoma in tumorsphere conditions: 500 mL of DMEM/F12 mixed with 10 mL of B-27 serum-free supplement minus vitamin A, 1 mL of amphotericin B, 2.5 mL 1M HEPES, 0.5 mL gentamicin (50 mg/mL). The following growth factors were added freshly to dishes; EGF and FGF (final concentration for each is 20 ng/mL). 4% FBS was supplemented in case of growing carcinoma cell lines.

Cryoprotective freezing medium: 90% complete medium (90% DMEM + 10% FBS) + 10% DMSO, in case of LLC1, as per manufacturer's recommendation, cryoprotective medium was prepared as follows; 95% complete medium + 5% DMSO.

10 mM Chloroquine: dissolved in distilled water, sterile filtered and stored at -20 °C, final concentration is 10 μM.

Polybrene: 6 mg/mL in ultrapure water, sterile filtered and stored at -20 °C.

Crystal violet: 0.5% Crystal violet in 20% Methanol/H2O, sterile filtered through a 0.45 μm PVDF filter; stored at 4 °C.

Doxycycline: 1 mg of Doxycycline is dissolved in 1 mL of sterile filtered ultrapure H_2O to produce 1 mg/mL stock concentration.

Laminin: 1 mg/mL stock concentration is diluted freshly before plates coating with 1× PBS to 1 µg/mL.

2.1.14.3. Nucleic acid isolation

Table 2.15. Kits and reagents used for RNA and genomic and plasmid DNA isolation and analysis

Kit/reagent	Company	Catalog number
RNeasy Mini Kit	Qiagen	74106
β-Mercaptoethanol	Sigma-Aldrich	M6250
RNase-Free DNase Set	Qiagen	79254
QIAshredder	Qiagen	79656
Diethylpyrocarbonate (DEPC)	Roth	K028
Monarch DNA gel extraction kit	NEB	T1020
Phusion Hot Start II High-Fidelity DNA polymerase	Thermo Scientific	F549L
PureLink genomic DNA mini kit	Invitrogen	K1820-01
DNA-spin Plasmid DNA purification kit	iNtRON biotechnology	17098
PureLink HiPure plasmid maxiprep kit	Invitrogen	K210007
T4 DNA ligase	Thermo Scientific	EL0011
SYBR Safe DNA gel stain	Invitrogen	S33102
Gel Loading Dye, Orange (6x)	NEB	B7022S
Pierce™ 16% Formaldehyde (w/v), methanolfree	Thermo Scientific	28908
Glycine	Roth	3908
p-APMSF	Cayman Chemical	14971
cOmplete™, Mini, EDTA-free Protease Inhibitor Cocktail	Roche	11836170001
RNase A	Thermo Scientific	EN0531
Proteinase K	Bioline	BIO-37037
nucleospin™ gel and pcr clean-up	Macherey&Nagel	740609.250
Protein A-Sepharose® CL-4B	GE Healthcare	17-0780-01
Protein G Sepharose® 4 Fast Flow	GE Healthcare	17-0618-01
NaCl	Roth	3957.1

LiCl	Sigma-Aldrich	L9650
NP-40	BioVision	2111
Deoxycholate	Roth	3484.2
EDTA	Sigma-Aldrich	E5134
SDS ultra pure	Roth	2326.1
Triton X-100	Sigma-Aldrich	T8787
Sonication beads	Diagenode	C03070001
Quantitative PCR human reference total RNA	Agilent	750500
Quantitative PCR mouse reference total RNA	Agilent	750600
Maxima H Minus First Strand cDNA Synthesis Kit	Thermo Scientific	K1652
2× PowerUp SYBR Green master mix for qPCR	Applied biosystems	A25743

DEPC-H2O: 1 mL Diethylpyrocarbonate was dissolved overnight in 1 liter distilled water and autoclaved subsequently.

1× TAE buffer: 40 mM TRIS, 20 mM glacial acetic acid, 1 mM EDTA.

Agarose gel: 0.8 to 2 % (w/v) Agarose NEEO ultra quality (Carl Roth, #2267.4).

2M Glycine: 30.028 g Glycine in 200 mL of distilled water.

Lysis buffer: 20 mL of 10% SDS, 4 mL of 0.5 M EDTA, 10 mL of 1 M Tris-HCl pH 8.1, filled up to 200 mL with double distilled water.

Dilution buffer: 200 µL of 10% SDS, 22 mL of 10% Triton X-100, 480 µL of 0.5 M EDTA, 33.4 mL of 1 M NaCl, 3.34 mL of 1 M Tris-HCl pH 8.1, filled up to 200 mL with double distilled water.

Low salt buffer: 2 mL of 10% SDS, 20 mL of 10% Triton X-100, 800 µL of 0.5 M EDTA, 30 mL of 1 M NaCl, 4 mL of 1 M Tris-HCl pH 8.1, filled up to 200 mL with double distilled water.

High Salt buffer: 2 mL of 10% SDS, 20 mL of 10% Triton X-100, 800 µL of 0.5 M EDTA, 100 mL of 1 M NaCl, 4 mL of 1 M Tris-HCl pH 8.1, filled up to 200 mL with double distilled water.

LiCl buffer: 40mL of 1.25 M LiCl, 20mL of 10% NP-40, 20 mL of 10% deoxycholate, 400 µL of 0.5 M EDTA, 2 mL of 1 M Tris-HCl pH 8.1, filled up to 200 mL with double distilled water.

TE buffer: 2 mL of 1 M Tris-HCl pH 8.1, 400 µL of 0.5 M EDTA, filled up to 200 mL with double distilled water.

2.1.14.4. Western blot

Table 2.16. Reagents used in various steps of protein analysis via western blot

Reagent	Company	Order number
Acrylamide 30%	Roth	3029.1
Tetramethylenediamine (TEMED)	Sigma-Aldrich	T9281
Ammonium persulfate (APS)	Sigma-Aldrich	A9164
Pierce ECL western blotting substrate	Thermo Scientific	32106
Western lightning Plus ECL	Perkin Elmer	NEL105001EA
SuperSignal West Pico PLUS Chemiluminescent Substrate	Thermo Scientific	34577
SuperSignal West Femto Maximum Sensitivity Substrate	Thermo Scientific	34094
Methanol	Sigma-Aldrich	34860
DC Protein Assay Reagents Package	Bio-rad	500-0116
Tween 20	Applichem	A49740100

Laemmli Lysis buffer: 10 mM Tris HCl, 2 % SDS, 2 mM EGTA, 20 mM NaF in distilled water.

Ammonium persulfate (APS): 1 g of powdered APS solved in 100 mL distilled water and stored in 1 mL aliquots at -20 °C.

Sample buffer: 40 mL 10 % SDS, 16 mL 1 M Tris pH 6.8, 20 mL 100% glycerol, 19 mL distilled water, stored in 800 µL aliquots, for usage mixed with 200 µL 1% bromophenol blue and 50 µL of β-Mercaptoethanol.

Lower buffer (for separating gel): 1.5 M Tris base, 0.4% SDS, in distilled water, pH adjusted to 8.8.

Upper buffer (for stacking gel): 0.5 M Tris base, 0.4% SDS, in distilled water, pH adjusted to 6.8.

8% PAGE separating gel: per 1 gel; 2.7 mL of 30% polyacrylamide, 2.6 mL Lower buffer, 4.65 mL distilled water, directly before pouring the solution in the cast, 100 µL APS (10%) and 5 µL TEMED are added for acrylamide polymerization.

12% PAGE separating gel: per 1 gel; 4 mL of 30% polyacrylamide, 2.6 mL Lower buffer, 3.5 mL distilled water, directly before pouring the solution in the cast, 100 µL APS (10%) and 5 µL TEMED are added for acrylamide polymerization.

15% PAGE separating gel: per 1 gel; 5.03 mL of 30% polyacrylamide, 2.6 mL Lower buffer, 2.4 mL distilled water, directly before pouring the solution in the cast, 100 µL APS (10%) and 5 µL TEMED are added for acrylamide polymerization.

4% Stacking gel: per 1 gel; 0.65 mL of 30% polyacrylamide, 1.3 mL upper buffer, 4.5 mL distilled water, directly before pouring the solution in the cast, 50 µL APS (10%) and 5 µL TEMED are added.

10× Running buffer: 250 mM Tris base, 2 M Glycine, 1% SDS in distilled water.

10× Wet Transfer buffer: 200 mM Tris base, 1.5 M glycine in distilled water.

1× Wet Transfer buffer: 1 L of 10× wet transfer buffer, 2 L methanol, and 7 L of distilled water.

Blocking buffer: 5% milk powder in 1× PBS-Tween 20 (0.1%).

Washing buffer: 1× PBS, 0.1% Tween 20 in distilled water.

Stripping buffer: 200 mM glycine, pH adjusted to 2.5, 0.05% Tween 20 in distilled water.

2.1.14.5. Immunofluorescence

Table 2.17. Reagents used in various steps of protein analysis via immunofluorescence

Reagent	Company	Order number
Paraformaldehyde (PFA)	Roth	0335.3
Dako fluorescence mounting medium	Dako	S3023
Normal goat serum (NGS)	Cell Signaling Technology	5425
Bovine serum albumin (BSA)	Serva	11946.02
4',6-diamidino-2-phenylindole (DAPI), stock concentration 1000 ng/mL	Invitrogen	D1306

4% PFA: 80 g PFA were dissolved in 1.5 liter of 1× PBS, adjusted the pH to 11 with 5 M NaOH and stirred until the solution gets clear. Afterwards the pH was adjusted to 7.4 and the solution filled up to 2 liter with 1× PBS. The solution was stored at -20°C.

Antibody dilution buffer: 1% BSA in 0.1% PBST.

2.1.14.6. Dual luciferase reagents

1× Passive lysis buffer: 5× Passive lysis buffer (Promega, #E194A), diluted to 1× with millipore water.

Luciferase Reagent A: 25 mM glycylglycine, 15 mM KH2PO4, 4 mM EGTA, 2 mM ATP, 1 mM dithiothreitol, 15 mM $MgSO_4$, 0.1 M coenzyme A, 75 µM beetle D-luciferin (Promega, #E1602).

Luciferase reagent B: 1.1 M NaCl, 2.2 M Na_2-EDTA, 0.22 M KH_2PO_4, 0.44 mg/mL BSA, 1.3 mM NaN_3.

Luciferase reagent C: 1.43 µM coelenterazine (Promega, #S2001), added freshly to luciferase reagent B in 1:50 ratio.

2.1.14.7. Animal experiments

Anesthesia: 9 mL 0.9% sterile NaCl solution, 2 mL of 10% Ketamine (bela-pharm GmbH, FS1670041), 0.5 mL of 2% Xylazin (CEVA Tiergesundheit GmbH).

D-Luciferin: D-Luciferin potassium salt (Regis Tech, #RE-1-360222-200) was dissolved with PBS to prepare 150 mg/kg solution, and stored at -20 °C.

3× Digestion buffer: 3 U/mL Collagenase I, 133 U/mL Collagenase IV, and 10 U/mL DNAse, 0.5 % BSA in 100 mL serum-free RPMI medium.

Wash buffer:2 mM EDTA in addition to 2% FBS in 5 mL serum-free RPMI.

Red Blood cell lysis buffer: Roche, #11814389001.

Collagenase I: Worthington Biochemical, # LS004194.

Collagenase IV: Worthington Biochemical, # LS004188.

2.2. Methods

2.2.1. Working with cell lines

2.2.1.1. Sub-culturing and passaging cells

U87MG, G55, A549, MDA-MB-231, LLC1, HEK293T were cultured in DMEM supplemented with 10% FBS on 10 cm tissue culture (TC) dishes (Sarstedt, #83.3902) under adherent conditions. A549-VIM-RFP and MDA-MB-231-VIM-RFP were cultured in DMEM/F12 medium supplemented with 10% FBS. H2030 cells were cultured in RPMI medium supplemented with 10% FBS. For passaging the cells, medium was discarded, cells were washed two times with 1× PBS, covered with 0.05% Trypsin-EDTA (e.g. 2 mL for 10 cm dish) and incubated at 37 °C for 3 to 5 minutes to detach the cells. For semi-adherent LLC1 cells, medium and PBS were collected instead of being discarded. Trypsin was inactivated with 4 mL of 10% FBS containing medium, cell suspension was collected in a falcon tube and centrifuged in a tabletop Rotina 420 centrifuge (Andreas Hettich, Germany) at 1000 rpm for 3 minutes. Medium was removed, and cell pellet was resuspended in fresh complete medium, and sub-cultured in different ratios according to the doubling time of the cell lines. Mycoplasma contamination was routinely monitored using PCR analysis (Pisal et al. 2016; Uphoff and

Drexler 2004, 2014). In case of contaminations, cells were treated with Plasmocin or Plasmocure according to the manufacturer's instructions, to eliminate mycoplasma.

2.2.1.2. Cryopreservation and thawing of cells

To cryopreserve established adherent cell lines in liquid nitrogen tanks, 70 to 80% confluent cells were washed with 1× PBS, then trypsinized as described in the previous section. Cell suspension was centrifuged at 1000 rpm for 3 minutes. Medium was removed, and cell pellet was resuspended in sterile-filtered freezing medium containing 10% DMSO. For LLC1 cells, 5% DMSO was used following the supplier's instructions. 1 mL cell suspension (approximately containing half of the cells from a 10 cm dish) was transferred to Cryovials (Greiner Bio-One, #123277) and placed in a container used to ensure a slow cooling in the vials (by isopropyl alcohol or Styrofoam). The container was placed in a -80 °C freezer for at least 24 hours, then transferred for long-term storage in liquid nitrogen tanks.

Cryopreserved cells were rapidly thawed in a water bath at 37 °C, after which the cell suspension was transferred to 10 cm TC dish filled with 10 mL of complete medium. The following day, medium was changed, and if necessary, replaced with medium containing antibiotics for selection of transduced cells.

2.2.1.3. Determination of cell count and viability

Cell number was determined using the CASY Cell Counter and Analyzer System Model TT (Roche Innovatis AG, #5651697). The counting principle is based on a current exclusion method: cells pass through a pore, generating an electric pulse as resistance signal which is registered by the counter. This approach determines cell number, size distribution, and percentage of viable cells, it also allows assessing the vital state of a cell as dead cells display a much weaker resistance due to a disrupted cell membrane. Cell counting was performed by diluting 100 µL of cell suspension in 10 mL of CASYton buffer following the manufacturer's recommendations, with individual programs stored for every cell line used.

2.2.1.4. Epithelial cells tumorsphere culture

To grow carcinoma cell lines in sphere culture, 10 mg/mL pHema coating was prepared by reconstituting 1 g of pHema in 100 mL of 95% Ethanol, mixture was heated to ensure complete dissolution. Solution was sterile filtered, then 10 cm TC dishes were coated with 5 mL pHema, dried, then rinsed with PBS. LLC1 cells grown in semi-adherent culture were trypsinized as described in section 2.2.1.1., and 8×10^5 cells were resuspended in tumorsphere medium (TSM) supplemented with 0.4% FBS, required for growth of epithelial cancer cells in 3D conditions, and seeded on pHema-coated dishes for at least 48 hours.

2.2.1.5. Treatments

2.2.1.5.1. TGFβ and α-KG treatments

For TGFβ time course treatment of U87MG, 8.5 × 10^5 cells were seeded under sphere conditions. Next day, TGFβ (final concentration 5 ng/mL) was added to the dishes for the indicated times (72, 48, or 24 hours) (Fig. 2.1a). For adherent and semi-adherent cells, such as MDA-MB-231, A549, and LLC1, 3.5, 2.5, or 1 × 10^5 cells were seeded in growth medium (with 10% FBS) under adherent conditions, respectively. The next day, the medium was replaced with 1% FBS-containing medium. On the third day, 5 ng/mL TGFβ was added to the dishes for the indicated times (96, 72, 48, 24, or 6 hours for MDA-MB-231 and A549) (Fig. 2.1b) and 72, 48, 24, 6, and 3 hours for LLC1) (Fig. 2.1c). Effect of TGFβ on EMT induction was assessed by RNA and protein analysis as described later.

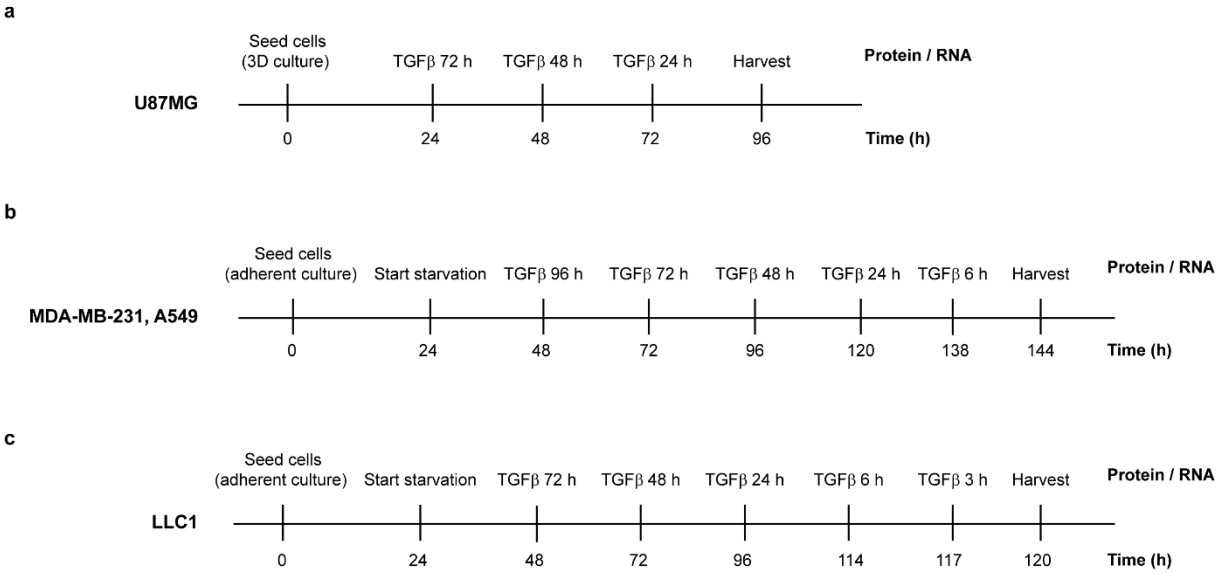

Figure 2.1. Experimental setups for TGFβ time course analyses.

Generally, for protein and RNA analysis experiments, 8.5-10 × 10^5 parental or genetically modified glioblastoma cells were seeded under sphere conditions, TGFβ treatment was started as described above on the next day, or on the same day three hours after seeding, for a duration of 72 hours. Carcinoma cell lines were seeded using same cell density mentioned earlier, under adherent condition, starved on the second day. On the third day, TGFβ was supplemented for 72 hours (Fig. 2.2a). For combined α-KG / TGFβ treatments, different concentrations of α-KG (2, 4, 6, and 8 mM) were used. Adherent cells were treated with α-KG after 72 hours of starvation for the last 24 hours. Depending on the setup of the experiment, treatment with 6 mM and/or 8 mM cell permeable Dm-α-KG was added for the indicated time points (6 or 24 hours) (Fig. 2.2b). Treatments duration varied according to the type of analysis,

detailed experimental setup is explained in the respective sections. Importantly, the pH of α-KG containing medium was adjusted to 7.4 by using 1N NaOH and 1N HCl, prior to starting the treatment, to prevent any unwanted effect of acidosis on cells. Medium was then sterile-filtered, and amounts corresponding to the designated α-KG concentrations were then added to the dishes or wells.

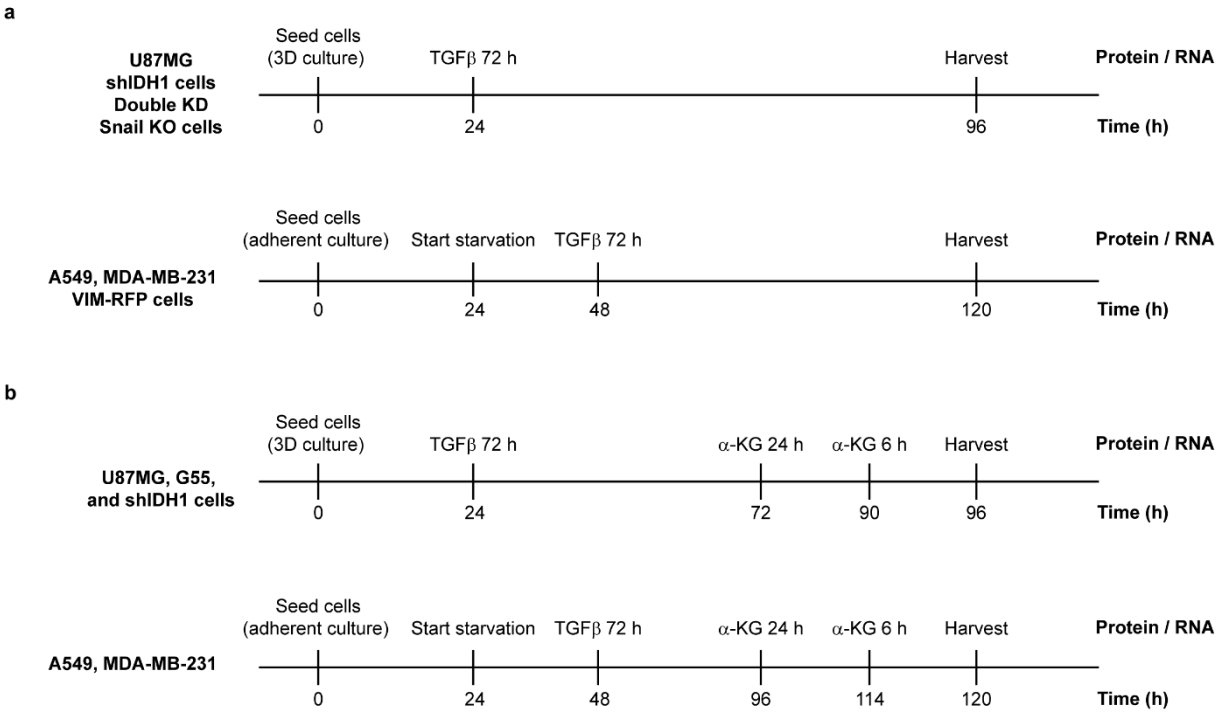

Figure 2.2. Experimental setups for the analyses of combined TGFβ / α-KG treatments.

2.2.1.5.2. Hypoxia incubation

Hypoxia treatment was carried out in an O_2 controlled Hypoxic Workstation (either Coy Laboratory Products Inc., USA; or Toepffer Lab Systems, Deutschland) with 1% O_2 at 37 °C. U87MG co and shIDH1 cells were seeded under normoxia in sphere conditions as described earlier. Depending on the experimental setup, cells were always placed in the hypoxic chamber starting from the second day, for the indicated durations, except for DLR assay where cells were placed three hours after splitting them in TSM. Cells were harvested under hypoxic conditions, at the same end point.

2.2.1.5.3. Inhibitor treatments

To inhibit the mTOR signaling pathway, 10 µM rapamycin (Rap), 10 µM U0126 (U0), 20 µM LY294002 (LY), 10 µM SB431542 (SB), 5 µM oligomycin (Oli), and 5 µM dorsomorphin (Dor) were added to the cells 2 hours before TGFβ treatment for 48 hours (Fig. 2.3a). For short treatments of oligomycin and dorsomorphin, treatments were started 5 minutes before TGFβ for 3, 6, or 24 hours (Fig. 2.3b).

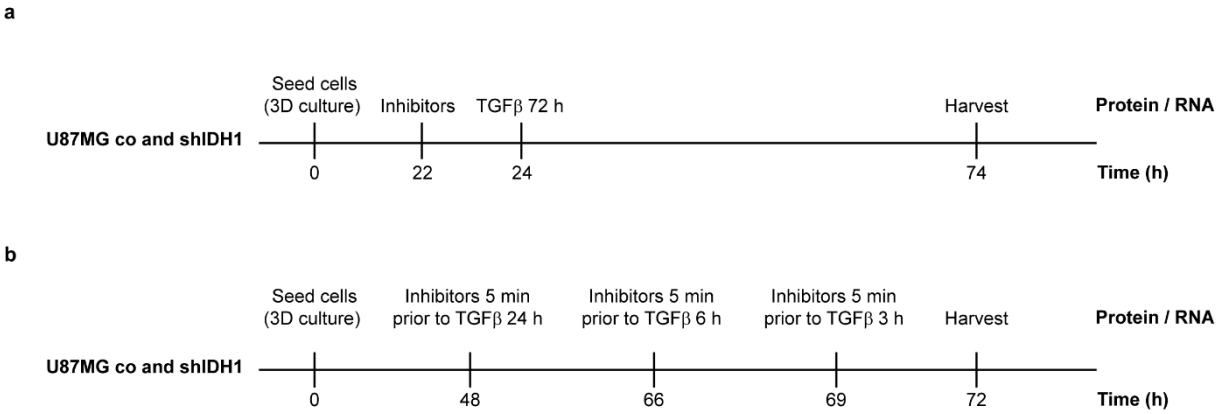

Figure 2.3. Experimental setups for the analyses of combined TGFβ / inhibitor treatments.

2.2.1.5.4. IDH1 overexpression

To induce IDH1 overexpression, pSLIK system, a Tetracycline-ON lentiviral vector, designed for conditional gene silencing or overexpression, was employed. The system uses a tetracycline response element (TRE) upstream of the gene/shRNA/miRNA of interest, and a reverse tetracycline-controlled transactivator (rtTA) that activates transcription only when doxycycline is added (Shin et al. 2006). U87MG pSLIK GFP (designated as control) and pSLIK IDH1 cells were seeded under sphere conditions, and doxycycline treatment was started right away to induce conditional IDH1 overexpression (stock concentration: 1000 µg/mL, working concentrations: 0.2, 0.4, or 0.8 µg/mL). Snail expression had to be initially induced to enable evaluation of the impact of IDH1 overexpression on EMT. To achieve this, cells were treated with 5 ng/mL TGFβ 3 hours after cells seeding for 72 hours (Fig. 2.4a), or cells were placed in hypoxic chamber for 6, 24, 48, 72, or 96 hours, one day after cell seeding and doxycycline treatment (Fig. 2.4b). Cells were harvested at the same time.

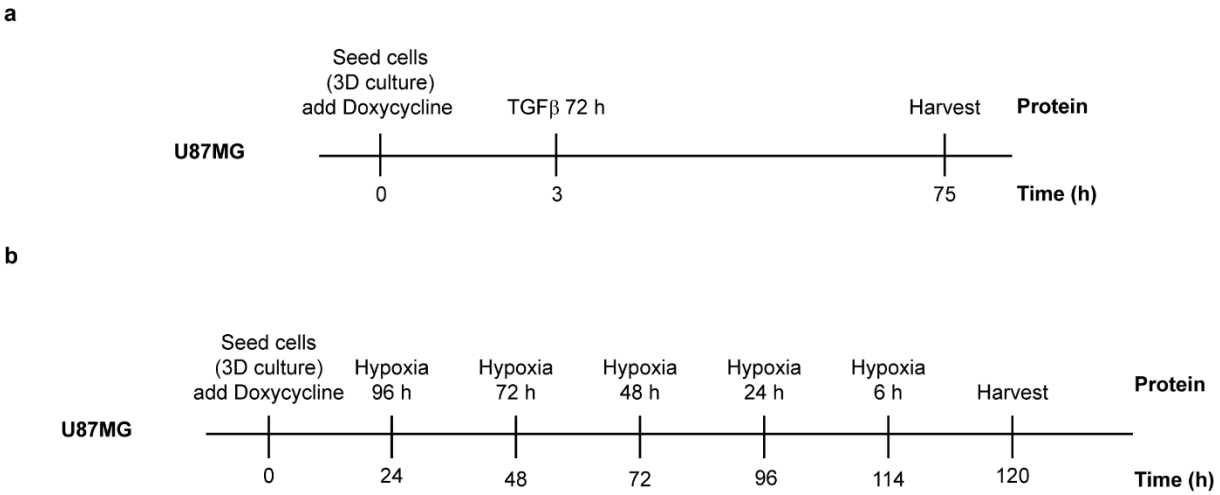

Figure 2.4. Experimental setups for the analyses of IDH1 overexpression.

2.2.1.6. Transfection and transduction

2.2.1.6.1. Virus production and concentration

All the following steps involving virus production, concentration, titration, and transduction were carried out in an S2 (biological safety level 2) laboratory. For each lentivirus described in section 2.1.7, three T75 cell culture flasks (Sarstedt, #83.3911) were used. In each flask, 4.5×10^6 HEK293T cells were seeded a day prior to the transfection, in 10 mL of complete medium. On the next day, two hours before transfection, medium was changed to 6 mL 1× DMEM + 10% FBS. In a sterile 1.5 mL reaction tube, 500 µL Opti-MEM was mixed with 7.5 µg of the specific plasmid-containing the to-be-expressed DNA. Additionally, 2.63 µg of the envelope plasmid pCI-VSVG as well as 4.88 µg of the packaging plasmid psPAX2 were added. 45 µL of room temperature (RT) equilibrated PEI in a 3:1 ratio with DNA were added to the plasmid and Opti-MEM mix, and vortexed for 10 seconds. The DNA/PEI mix was incubated at RT for 20 minutes. Meanwhile, 6 µL of 10 mM chloroquine were added to the cells and mixed well. The DNA/PEI mix was then added in a dropwise manner to the cells, while lightly swirling the flasks. Flasks were kept for up to 24 hours at 37 °C. On day three, medium was changed to 9 mL of DMEM + 10% FBS. 48 hours post-transfection, the recombinant virus-containing supernatant was collected in 50 mL tubes, centrifuged at 250 g for 5 minutes, and filtered using a 0.45 µm PVDF filter (Carl Roth, #P667.1), then kept at 4 °C until next day. Cells were then replenished with 9 mL of fresh complete medium. 72 hours post-transfection, virus-containing supernatant was again collected, centrifuged at 250 g for 5 minutes, and filtered using a 0.45 µm PVDF filter.

To obtain high viral titers, lentiviral particles were concentrated. First, 6 ultracentrifugation tubes (Herolab, #253060) were added to each centrifuge bucket (Thermo Fisher Scientific, #52427). To each ultracentrifugation tube, approximately 28 mL of centrifuged and filtered virus supernatant was added in a way that all buckets end up with the same weight to ensure balance during the ultracentrifugation step, plain DMEM + 10% FBS medium was used to reach the same weight if needed. Viruses were then centrifuged at 20,000 rpm (or 22,500 rpm) for four hours (or 1.5 hours) at 4 °C in Sorvall WX ultracentrifuge (Thermo Scientific) using the AH-629 rotor (Thermo Scientific). After centrifugation, supernatant was removed, and tubes were left upside-down to dry on UV-lighted tissue paper to ensure complete removal of medium. Then, each pellet was resuspended in 120 µL plain DMEM medium without FBS, and incubated at 4 °C for 30 minutes. Subsequently, viruses of the same plasmid were resuspended again and combined in a 1.5 mL reaction tube, centrifuged using Heraeus

Fresco 17 centrifuge for three minutes at 13,000 rpm at 4 °C. The supernatant was then aliquoted and frozen to -80 °C for storage.

2.2.1.6.2. Virus titration

To titer viruses, 5 × 10^4 G55TL cells were seeded in 6-well TC plates (Sarstedt, #83.3920), 9 wells per virus to be titered. On the following day, virus aliquots were thawed on ice, and 10-fold serial dilutions of the virus were prepared in dilution medium (DMEM + 10% FBS+ 8 µg/mL Polybrene). 11 µL of virus was resuspended well in 1089 µL of dilution medium. From the first dilution, 110 µL was transferred to 990 µL of dilution medium and resuspended well. This was repeated six times until reaching 10^{-9} dilution, last well was used as a mock control without any virus transduction. After that, the medium on the cells was replaced with the prepared serial dilutions. 24 hours after transduction, medium was changed to fresh DMEM + 10% FBS. On the following day, the medium was replaced with DMEM + 10% FBS containing selective antibiotics, as defined by the plasmid sequence, and in the amount tolerated by the transduced cells and determined by kill-curve experiments (cell line-specific). The antibiotic containing medium was refreshed every 2 to 3 days, usually up to 16 days, until all cells in the mock control have died. At the end of the experiment, cell colonies were stained. For this, cells were washed twice with 1× PBS. Then, for each well, 100 µL of Crystal violet was diluted in 1 mL of DMEM, and 1 mL of the mix was added to each well. Cells were incubated for 15 minutes at RT. After this, staining solution was discarded, and cells were washed up to three times with 1× PBS until the colonies were well visible. Subsequently, the plates were scanned using EPSON Perfection V700 Photo Scanner, and colonies were counted manually. The titer in transducing units per mL (TU/mL) was calculated using the following formula, where the mean of the number of colonies multiplied by the dilution factor in 2 wells was determined.

(n1 x d1+ n2 x d2) / 2 = # TU/mL

where n is the number colonies of a dilution and d is the dilution factor (e.g. 10^7).

2.2.1.6.3. Stable lentiviral transduction

Depending on the cell line and the desired multiplicity of infection (MOI), 2 × 10^3, 5 × 10^3, 2 × 10^4, or 5 × 10^4 were seeded in 96-, 48-, 24-, or 12-well TC plates in 1× complete medium one day prior to transduction, respectively. On the next day, medium was changed to 1× complete medium with 8 µg/mL Polybrene. Concentrated virus particles were added to the cells according to the defined MOI, cells were then incubated for up to 24 hours at 37 °C. On the following day, medium was changed to 1× DMEM, RPMI, or DMEM/F12 + 10% FBS. One day later, the medium was replaced with complete medium containing selective antibiotics

according to the plasmid sequence, and in the amount tolerated by the transduced cells and determined by kill-curve experiments. The antibiotic containing medium was refreshed every 2 to 3 days, and the cells were expanded whenever they reached 80% confluency.

2.2.1.6.4. Transient transfection for RNP-mediated gene knockout

To knockout SNAI1 gene using a CRISPR-Cas9 system, the ribonucleoprotein (RNP) Alt-R CRISPR-Cas9 2-part guide RNA system from IDT was deployed. Firstly, Alt-R-CRISPR-Cas9 crRNA specific to the gene of interest was purchased along with Alt-R-CRISPR-Cas9 HPRT positive control, Alt-R-CRISPR-Cas9 negative control, and Alt-R-CRISPR-Cas9 tracrRNA-ATTO550 from IDT. RNA oligonucleotides were resuspended in nuclease-free duplex buffer (30 mM HEPES, pH 7.5, 100 mM potassium acetate) to 100 µM stock concentration. The 2-step protocol starts by forming the gRNA complexes by mixing equimolar amounts of Alt-R crRNA and Alt-R tracrRNA in nuclease-free duplex buffer, creating a duplex concentration of 1 µM. This solution was incubated at 95 °C for 5 minutes and left slowly cooling to RT. Next, for each single well in a 24-well TC plate (Sarstedt, #83.3922), 6 µL of diluted Alt-R S.p. HiFi Cas9 Nuclease V3 (working concentration 1 µM) was combined with 6 µL of gRNA and 88 µL of OptiMEM, which was left for 5 minutes at RT to allow assembly of the RNP complex. Finally, 100 µL of RNP complex was mixed with 6 µL of Lipofectamine RNAiMAX (Invitrogen, #13778150), and opti-MEM in a final volume of 200 µL, transfection mix was incubated at 37 °C for 20 minutes. Next, 5×10^4 U87MG or MDA-MB-231-POR cells diluted in 200 µL of medium were mixed with a final concentration of RNP complex of 15 nM. Cells were incubated with transfection mix for 48 hours, then splitted and cultured. Alt-R-CRISPR-Cas9 tracrRNA-ATTO550 was used to confirm successful transfection by fluorescence microscopy visualization, 24 hours after transfection. Cells transfected with Alt-R-CRISPR-Cas9 HPRT were included in preliminary experiments as positive controls to test for knockout efficiency but were not included in the presented results.

2.2.1.6.5. Transient transfection for dual luciferase reporter assay

SNAI1 gene promoter activity was assessed using a dual luciferase reporter (DLR) assay. For this purpose, cells were co-transfected with two plasmids; 1000 ng/µL Snail-pGL3#1 or Snail-pGL3#2 containing a partial promoter sequence of SNAI1 fused with a firefly luciferase, in combination with 10 ng/µL of control reporter vector; a plasmid encoding for a stable viral promoter (SV40) with Renilla luciferase, used to estimate numbers of viable cells. Cells were always co-transfected at 1:1000 ratio between Renilla and firefly luciferase. 3.5×10^5 U87MG co and U87MG shIDH1 cells were seeded in 6-well TC plate one day prior to transfection. The next day, a total of 1 µg of DNA was mixed with Fugene HD (4 µL) at a ratio

of 1:4 (Promega, #E2311) in Opti-MEM in a total volume of 100 µL. To transfect the same amount of DNA in each well, DNA amounts were adjusted with empty pcDNA3.1 vector to a total of 1 µg. The transfection mix was incubated at RT for 15 minutes, then added to each well in a dropwise manner, and cells were incubated for 24 hours. On the third day, cells were split in triplicate into 24-well suspension plates (Sarstedt, #83.3922500), under sphere conditions. 5 ng/mL TGFβ treatment was started after 3 hours for 48 hours (Fig. 2.5a), or was started next day for 6 hours (Fig. 2.5b). Hypoxia treatment was started after 3 hours for 24 hours (Fig. 2.5c). On the other hand, α-KG treatment started on the next day for 3 hours (Fig. 2.5d). At the end of the treatments, the cells were collected and lysed in 1× passive lysis buffer. Renilla luciferase and firefly luciferase activity were measured using the Dual-Luciferase Reporter Assay System (Promega) in a microplate reader (TriStar LB 941, Berthold Technologies), using white 96-well plates (Greiner, 655075). Firefly luciferase signal was normalized to Renilla luciferase activity and plotted as relative luciferase units (RLU). pGL3-basic and pGL3-control were used as controls but were not included in the final figures.

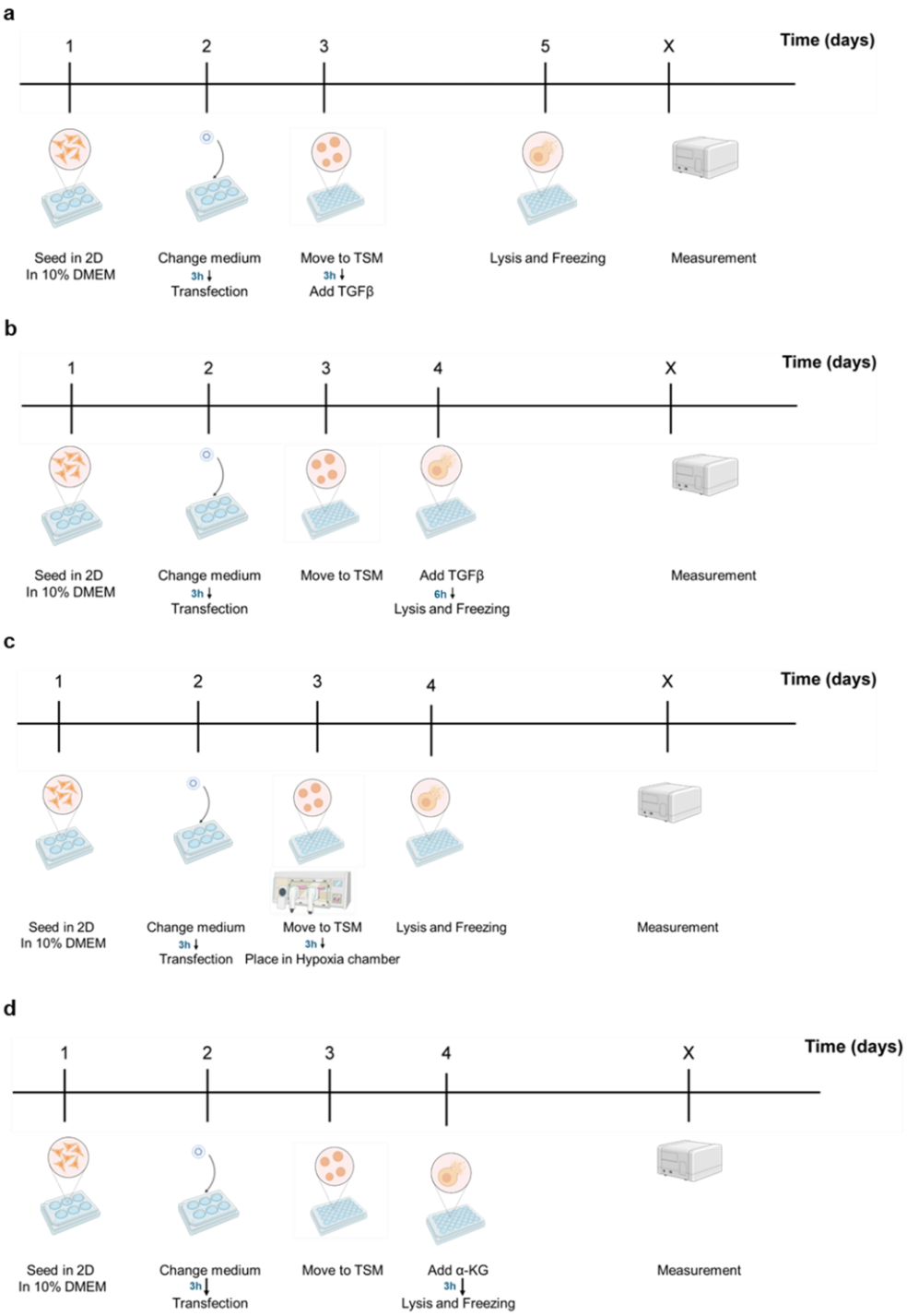

Figure 2.5. Experimental setups for dual luciferase assays.

2.2.1.6.6. Transient transfection for siRNA-mediated gene knockdown

siRNAs against HIF-1α, HIF-2α, FoxK1, FoxK2, c-Myc, SNAIL or non-targeting control siRNA were obtained as a pool of 4 siRNA oligos (ONTARGETplus SMART pool, Dharmacon) as described in section 2.1.8. Lyophilized siRNA pools were resuspended in 1x diluted siRNA buffer (5x siRNA buffer, Dharmacon, #B-002000-UB-100) to a final concentration of 20 µM (20 pmol/µL), aliquoted, and stored frozen at -80 °C. Reverse siRNA

transfection of 4.5 × 10^5 U87MG co and shIDH1 cells was performed in 6-well TC plate using Lipofectamine RNAiMAX, according to the manufacturer's instructions. 60 nM-180 nM of total siRNAs is diluted in 500 µL of Opti-MEM reduced serum medium (Table 2.18), in addition to 4 µL of Lipofectamine RNAiMAX, then the transfection mix is transferred to the wells and incubated at 37 °C for 20 minutes. After the incubation, the required amount of cells resuspended in 500 µL of antibiotic-free DMEM + 10% FBS is added into the wells. 24 hours after transfection, cells were trypsinized and reseeded to sphere culture conditions in 10 cm Petri dishes (Greiner, #633161). Three hours later, 5 ng/mL TGFβ was added to the cells for 48 hours for protein and RNA analysis. When siRNA transfection is combined with DLR assay, cells were reverse transfected as explained above, and on the following day transfection with luciferase plasmids was started. Cells were then split to 24-well suspension plates and treatment with TGFβ or hypoxia for 24 hours was conducted (Fig. 2.6). To ensure a consistent total siRNA concentration during transfection, non-targeting control siRNA was supplemented as needed to reach the desired final concentration.

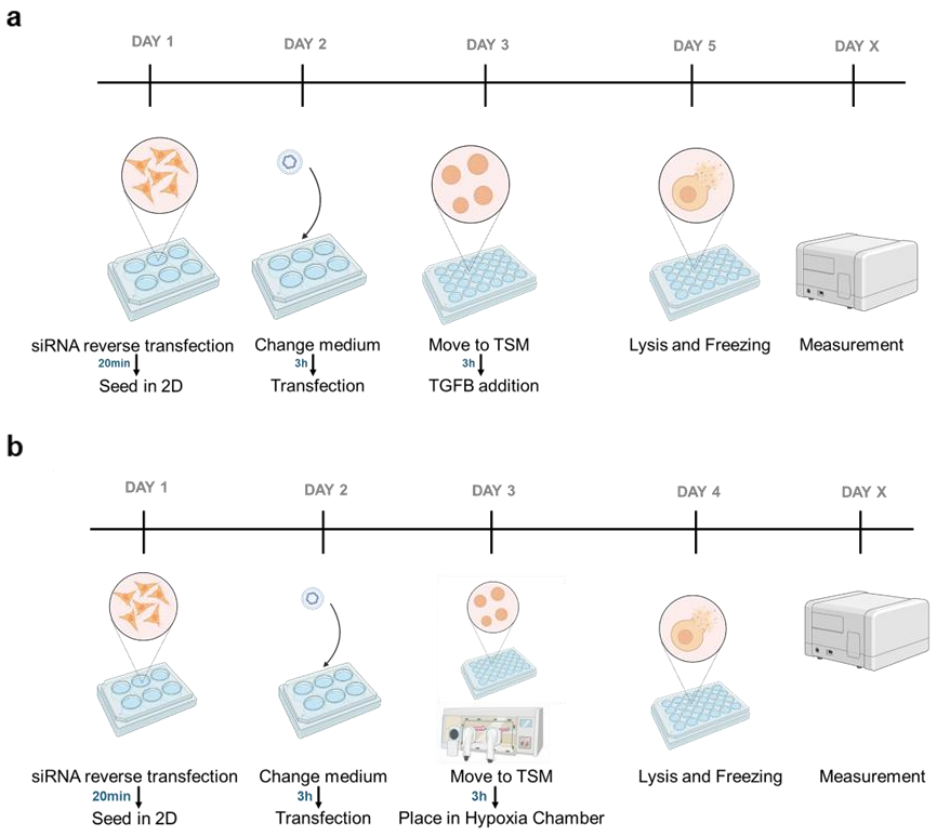

Figure 2.6. Experimental setups for dual luciferase assay including siRNA treatments.

Table 2.18. Final single siRNA concentration used in reverse siRNA transient transfection

siRNA	Final concentration (nM)
HIF-1α	20
HIF-2α	100
Snail	120
c-Myc	60
FoxK1	60
FoxK2	60

2.2.1.7. Collagen invasion assay

To test the invasiveness of tumor cells grown in 3D culture medium a collagen matrix was prepared. This consists of 50% PureCol bovine collagen type I, 2% B-27 Serum-Free Supplement, combined with 48% tumorsphere culture medium containing DMEM/F12, HEPES, Amphotericin B, gentamycin, 20 ng/mL bFGF, 20 ng/mL EGF and 0.4% FBS. 12-well TC plates (Sarstedt, #83.3921) were covered with 300 µL of collagen gel and the gel was polymerized for 1 hour at 37 °C. LLC1 tumor spheroids of equal size were then picked using 10 µL pipette and plated in a second layer of 360 µL of non-polymerized collagen matrix. The first image was taken 2 hours after experiment was set, afterwards images were taken every 24 hours for a duration of 96 hours. Images were taken with a 4× objective. The invasion of the spheres was analyzed with the programs Affinity Photo and ImageJ (Schneider, et al., 2012). Affinity Photo was used to select the spheres, isolate and excise them using the Flood select tool, while ImageJ was used for thresholding and quantification of the area of invasion by the spheroids. Eight out of twelve spheres were qualified to be pictured and counted.

2.2.1.8. Modified Boyden chamber assay

Invasiveness of the cells was assessed using a modified Boyden chamber assay. The main difference between the modified version of the protocol and the original assay is that in the modified Boyden chamber assay cells must first invade through an ECM matrix such as Matrigel, in order to migrate through the porous membrane, whereas in the original assay cells are only allowed to migrate through the pores of the membrane from upper to lower compartment by chemotaxis, without passing through Matrigel (Chen 2005). 1-1.5 × 10^5 cells (U87MG, MDA-MB-231, A549) were seeded in complete medium containing 10% FBS in 6 cm TC dishes (Sarstedt, 83.3901). On the second day, cells were starved as described earlier by replacing the medium with 1% FBS containing medium. On the following day, TGFβ treatment was started for 72 hours. Two concentrations of Dm-α-KG (6 mM and 8 mM) were added to

the medium in the last 24 hours. After the end of the treatment, cells were trypsinized and counted as described earlier. Next, 3-5 × 10^4 cells were resuspended in 100 µL diluted Matrigel (1:10 in 1% FBS containing DMEM) and kept on ice to avoid premature solidification. They were then seeded in the upper compartment of one transwell filter with a pore size of 8.0 µm (Corning, #3422). Four to six wells were seeded per condition. The suspension was allowed to polymerize at 37 °C for 1 hour. Next, the polymerized Matrigel containing suspended cells were carefully overlaid with 100 µL of 1% FBS supplemented medium, while 600 µL of complete growth medium (10% FBS) was added to the lower compartment. This generated a chemical gradient via a difference in the concentration of nutrients and chemokines, effectively stimulating cell invasion through the porous membrane. Cells were kept in Boyden chambers for 24 or 48 hours (Fig. 2.7a,b). To check the effect of α-KG in reversing invasion without the prior induction by TGFβ, MDA-MB-231 cells were seeded as described above in 6 cm TC dishes, starved on the next day, and were treated on the fifth day with two concentrations of Dm-α-KG for 24 hours. Cells were trypsinized at the end of the treatment and seeded in Transwells as described above for 48 hours (Fig. 2.7c). MDA-MB-231 cells invasiveness was also examined upon pre-treatment with TGFβ for 72 hours prior to seeding cells in the transwells (Fig. 2.7d). Finally, to test the preventative effect of α-KG on TGFβ-induced invasion, starved A549 cells were treated with increasing concentrations of Dm- α-KG from 2 mM to 8 mM in 2 mM increments for 72 hours. TGFβ was supplemented three hours later. At the end of the treatment, cells were processed for Boyden chamber assay (Fig. 2.7e). For U87MG single, double knockdown, or Snail knockout cells, 5 × 10^4 cells were directly resuspended in 100 µL diluted Matrigel (1:10 in 1% FBS containing DMEM) and seeded in the Transwells as explained above.

Depending on the condition, 10% and 1% FBS containing medium were either supplemented with TGFβ, 6 mM or 8mM Dm-α-KG, TGFβ in addition to 6 mM or 8mM Dm-α-KG, or no treatments, to maintain similar conditions used before trypsinization. With the exception of U87MG knockout and knockdown cells, where cells were not treated prior to seeding in Boyden chamber, and no treatment was added in the wells, only a gradient of FBS was kept between upper and lower compartments. Depending on the cell line, after 24 to 48 hours, cells were washed first by replacing the medium in the lower compartment with 1× PBS, then fixed at RT for 10 minutes in 70% ethanol. Cells were then rehydrated with 1× PBS for 10 minutes. The nuclei of both invaded cells (located on the lower side of the porous membrane) and nuclei of remaining cells suspended in Matrigel were stained with DAPI (1:1000 in 1× PBS) in the dark for 10 minutes. The inserts were then washed for 10 minutes in 1× PBS, after

which pictures were acquired for the DAPI stained non-invading nuclei in the upper compartment using a LEICA BM IL LED inverted fluorescence microscope with a 4× objective and with a LEICA DFC420C camera. Medium was then completely removed from the lower and upper compartments, and remaining cells in the upper compartment were removed using cotton swabs. Membranes were carefully separated from the insert walls and placed on glass slides with the lower side facing upwards. A drop of fluorescent mounting medium was placed on top of the membranes, which were then sealed to the slide with a cover glass. Afterwards, fluorescent pictures of the lower compartment were taken with a 4× objective. The number of DAPI stained upper and lower cells was quantified using Fiji (v.1.53q, https://Fiji.nih.gov/ij/). Invasion rate was calculated as the mean of the ratio of invaded cells to the non-invading cells. To select for more invasive cells, MDA-MB-231 cells mixed with diluted Matrigel matrix were allowed to invade through the 8-µm pore insert membranes for 48 hours. Cells that didn't cross the membrane, and remained in Matrigel, were collected, washed, then cultured and were designated as non-invasive (ni). Cells that crossed and were on the lower surface of the membrane, were collected by trypsinization, and reapplied to the Boyden chamber. This procedure has been repeated for 10 times. Cells invading through the membrane after the 10^{th} round were collected as mentioned above, propagated, and were designated as invasive (i10). Pre-treatments for follow-up Boyden chamber assays were done as described above (Fig. 2.7c,d).

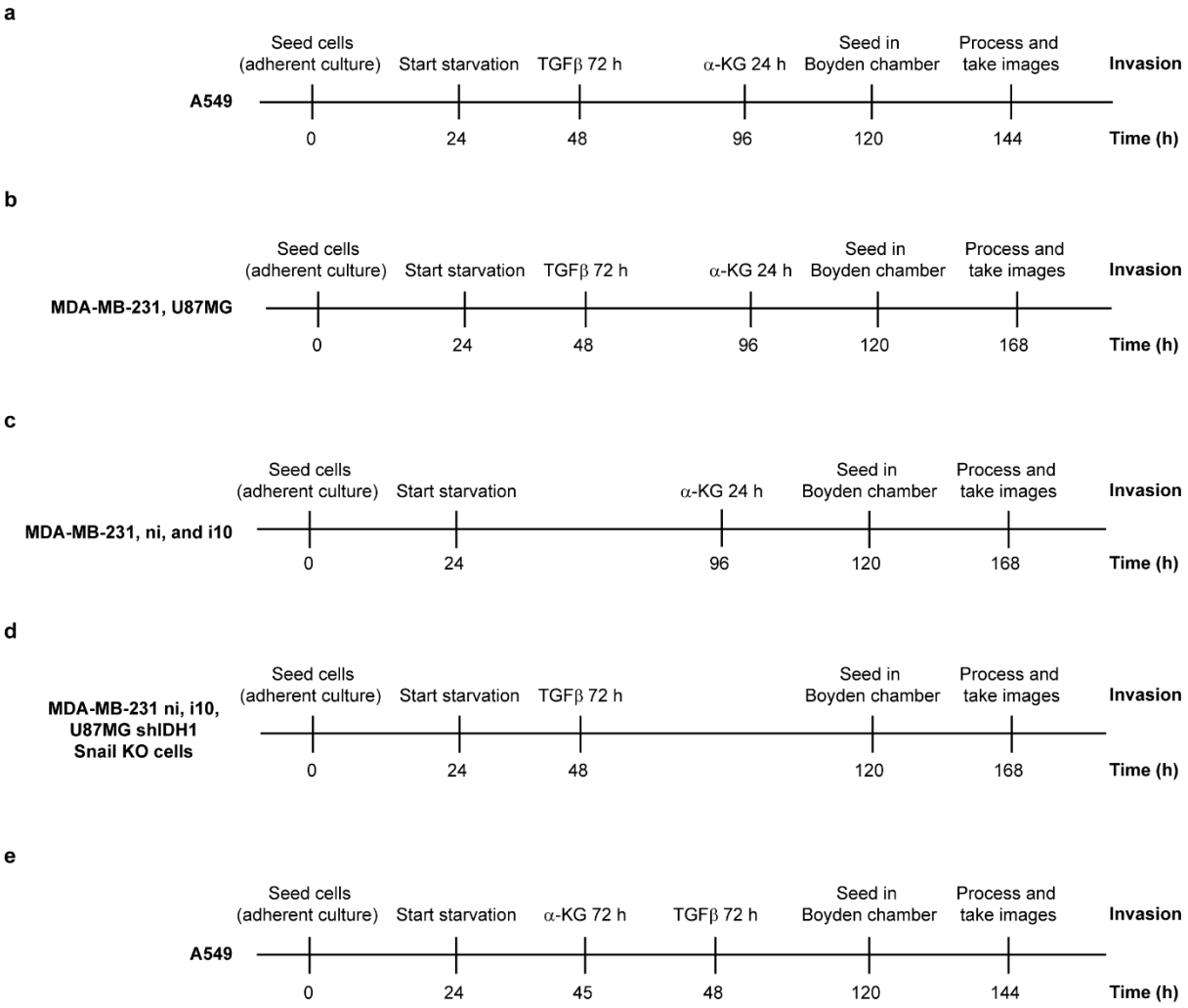

Figure 2.7. Experimental setups for the pre-treatment with TGFβ and / or α-KG prior to modified Boyden chamber invasion assay.

2.2.1.9. Proliferation assay

To test if α-KG influences cell proliferation and viability, a proliferation assay was conducted. U87MG, A549, and MDA-MB-231 cells were seeded at different densities (40, 18, or 13 × 10^3, respectively) in 12-well TC plates. On the following day, medium was changed to 1500 µL of 1% FBS containing DMEM. On day three, medium was replaced to 1500 µL 1% FBS containing DMEM with or without TGFβ treatment (5 ng/µL). At defined time points 6 mM or 8 mM Dm-α-KG were added to pre-incubated medium containing 1% FBS. The pH was set to 7.4, the medium was sterile-filtered and 500 µL of plain, TGFβ, or TGFβ plus 6 or 8 mM Dm-α-KG containing medium was added for 72, 48, or 24 hours (Fig. 2.8). In case of 72 hours α-KG treatment, medium was added around 3 hours after TGFβ treatment had started (Fig. 2.8). Each condition was performed in three biological replicates per experiment. Experiments were repeated twice. At the end of the treatment, cells were trypsinized, collected, and counted as described in 2.2.1.3, without any centrifugation step in between to reduce cell loss. The

percentage and total number of viable cells was determined using the CASY device. The cell counts of the individual treatment conditions were divided by those of the control and presented as relative cell proliferation.

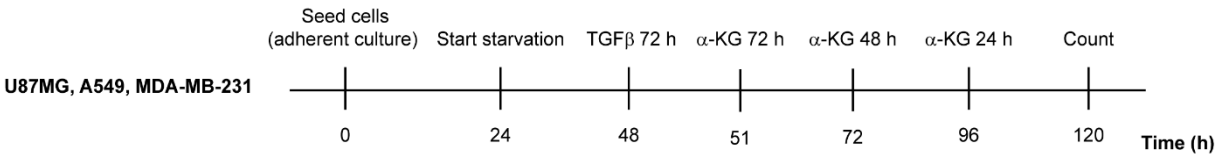

Figure 2.8. Experimental setup to detect the effect of α-KG treatment on cell proliferation and viability.

2.2.1.10. Measurement of the cellular ATP/ADP ratio

96-well white with clear flat bottom plates (Corning, #3903) were coated with 1 µg/mL Laminin in PBS, and incubated for three to six hours at 37 °C. Wells were washed, then U87MG cells were seeded in TSM at 1×10^4 cells per well with or without TGFβ for 72 hours, and pH-adjusted Dm-α-KG-containing medium (6 or 8 mM) was added for the last 3 hours. The experiments were performed in three biological replicates (Fig. 2.9a). ATP/ADP ratios were measured by using EnzyLight ADP/ATP Ratio Assay Kit (BioAssay Systems, ELDT-100), luminescence was read using TriStar LB 941 microplate reader (Berthold Technologies). The ATP synthase inhibitor oligomycin was used as a positive control. Shorter α-KG treatment duration was decided based on preliminary experiments and the well-established rapid negative impact of α-KG and oligomycin on ATP synthase activity (Chin et al. 2014).

2.2.1.11. Measurement of the cellular ATP levels

U87MG, U87MG co and shIDH1 cells were seeded in TSM with or without TGFβ for 72 hours in 96-well white with clear flat bottom plates, pre-coated with Laminin at 1×10^4 cells per well. pH-adjusted Dm-α-KG-containing medium (6 or 8 mM) was added for the last 3 hours (Fig. 2.9b). The experiments were done in 3-4 biological replicates. ATP levels were measured using the CellTiter-Glo 3D cell viability assay (Promega, G9681), and luminescence was read using TriStar LB 941 microplate reader (Berthold Technologies). Protein concentration was measured afterwards using DC protein assay. ATP levels were normalized to protein content. The ATP synthase inhibitor oligomycin was used as a positive control.

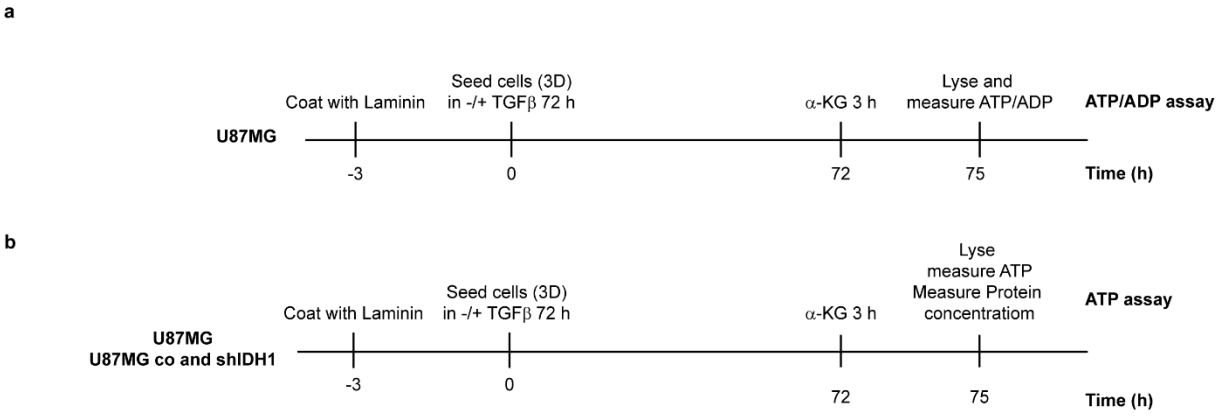

Figure 2.9. Experimental setups for ATP/ADP and ATP assays.

2.2.2. Working with RNA

2.2.2.1. RNA extraction

Adherent cells were washed with PBS, then scraped and lysed in 350 µL RLT+ buffer (1 mL RLT buffer + 10 µL β-Mercaptoethanol). For semi-adherent cells such as LLC1, cell suspension was collected, and the remaining adherent cells were washed two times with PBS and collected. Total cell suspension was divided for protein and RNA analysis, spun down at 1000 rpm for 3 minutes, and cell pellet was then lysed in 350 µL RLT+ buffer. For cells grown under tumorsphere conditions, cell suspension was collected, divided for protein and RNA analysis, and centrifuged at 1000 rpm at 4 °C for 3 minutes. Cell pellet was also lysed in 350 µL RLT+ buffer. All cell lysates were directly frozen at -80 °C until further processing. RNA was then extracted using the RNAeasy Mini Kit, following the manufacturer's instructions. Centrifugations were done using Heraeus Fresco 17 or Heraeus Pico 17 centrifuges (Thermo Scientific). The optional on-column DNase digestion was performed using the RNAse-Free DNase Set in order to remove residual DNA. RNA concentration was determined by NanoDrop (Peqlab) photometric measurement at a wavelength of 260 nm. The quality of RNA was assessed by measuring the 260/280 and 260/230 absorbance ratios. The isolated total RNA was stored at -80 °C.

2.2.2.2. cDNA synthesis

Following the manufacturer's instructions (Maxima H Minus First Strand cDNA Synthesis Kit), 1 µg of RNA was mixed up with 1 µL of each of oligo $(dT)_{18}$ primer, random hexamer primer, and 10 mM dNTP mix. The mix was filled up to 15 µL with DEPC-treated H_2O, incubated at 65 °C for 5 minutes to unfold secondary structures, then cooled down immediately on ice. 4 µL of RT buffer in addition to 1 µL of Maxima H Minus enzyme mix were then added per reaction, and the reaction mix was then incubated for 10 minutes at 25 °C followed by 30 minutes at 50 °C, then 5 minutes at 85 °C in a ProFlex PCR System

thermalcycler (Thermo Fisher Scientific). Samples were then cooled down at 4 °C. For further analysis, cDNA was diluted 1:10 with 180 µL of DEPC-treated H_2O and stored at -20°C.

2.2.2.3. RT-qPCR

Analysis of gene expression at mRNA level was achieved by quantitative real time PCR using the QuantStudio 3 Real-Time PCR system (Applied Biosystems). Reactions were performed in technical triplicates, with 4 µL corresponding to 20 ng of cDNA, 4 µL of 1 µM forward and reverse primers mix, 10 µL of 2× PowerUp SYBR Green master mix, and DEPC-treated H_2O in a total volume of 20 µL. 2× PowerUp SYBR Green master mix constitutes of the polymerase, dNTPs, buffer, SYBR green dye, ROX dye passive reference, as well as Heat-labile Uracil-DNA Glycosylase. The routinely used amplification program is presented in Table 2.19. Analysis of relative gene expression was performed using the double delta C_t ($2^{-\Delta\Delta C_t}$) method (Livak and Schmittgen 2001), with first calculating the difference between target gene expression level and housekeeping gene (HPRT or ACTB (β-actin)) levels, defined by Cycle threshold (C_t) values, followed by normalizing these differences between experimental conditions and the respective control sample. Data are presented as normalized fold change of average from three technical replicates. Any primer pair used in this study was tested for its efficiency using a serial dilution of reverse transcribed human reference total RNA (Stratagene, #750500) or mouse reference total RNA (Stratagene, #750600). Only PCR reactions with efficiency between 90 and 110% were used. All primers used in this study are listed in table 2.6.

Table 2.19. Standard RT-qPCR amplification program using SYBR green

Step	Temperature	Time	Number of cycles
Uracil-DNA glycosylase activation	50 °C	2 min	1
Initial Denaturation, Taq activation	95 °C	2 min	1
Denaturation	95 °C	30 sec	45 cycles
Annealing	60 °C	30 sec	
Extension	72 °C	35 sec	
Denaturation	95 °C	1 min	
Annealing/Extension	60 °C	1 min	1
Melt curve/ Dissociation	95 °C	15 sec	0.1 °C stepwise increase in temperature
End	4 °C	hold	

2.2.2.4. Bulk RNA-seq

According to the observed upregulation of Snail in time course experiments described earlier in section 2.2.1.10.1, two TGFβ time points were chosen for each cell line; U87MG, MDA-MB-231, and A549. In specific, 5 ng/mL TGFβ was added for 48 or 72 hours in U87MG and A549 (Fig. 2.10a,b), and for 6 or 24 hours in MDA-MB-231 (Fig. 2.10c). U87MG co and shIDH1 cells were seeded under TSM conditions, 5 ng/mL TGFβ was added and incubated for 72 hours. Additionally, 6 mM Dm-α-KG was introduced at two distinct time points: 72 hours; added 3 hours after start of TGFβ, or 6 hours before harvesting (Fig. 2.8d). Treatments were conducted in 10 cm TC or petri dishes. Three biological replicates were prepared for each condition. Cells were harvested, and RNA was extracted using RNeasy Mini Kit, combined with on-column DNase digestion to avoid contamination by gDNA, as described in section 2.2.2.1. 2 µg RNA in 10 µL RNase-free water were prepared and sent to Deep sequencing platform of the Max Planck Institute for Heart and Lung Research, (Bad Nauheim, Germany) led by Dr. Stefan Günther. RNA samples were processed according to the specifications of the sequencing facility. Library preparation integrity was verified with LabChip Gx Touch 24 (Revvity). 400 ng of total RNA was used as input for the VAHTS Stranded mRNA-seq Library Preparation V6 according to the manufacturer's protocol (Vazyme). Sequencing was performed on a NextSeq 500 instrument (Illumina) using v2 chemistry resulting in an average of 33.3M reads per library, with a 1 x 75 bp single end setup. The resulting raw reads were assessed for quality, adapter content and duplication rates with FastQC. Trimmomatic v.0.39 was used to trim reads after a quality drop below a mean of Q15 in a window of five nucleotides, keeping only filtered reads longer than 15 nucleotide. Reads were aligned against the Ensembl human genome with STAR. The number of reads aligning to genes were counted using the FeatureCounts from the Subread package. The reads that were admitted and aggregated per gene were the ones that mapped at least partially inside exons. Reads that were overlapping multiple genes or aligning to multiple regions were excluded. Differentially expressed genes (DEG) were identified using DESeq2. Genes were classified as significantly differentially expressed at average count greater than five, multiple testing $P_{adj} < 0.05$ and $-0.585 < \log_2$ fold change > 0.585. The annotation was enriched with UniProt data based on Ensembl gene identifiers.

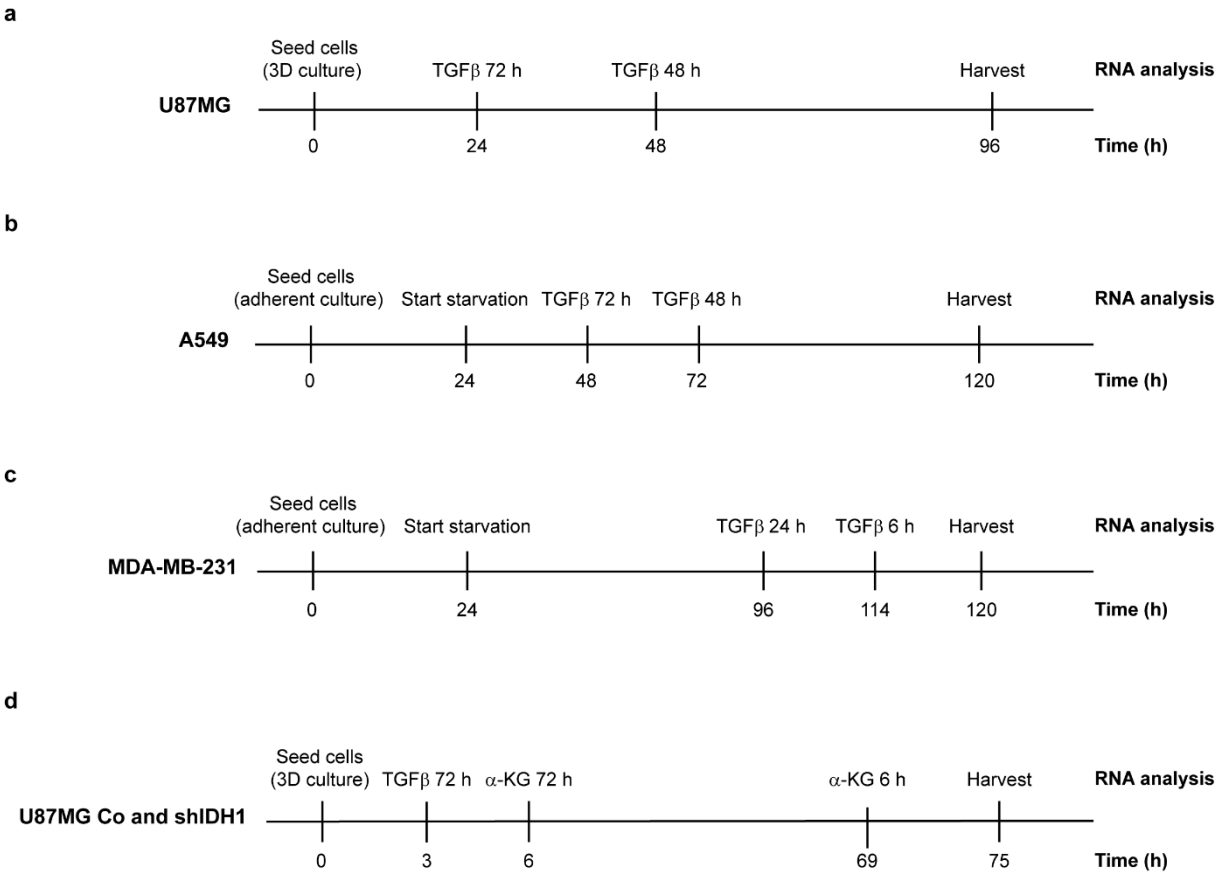

Figure 2.10. Experimental setups for the treatments of cells subjected to RNA-seq analyses.

2.2.3. Working with proteins - western blotting

2.2.3.1. Cell lysis and protein extraction

To prepare protein extracts from adherent cells grown in 10 cm TC dishes, cells were washed once with 1× PBS, then they were scraped off the dish using a cell scraper (TPP Techno Plastic Products AG, Switzerland) with an appropriate amount of Laemmli lysis buffer (usually between 80-120 µL depending on cell confluence). For semi-adherent cells, and cells grown under sphere conditions, cell suspension was collected, and divided in two tubes, transferred on ice immediately, centrifuged at 2500 rpm for 1 minute at 4 °C. After aspiration of supernatant, one cell pellet was processed for RNA (as described in section 2.2.2.1) and the other cell pellet for protein extraction and subsequent analyses. Cell pellets intended for protein analysis were typically resuspended in 100 µL of Laemmli lysis buffer. Higher amounts of Laemmli buffer (350 µL) were used for the denser LLC1 cells. Cell lysates were then collected in 1.5 mL Eppendorf tubes. The lysates were first heated at 95 °C for 5 minutes, then sonicated for 30-60 seconds, at 90% amplitude with 0.5 seconds pulse (Bandelin electronic sonifier, Germany) to shear genomic DNA. Protein lysates were stored at -20 °C until further use.

2.2.3.2. Determination of protein concentration

Protein concentration was determined using the colorimetric DC Protein Assay Reagents Package, a two-step reactions which lead to color development, based on the Lowry method (Lowry et al. 1951). The alkaline copper tartrate solution (Reagent A), the diluted Folin Reagent (Reagent B) and Reagent S were prepared according to the manufacturer's instructions. 25 µL of the mixture of reagent A and S (20 µL of reagent S in 1000 µL of reagent A), were added to the sample (5 µL of protein lysate) and combined with 200 µL of reagent B in a 96 well plate (Greiner, #655101). After a gentle agitation of the plate to mix the reagents, the plate was incubated for 15 minutes at RT, then the absorbance was measured at 750 nm in a microplate reader (Berthold Technologies). Each sample was measured in duplicates. Laemmli buffer without bromophenol blue was used as a blank measurement. The protein concentration was determined using a calibration curve calculated with increasing concentrations of BSA.

2.2.3.3. Sample preparation

To prepare samples for immunoblotting and load equal amounts in equal volumes for all samples, 30 to 80 µg of total protein was mixed with 4× Sample Buffer and filled up to a final volume of 20 µL using Laemmli buffer. Samples were heated at 95 °C for 5 minutes to reduce viscosity and denature any remaining high molecular weight DNA.

2.2.3.4. Western Blot and Sodium-Dodecyl-Sulfate-PolyAcrylamide Gel Electrophoresis (SDS-PAGE)

The denatured proteins were separated according to their size using SDS-PAGE. Here, addition of SDS renders the proteins identically charged per unit mass, which enables the size-dependent separation. Depending on the size of the proteins being analyzed, 8% / 12% or 8% / 15% (upper/lower half) separating gels, or 12% separating gels were prepared. Samples were loaded onto the gel in a Mini-PROTEAN 3 system (Bio-Rad Laboratories) and run initially at a voltage (V) of 80 V, and then at 130 V after the proteins crossed the 4% stacking gel. Separated proteins were transferred to 0.45 µm PVDF transfer membranes (Thermo Fisher Scientific, #88518) at 125 mA per blot using the Wet-blot Mini-PROTEAN 3 system (Bio-Rad) for two hours. Membranes were then incubated for 1 hour at RT in the 5% milk blocking buffer to prevent unspecific antibody binding under continuous shaking. Next, membranes were cut according to the size of the proteins of interest and incubated overnight at 4 °C with the designated primary antibody diluted in the blocking buffer. Next day, the blots were rinsed 3 times (15 minutes each) in PBST washing buffer to remove unbound antibodies and incubated for 1 hour at RT with the appropriate secondary HRP-conjugated antibody diluted in blocking buffer. To detect protein bands, after three times washing with washing buffer and once with

1× PBS, chemiluminescent detection was performed by incubating the membranes for up to 3 minutes with the signal developing solution of the ECL Western Blotting Detection System, ECL plus System, or 9:1 mixture of SuperSignal West Pico PLUS Chemiluminescent Substrate and Super Signal West Femto Maximum Sensitivity Substrate, depending on the abundance of the protein and peroxidase activity of the secondary antibody. The membrane was placed into a developing cassette and the luminescent signals were then detected with an X-ray film (Thermo Scientific, #34089) with exposure times of 5 seconds to 1 hour, depending on the signal strength.

2.2.3.5. Stripping of western blot membranes

To detect another protein in the same western blot membrane, membranes were stripped of bound antibodies through incubation in the stripping buffer for two times each for 30 minutes at RT while shaking. Afterwards, membranes were washed three times for 10 minutes in PBST washing buffer to remove the acidic buffer. Then, membranes were blocked with blocking buffer for at least one hour again and probed with the next primary antibody. The procedure was continued as described above.

2.2.4. Working with proteins - immunofluorescence

2.2.4.1. Immunofluorescence analysis of Snail protein

To assess the effect of TGFβ and α-KG treatments on Snail localization and signal, immunofluorescence staining was applied. 8×10^3 A549 or U87MG, or 7×10^3 MDA-MB-231 cells were seeded onto sterile cover slips in 24-well TC plate, and medium starvation started on the second day, by replacing existing medium with 5% FBS DMEM. On the third day, A549 and U87MG were treated with TGFβ for 72 hours and increasing concentrations of α-KG for the last 24 hours (Fig. 2.11a). While MDA-MB-231 cells were treated with TGFβ for 24 hours and increasing concentrations of α-KG for the last 6 hours (Fig. 2.11b). Shorter treatments exposure in MDA-MB-231 was dependent on the TGFβ time points when Snail mRNA and protein expression levels were induced the most. At the end of the treatment, cells were washed once with 1× PBS and incubated with 4% PFA at RT for 10 minutes. Next, cells were washed three times with 1× PBS, and permeabilized with 0.3% Triton X-100 in PBS for 15 minutes. Coverslips were then placed on parafilm, and the following staining steps were performed: Cells were blocked in Blocking buffer (1× PBS / 5% NGS / 1% BSA / 0.1% Triton X-100) for 1 hour, followed by incubation with the primary antibody (Rat-anti-Snail, 1:100 dilution) in the antibody dilution buffer overnight at 4 °C in a humidified chamber. Next day, coverslips were washed 3 times with washing buffer, followed by incubation with fluorophore-conjugated secondary antibody (Goat anti-rat AlexaFluor 488, 1:200) diluted in the antibody dilution buffer

at RT in the dark for 1 hour. After 3 times washes with washing buffer, once with PBS, nuclei were stained with DAPI (1:3000 in 1× PBS) for 10 minutes at RT, followed by three final washing steps with washing buffer, once with PBS, and once in dH_2O. Finally, a drop of fluorescent mounting medium was placed on the coverslips and they were embedded on microscope slides. At least 10 images per condition were taken using Leica DMi8 S inverted microscope at 40× magnification, and LAS X software. Quantification of fluorescence intensity was performed using the Fiji software. DAPI staining (blue channel) was used to create a binary image, and nuclei were then defined as Regions of interest (ROIs). These ROIs were then applied to the green channel where Snail fluorescent signal intensities were measured. Corrected total nucleus fluorescence (CTNF) was calculated based on the following formula: CTNF = Integrated Density – (Area of selected nucleus × Mean fluorescence of background readings). Integrated density and area are measurements selected from Analyze menu > Set measurements.

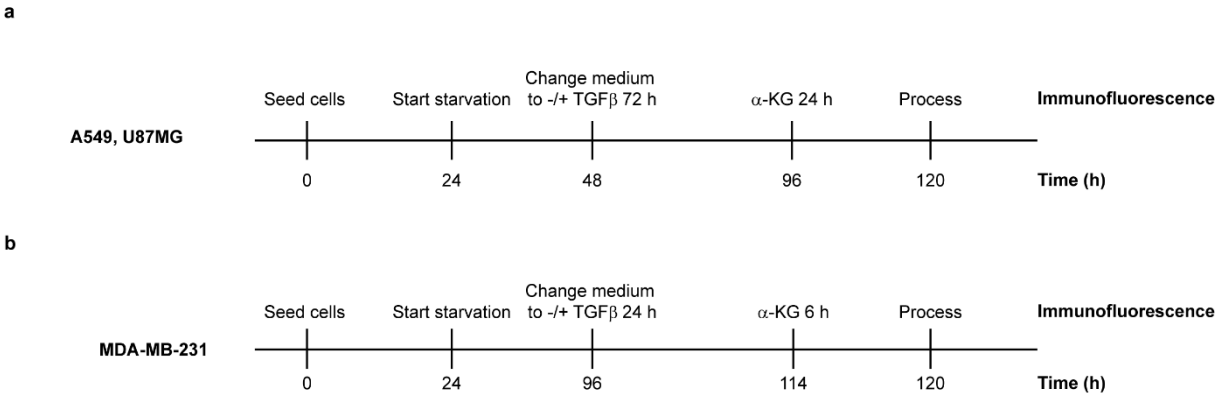

Figure 2.11. Experimental setups for immunofluorescence analyses of Snail.

2.2.4.2. Immunofluorescence analysis of Vimentin protein

Cells were seeded and starved as described in the previous section. Next, cells were treated with 5 ng/mL TGFβ and increasing concentrations of α-KG (6 mM and 8 mM) for 72 hours (Fig. 2.12). After the end of the treatment, cells were washed once with 1× PBS and incubated with 4% PFA at RT for 10 minutes. Next, cells were washed three times with 1× PBS, permeabilized with 0.1% Triton X-100 in PBS for 5 minutes, washed 3 times with PBS, then incubated in 100% methanol for 20 minutes at -20 °C, followed by incubation in 50% methanol for 5 minutes at 4 °C. Methanol was then replaced with PBS and the cells were incubated at RT for 15 minutes for rehydration. Coverslips were then placed on parafilm, and the following staining steps were performed: Cells were blocked in Blocking buffer (1x PBS / 5% NGS / 1% BSA / 0.1% Triton X-100) for 1 hour, followed by incubation with the primary antibody (mouse anti-vimentin, 1:500 dilution) in the antibody dilution buffer overnight at 4 °C

in a humidified chamber. Next day, coverslips were washed 3 times with washing buffer, followed by incubation with fluorophore-conjugated secondary antibody (Goat anti-mouse AlexaFluor 568, 1:200) diluted in the antibody dilution buffer at RT in the dark for 1 hour. After 3 times washes with washing buffer, once with PBS, nuclei were stained with DAPI for 10 minutes at RT, followed by three final washing steps with washing buffer, once with PBS, and once in dH_2O. Finally, a drop of fluorescent mounting medium was placed on the coverslips and they were embedded on microscope slides. Around 10 images per condition were taken using Leica using Leica DMi8 S inverted microscope at 40× magnification, and LAS X software. Quantification of fluorescence intensity was performed using Fiji software. Red channel was used to create a binary image, and single cells were defined as ROIs. These ROIs were then applied again to the red channel where vimentin fluorescent signal intensities were measured. Corrected total cell fluorescence (CTCF) was calculated based on the following formula:

CTCF = Integrated Density – (Area of selected cell × Mean fluorescence of background readings). Integrated density and area are measurements selected from Analyze menu > Set measurements.

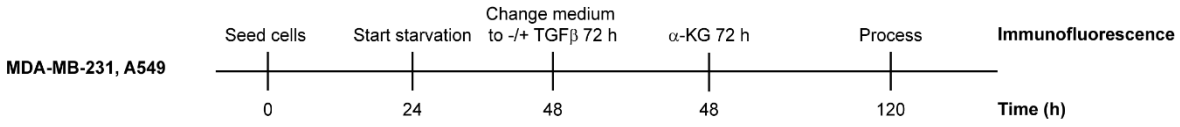

Figure 2.12. Experimental setups for immunofluorescence analysis of Vimentin.

2.2.4.3. Immunofluorescence analysis of E-cadherin protein

After treatment with 5 ng/mL TGFβ for 96 hours and increasing concentrations of α-KG (6 mM and 8 mM) for 72 hours, under 2% FBS containing medium (Fig. 2.13), cells were washed once with 1× PBS and incubated with 4% PFA at RT for 10 minutes. Next, cells were washed three times with 1× PBS, permeabilized with 0.1% Triton X-100 in PBS for 15 minutes. Coverslips were then placed on parafilm, and the following staining steps were performed: Cells were blocked in Blocking buffer (1× PBS / 4% NGS / 2% BSA / 0.1% Triton X-100) for 1 hour, followed by incubation with the primary antibody (mouse anti-E-cadherin, 1:50 dilution) in the blocking buffer overnight at 4 °C in a humidified chamber. Next day, coverslips were washed 3 times with washing buffer, followed by incubation with fluorophore-conjugated secondary antibody (Goat anti-mouse AlexaFluor 488, 1:200) diluted in the blocking buffer at RT in the dark for 1 hour. After 3 times washes with washing buffer, once with PBS, nuclei were stained

with DAPI for 10 minutes at RT, followed by three final washing steps with washing buffer, once with PBS, and once in dH_2O. Finally, a drop of fluorescent mounting medium was placed on the coverslips and they were embedded on microscope slides. At least 5-10 images per condition were taken using Leica DMi8 S inverted microscope at 40× magnification, and LAS X software. Experiment was conducted once. No quantification was possible, due to lack of control cellular membrane marker.

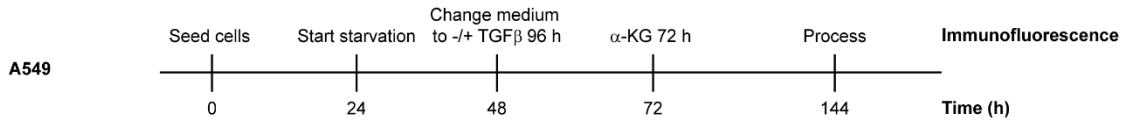

Figure 2.13. Experimental setups for immunofluorescence analysis of E-cadherin.

2.2.5. Flow cytometry

Upon 72 hours TGFβ and α-KG treatments under starvation, A549 and MDA-MB-231 VIM-RFP cells were dissociated into a single-cell suspension by accutase treatment for 15 minutes at 37 °C. Cells were stained with SYTOX Blue (Invitrogen, #CD133/2-PE) nucleic acid stain to gate out dead cells. Flow cytometry was performed using a Sony spectral cell analyzer (BD Biosciences). Four biological replicates were measured for each condition. Data were analyzed using FlowJo v7/9 (Tree Star) by gating for live cells based on SYTOX staining, forward and side scatter gates were used to discriminate doublets and debris, followed by gating for RFP positive populations.

To evaluate the tumor microenvironment labeling ability of sLP-mCherry–expressing tumor cells *in vivo*, Fluorescence-activated cell sorting (FACS) was employed. Parental LLC1 cells, LLC1 pCDH-B3, LLC1 sLP-mCherry, and double-labeled LLC1 cells were used to establish fluorescence-based gating parameters using BD FACSMelody cell sorter. LLC1 parental cells treated with 100% ethanol were stained with DRAQ7 dye (Invitrogen, #D15106) to exclude non-viable cells. A single-cell suspension of digested and dissociated tumor tissue was analyzed by flow cytometry. Cells were first gated for viability based on DRAQ7 exclusion, followed by forward and side scatter to eliminate doublets and debris. mCherry-positive populations were then identified, and further gating distinguished GFP-positive / mCherry-positive tumor cells from GFP-negative / mCherry-positive stromal cells.

2.2.6. Working with bacteria

2.2.6.1. Preparation of LB medium and LB agar plates

LB medium and LB agar were prepared using distilled water as recommended by the manufacturer, and as described in the materials section 2.1.14.1. The mixtures were sterilized by autoclaving at 121 °C under 20 pounds per square inch (psi) for around 30 minutes. After cooling down to approximately 50 °C, ampicillin was added to a final concentration of 100 µg/mL. LB agar was poured into 10 cm Petri dishes under the sterile hood. After solidification, the plates were either directly used or stored at 4 °C for up to 4 weeks. LB medium was also stored at 4°C.

2.2.6.2. Bacterial transformation

Transformation of plasmid DNA was carried out by adding 5 µL of a ligation reaction to 50 µL chemically competent *Stbl3 E. coli*. The tubes were flicked several times and incubated for 30 minutes on ice. Heat shock (42 °C) was applied to the bacteria for 45 seconds. Subsequently, bacteria were incubated on ice for two minutes. 250 µL of S.O.C. medium (Gibco, # 15544034) was added to the transformed cells, and cells were incubated in a 37 °C heat block with continuous shaking at 800 rpm for up to one hour. 100-200 µL of the bacterial culture was streaked onto LB agar plates containing the appropriate amount of antibiotics and incubated at 37 °C overnight. As a positive control for ligation, bacteria were transformed with the empty vector plasmid DNA.

2.2.6.3. Inoculation of liquid culture

Single bacterial colonies were picked and transferred in 5 mL of LB medium containing the appropriate antibiotics. These liquid cultures were incubated at 37 °C with shaking at 225 rpm overnight in a Multitron Incubator Shaker (Infors AG, Switzerland). They were subsequently used for small-scale plasmid purification, the inoculation of large-scale cultures or preparation of glycerol stocks. Glass and metal surfaces were sterilized using a Bunsen burner.

2.2.6.4. Preparation of glycerol stocks

For long-term storage of the plasmid-containing bacteria, glycerol stocks of bacterial suspensions were prepared by mixing 500 µL autoclaved 60% glycerol prepared in LB medium, and 500 µL of the liquid cultures. Glycerol stocks were stored at -80 °C.

2.2.7. Working with DNA

2.2.7.1. Chromatin immunoprecipitation (ChIP)

In total, 6×10^5 MDA-MB-231 cells were seeded per 15 cm TC dishes (Sarstedt, 83.3903), under adherent conditions and TGFβ was added on the third day for 72 hours (Fig. 2.14a). $2–2.5 \times 10^6$ U87MG co and shIDH1 cells were seeded in 15 cm petri dishes (Sarstedt, 82.1184.500), under tumorsphere conditions. TGFβ treatment started three hours after seeding, and 6 mM α-KG was supplemented three hours later for 72 hours (Fig. 2.14b). At the end of treatment, proteins bound to DNA were cross-linked with 1% ChIP-grade formaldehyde added directly to the medium. After 5 minutes incubation at RT, glycine with a final concentration of 0.1 M was added for 5 minutes to stop cross-linking. Plates were rocked manually during this time. Then, cells were collected by scraping and centrifuged at 1600 ×*g* for 5 minutes at 4 °C. Next, cells were resuspended and washed in ice-cold PBS containing 0.5 µM p-APMSF and centrifuged again. Cell pellets were shock frozen in liquid nitrogen, and stored at -80 °C. Four plates of U87MG cells were lysed with sonification beads (Diagenode, C01020031) in 1 mL ChIP lysis buffer, to which 0.5 µM PMSF and 0.15× Roche protease inhibitor cocktail were added freshly. Chromatin was sheared for 28 cycles 30 seconds on/ 30seconds off, at 4 °C using the Bioruptor Pico (Diagenode) device. In the case of MDA-MB-231 cells, each plate was lysed for 5 minutes at RT, then 5 minutes on ice in 900 µL of ChIP lysis buffer with freshly added 0.5 µM PMSF and 0.15× Roche protease inhibitor cocktail. Chromatin was sheared for 5 cycles 20 seconds on/ 30 seconds off, using Bioruptor Pico at 4 °C. Lysates were cleared by centrifugation at 13200 rpm at 4 °C for 15 minutes. For determination of DNA concentration, 20 µL of sheared lysate was diluted with 100 µL TE buffer including 10 µg/mL RNase A. After 30 minutes at 37 °C, 3.8 µL proteinase K (20 mg/mL) and 1% SDS was added and incubated for 2 hours at 37 °C followed by overnight incubation at 65 °C for reversal of the cross-linking. Samples were resuspended in 240 µL NTB buffer from the NucleoSpin® Gel and PCR Clean-Up Kit and DNA was purified according to the manufacturer's instructions. DNA was eluted with 50 µL elution buffer (5 mM Tris pH 8.5) and concentration was determined by NanoDrop. For the IP reactions, the following antibody amounts were added to precleared-lysate volumes equivalent to 10 µg of DNA: 2 µg anti-H3K27ac, 10 µg anti-H3K4me3, 2 µg anti-H3K27me3, and 2 µg IgG. The volume was adjusted to 100 µL with lysis buffer. Next, 30 µL of a protein A/G sepharose mixture, pre-equilibrated in ChIP dilution buffer were diluted in 900 µL of ChIP dilution buffer, and mixed with the samples and antibodies, and were incubated at 4 °C while rotating overnight. Next day, the beads were collected by centrifugation, washed once in ChIP low salt buffer, once in ChIP high salt buffer, once in ChIP LiCl buffer, and twice in ChIP TE

buffer for 5 minutes each while rotating at 4 °C. Beads were finally resuspended in 100 µL TE buffer including 10 µg/mL RNase A. In parallel, 1/10 volume of the initial lysate (10% input samples) were treated accordingly. After 30 minutes at 37 °C, 3.8 µL proteinase K (20 mg/mL) and 1% SDS were added and both input and immunoprecipitated fractions were incubated for at least 2 hours at 37 °C followed by overnight incubation at 65 °C for reversal of cross-linking. DNA was purified using the NucleoSpin® Gel and PCR Clean-Up Kit. DNA was eluted with 50 µL elution buffer and stored at −20 °C until further use. Regions of the genome were determined by previous studies (Smith et al. 2009; Zhang et al. 2013; Zhu et al. 2013), as well as the UCSC's built-in track JASPAR 2020 transcription factor binding site database. Selected regions were analyzed by real-time qPCR using the QuantStudio 3 Real-Time PCR system, using primers in Table 2.7. The reaction mixture contained 2 µL of ChIP or input DNA (diluted 1:10 to represent 1% of input DNA), 4 µL of 1 µM of specific primer mix and 10 µL of PowerUp SYBR Green master mix in a total volume of 20 µL. PCR cycles are described in Table 2.20. Calculation of enrichment by immunoprecipitation relative to the signals obtained for 1% input DNA was performed based on the percent input method. In brief, input is adjusted to 100% by subtracting log2 of 100 or 6.644 from the input Ct value. Then % input (IP) is calculated based on the following equation: 100 * 2^(Adjusted input - Ct (IP)), where Ct(IP) is the Ct value of the antibodies of interest in each sample.

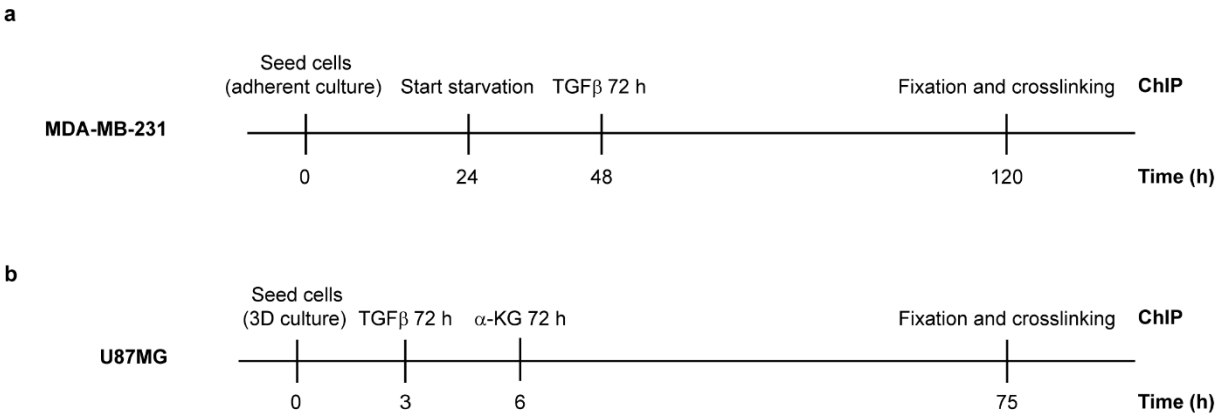

Figure 2.14. Experimental setups for ChIP-qPCR analyses.

Table 2.20. Standard ChIP-qPCR amplification program using SYBR green

Step	Temperature	Time	Number of cycles
Uracil-DNA glycosylase activation	50 °C	2 min	1
Initial Denaturation, Taq activation	95 °C	2 min	1
Denaturation	95 °C	1 sec	50 cycles
Annealing/extension	60 °C	30 sec	
Denaturation	95 °C	15 sec	1

Annealing/extension	60 °C	1 min	
Melt curve/ Dissociation	95 °C	15 sec	0.1 °C stepwise increase in temperature
End	4 °C	hold	

2.2.7.2. Genomic DNA isolation

Genomic DNA was extracted from cells using PureLink genomic DNA mini kit. G55 cells from a 70% confluent 10 cm TC dish were harvested through trypsinization and processed according to the manufacturer's instructions.

2.2.7.3. Plasmid DNA isolation

To isolate plasmid DNA from bacteria, different kits were used depending on the experimental need. For small-scale plasmid DNA purification used for determining the sequence of the plasmids, 4 to 6 mL of starter liquid culture was processed with the DNA-spin Plasmid DNA Purification Kit, according to the manufacturer's instruction. For large-scale plasmid purification, the starter liquid culture was incubated in up to 200 mL of LB medium with the appropriate antibiotics overnight, and the PureLink HiPure Plasmid Maxiprep Kit was then used according to the manufacturer's protocol.

2.2.7.4. Plasmid DNA sequencing

To verify the correct sequences of plasmids, plasmid DNA were sent for sequencing to Microsynth AG (Switzerland) according to the requirements set by the service provider. In general, 1 µg of DNA in 12 µL of TE buffer were sent for sequencing in case of available sequencing primers at Microsynth. Alternatively, for specific primer sequences, 3 µL of 10 µM primer was added to the DNA sample.

2.2.7.5. PCR cloning

To have an extended SNAI1 gene promoter sequence for DLR assay which includes transcription starting site (TSS), Phusion high-fidelity DNA polymerase was used to amplify the fragments of interest -1041 bp to +38 bp of the SNAI1 promoter sequence from genomic DNA of G55 cells, using primers listed in Table 2.8. A 50 µL reaction mix contained 0.5 µL Phusion polymerase, 10 µL 5× Phusion green HF buffer, 1 µL of 10 mM dNTPs, 1.5 µL DMSO, 2.5 µL of each forward and reverse primer (10 µM) in DEPC-treated water. The cycling program is shown in Table 2.21.

Table 2.21. Amplification program for SNAI1 promoter

Step	temperature	time	Number of cycles

Initial denaturation	98 °C	30 sec	1
Denaturation	98 °C	10 sec	35
Annealing	62 °C	30 sec	
Extension	72 °C	30 sec	
Final extension	72 °C	10 min	1

2.2.7.6. Restriction digestion

To clone the desired insert into a vector, namely partial sequences of SNAI1 gene promoter used for DLR assay, first a pGL2 vector encompassing SNAI1 promoter sequence (Fujita et al. 2003) and the pGL3-basic vector were digested with HindIII and KpnI. The 40 µL reaction mix consisted of 2 µg of plasmid DNA, 10× Tango buffer, and 16 µL of both KpnI and HindIII, and nuclease-free water and it was incubated at 37 °C for four hours. In order to create pGL3-Snail#2, up to 200 ng of the desired amplified and gel-extracted SNAI1 promoter sequence was mixed with 2 µL of 10× FastDigest Green Buffer, and 1 µL each of FastDigest MluI and FastDigest XhoI, and filled up to 30 µL with nuclease-free water, incubated at 37 °C for 20 minutes. Heat inactivation was used to stop the reaction at 80 °C for 20 minutes. Double digestions were usually conducted as recommended on the following website. https://www.thermofisher.com/de/de/home/brands/thermo-scientific/molecular-biology/thermo-scientific-restriction-modifying-enzymes/restriction-enzymes-thermo-scientific.html

2.2.7.7. Agarose gel electrophoresis

For separation and analysis of DNA after chromatin decrosslinking, PCR amplification, or double digestion, agarose gel electrophoresis was used. Depending on the size of the DNA fragments 0.8-2% gels were casted. The appropriate amount of agarose (0.8 to 2g) was dissolved in 100 mL 1× TAE through boiling in a microwave. Volume was adjusted to the respective gel tray. 4 µL of 10 mg/mL SYBR Safe DNA gel stain solution was added to allow detection of DNA bands under UV light, and the gel was poured into the gel tray. The gel was left to solidify for at least 30 minutes. 6× gel loading dye was added to the samples, which were then loaded onto the gel placed in a gel electrophoresis chamber (Thermo Fisher Scientific) filled with 1× TAE buffer. Appropriate DNA ladders were used to determine DNA fragment lengths. The electrophoresis ran for about 40 minutes at 120V. Afterwards, the DNA was visualized using a blue/green light-equipped FastGene FAS-V imaging system (NIPPON Genetics EUROPE).

2.2.7.8. Gel extraction of DNA fragments from agarose gels

If elution of the DNA was desired, the correct DNA fragments were excised using a clean scalpel. The gel slices were transferred to a 2 mL microcentrifuge tube and stored at -20 °C until further use. The recovery of DNA from gel slices was performed using the Monarch DNA gel extraction kit according to the manufacturer's instructions. The DNA was eluted in 10 µL DNA elution buffer.

2.2.7.9. Determination of DNA concentration

DNA concentration and quality were measured on a NanoDrop 2000 Spectrophotometer (Thermo Fisher Scientific). For determination of DNA concentration, the absorbance at 260 nm was measured. To assess the purity of the DNA sample, the ratio of absorbance at 260 nm and 280 nm vs. 230 nm was calculated. A clean and pure DNA preparation should have a 260/280 ratio of around 1.8 and a 260/230 ratio of around 2.0-2.2.

2.2.7.10. Ligation

For ligation reaction, 1 µL of around 20 ng of pGL3-basic linearized vector, 5 µL of insert (purified extracted DNA), 1 µL of 10× T4 DNA ligase buffer, and 0.5 µL of T4 DNA ligase were mixed and filled up to 10 µL with DEPC-water in a sterile 1.5 mL tube. The reaction was performed at RT for 1 hour.

2.2.8. Animal experiments

Animal experiments were approved by the veterinary department of the regional council in Darmstadt, Germany (V 54 - 19 c 20/15 - FR/1018). All experiments were performed in 6-8 week-old female C57BL/6 or NMRI nu/nu mice (Charles River) that were kept in a specific pathogen-free animal facility according to the institutional guidelines.

2.2.8.1. Subcutaneous models

Prior to the injection of tumor cells, animals were anesthetized with ketamine and xylazine anesthesia mix. For transplantation, 100 µL of tumor cell suspension containing 1×10^6 LLC1 cells per animal were injected subcutaneously into the right flank of C57BL/6 mice. 5×10^6 H2030 cells were resuspended in 100 µL of 1:1 PBS / Matrigel mix and injected subcutaneously into the right flank of NMRI nu/nu mice.

2.2.8.2. Tumor growth measurement

To estimate tumor volume, measurements of subcutaneous tumors were taken twice weekly with a caliper, and the volume calculated according to the following formula: Volume = (Length × Width^2)/2. Mice were maintained until the tumor exceeded a volume of 2000 mm^3, or upon the onset of morbidity symptoms (>20% weight loss, or tumor ulceration). Primary tumors were isolated and fixed at 4% PFA for 24 hours. Wounds were closed with application

of surgical Michel clips (FST, 12040-01). In the postoperative period, animals were administered analgesia (5 mg/kg of Rimadyl, Zoetis) directly after operation and 24 hours later, to relieve pain. Animals were kept for another 8 weeks to check for lung metastasis. When no metastasis was formed, mice were scarified by deep anesthesia followed by cervical dislocation. The mice were processed at the same time point, whenever it is possible.

2.2.8.3. Intravenous models

Prior to the injection of tumor cells, animals were anesthetized with ketamine and xylazine anesthesia mix, mice were placed in a plastic restrainer, and tails were warmed by incubating in warm water for 1 minute, to promote vasodilation. For intravenous transplantation, 100 µL of tumor cell suspension containing 1-5 × 10^6 LLC1 or 2.5 × 10^6 H2030 cells per animal were injected into the distal end of the tail vein of C57BL/6 or NMRI nu/nu mice, respectively.

2.2.8.4. *In vivo* bioluminescence imaging

In vivo bioluminescence imaging (BLI) of the LLC1-transplanted mice was performed with the help of the Lumina II *in vivo* imaging system (IVIS Lumina II, PerkinElmer). In brief, animals were imaged under general anesthesia with isoflurane (1-3%) administered via an inhalational anesthesia system (PerkinElmer). For detection of *in vivo* bioluminescence, 8 minutes prior to image acquisition mice were given a solution of D-luciferin by intraperitoneal injection at 150 mg/kg. Image analysis was done using the LivingImage 4.2 software (PerkinElmer).

2.2.8.5. Tissue dissociation and sample preparation

To determine if cancer cells expressing sLP-mCherry construct were able to label surrounding cells in the tumor microenvironment, mice were sacrificed, lungs were excised after intracardiac perfusion with 1× PBS to remove blood from the circulatory system, and tumors were minced with scissors on ice in 1× digestion buffer, diluted by serum-free RPMI. The minced tumor fragments were then digested at 37 °C for 30 minutes, with continuous mixing every 5 minutes, then passed through an RPMI-pre-moistened 70 µm MACS SmartStrainer (Miltenyi Biotec, #130-098-462). Remaining tumor aggregates were smashed mechanically using a 2.5 mL syringe plunger. The cells were washed with washing buffer, centrifuged at 1500 rpm for 5 minutes, at 4 °C, and supernatant was discarded. Red blood cells were lysed with 3 mL RBC lysis buffer for 3 minutes at RT, and then washed with 10 mL RPMI, filtered through 70 µm MACS SmartStrainer, and centrifuged. The cell pellets were resuspended in FACS buffer (1x PBS, 0.5% BSA, 2,5M EDTA), and processed as described in section 2.2.5.

2.2.9. Bioinformatic analysis

Correlations between patient survival, molecular GBM subtype (mesenchymal), and SNAI1 or IDH1 mRNA expression were determined through analysis of the Cancer Genome Atlas (TCGA) GBM database, which is available through GlioVis webserver (http://gliovis.bioinfo.cnio.es), using optimal cutoff. The correlation between SNAI1 or IDH1 mRNA levels and overall survival was evaluated with the Cox proportional hazards regression model, using the Kaplan–Meier plotter (KM-plotter) website (https://kmplot.com/analysis/) in breast cancer with positive lymph node metastasis, and in lung adenocarcinoma. To evaluate the combinatorial effect of SNAI1 and IDH1 expression on patient survival, datasets were obtained from KM-plotter for breast cancer patients with lymph node positive metastasis and for lung adenocarcinoma. The datasets were manually stratified into two groups: (1) IDH1 high / SNAI1 low and (2) IDH1 low / SNAI1 high. Stratification was performed by first dividing patients based on IDH1 expression (high or low), followed by further subdivision according to SNAI1 expression levels (high or low). Time until censoring or death in days were plotted against event, which could be either 1, which is equivalent to death, or 0, where the subject was instead censored at this time.

2.2.10. Visualization of sequencing data

To assess the binding of transcription factors c-Myc and HIFs (HIF-1α, HIF-2α, HIF-1β) to the SNAI1 promoter, publicly available ChIP-seq datasets were retrieved from the NCBI Gene Expression Omnibus (GEO) repository. The search was refined to include ChIP-seq experiments specific to Myc or HIF family members in cancer cells, with a particular focus on BigWig-formatted files, which allow efficient upload on UCSC genome browser in a later step. The retrieved BigWig files were initially examined using the Integrated Genome Browser (IGB) to assess the presence or absence of transcription factor binding signals over the promoter and gene body region of SNAI1 using the human genome assembly (hg38). Subsequently, selected BigWig datasets were uploaded to the Galaxy web platform (https://usegalaxy.org/) to generate publicly accessible URLs. These URLs were then imported into the UCSC Genome Browser by creating custom tracks. This approach enabled direct comparison of transcription factor binding profiles across the SNAI1 locus from various cancer cell lines. In addition to the user-defined custom tracks, UCSC's built-in ENCODE regulation track for histone modifications, such as H3K4me3 and H3K27ac, was used to provide epigenetic regulation information at the SNAI1 promoter. High resolution screenshots of the ChIP-seq alignment results alongside regulatory annotations of SNAI1 gene were captured using UCSC genome browser view and export tools.

2.2.11. Statistical analysis

All statistical analyses were performed using GraphPad Prism software. Statistical significance was calculated by two-tailed unpaired Student's *t*-tests or one-way Anova followed by post hoc analysis using Dunnett or Tukey's multiple comparison tests (*$P < 0.05$; **$P < 0.01$; ***$P < 0.001$). Detection of mathematical outliers was performed using the Grubbs' test in GraphPad. At least two to three independent replicates were performed with similar results, unless stated otherwise. Data are presented as means + standard error of means (SEM), unless otherwise specified. Statistical significance in Kaplan-Meier survival plots was assessed with log-rank P-values obtained from the KM plotter/ GlioVis websites or using the GraphPad Prism software.

3. Results

3.1. Snail is the sole EMT transcription factor consistently and highly upregulated by TGFβ across brain, breast and lung tumor cell lines

To investigate the role of α-KG in regulating EMT and invasion induced by either hypoxia or TGFβ in shIDH1 cells, we first revisited the effect of TGFβ on EMT induction in parental cells. To this end, bulk RNA-seq was performed on U87MG glioblastoma, MDA-MB-231 breast carcinoma, and A549 lung adenocarcinoma cells treated with 5 ng/mL TGFβ for the time points indicated on Fig 3.1. These time points were selected based on a TGFβ time-course experiment conducted on the same cell lines (data not shown, see Fig. 2.1 for experimental setup). Two time points were chosen according to the highest induction of SNAI1, as increased SNAI1 levels were observed upon TGFβ treatment in IDH1-depleted cells (Fig. 1.9) (Bögürcü-Seidel 2018). Notably, among the EMT regulators listed in the PMT gene set (Karsy et al. 2016), and the EMT transcription factors consensually defined by Lambert and Weinberg (2021) and Yang et al. (2020), SNAI1 was strongly and robustly upregulated across all three cancer cell lines (Fig. 3.1a). This observation was further validated by RT-qPCR (Fig. 3.1b), showing an over fifty-fold, two-fold, and almost twelve-fold increase in SNAI1 transcript levels following TGFβ stimulation in U87MG, MDA-MB-231, and A549, respectively. Interestingly, none of the PMT TFs were upregulated, whereas PRRX1 and FOXC1 showed increased expression following TGFβ treatment only in U87MG (Fig. 3.1a). A TGFβ time course experiment conducted in LLC1 mouse Lewis lung carcinoma cells showed a comparable pattern of core EMT TF induction. After TGFβ treatment, specifically at earlier time points (3 and 6 hours), Snail expression exceeded that of other EMT transcription factors both at the protein level (Fig. 3.1c) and at the mRNA level (Fig. 3.1d). This was followed by a subsequent downregulation of epithelial marker Cdh1 (E-cadherin), a direct transcriptional target of Snail, at 6 hours, and peaking of the mesenchymal marker Cdh2 (N-cadherin) quickly at 3 hours (Fig. 3.1d). Other core EMT TFs were either not consistently upregulated across the different cell lines or were not induced upon TGFβ treatment (Fig. 3.1a,d). These results supported earlier observations in our laboratory (Fig. 1.9) (Bögürcü-Seidel 2018), emphasizing the role of Snail as a master EMT regulator in the three cancer types, and prompted us to explore the link between α-KG and Snail in greater depth.

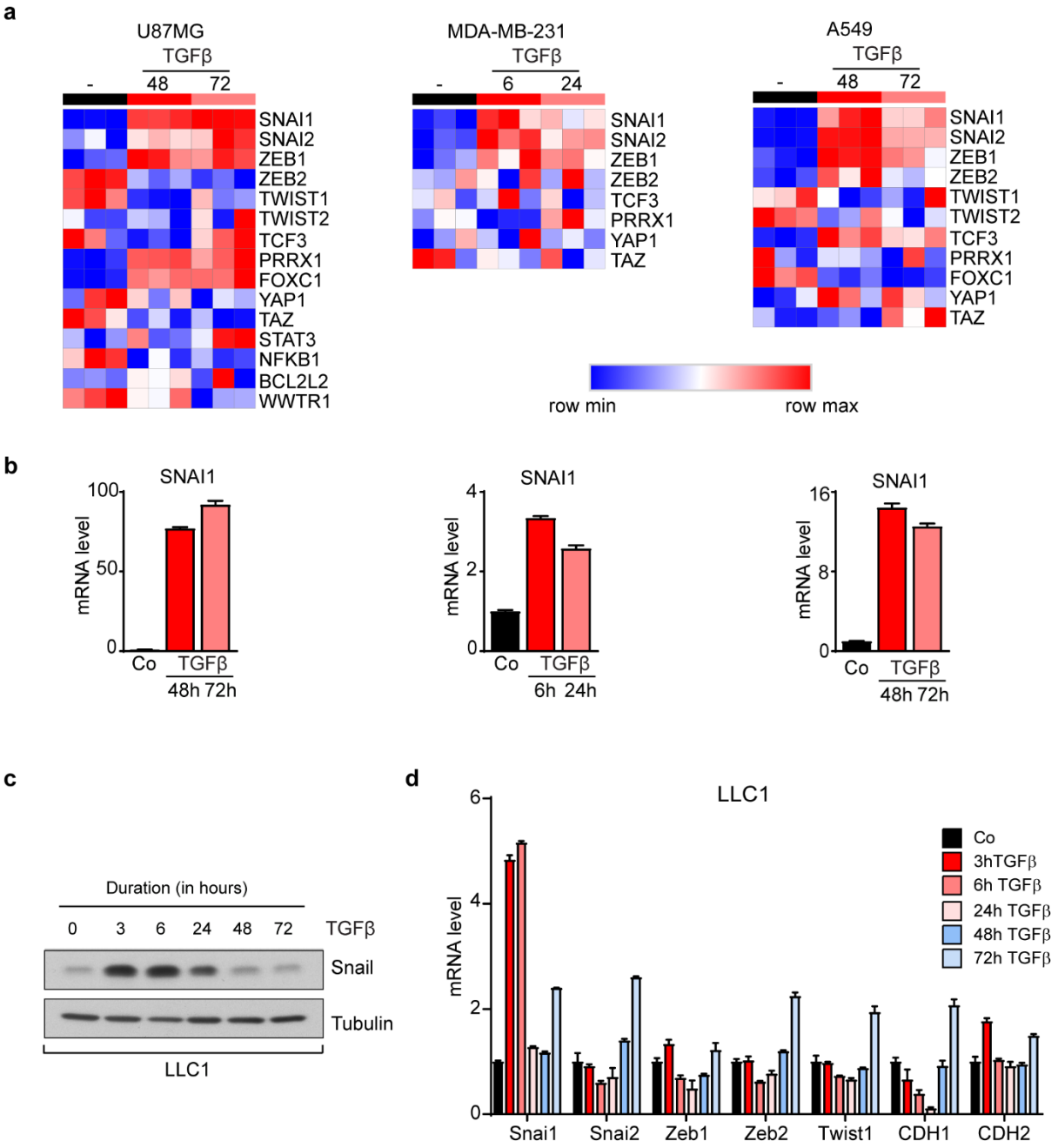

Figure 3.1.TGFβ stimulation increases Snail level in different cancer cell types. a. Heatmap derived from bulk RNA-seq depicting the differential expression of PMT (Karsy et al. 2016) and EMT (Lambert and Weinberg 2021; Yang et al. 2020) transcription factors in U87MG, MDA-MB-231, and A549 cells following TGFβ treatment at two time points. Columns represent individual replicates (n=3 biological replicates), grouped by conditions, rows represent DEG, color denotes row scaled (Z-score) expression values, with darkest blue as lowest expression and darkest red as highest). **b.** RT-qPCR analysis of the EMT transcription factor Snail in the three cell lines, under the indicated conditions (n=3 technical replicates). Graphs are representative of four independent experiments. **c.** Western blot detection of Snail levels in LLC1 cells treated with 5 ng/mL TGFβ for different time points (n=1). **d.** RT-qPCR determination of mRNA levels of EMT TFs and markers in LLC1 cells under the same conditions (n=3 technical replicates). The treatments and western blot were carried out with the help of Anna Gomeniuk, whereas RT-qPCR was carried out in collaboration with Anna Gomeniuk and Weam Maddadeh. Here and in subsequent western blots, Tubulin served as a loading control. Data are normalized to the control condition. Results are presented as means + standard error of means (SEM) (**b,d**).

3.2. TGFβ-induced Snail is suppressed by α-KG addition

To determine the concentration of α-KG required to downregulate Snail expression, and to validate previous findings of our lab, MDA-MB-231 and A549 cells were treated with TGFβ for 72 hours to induce Snail expression. During the final 24 hours of TGFβ treatment, increasing concentrations (in 2 mM increments) of a cell-permeable form of α-KG (Dm-α-KG) were added (Fig. 2.2b). Here, 6 mM and 8 mM Dm-α-KG remarkably reduced Snail protein levels (Fig. 3.2a). Slug levels, although slightly reduced, remained largely unchanged across different α-KG concentrations in both cell lines. To further corroborate the role of α-KG in regulating Snail levels, we first conducted RT-qPCR analyses on U87MG, G55, MDA-MB-231, and A549 cells treated with TGFβ for 72 hours, and with 6 mM or 8 mM Dm-α-KG in the last 24 or 6 hours (Fig. 2.2b), focusing on mRNA levels of core EMT transcription factors (SNAI1, SNAI2, ZEB1, ZEB2, TWIST1 and TWIST2). Indeed, the most pronounced changes were observed for SNAI1, which mRNA levels were strongly upregulated by TGFβ and downregulated upon subsequent α-KG treatment in a dose- and time-dependent manner across all four cell lines (Fig. 3.2b), with the exception of A549, where 6 hours-treatment of α-KG showed lower SNAI1 mRNA levels compared to 24 hours. SNAI2 mRNA levels were moderately increased following TGFβ treatment in carcinoma cell lines (MDA-MB-231 and A549), but not in glioblastoma cell lines. Moreover, its levels in carcinoma cells were also reduced upon α-KG treatment. Notably, TWIST1 and TWIST2 were not detectable in MDA-MB-231 cells. Consistently, western blot analyses confirmed an increase in Snail and Slug levels upon TGFβ induction, then a gradual reduction in Snail following α-KG treatment across all cell lines, while Slug level remained unchanged in G55, but was reduced in MDA-MB-231 and A549 cells (Fig. 3.2c), consistent with its differential mRNA expression. Generally, extended α-KG exposure (24 hours) and/or higher concentrations (8 mM) led to a more substantial decrease in both Snail mRNA and protein levels compared to shorter treatment (6 hours) and/or lower concentration (6 mM). These results highlight that Snail levels are strongly induced upon TGFβ treatment in various cancer cell types and clearly reduced upon α-KG supplementation.

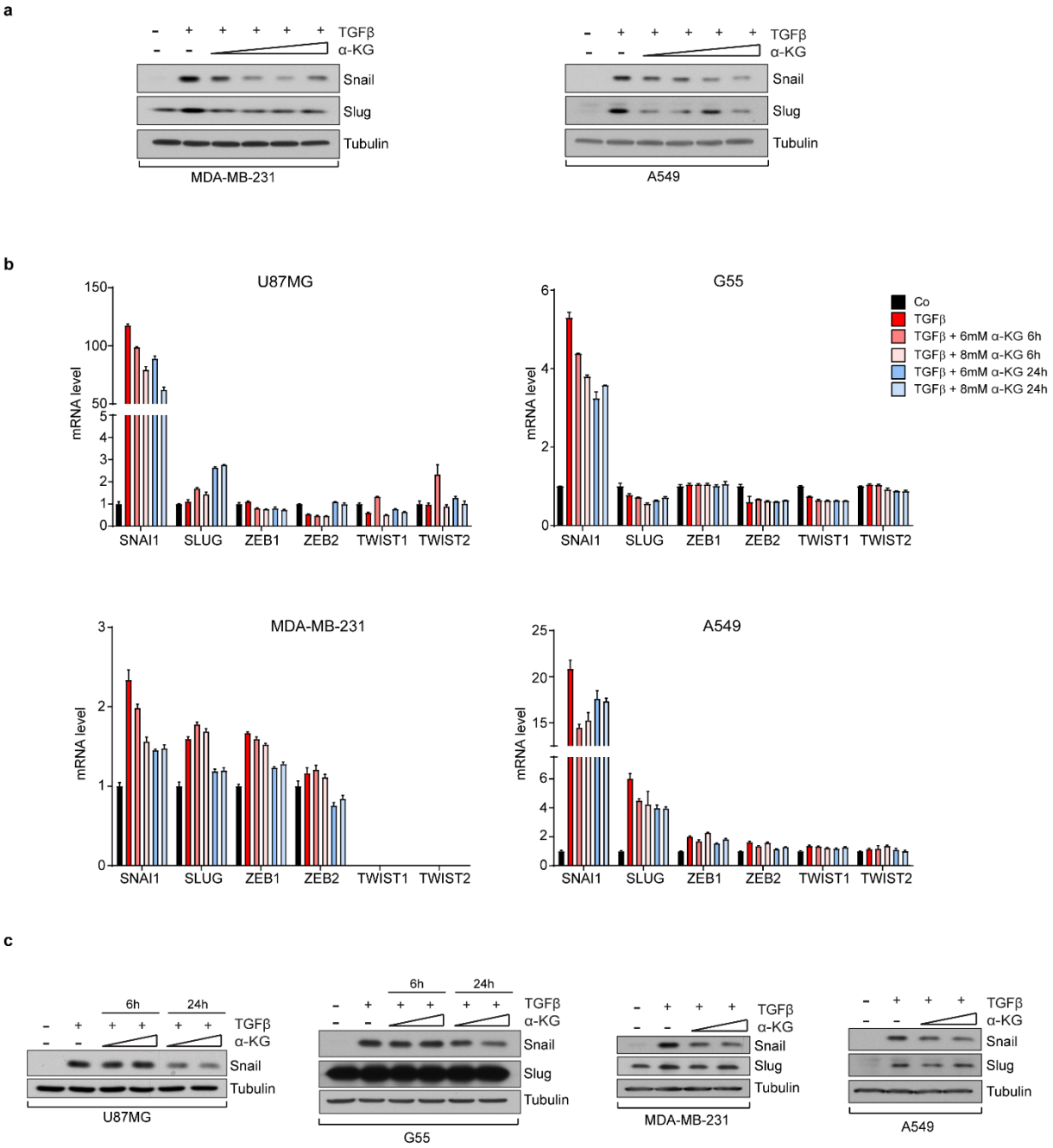

Figure 3.2. α-KG treatment reduces TGFβ-induced EMT induction. a. Western blots of Snail and Slug in MDA-MB-231 and A549 cells upon treatment with 5 ng/mL TGFβ for 72 h and increasing concentrations of α-KG (2 mM up to 8 mM in 2 mM increment) in the last 24 h (n=3). **b.** RT-qPCR analysis of the expression of the core EMT TFs SNAI1, SNAI2, ZEB1, ZEB2, TWIST1, and TWIST2 in glioblastoma cell lines U87MG and G55, breast cancer cell line MDA-MB-231, and lung cancer cell line A549 upon treatment with TGFβ for 72 h, and Dm-α-KG for the last 6 h or 24 h in increasing concentrations (6 mM and 8 mM), (n=3 technical replicates). Shown are representative examples of two independent experiments with similar results. **c.** Expression levels of EMT TFs Snail and Slug in the same cell lines, upon treatment with TGFβ for 72 h and Dm-α-KG for the indicated time points or 24 h if not indicated, determined using western blotting. Shown are representative immunoblots of 2 independent experiments with similar results. Data are normalized to control condition. Results are presented as means + SEM (**b**).

3.3. α-KG inhibits TGFβ-mediated EMT activation

Immunofluorescence staining of Snail validated previous observations (Fig. 2.11), showing that Snail signal intensity and nuclear localization were massively induced upon TGFβ treatment, and subsequently, significantly reduced upon α-KG supplementation in all three cancer cell lines (Fig. 3.3a-c). The nuclear localization of Snail correlates well with its TF function. Vimentin, another established mesenchymal marker was also assessed (Fig. 2.12), and a clear increase in the immunofluorescence signal was detected in both MDA-MB-231 and A549 cells following TGFβ addition. The increase was reversed to baseline levels in MDA-MB-231 and was reduced to almost 80% in A549 upon α-KG treatment (Fig. 3.3d). Remarkably, TGFβ-induced changes in Vimentin's subcellular distribution were also observed. Vimentin levels have been previously found unaffected by TGFβ supplementation in GBM cells (Goos 2015) and thus not investigated here. Further immunofluorescence (Fig. 2.13), and western blot analyses (Fig. 3.3e,f) of the epithelial marker transmembrane cell adhesion molecule E-cadherin in A549 cells revealed its downregulation following TGFβ treatment, consistent with Snail induction. This downregulation was also reflected at the mRNA level, alongside increased expression of the mesenchymal markers N-cadherin and Vimentin (Fig. 3.3g). Remarkably, neither 72 hours (Fig. 3.3e) nor 24 hours (Fig. 3.3f,g) of α-KG treatment reversed E-cadherin expression.

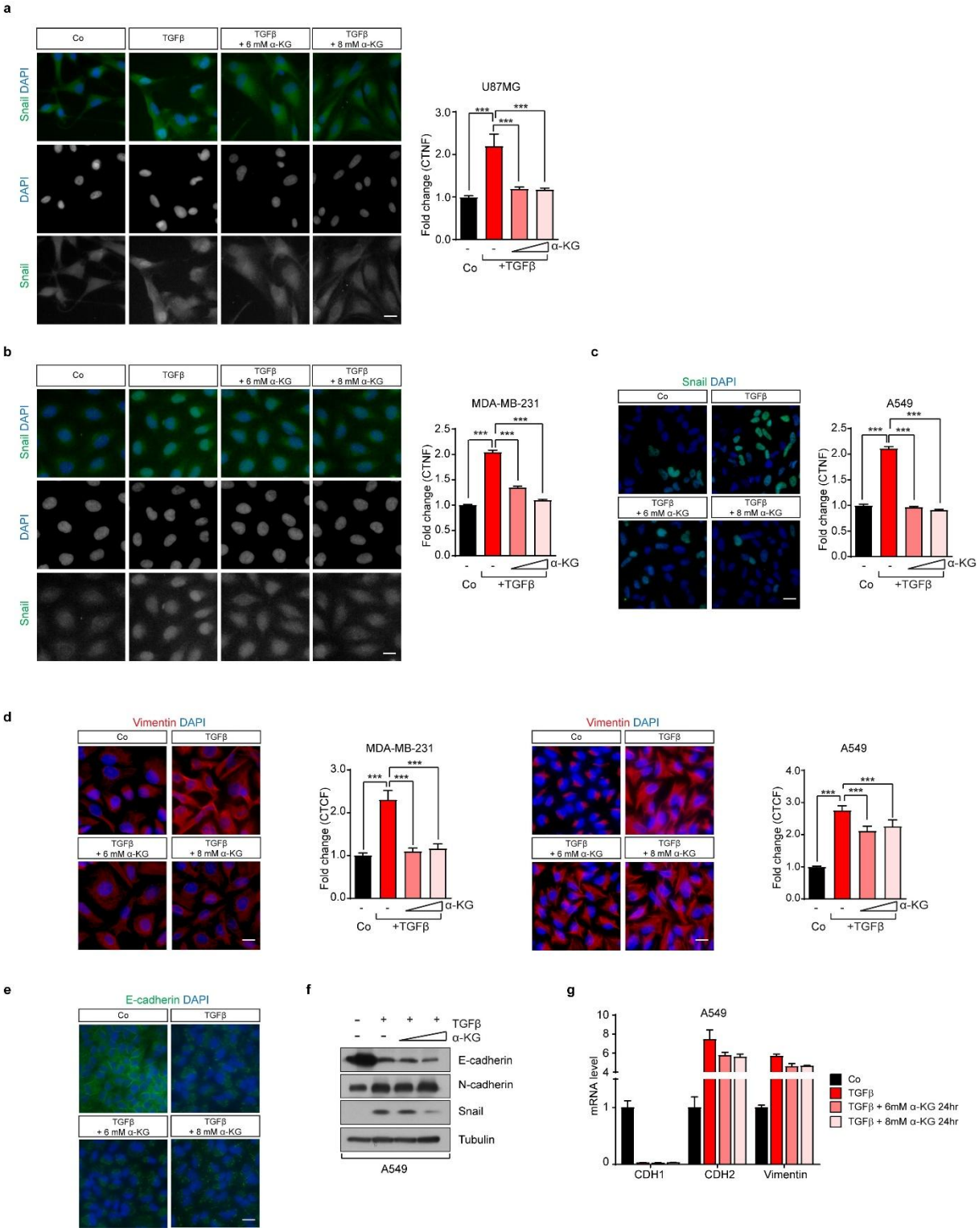

Figure 3.3. Immunofluorescence analyses of α-KG-mediated suppression of TGFβ-induced EMT. **a.** Immunofluorescence staining of EMT TF Snail in cells treated with 5 ng/mL TGFβ for 72 h and Dm-α-KG (6 mM and 8 mM) for 24 h in U87MG. **b.** Immunofluorescence staining of EMT TF Snail in cells treated with 5 ng/mL TGFβ for 24 h and Dm-α-KG (6 mM and 8 mM) for 6 h in MDA-MB-231. **c.** Immunofluorescence staining of EMT TF Snail in cells treated with 5 ng/mL TGFβ for 72 h and Dm-α-KG (6 mM and 8 mM) for 24 h in A549. The graphs in (**a,b,c**) to the right of the images show the fold change of corrected total nucleus fluorescence (CTNF) for Snail staining. Results are from two biological replicates, with average of 20 areas per condition imaged and analyzed. Scale bars indicate 20 µm. **d.** Immunofluorescence staining of mesenchymal marker Vimentin in MDA-MB-231 and A549 cells treated with 5 ng/mL TGFβ and Dm-α-KG (6 mM and 8 mM) for 72 h. The graphs to the right of

the images show the fold change of corrected total cell fluorescence (CTCF) for Vimentin staining signal in the entire cells. Results are from two biological replicates, with an average of 20 areas per condition imaged and analyzed. Scale bars indicate 20 µm. **e.** Immunofluorescence staining for epithelial marker E-cadherin in A549 cells treated with 5 ng/mL TGFβ for 96 h and Dm-α-KG (6 mM and 8 mM) for 72 h. No quantification was possible due to the absence of a plasma membrane marker. Results are from one biological replicate, with average of 10 areas per condition imaged. Scale bar indicates 20 µm. **f,g.** Expression levels of EMT markers E-cadherin, N-cadherin, Vimentin in A549 upon treatment with 5 ng/mL TGFβ for 72 h and increasing concentrations of Dm-α-KG (6 mM and 8 mM) for 24 h determined by immunoblotting (**f**) and RT-qPCR (**g**). Data are normalized to control condition, and results are presented as means + SEM (**a-d,g**). Statistical analysis was performed using one-way ANOVA, followed by Dunnett's multiple comparisons test (**a-d**), versus TGFβ treatment. ***p<0.001.

To further reinforce our findings, we employed MDA-MB-231-VIM-RFP and A549-VIM-RFP cells, which are engineered by CRISPR-Cas9 technology to stably express RFP-tagged Vimentin. Flow cytometry analysis under the same treatment conditions, revealed that α-KG supplementation significantly reduced the percentage of Vim-RFP-positive cells compared to TGFβ-treated condition (Fig. 3.4a). This observation was further reinforced by a concomitant decrease in Vimentin and Snail protein levels in the same cell lines, as determined by western blot analysis (Fig. 3.4b). Together, these results support the role of α-KG as a negative regulator of EMT, by suppressing both Snail and Vimentin expression.

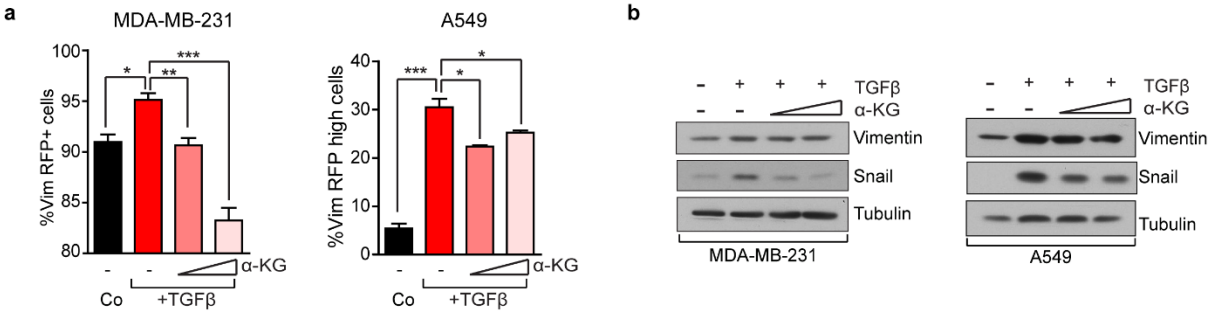

Figure 3.4. Flow cytometry analyses of α-KG-mediated suppression of TGFβ-induced EMT. a. FACS analysis of Vimentin-RFP+ fractions in MDA-MB-231-VIM-RFP and A549-VIM-RFP upon treatment with 5 ng/mL TGFβ and Dm-α-KG (6mM and 8mM) for 72 h (n=4). Treatment and FACS analysis were conducted by Nuray Bögürcü-Seidel and Sascha Seidel. Data are normalized to control condition. Results are presented as means + SEM. Statistical analysis was performed using one-way ANOVA, followed by Dunnett's multiple comparisons test, versus TGFβ treatment. *p<0.05; **p<0.01; ***p<0.001. **b.** Supplementary western blot analyses of Vimentin and Snail in the same cell lines upon treatment with 5 ng/mL TGFβ for 72 h and Dm-α-KG (6 mM and 8 mM) for 24 h. Shown are representative immunoblots of two independent experiments with similar results.

3.4. α-KG suppresses TGFβ-induced cellular invasion

EMT induction in carcinomas as well as mesenchymal transition in glioblastomas represent an initial and critical step in invasion and metastasis. We sought to investigate the role of α-KG in reversing invasive potential, by treating cells with TGFβ and α-KG as indicated earlier, then performing modified Boyden chamber assay, in which cells must traverse a Matrigel layer prior to migrating through a porous membrane (see Fig. 2.7a,b for treatment setups). Treating all three cancer cell types with TGFβ markedly enhanced their invasive

capacity, whereas supplementation with increasing concentrations of α-KG in the last 24 hours significantly reversed their invasion (Fig. 3.5a). A549 cells exhibited the most pronounced TGFβ-induced invasiveness yet showed the least reversal upon α-KG treatment. To assess whether α-KG could also prevent invasion, cells were first pre-treated with increasing concentrations of α-KG (in 2 mM increments) 3 hours prior to a 72 hours TGFβ treatment, followed by analysis in the modified Boyden chamber assay for another 24 hours (Fig. 2.7e). Interestingly, increasing α-KG concentrations gradually, but mildly suppressed invasive capacities of A549 cells apart from the 8 mM treatment condition (Fig. 3.5b). Furthermore, the anti-invasive role of α-KG in the absence of a microenvironmental cue, such as TGFβ, was evaluated. MDA-MB-231 cells, which are more at the mesenchymal end of the EMP spectrum, were treated with α-KG for 24 hours without prior TGFβ stimulation (Fig. 2.7c). Intriguingly, α-KG significantly diminished the intrinsic invasive capacity of these cells, as revealed by a Boyden chamber assay, and concurrently reduced Snail protein levels, as shown by western blot analysis (Fig. 3.5c).

To independently validate these findings, we generated a subpopulation of MDA-MB-231 cells with stably enhanced invasive properties. This was achieved by subjecting the cells to 10 consecutive rounds of selection using the modified Boyden chamber assay. Cells that invaded through the Matrigel-coated Transwell membrane were collected and propagated after each round. The final selected highly invasive cells were designated as i10, while cells which did not initially pass through to the lower chamber from the first round, were designated as non-invasive (ni) cell population (Fig. 3.5d, see section 2.2.1.13). MDA-MB-231 i10 cells displayed substantially elevated invasive potential relative to ni cells, in the presence or absence of TGFβ (Fig. 3.5e, Fig. 2.7d for setup). Importantly, supplementation with α-KG significantly and strongly inhibited i10 cells invasiveness in the absence of TGFβ treatment (Fig. 3.5f, Fig. 2.7c for setup).

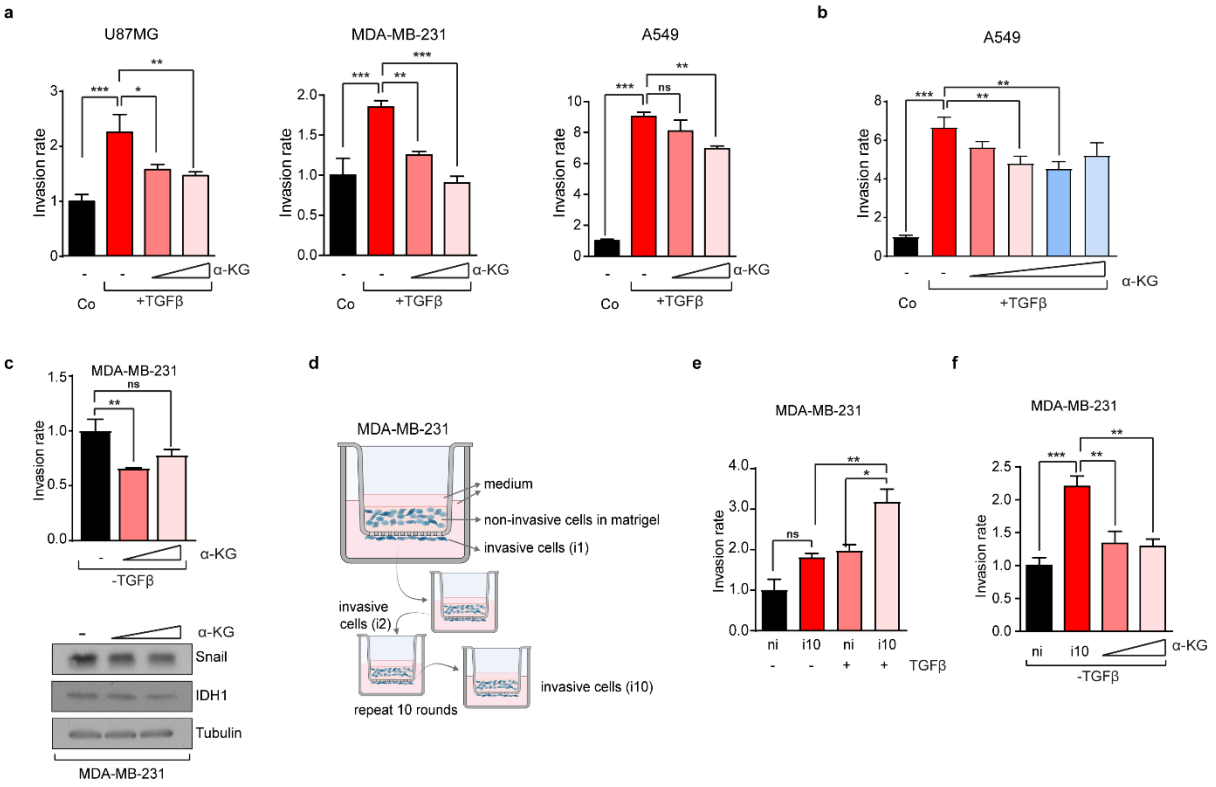

Figure 3.5. α-KG attenuates tumor cell invasion. **a.** Invasion rates of U87MG, MDA-MB-231, and A549 cells treated with 5 ng/mL TGFβ for 72 h and Dm-α-KG for last 24 h in increasing concentration (6 mM and 8 mM), followed by conducting Boyden chamber assay for an extended 24 or 48 h. (n=5-6 biological replicates per condition). **b.** Invasion rates of A549 treated with increasing concentration of α-KG (2 mM up to 8 mM in 2 mM increment) 3 h before addition of 5 ng/mL TGFβ for 72 h, followed by conducting Boyden chamber assay for an extended 24 h with same treatment conditions (n=4-6 biological replicates per condition). **c.** MDA-MB-231 as a MET model, cells were treated with Dm-α-KG (6 mM and 8 mM) for 24 h, followed by 48 h in Boyden chamber (upper) (n=5 biological replicates per condition). Expression levels of Snail were determined using Western blotting upon same treatment conditions (lower). **d.** Schematic illustration of the generation of non-invasive (ni) and invasive cells (i10). The selection was done, and the BioRender scheme was created by Nuray Bögürcü-Seidel. **e.** Invasion rates of MDA-MB-231 ni and i10 cells pre-treated with 5 ng/mL TGFβ for 72 h followed by a Boyden chamber assay for additional 48 h (n=4 biological replicates per condition). **f.** Invasion rates of MDA-MB-231 ni and i10 cells pre-treated with Dm-α-KG for 24 h in increasing concentration (6 mM and 8 mM) without prior TGFβ treatment followed by a Boyden chamber assay for additional 48 h (n=5-6 biological replicates per condition). Data are normalized to control condition. Results are presented as means + SEM. Statistical analysis was performed using one-way ANOVA, followed by Tukey's (**e**) or Dunnett's multiple comparisons test (versus TGFβ treatment) when appropriate. *p<0.05; **p<0.01; ***p<0.001.

To exclude the possibility that reduced invasiveness observed following α-KG treatment was due to impaired cell proliferation or increased cell death, we performed proliferation assay on all three cancer cell types following treatment with TGFβ for 72 hours, in addition to α-KG for 24, 48, or 72 hours (check Fig. 2.8 for experimental setup). We monitored the cell count and the percentage of viable cells using a CASY Cell Counter and Analyzer System. While α-KG treatment led to a significant reduction in U87MG cell count compared to TGFβ-treated cells (Fig. 3.6a), the percentage of viable cells remained largely unchanged with an average of

92.96% ± 0.95% (mean + standard deviation) viable cells (Fig. 3.6b). A variation in proliferation between treatment conditions in MDA-MB-231 was also evident, with a non-significant decrease in cell count in the 24 hours α-KG conditions (Fig. 3.6c). While serum deprivation reduced viability to an average of 90.31 % ± 2.39 %, additional treatments had no further measurable effect on viability (Fig. 3.6d). Finally, A549 showed the least variability of cell count between treatment conditions (Fig. 3.6e). They also showed the highest and least variable viability with an average of 95.23% ± 0.76% (Fig. 3.6f). Notably, U87MG cell treatments were conducted under TSM conditions, rather than adherent conditions, except during Boyden chamber assay pre-treatment. Collectively, while a modest effect on U87MG proliferation was observed, these results support a role for α-KG in suppressing the invasive potential of various cancer cell types without substantial cytotoxic or antiproliferative effects.

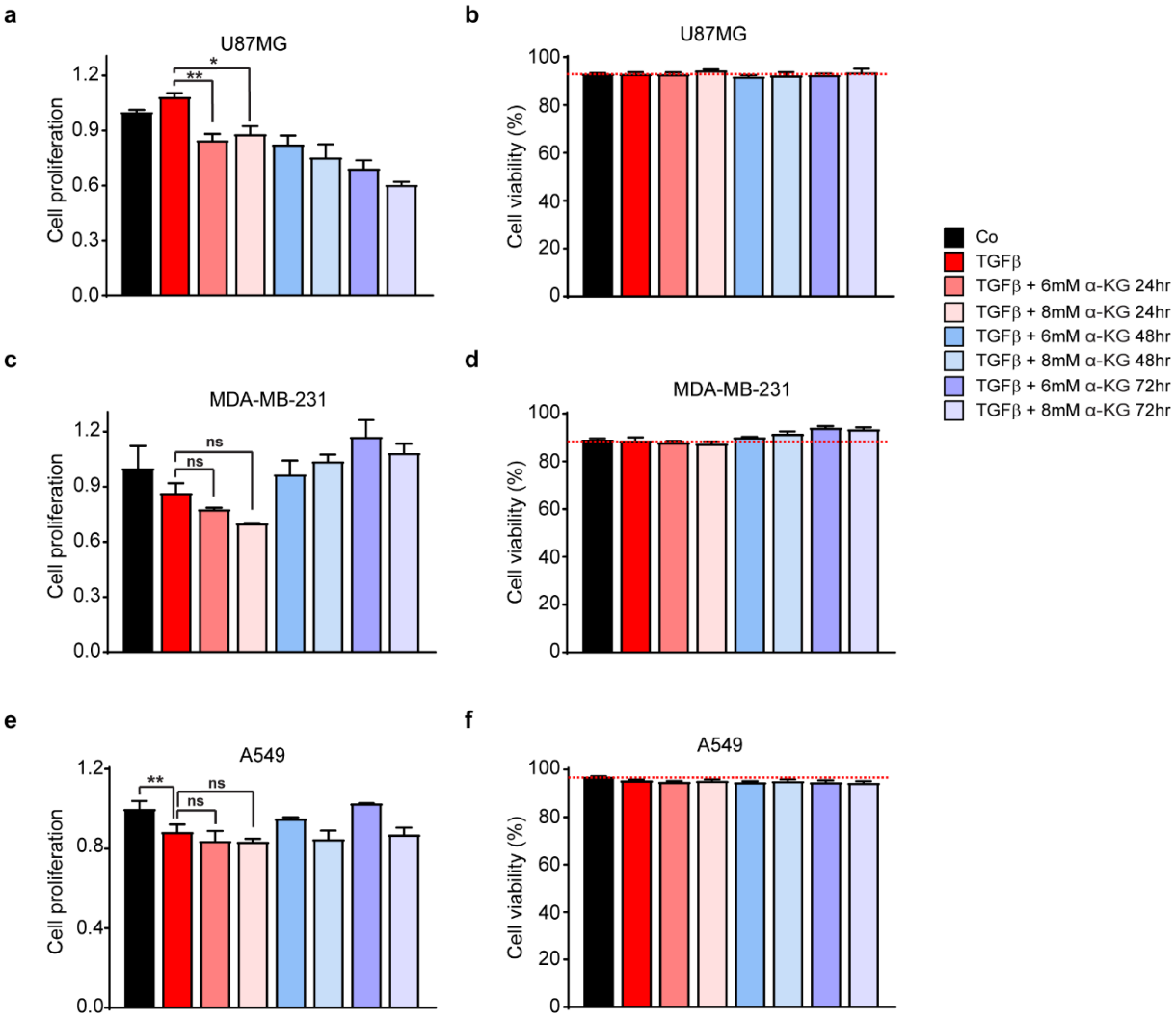

Figure 3.6. α-KG has minor effect on cell proliferation and no remarkable impact on viability. **a,c,e.** Analysis of cell proliferation by end-point cell counting. U87MG (**a**), MDA-MB-231 (**c**), and A549 (**e**) cells were treated with 5 ng/mL TGFβ for 72 h and Dm-α-KG for the last 72, 48, or 24 h in increasing concentration (6 mM and 8 mM), (n=3 biological replicates, representative of two independent experiments). Results are presented as means + SEM. **b,d,f.** Analysis of percentage cell

viability at the end of the described treatment in U87MG (**b**), MDA-MB-231 (**d**), A549 (**f**). Dashed red line is showing the threshold of viability in control conditions. (n=3 biological replicates, representative of two independent experiments). Results are presented as means + standard deviation (SD). Data in (**a,c,e**) are normalized to control condition. Statistical analysis was performed using one-way ANOVA, followed by Dunnett's multiple comparisons test (versus TGFβ treatment). *p<0.05; **p<0.01; ***p<0.001.

3.5. IDH1 regulates EMT and invasion

To confirm prior findings of our laboratory, we reassessed Snail and IDH1 expression at protein and mRNA levels in U87MG control (co) and shIDH1 cells treated with TGFβ for 72 hours (see Fig. 2.2a for experimental setup). Consistent with earlier results (Fig. 1.9), IDH1 expression was effectively depleted in shIDH1 cells, accompanied by a concomitant increase in SNAI1 mRNA levels compared to control cells. This upregulation was further induced upon TGFβ treatment at both protein and mRNA levels (Fig. 3.7a). Moreover, U87MG shIDH1 cells exhibited a significantly enhanced invasive capacity compared to control cells (Fig. 3.7b). Remarkably, additional supplementation with α-KG notably reduced Snail protein levels in U87MG shIDH1 cells (Fig. 3.7c). These findings were further validated across multiple cancer cell lines, including MDA-MB-231-VIM-RFP as a breast cancer model (Fig. 3.7d), as well as LLC1 pCDH B3 (Fig. 3.7e) and LLC1 pCDH B3/ sLP mCherry B2 co and shIDH1 cells (Fig. 3.7f) as lung cancer models. Efficient IDH1 knockdown was confirmed at both protein and mRNA levels, in addition to coinciding Snail upregulation in shIDH1 cells, with or without TGFβ treatment (Fig. 3.7d-f). To achieve robust knockdown of IDH1 in LLC1 cells, various mouse shIDH1 constructs and MOIs were tested (data not shown), among which shIDH1#3 with a MOI of 100 demonstrated the highest knockdown efficiency and was therefore used in subsequent experiments. Although Snai1 mRNA levels were not elevated in LLC1 shIDH1 cells compared to control cells, its expression at protein levels was markedly increased in shIDH1 cells (Fig. 3.7e,f). Notably, among several EMT TFs, Snail was the only TF induced upon IDH1 knockdown and/or TGFβ stimulation in LLC1 pCDH3/ sLP mCherry B2 cells within the 6-hours induction period (Fig. 3.7f).

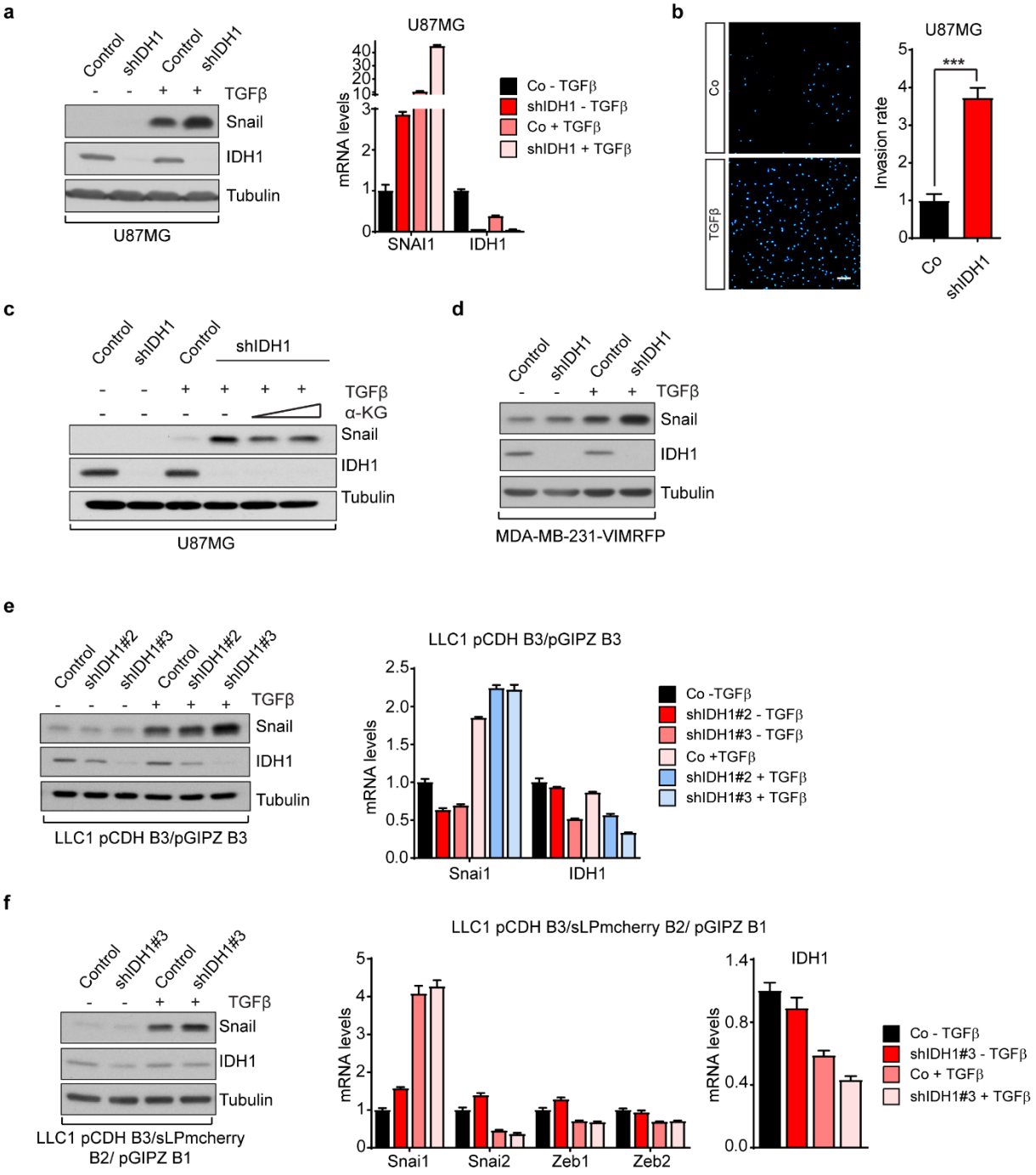

Figure 3.7. IDH1 depletion induces the EMT TF Snail and invasion. a. Snail (SNAI1) and IDH1 expression levels determined using western blotting (left) and RT-qPCR (right) upon IDH1 knockdown in U87MG cells, following 5 ng/mL TGFβ treatment for 72 h. (co) for control cells and (shIDH1) for IDH1-depleted cells. Shown is representative of three independent experiments. **b.** Invasion rates of U87MG co and shIDH1 cells as assessed by modified Boyden chamber assay (n=5-6 biological replicates per condition). Cells were seeded directly in Boyden chamber without pre-treatment and kept for 24 h. Representative images showing invading tumor cells on the left, and quantification of the area covered by invaded cells in the lower compartment, normalized to the area covered by non-invaded cells in the upper compartment is shown on the right. Scale bar indicates 200 µm. **c.** Snail and IDH1 expression levels determined using western blotting in U87MG upon 5 ng/mL TGFβ treatment for 72 h and Dm-α-KG for the last 24 h in increasing concentration (6 mM and 8 mM). **d.** Snail and IDH1 expression levels determined using western blotting following IDH1 knockdown in MDA-MB-231-VIM-RDP cells, upon 5 ng/mL TGFβ treatment for 72 h. **e-f.** Snail (Snai1) and IDH1 expression levels determined using western blotting (left) and RT-qPCR (right) following IDH1 knockdown in LLC1

pCDH B3/ pGIPZ B3 cells (**e**) or LLC1 pCDH B3/ sLP mCherry B2/ pGIPZ B1 (**f**), in addition to examining other EMT TFs in LLC1 pCDH B3/ sLP mCherry B2/ pGIPZ B1 using RT-qPCR upon 5 ng/mL TGFβ treatment for 6 h (**f**). (n=3 technical replicates for all RT-qPCR). RT-qPCR Data are normalized to control condition. Results are presented as means + SEM (**a,b,e,f**). p values were calculated by two-tailed unpaired Student t-test. ***p<0.001.

In contrast, doxycycline-induced overexpression of IDH1 resulted in a clear reduction in Snail protein levels in TGFβ-treated U87MG cells (Fig. 3.8a, see Fig. 2.4a for experimental setup). No appreciable change in Snail and IDH1 levels was detected in corresponding control cells, transduced with pSLIK-GFP, in the presence or absence of doxycycline induction. Snail levels were found to be higher in pSLIK IDH1-transduced cells compared to control cells following TGFβ supplementation, without doxycycline treatment. Importantly, as IDH1 knockdown was previously shown to induce HIF-α stability at protein levels (Fig. 1.9), induced IDH1 overexpression markedly suppressed HIF-1α and HIF-2α levels over extended duration of hypoxic incubation (see Fig. 2.4b for experimental setup), particularly at 6 and 72 hours of low oxygen exposure (Fig. 3.8b). Although doxycycline alone had a slight effect on HIF-α levels in control cells, the diminished levels observed upon doxycycline-induced overexpression of IDH1 remained evident despite this baseline reduction. Taken together, these results establish a role for IDH1 in modulating Snail expression, invasion and HIF-α stability, via regulating α-KG homeostasis.

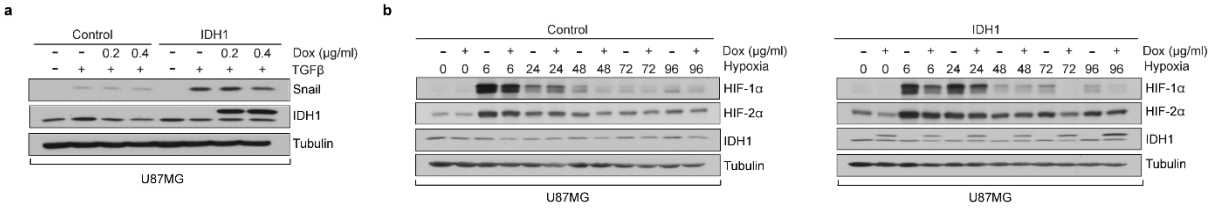

Figure 3.8. IDH1-induced overexpression reduces EMT induction. a. Snail and IDH1 expression levels following IDH1 overexpression in U87MG induced by doxycycline treatment in increasing concentrations (0.2 and 0.4 μg/mL), and 5 ng/mL TGFβ treatment for 72 h. **b.** HIF-1α, HIF-2α, and IDH1 expression levels following induced IDH1 overexpression in U87MG treated with 0.8 μg/mL doxycycline and increasing durations of hypoxia. Shown are representative immunoblots of 2 independent experiments with similar results.

3.6. Snail as a critical mediator of IDH1 depletion-driven invasiveness

To delineate the relationship between IDH1 knockdown, Snail upregulation, and increased invasiveness, we first depleted Snail in both U87MG control and shIDH1 cells. This resulted in pronounced reduction in invasiveness, as assessed by modified Boyden chamber assay (Fig. 3.9a). Indeed, the enhanced invasive capacity conferred by IDH1 depletion was effectively abrogated upon further Snail knockdown. This was coupled with efficient Snail depletion, specifically evident under TGFβ treatment in both U87MG shIDH1 / shSnail, and MDA-MB-231-POR shIDH1 / shSnail cells, determined by western blotting (Fig. 3.9b). To further support these findings, we employed an independent approach utilizing the RNP-based

CRISPR-Cas9 system to knockout Snail in U87MG and MDA-MB-231-POR shIDH1 cells. Snail knockout significantly reversed the enhanced invasiveness characteristic of shIDH1 cells (Fig. 3.9c) and was associated with a substantial reduction in Snail protein levels in both U87MG and MDA-MB-231-POR shIDH1 cells with sgSnail (Fig. 3.9d). Interestingly, partial depletion of Snail expression using sgSnail#1 resulted in a greater reduction in invasiveness compared to complete abolishment of Snail achieved by sgSnail#2 (Fig. 3.9c,d).

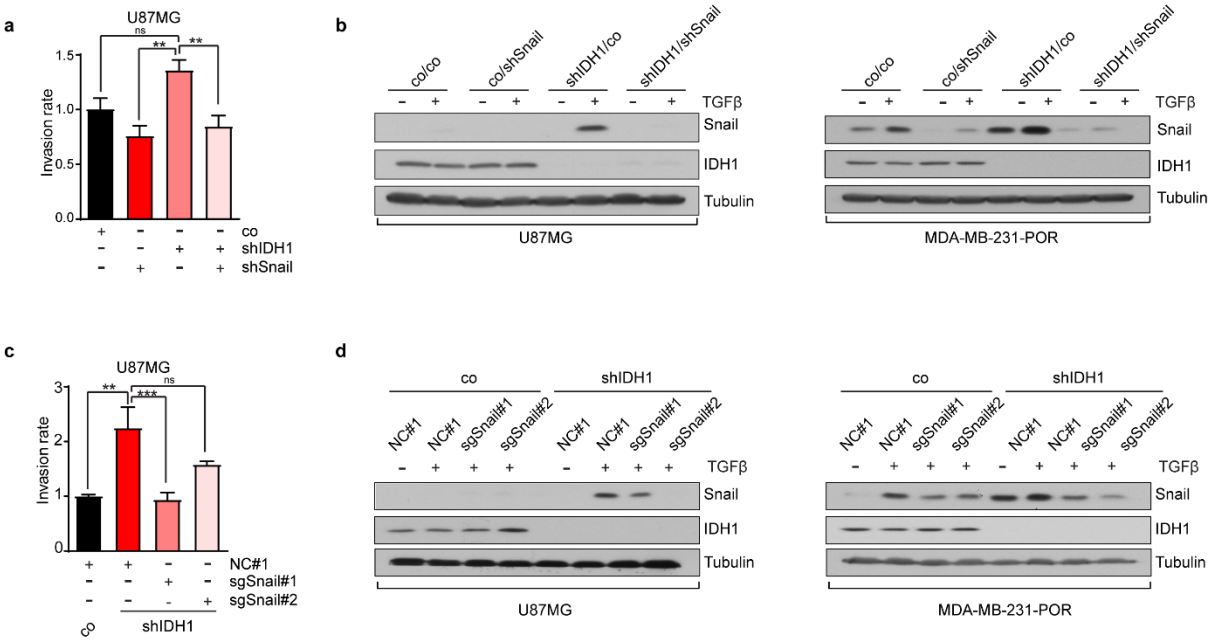

Figure 3.9. Snail knockdown mitigates IDH1 loss-induced invasion. a. Invasion rates of U87MG control (co), shIDH1 and/or shSnail, measured by modified Boyden chamber assay (n=4-5 biological replicates per condition). Cells were directly seeded in Boyden chamber for 24 h without prior pre-treatment. **b.** Snail and IDH1 expression determined by western blot in U87MG and MDA-MB-231-POR co/co, co/shSnail, shIDH1/co, or shIDH1/shSnail cells treated with 5 ng/mL TGFβ for 72 h. Shown is representative for two independent experiments. **c.** Invasion rates of U87MG co or shIDH1 transfected with non-targeting control (NC#1), or sgSNAI1 (#1 or #2), pre-treated with TGFβ for 72 h, followed by incubation in modified Boyden chamber assay for 48 h (n=5-6 biological replicates per condition). **d.** Snail and IDH1 expression determined by western blot in U87MG and MDA-MB-231-POR co and shIDH1 upon SNAI1 knockout under TGFβ treatment for 72 h. Shown is representative for two independent experiments. Data are normalized to control condition. Results are presented as means + SEM (**a**,**c**). Statistical analysis was performed using one-way ANOVA, followed by Dunnett's multiple comparisons test (versus shIDH1 cells). *p<0.05; **p<0.01; ***p<0.001.

To further dissect the transcriptomic consequences of IDH1 depletion, and the potential rescue effect of α-KG supplementation on EMT onset and invasiveness, we performed bulk RNA-seq on U87MG control and shIDH1 cells treated with TGFβ for 72 hours and supplemented with α-KG for either the last 6 or 72 hours (Fig. 2.10d). A comprehensive list of potential Snail target genes was manually curated, and a selected list of genes characteristic of epithelial and mesenchymal states, as well as genes involved in cell adhesion, movement, and invasion, were assessed (Cano and Nieto 2016; Nieto 2002; Yastrebova et al. 2021). A heatmap

of the genes, which are differentially expressed under the described treatment conditions, is shown in Fig. 3.10a. We focused on genes that were upregulated following IDH1 knockdown and/or TGFβ stimulation, and downregulated following α-KG treatment, consistent with changes in SNAI1 expression. Among the genes that fulfilled these criteria were MMP7, MMP13, MMP15, JUP, COL3A1, COL8A2, and COL14A1. We validated the expression profiles of MMP7, MMP15, and COL14A1 at mRNA levels using RT-qPCR, which were found to be clearly upregulated upon IDH1 knockdown and/or TGFβ treatment. Their expression was dramatically reduced following α-KG supplementation for 72 hours, but not 6 hours, exhibiting a comparable expression profile to SNAI1 (Fig. 3.10b). We further determined the effect of TGFβ and α-KG on these potential Snail targets in parental cells by RT-qPCR (Fig. 3.10c). MMP7 expression regulation by both TGFβ and α-KG was inconsistent across the different cell lines, whereas MMP15 and COL14A1 were robustly upregulated following TGFβ treatment, and reduced upon α-KG supplementation. Interestingly, COL14A1 seems to be mainly expressed in GBM cells (Fig. 3.10c). Collectively, these results support Snail's essential role in mediating EMT and invasion in IDH1-deficient cells, potentially through MMPs and collagens, with Snail depletion recapitulating the suppressive effect of α-KG.

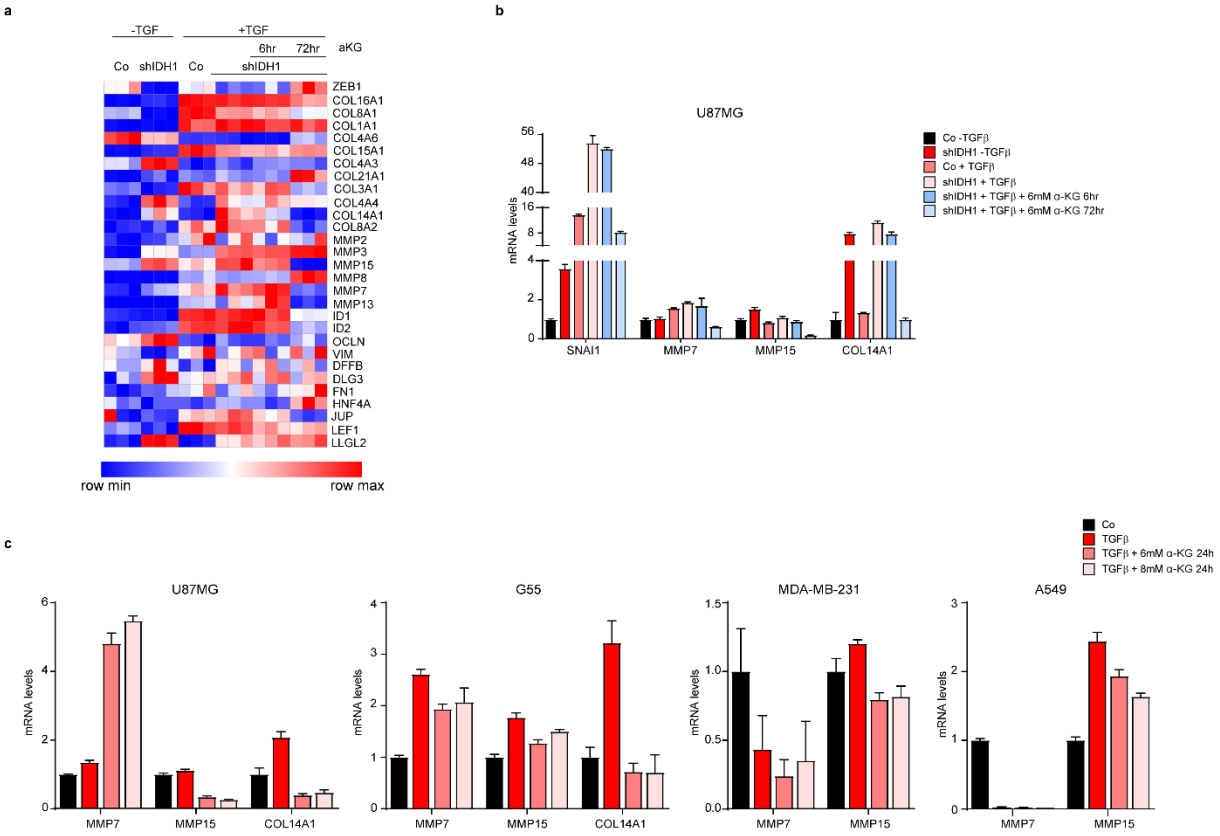

Figure 3.10. α-KG inhibits Snail transcriptional regulation and suppresses EMT program. a. Heatmap derived from bulk RNA-seq depicting the differential expression of a selected Snail downstream targets in U87MG co and shIDH1 cells upon treatment with 5 ng/mL TGFβ for 72 h in addition to 6 mM Dm-α-KG treatment for the last 6 h or 72 h. Columns represent individual replicates

(n=3 biological replicates), grouped by conditions, rows represent DEG, color denotes row scaled (Z-score) expression values, with darkest blue as lowest expression and darkest red as highest). **b.** RT-qPCR analysis of the expression of SNAI1, in addition to MMP7, MMP15 and COL14A1 mRNA levels as potential downstream targets of Snail TF, in U87MG co and shIDH1 cells under the same indicated conditions, (n=3 technical replicates). Shown are representative examples of two independent experiments with similar results. **c.** RT-qPCR analysis of the expression of MMP7, MMP15 and COL14A1 mRNA levels in U87MG, G55, MDA-MB-231, and A549 cells upon treatment with 5 ng/mL TGFβ for 72 h in addition to increasing concentrations of Dm-α-KG treatment (6 mM and 8mM) for the last 24 h, (n=3 technical replicates). Data are normalized to control condition. Results are presented as means + SEM (**b,c**).

3.7. α-KG negatively regulates Snail expression partially through the ATP synthase-mTORC1-c-Myc axis

Previous results in our lab identified that Snail levels are regulated by the IDH1-α-KG-PHD-HIF signaling pathway (Fig. 1.9). However, HIF1/2-α knockdown only resulted in partial Snail reduction at both protein and mRNA levels (Bögürcü-Seidel 2018), suggesting that additional α-KG-dependent mechanisms might also contribute to Snail regulation. Given that α-KG has been shown to directly inhibit ATP synthase, thereby repressing mTORC1 signaling (Chin et al. 2014), we investigated whether the IDH1-ATP synthase-mTORC1 signaling pathway plays a role in modulating Snail expression.

First, we investigated the impact of α-KG on ATP levels as an indirect readout for ATP synthase activity, by supplementing TGFβ-treated U87MG cells with increasing concentrations of α-KG for 3 hours (see Fig. 2.9 for experimental setup). α-KG significantly reduced both ATP/ADP ratio (Fig. 3.11a) as well as ATP levels (Fig. 3.11b). The effect was comparable to that of oligomycin, an established ATP synthase inhibitor. A similar trend was observed in U87MG co and shIDH1 cells pre-treated with TGFβ for 72 hours, where supplementation with increasing concentrations of α-KG for 3 hours dramatically reduced ATP levels compared to shIDH1 cells treated with only TGFβ. Co-treatment of oligomycin with α-KG further reduced ATP levels. Notably, significantly lower ATP levels were observed in TGFβ-treated shIDH1 cells as compared to control cells (Fig. 3.11c). Taken together, the results revealed a potent and quick inhibitory effect of α-KG on ATP synthase.

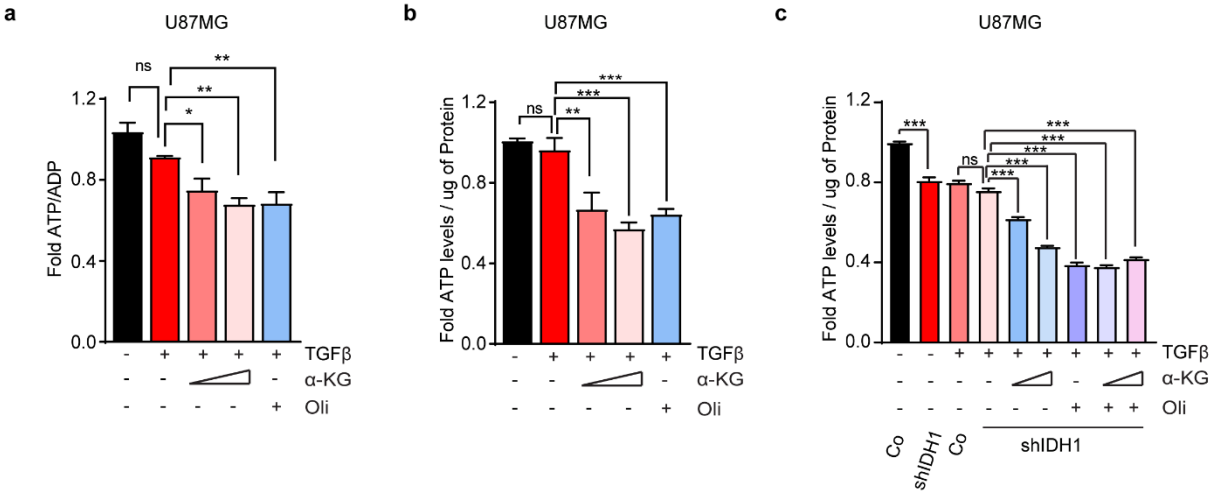

Figure 3.11. α-KG reduces ATP levels and the ATP/ADP ratio. a. Effect of Dm-α-KG on ATP/ADP ratio upon treatment of U87MG with 5 ng/mL TGFβ for 72 h and Dm-α-KG treatment (6 mM and 8 mM) for the last 3 h in U87MG, Oligomycin (Oli, 5μM) was used as a positive control. Results are from 6 biological replicates from two independent experiments. **b.** Effect of Dm-α-KG on ATP levels upon treatment of U87MG with 5 ng/mL TGFβ for 72 h and Dm-α-KG treatment (6 mM and 8 mM) for the last 3 h in U87MG. Oli was used as a positive control. Values were normalized to protein concentration in μg. Results are from 6 biological replicates from two independent experiments. **c.** Effect of Dm-α-KG on ATP levels upon treatment of U87MG co and shIDH1 with 5 ng/mL TGFβ for 72 h and Dm-α-KG treatment (6 mM and 8 mM) for the last 3 h. Oli was used as a positive control. Values were normalized to protein concentration in μg. Results are presented from four biological replicates. Data are normalized to control condition. Results are presented as means + SEM. Statistical analysis was performed using one-way ANOVA, followed by Dunnett's (**a,b**; versus TGFβ treatment) or Tukey's (**c**) multiple comparisons test when appropriate. *p<0.05; **p<0.01; ***p<0.001.

Next, we examined mTORC1 activity by western blot analysis of the phosphorylation status of its downstream effectors, P70S6K and 4EBP1, following treatment with TGFβ for 72 hours, and increasing concentrations of α-KG in the last 24 hours in U87MG, MDA-MB-231, and A549 cells (Fig. 3.12a-c). Interestingly, in U87MG, TGFβ robustly increased phosphorylation, and thus activity of both effectors, which were suppressed by α-KG supplementation in parallel with changes in Snail protein levels (Fig. 3.12a). In contrast, changes in phosphorylation of only 4-EBP1 but not P70S6K were evident in MDA-MB-231 and A549 cells, under the indicated conditions (Fig. 3.12b,c). Moreover, a marked increase in P70S6K phosphorylation was observed following TGFβ treatment in MDA-MB-231, which was reduced only upon 6 mM α-KG addition (Fig. 3.12b). As ATP can activate mTORC1 directly through its binding motif in the active site of mTOR protein, and indirectly by inhibiting the activity of AMPK, we also determined the activation or inhibition of AMPK phosphorylated targets TSC2, and Raptor, respectively. Upon AMPK activation after ATP:AMP ratio reduction, phosphorylation of TSC2 on Ser1387 is achieved, enabling TSC2 inhibitory effect on mTOR. Moreover, active AMPK phosphorylates Raptor on Ser792, disturbing its binding to mTOR thus halting the activity of mTORC1 complex. Activating phosphorylation of TSC2 was evident in both MDA-MB-231 and A549 (Fig. 3.12b,c), but not U87MG (Fig. 3.12a), upon

α-KG treatment. Conversely, inactivating phosphorylation of Raptor was only observed in A549 (Fig. 3.12c). Moreover, no change in ERK phosphorylation was observed across the cell lines. Conversely, TGFβ-treatment-induced increased phosphorylation of AKT was observed in A549 cells (Fig. 3.12c), while a decrease of p-AKT was apparent in MDA-MB-231 cells (Fig. 3.12b). However, α-KG supplementation reduced p-AKT levels in both cell lines (Fig. 3.12b,c).

As c-Myc and FoxK1 are mTORC1-regulated transcription factors, and established SNAI1 activators (Chen et al. 2017; Smith et al. 2009; H. Xu et al. 2018), we also sought to examine their expression. α-KG suppressed TGFβ-induced c-Myc in all three cell lines, whereas TGFβ-upregulated FoxK1 levels remained unchanged upon α-KG treatment (Fig. 3.12a-c), suggesting that c-Myc may link α-KG-ATP synthase-mTORC1 signaling to Snail regulation.

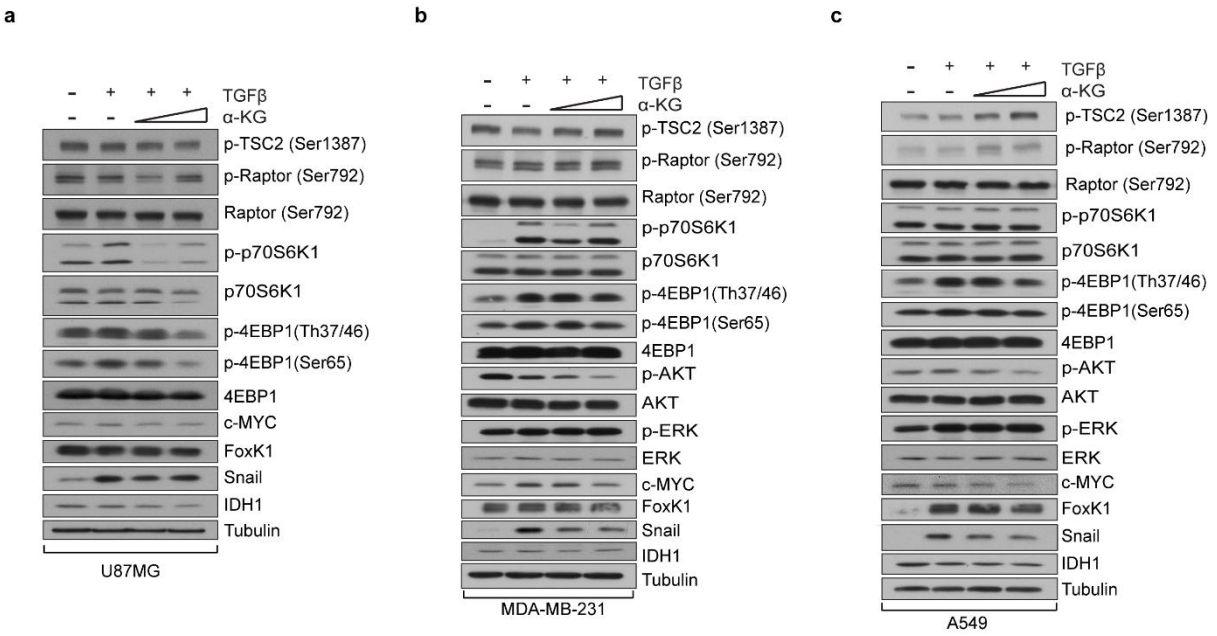

Figure 3.12. α-KG simultaneously reduces Snail levels, ATP synthase-mTORC1 activity and c-Myc levels. a-c. Western blot analyses of the activation and phosphorylation levels of mTORC1 effectors P70S6K and 4EBP1, in addition to activating phosphorylation of TSC2, an upstream negative regulator of mTORC1, and an inactivating phosphorylation of Raptor, an mTOR binding partner. c-Myc and FoxK1 TF levels, and activity status of upstream regulators of mTORC1, AKT and ERK are also shown. U87MG (**a**), MDA-MB-231 (**b**), and A549 (**c**) cells were treated with 5 ng/mL TGFβ for 72 h and Dm-α-KG (6 mM and 8 mM) for the last 24 h in. Shown are representatives of two independent experiments.

To further confirm our findings in IDH1-depleted cells and emphasize the α-KG-dependent control of Snail, we pharmacologically targeted key members of the TGFβ-mTORC1 signaling axis in U87MG shIDH1 cells under TGFβ treatment (Fig. 3.13a-c). Intriguingly, treating cells with a TGFβ inhibitor (SB431542), PI3K inhibitor (LY294002) or

mTOR inhibitor (Rapamycin), effectively blocked TGFβ- and IDH1-knockdown-induced Snail expression and mTORC1 activation, while MEK inhibition (U0126) had no effect on Snail expression (Fig. 3.13a,c). Similarly, treatment with either the ATP synthase inhibitor oligomycin, or dorsomorphin, an ATP-competitive inhibitor of AMPK which also inhibits the BMP/AKT pathway, attenuated mTORC1 signaling, and decreased Snail levels (Fig. 3.13b,c). Interestingly, AKT and ERK were activated following both IDH1 knockdown and TGFβ stimulation and were downregulated following the pharmacological inhibition of their upstream signaling molecules (Fig. 3.13a-c). Collectively, these results demonstrate that α-KG dependent Snail regulation could be driven in part by the ATP-synthase-mTORC1 signaling axis. Moreover, our findings highlight that Snail regulation is also mediated by TGFβ-PI3K-AKT-mTORC1 but not TGFβ-MEK-ERK-mTORC1 signaling.

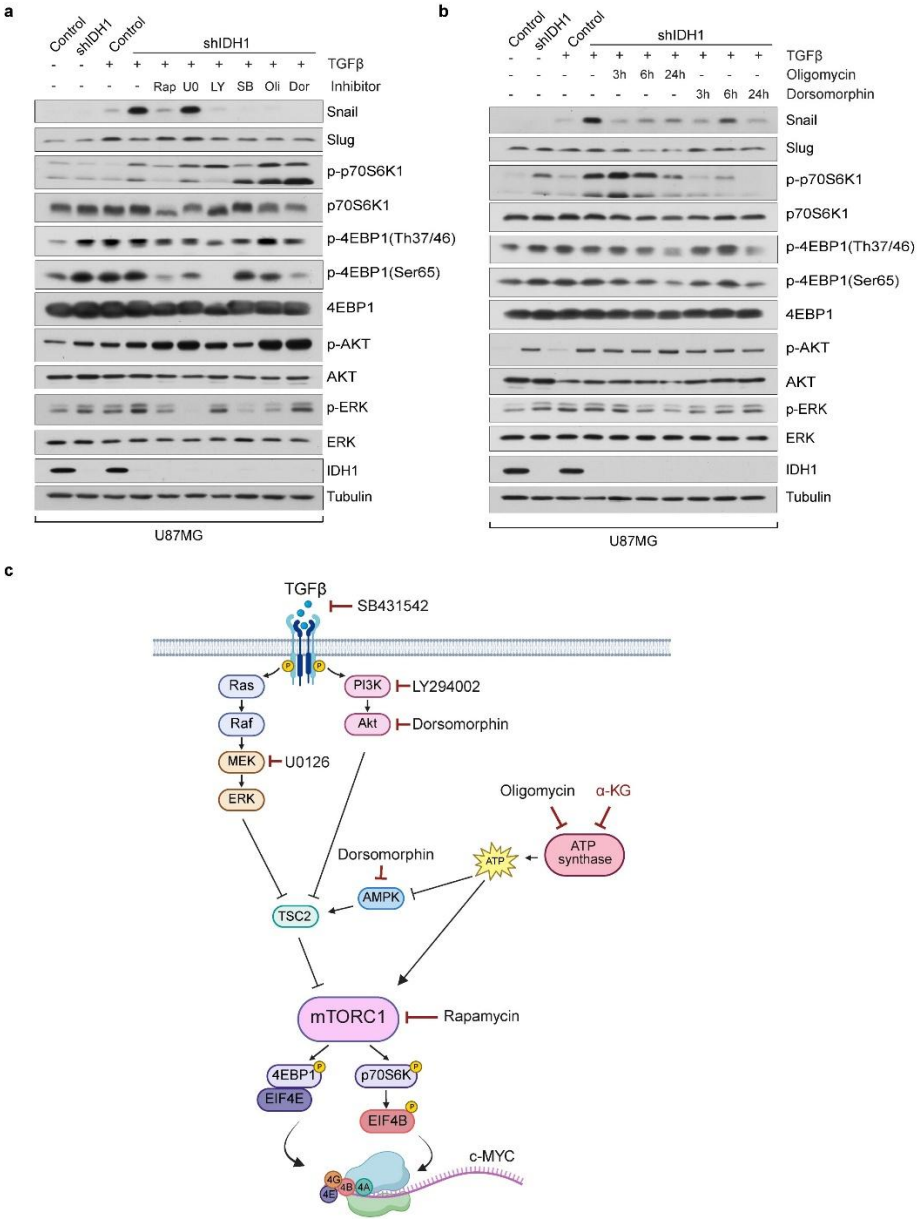

Figure 3.13. Snail regulation is mediated through two pathways converging on mTORC1. a. The activity of upstream and downstream factors of mTORC1 signaling and Snail expression levels were determined using western blotting upon inhibition of several factors in the TGFβ-mTORC1 signaling cascade using Rapamycin (Rap, 10μM), U0126 (U0, 10μM), LY294002 (LY, 20μM), SB431542 (SB, 10μM), Oligomycin (Oli, 5μM), and Dorsomorphin (Dor, 5μM) in addition to treatment with 5 ng/mL TGFβ for 72 h. The treatments with inhibitors started 2 hours prior to TGFβ addition. Shown are representative examples of two independent experiments **b.** The activity of upstream and downstream factors of mTORC1 signaling and Snail expression levels were determined using western blotting upon inhibition of several factors in the TGFβ-mTORC1 signaling cascade using Oligomycin (Oli, 5μM), and Dorsomorphin (Dor, 5μM) along with TGFβ treatment (5 ng/mL) for 3, 6, or 24 h. The treatments with the inhibitors started 5 min prior to TGFβ addition. Shown are representative examples of two independent experiments. **c.** Diagram showing the TGFβ-mTORC1-c-Myc and α-KG-ATP synthase-mTORC1-c-Myc axis and the targets of the inhibitors used in (**a,b**). Created by Biorender.com.

3.8. α-KG negatively regulates Snail expression synergistically through PHD-HIF and ATP synthase-mTORC1-c-Myc pathways

c-Myc, FoxK1 and FoxK2 are direct targets of mTOR signaling and all three TFs are known to bind regulatory regions of the SNAI1 gene (Chen et al. 2017; Smith et al. 2009; H. Xu et al. 2018). To test whether they could mediate Snail expression upon IDH1 knockdown and TGFβ stimulation, we transiently transfected U87MG shIDH1 cells with siRNAs targeting each factor, followed by TGFβ treatment. Among the three factors, only c-Myc downregulation resulted in partial reduction in Snail expression at both protein and mRNA levels (Fig. 3.14a,b). In contrast, despite efficient silencing of FoxK1, and partial knockdown of FoxK2, Snail levels remained largely unaffected. We also confirmed the knockdown efficiency of these transcription factors at mRNA levels by RT-qPCR (Fig. 3.14c).

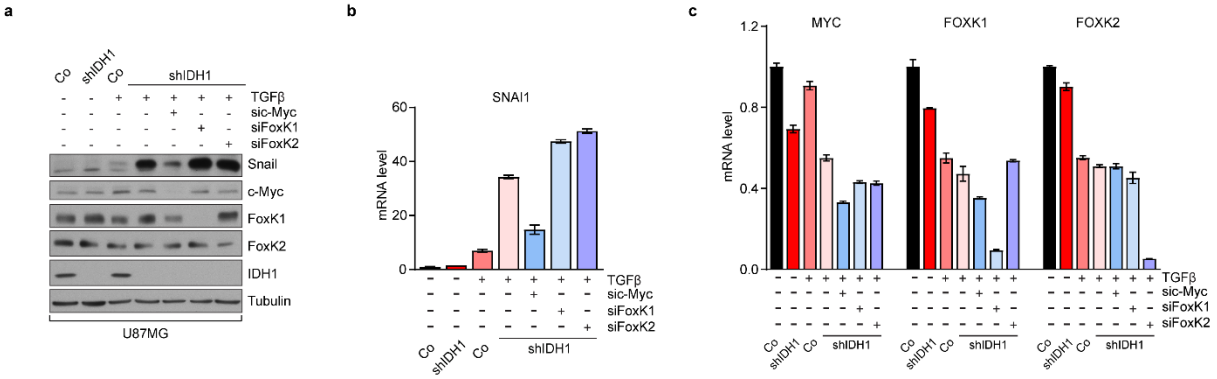

Figure 3.14. α-KG controls Snail levels partially through c-Myc. a-b. Effects of siRNA-mediated cMyc, FoxK1, and FoxK2 knockdown on Snail levels under 5 ng/mL TGFβ treatment for 48 h, determined by immunoblotting (**a**) and RT-qPCR (**b**). **c**. RT-qPCR analysis of MYC, FOXK1, FOXK2 knockdown efficiency in U87MG shIDH1 cells under TGFβ treatment for 48 h. Data in (**b,c**) are from n=3 technical replicates within a single experiment. siRNA knockdown experiments were conducted by Sascha Seidel. Shown are representative examples of three independent experiments. Data are normalized to control condition. Results are presented as means + SEM (**b,c**).

To further assess the potential cooperative contribution of HIF-α and c-Myc in regulating Snail level, we silenced HIF-1/2α, c-Myc, or the combination of them in U87MG shIDH1 cells using siRNAs, followed by TGFβ stimulation. Snail siRNA served as a positive

control. Interestingly, simultaneous depletion of HIF-1/2α and c-Myc resulted in further abrogation of Snail expression at both protein and mRNA levels, compared to individual knockdowns, as determined by western blotting and RT-qPCR (Fig. 3.15a-c). Taken together, these data and previous data from the lab support a model in which α-KG inhibits Snail levels through converging pathways, including the PHD-HIF axis, as well as ATP synthase-mTORC1-c-Myc signaling.

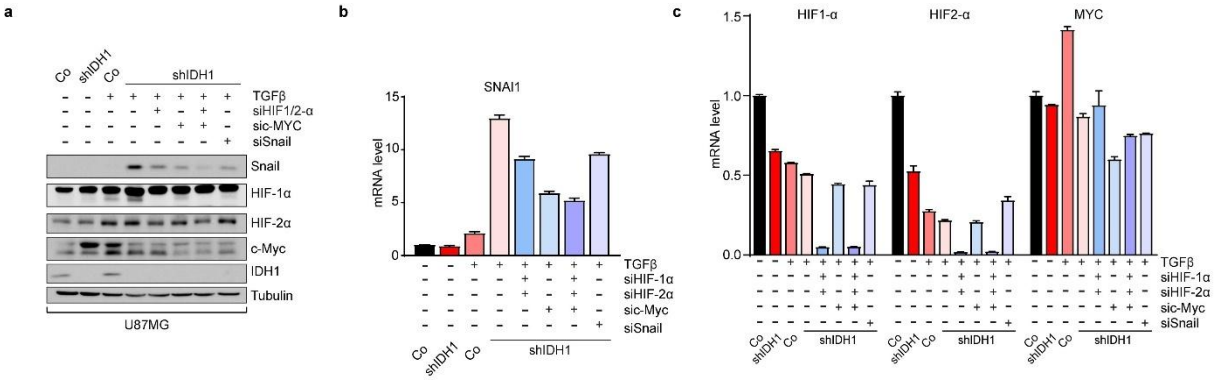

Figure 3.15. α-KG suppresses Snail levels through converging pathways. a-b. Effects of siRNA-mediated HIF-1/2α (HIF-1α and HIF-2α) and/or c-Myc knockdown on Snail levels under 5 ng/mL TGFβ treatment for 48 h, determined by immunoblotting (**a**) and RT-qPCR (**b**). **c**. RT-qPCR analysis of HIF-1α, HIF-2α, and MYC knockdown efficiency under TGFβ for 48 h. Data in (**b,c**) are from n=3 technical replicates within a single experiment. Shown are representative examples of two independent experiments. Data are normalized to control condition. Results are presented as means + SEM (**b,c**).

3.9. IDH1 depletion-mediated Snail regulation occurs at the transcriptional level

Given our interest in SNAI1 gene regulation and considering α-KG as a co-substrate for several JmjC domain-containing KDMs, we initially examined global histone modification changes in MDA-MB-231 and A549 cells, following TGFβ and α-KG treatment via western blotting. No gross changes were observed under either condition (Fig. 3.16a,b), suggesting that α-KG-dependent chromatin changes are more subtle and require locus-specific investigations.

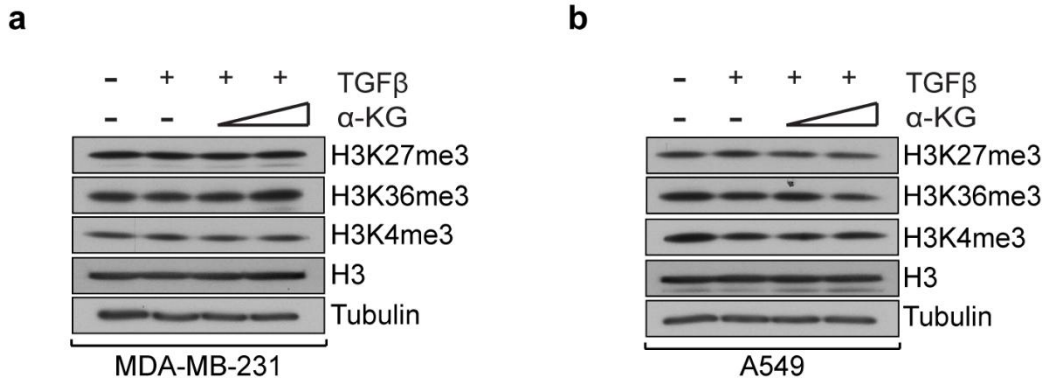

Figure 3.16. α-KG supplementation does not affect global pattern of histone modification. a-b. Western blot analyses of H3K27me3, H3K36me3, and H3K4me3 levels in MDA-MB-231 (**a**) and A549 (**b**) upon treatment with 5 ng/mL TGFβ for 72 h and Dm-α-KG treatment (6 mM and 8 mM) for the last 24 h (n=1).

To evaluate chromatin changes at the SNAI1 locus, we first performed ChIP-qPCR in MDA-MB-231 cells treated with TGFβ (Fig. 2.14a), using an H3K27ac antibody and primer sets spanning regions associated with active chromatin remodeling and known c-Myc and HIF binding sites (Fig. 3.17a), primers were designed based on previous studies (Smith et al. 2009; Zhang et al. 2013; Zhu et al. 2013), or using the JASPAR 2000 transcription factor binding site database track in UCSC genome browser. This analysis revealed an enrichment of the active histone mark H3K27ac at the proximal TSS region, and at nearby E-box/HRE elements (Fig. 3.17b), which are established binding sites for c-Myc and HIF TFs.

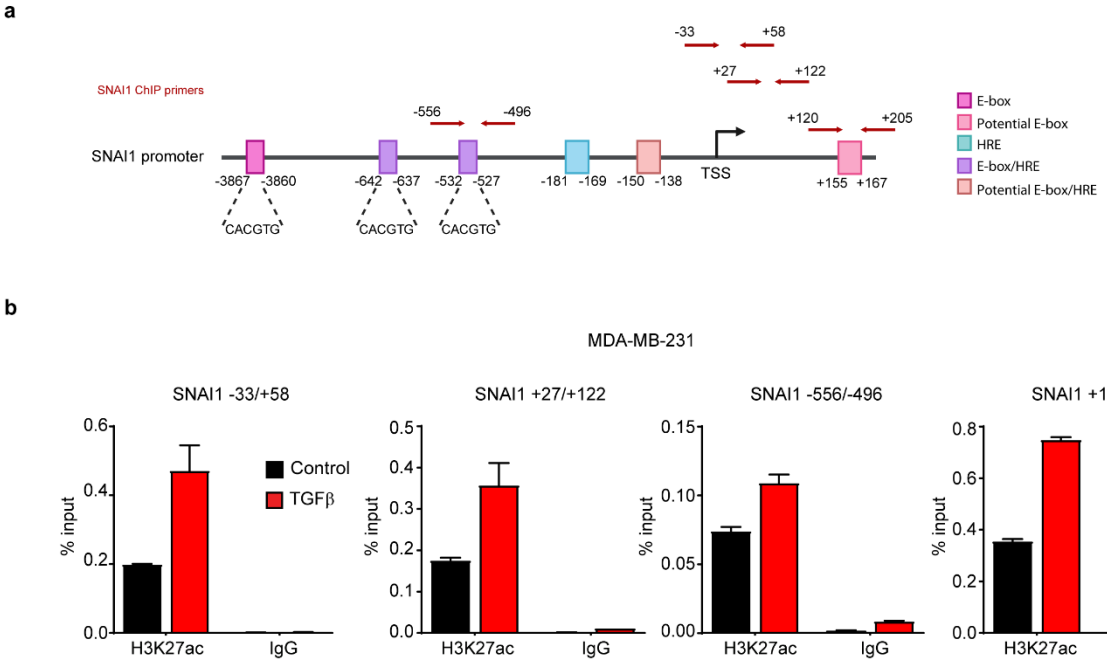

Figure 3.17. TGFβ-induced chromatin regulation the SNAI1 gene promoter. a. Schematic illustration of ChIP-qPCR primers targeting regions up and downstream of the SNAI1 gene TSS. Established E-Boxes and HREs are shown, or identified by sequence analyses (potential E-Box, E-Box/HREs) are indicated. Created by Biorender.com. **b.** ChIP-qPCR analysis of the H3K27ac active chromatin marker at the Snail promoter in MDA-MB-231 upon treatment with 5 ng/mL TGFβ for 72 h. Shown are representative examples of two independent experiments. Results are presented as means + SEM.

We next conducted ChIP-qPCR in U87MG control and shIDH1 cells treated with TGFβ and α-KG for 72 hours (Fig. 2.14b) using the primers depicted in Fig. 3.17a. Here, we also observed increased enrichment of the active histone marks H3K27ac and H3K4me3 around the TSS (Fig. 3.18a), as well as at c-Myc and HIF binding regions (Fig. 3.18b). This enrichment was enhanced upon both IDH1 depletion and TGFβ treatment and was attenuated upon α-KG supplementation. In contrast, the repressive histone mark H3K27me3 showed no substantial changes across most regions tested, except for an α-KG-induced enrichment at SNAI1+120/+205, which harbors a putative c-Myc E-box element (Fig. 3.18b, right). In line with this, H3K27me3 occupancy was at this site higher in U87MG co compared to U87MG

shIDH1, regardless of TGFβ treatment. These findings indicate that IDH1 depletion and/or TGFβ treatment contribute to gene promoter activation at the SNAI1 locus, whereas α-KG acts to reverse these changes.

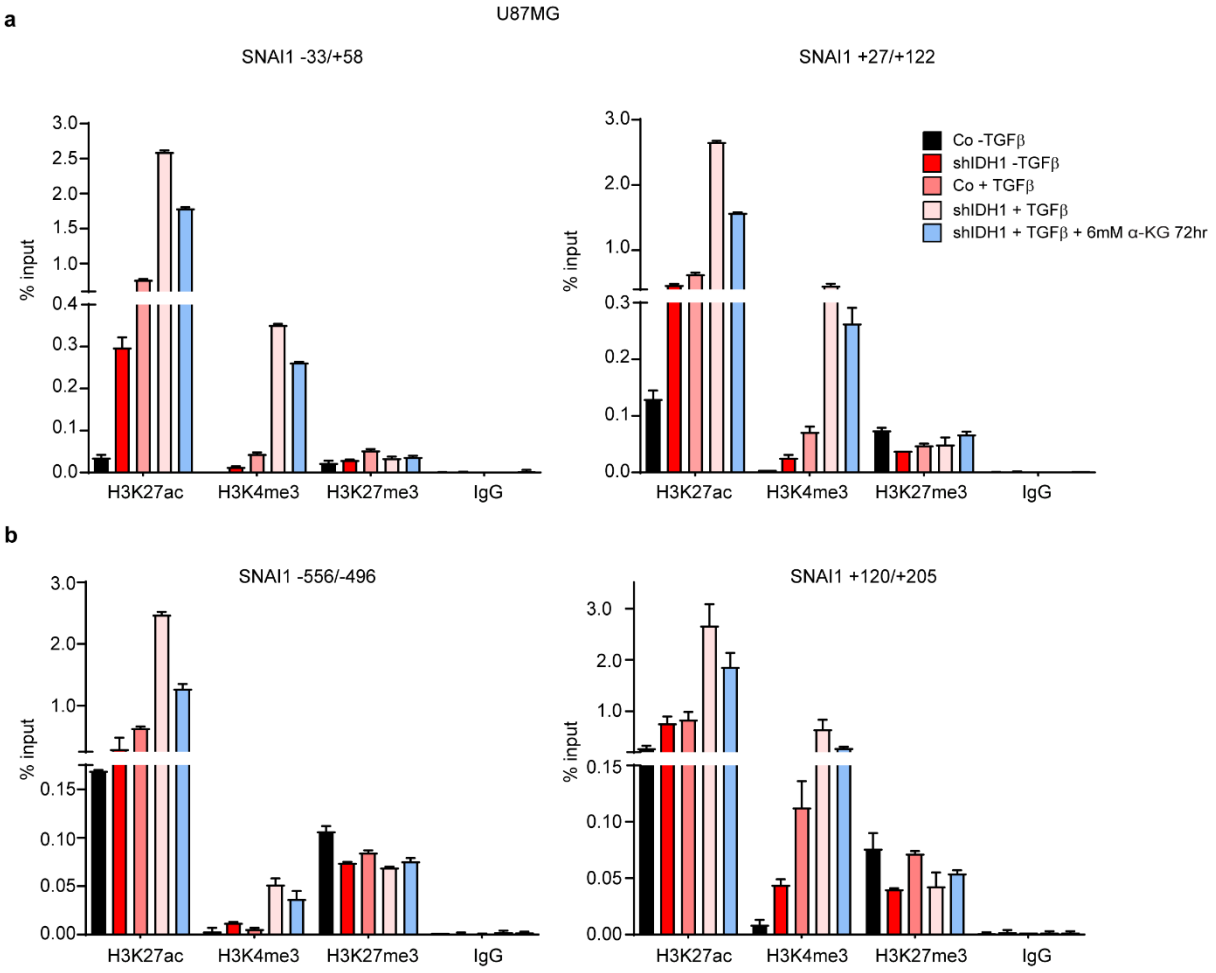

Figure 3.18. α-KG regulates Snail at promoter level. a. Promoter-proximal and **b.** promoter-distal ChIP-qPCR analyses of the active chromatin marks H3K27ac, H3K4me3, and the inactive chromatin mark H327me3 at the SNAI1 gene locus in U87MG co and shIDH1 cells upon 5 ng/mL TGFβ and 6 mM Dm-α-KG treatments for 72 h. Shown are representative examples of two independent experiments for H3K27ac and IgG. Treatment, ChIP and Snail -33/+58 qPCR were conducted by Nuray Bögürcü-Seidel. Data are presented as means + SEM.

Due to unsuccessful pulldown of c-Myc and HIF-bound DNA fragments in ChIP experiments, we only mined publicly available ChIP-seq datasets from the GEO database, and visualized the data aligned with the SNAI1 locus and active histone marks using the UCSC Genome Browser with the integrated ENCODE regulation track. This analysis revealed c-Myc enrichment at regions upstream of SNAI1 in various human cancer cell lines, coinciding with elevated levels of H3K27ac and H3K4me3 (Fig. 3.19a), indicative of transcriptionally active chromatin. Similarly, HIF-1β, HIF-1α, and HIF-2α ChIP signals were detected in close proximity to c-Myc binding regions, overlapping with E-Box/HRE elements and with sites marked by H3K27ac and H3K4me3. In contrast to HIF-2α, however, HIF-1β and HIF-1α

signals appear to be either dispersed across the gene or lack specificity (Fig. 3.19b). These findings support the hypothesis that both c-Myc and HIFs can directly regulate Snail transcription through interaction with promoter elements, potentially acting in combination with the epigenetic activation observed under TGFβ stimulation and/or IDH1 knockdown.

Figure 3.19. c-Myc and HIFs bind to the Snail promoter. a. Visualization of c-Myc binding on Snail promoter using c-Myc ChIP-seq datasets obtained from the GEO repository and imported in UCSC custom tracks. GEO accession numbers, as well as cell types are shown on the left. **b.** Visualization of HIF-1β, HIF-1α, and HIF-2α binding on Snail promoter using their respective ChIP-seq datasets obtained from GEO repository and imported in UCSC custom tracks. GEO accession numbers, as well as cell types are shown on the left, HIF labels are on the right. Layered H3K4me3 and H3K27ac tracks in (**a**) and (**b**) were obtained from ENCODE regulation tracks.

Next, we assessed SNAI1 promoter activity using a dual luciferase assay. For this, we used a firefly luciferase reporter under the control of SNAI1 promoter sequences, labeled as pGL3_Snail#1 and pGL3_Snail#2, with the latter also encompassing the TSS. The reporters were co-transfected with a Renilla luciferase control in U87MG co and shIDH1 cells (Fig. 3.20a). We observed an increase in SNAI1 promoter activity in shIDH1 relative to control cells,

both in the presence or absence of TGFβ, with TGFβ eliciting an almost two-fold increase in activity (Fig. 3.20b,c; see Fig. 2.5a,b for experimental setup). Empty pGL3-basic without our promoter of interest was used as a control. Although a four-fold increase in activity of pGL3 vector in shIDH1 cells under TGFβ was observed (Fig. 3.20b), however, there was an almost seven-fold and twenty-fold increase in SNAI1 promoter activity in co and shIDH1 cells, respectively. Moreover, no change in pGL3-basic was observed in hypoxia, normoxia, non-TGFβ treated cells (data not shown).

Additionally, Snail promoter activity was robustly upregulated upon IDH1 knockdown and/or hypoxic exposure (Fig. 3.20d; Fig. 2.5c). Most importantly, α-KG supplementation for 3 hours significantly suppressed Snail promoter activity in U87MG shIDH1 in the absence of TGFβ pre-treatment (Fig. 3.20e; Fig. 2.5d). Interestingly, transient knockdown of both HIF-1/2α and c-Myc dramatically reduced Snail promoter activity in U87MG shIDH1 cells upon TGFβ treatment for 24 hours using pGL3_Snail#2 (Fig. 3.20f; Fig. 2.6a), and after 48 hours of TGFβ stimulation using pGL3_Snail#1 (data not shown), as well as under hypoxic conditions (Fig. 3.20g; Fig. 2.6b). Taken together, ChIP-qPCR results, ChIP-seq data analyses, as well as dual luciferase assay results indicate that Snail transcription is regulated through TGFβ supplementation, hypoxia exposure, and most importantly, IDH1 depletion. They also confirm a robust α-KG-dependent regulation of the SNAI1 promoter in which the HIF and c-Myc TFs are involved.

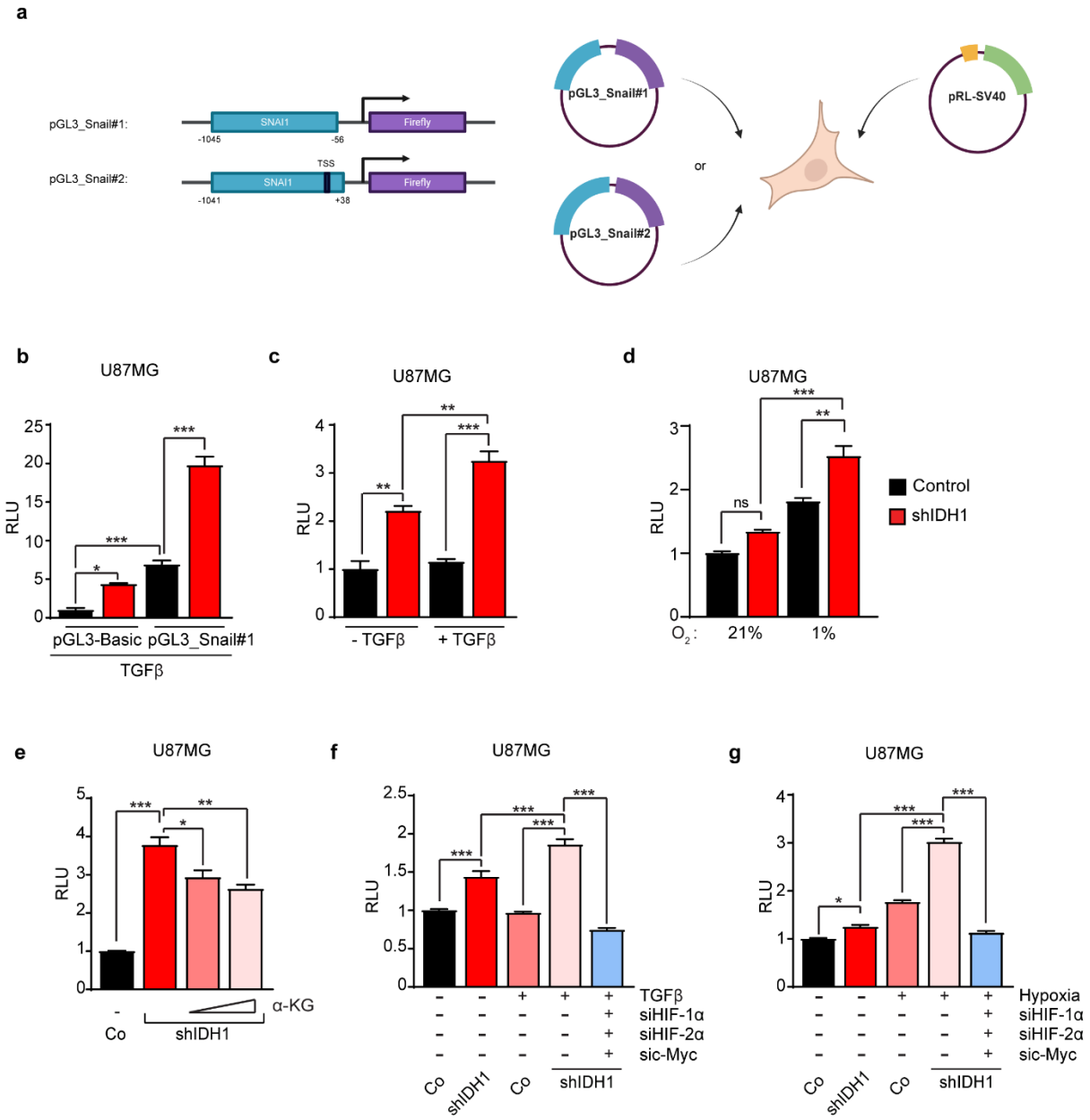

Figure 3.20. The Snail promoter is regulated by IDH1 depletion, TGFβ, and hypoxia. a. Schematic of the dual-luciferase reporter assay used to assess Snail promoter activity created by Biorender.com. Two Snail promoter–Firefly luciferase constructs were generated: pGL3_Snail#1 (–1045 to –56) and pGL3_Snail#2 (–1041 to +38). Each construct was co-transfected with a Renilla luciferase control plasmid into U87MG control and shIDH1 cells. **b.** Snail promoter activity was measured in U87MG co and shIDH1 using pGL3_Snail#1 upon treatment with 5 ng/mL TGFβ for 48 h. pGL3-basic was used as a control. Results are presented from three biological replicates. **c**. Snail promoter activity was measured in U87MG co and shIDH1 using pGL3_Snail#2 upon treatment with 5 ng/mL TGFβ for 6 h. Results are presented from three biological replicates. **d.** Snail promoter activity was measured in U87MG co and shIDH1 under normoxic (21% O_2) or hypoxic (1% O_2) conditions for 24 h, using pGL3_Snail#1. Results are presented from three biological replicates. **e.** Snail promoter activity was measured in U87MG co and shIDH1 upon Dm-α-KG treatment (6 mM and 8 mM) for 3 h, using pGL3_Snail#2. Results are presented from three biological replicates. **f.** Snail promoter activity was measured in U87MG co and shIDH1 after transfection with siRNAs against HIF1/2-α and c-Myc, followed by dual luciferase assay using pGL3_Snail#2. Cells were treated with 5 ng/mL TGFβ for 24 h. Results are presented from three biological replicates. **g.** Snail promoter activity was measured in U87MG co and shIDH1 after transfection with siRNAs against HIF1/2-α and c-Myc, followed by dual luciferase assay in which pGL3_Snail#1 was introduced. Cells were exposed to 1% O_2 for 48 h. Results

are presented from three biological replicates. Data are normalized to control condition. Results are presented as means + SEM. Statistical analysis was performed using two-tailed unpaired Student t-test (**b**), one-way ANOVA, followed by Tukey's (**c,d,f,g**) or Dunnett's (**e**; versus TGFβ treatment) multiple comparisons test when appropriate. *p<0.05; **p<0.01; ***p<0.001.

3.10.α-KG producing and consuming enzymes are regulated by TGFβ treatment

We observed that TGFβ treatment markedly suppressed the expression of IDH1, the cytosolic isoform of isocitrate dehydrogenase, at both protein and mRNA levels, as demonstrated by western blotting and RT-qPCR analyses in U87MG, MDA-MB-231, and A549 cells (Fig. 3.21a). In contrast, the mRNA levels of the mitochondrial isoforms, IDH2 and IDH3 subunit alpha (IDH3A), remained largely unaltered following TGFβ treatment, as assessed by RT-qPCR (Fig. 3.21b).

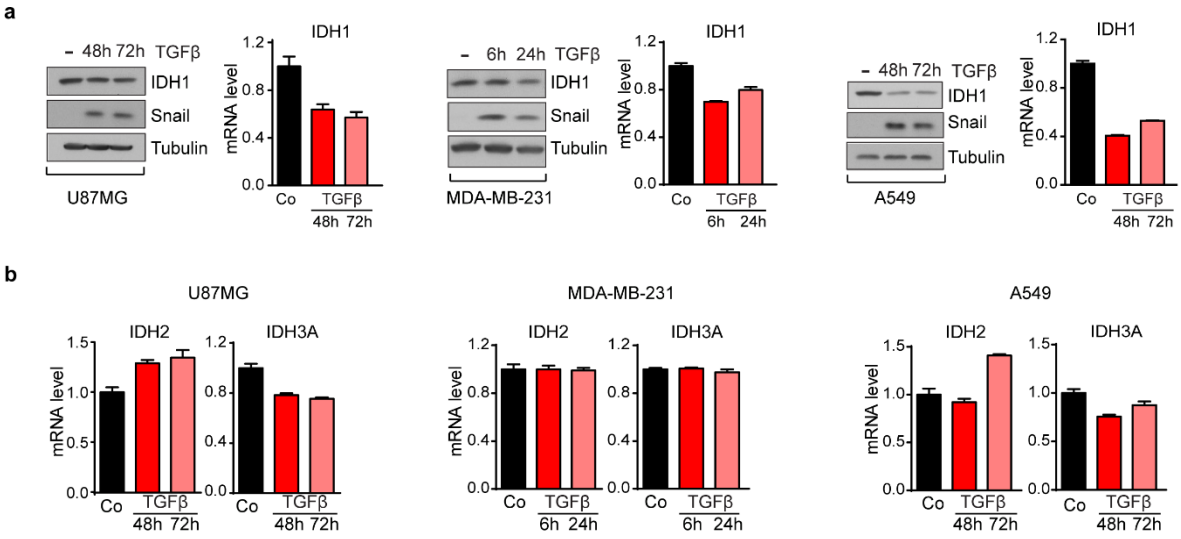

Figure 3.21. TGFβ downregulates IDH1 expression. a. IDH1 protein and mRNA levels in U87MG, MDA-MB-231 and A549 cells treated with 5 ng/mL TGFβ for the indicated times (n=3 technical replicates). Graphs are representative of five independent experiments. **b.** IDH2 and IDH3A mRNA levels were analyzed by RT-qPCR in the indicated cell lines and conditions, (n=3 technical replicates of one experiment). Data are normalized to control condition. Results are presented as means + SEM.

These findings prompted us to further investigate whether TGFβ modulates other enzymes involved in the production and consumption of α-KG. For this, we have selected some direct and indirect α-KG-regulating enzymes based on their relevance to α-KG homeostasis. Notably, PSAT1 and GLUD1 expression were reduced upon TGFβ stimulation in U87MG cells (Fig. 3.22a), while GLUD1 levels exhibited a striking and robust downregulation in both MDA-MB-231 and A549 cells (Fig. 3.22b,c). In addition, modest decreases in PSAT1 and GOT1 transcript levels were observed in A549 cells (Fig. 3.22c). Although we only examined a subset of enzymes responsible for maintaining intracellular α-KG levels, our results indicate that TGFβ selectively targets IDH1 for transcriptional repression in all three cancer cell types, in addition to a potential regulation of GLUD1. Further investigations are required to elucidate

the mechanistic link between TGFβ signaling and downregulation of α-KG-regulating enzymes.

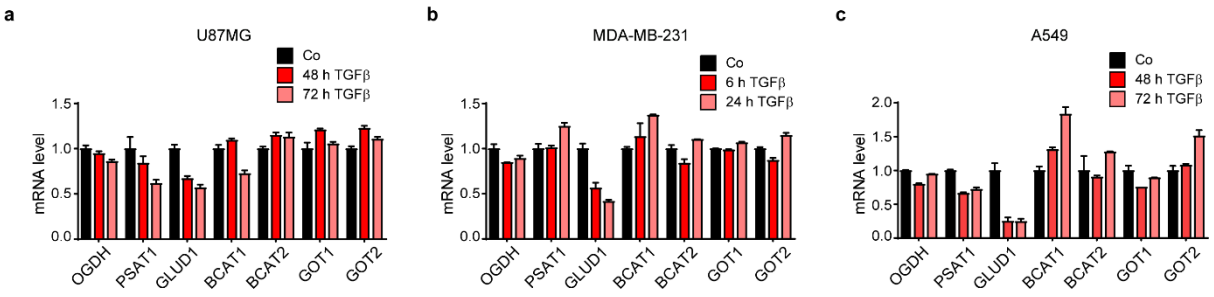

Figure 3.22. TGFβ controls α-KG-regulating enzymes. a-c. α-KG homeostasis-regulating enzyme mRNA levels were analyzed by RT-qPCR in U87MG (**a**), MDA-MB-231 (**b**), and A549 (**c**) following TGFβ treatment at two distinct time points, (n=3 technical replicates). Graphs are representative of two independent experiments. Data are normalized to control condition. Results are presented as means + SEM.

3.11.Reduced IDH1 levels correlate with poor patient prognosis

To assess the clinical relevance of our data, and analyze the prognostic impact of Snail and IDH1, we analyzed glioblastoma, breast cancer, and lung cancer patient data from GlioVis and KM-plotter (Bowman et al. 2017; Győrffy 2024), and conferred the relationship between IDH1 and Snail gene expression, and patients' overall survival. Analyzing RNA-seq data from The TCGA glioblastoma cohort in GlioVis indicated that low IDH1 levels are significantly correlated with worse prognosis, specifically in the mesenchymal subtype (Fig. 3.23a), as well as in the classical, but not in the proneural subtype (not shown). Low IDH1 levels show a tendency, but no significant correlation, with worse overall survival in the combined cohort of all glioblastoma patients (Fig. 3.23b). A similar analysis of SNAI1 revealed a negative correlation between high SNAI1 levels and overall survival of glioblastoma patients (Fig. 3.23c). Comparably, KM-plotter analyses of the mRNA gene chip data of stratified breast carcinomas with lymph node metastasis and lung adenocarcinomas showed significant correlation of low IDH1 or high SNAI1 with overall poor prognosis (Fig. 3.23d,e). In addition, we further stratified the combined status of IDH1 and SNAI1 into two groups using KM-plotter data: $IDH1^{high}/SNAI1^{low}$, and $IDH1^{low}/SNAI1^{high}$. Interestingly, $IDH1^{low}/SNAI1^{high}$ was significantly associated with poor survival in breast cancer patients with positive lymph node metastasis (Fig. 3.23f), and in lung adenocarcinoma patients (Fig. 3.23g). Unfortunately, stratification of glioblastoma patient data was not feasible due to the limited number of available samples. Similarly, a combined analysis of IDH1 and SNAI1 expression across all breast and lung cancer cohorts from KM-plotter could not be conducted, owing to mismatched patient numbers between the two gene datasets and the unavailability of individual patient identifiers.

Overall, low IDH1 and high SNAI1 mRNA levels indicate a worse prognosis in all three cancer types and in the indicated subtypes.

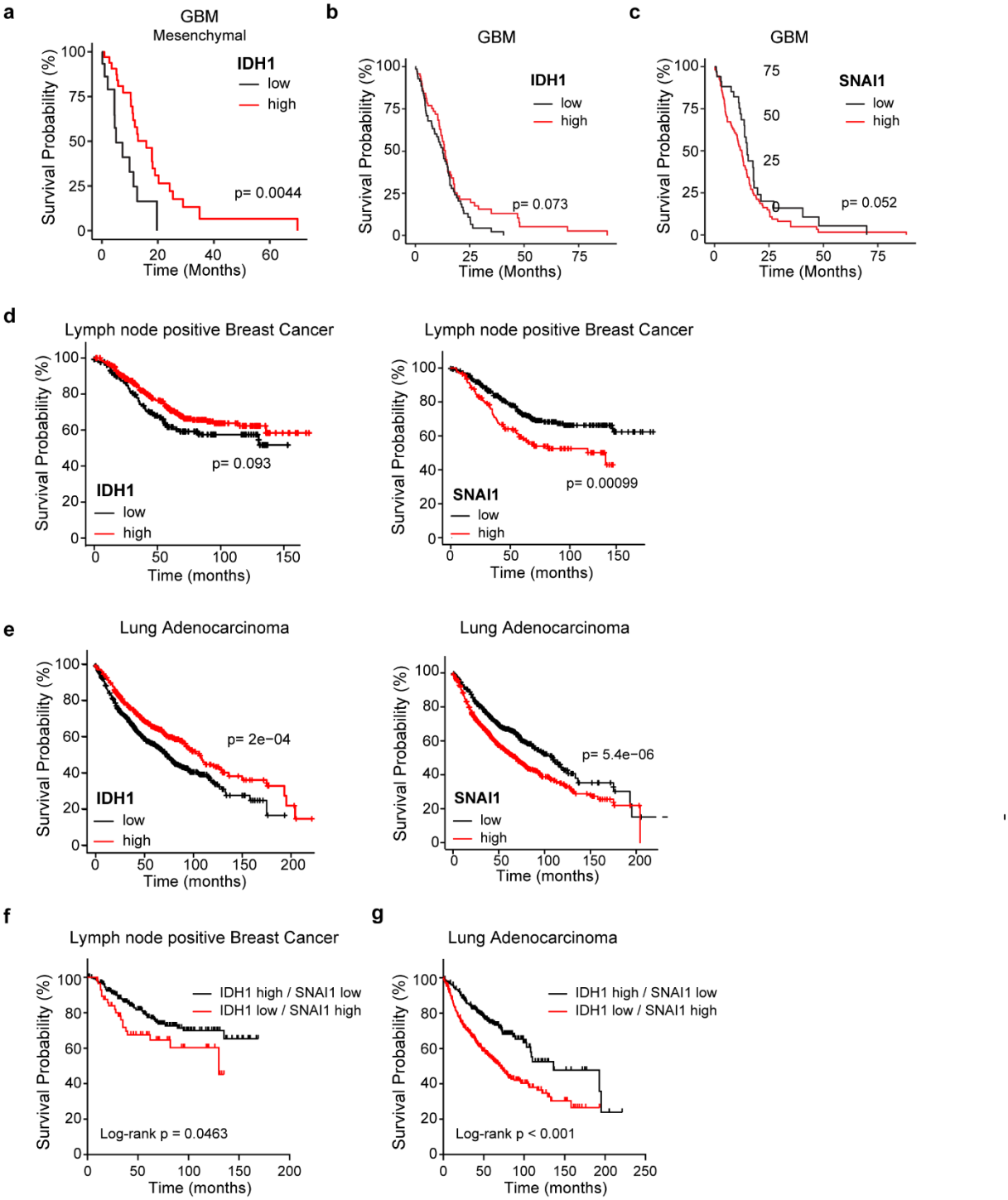

Figure 3.23. Low IDH1 and high SNAI1 expression levels are associated with worse survival. a. Correlation analysis of survival and IDH1 expression of IDH1 WT mesenchymal subtype GBM patient data from the TCGA_GBM, RNA-seq cohort using the GlioVis tool (n=49). **b-c**. Correlation analyses of survival and IDH1 (**b**) or SNAI1 (**c**) expression of IDH1 WT GBM patient data from the TCGA_GBM, RNA-seq cohort using the GlioVis tool (n=142). **d.** Correlation analyses of overall survival and IDH1 (left) or SNAI1 (right) expression of lymph node positive breast cancer patient mRNA gene chip data using the KM-plotter (n=452). **e.** Correlation analyses of overall survival and IDH1 (left) or SNAI1 (right) expression of lung adenocarcinoma patient mRNA gene chip data using the KM-plotter (n=1161). **f-g.** Correlation analyses of overall survival of lymph node positive breast

cancer patients (**f**), and lung adenocarcinoma (**g**) from the KM-plotter dataset stratified according to IDH1^{low}/SNAI1^{high} and IDH1^{high}/SNAI1^{low} (n=452 for breast cancer; n=1161 for lung adenocarcinoma). Log-rank p values were either obtained directly from GlioVis or KM-plotter, or calculated in GraphPad Prism.

3.12.Testing growth and invasion capacity of LLC1 cells grown as spheres

As conventional adherent culture conditions do not accurately recapitulate the physiological environment of tumor cells, we established conditions to grow LLC1 cells in 3D culture. Using a modified tumorsphere culture medium typically used for glioblastoma cell lines, supplementing it with 0.4% FBS, LLC1 cells were growing as spheres (Fig. 3.24a). To assess their invasive potential, we performed a collagen invasion assay. Spheres generated from LLC1 cells were carefully transferred into a collagen matrix, enabling three-dimensional invasion. Over a course of 96 hours, cells exhibited a robust invasion into the collagen matrix, with a significant increase in invading area observed at 72 and 96 hours post-embedding (Fig. 2.24b,c). These data demonstrate that LLC1 cells can adapt to 3D culture and exhibit strong invasive capabilities in a physiologically relevant matrix environment, a finding that provides a basis for future experiments under sphere culture conditions.

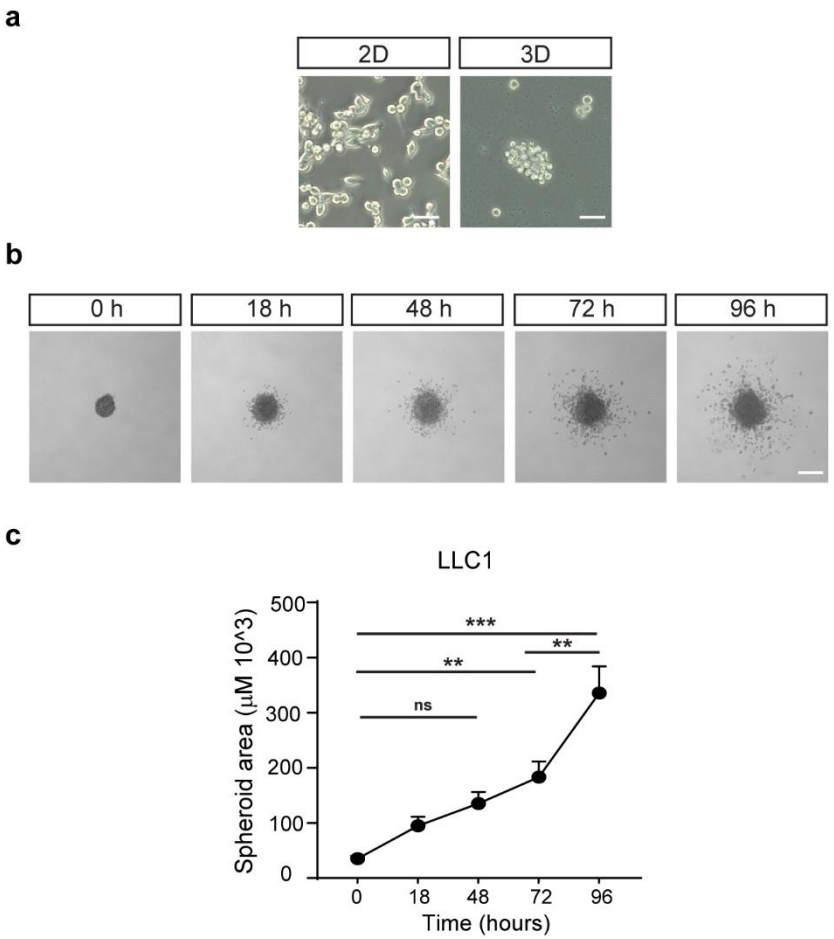

Figure 3.24. LLC1 cells are growing and invading in tumorsphere culture. a. LLC1 cells grown in semi-adherent and tumorsphere conditions. Scale bars indicate 100 µm. **b.** Invasion of LLC1 cells grown in tumorsphere medium using collagen invasion assay. Cell invasion was monitored and recorded over

a course of 96 hours. Representative images series of 8 biological replicates. Scale bars indicate 500 µm. **c.** Quantification of the spheroid area against the number of hours the spheroids were embedded within the 3D collagen gel. Data are presented as means + SEM. Statistical analysis was performed using one-way ANOVA, followed by Tukey's multiple comparisons test. **p<0.01; ***p<0.001.

3.13.Testing growth of LLC1 *in vivo*

To evaluate the impact of IDH1 depletion on tumor growth and metastasis in lung cancer model, we performed *in vivo* experiments. First, we tested the tumorigenicity of LLC1 pCDH B3 cells, as a lung cancer syngeneic model, by subcutaneously injecting the cells, and monitoring tumor growth using bioluminescence imaging (BLI) (Fig. 3.25a). By day 5 post-inoculation, tumors started to grow rapidly, reaching volumes of approximately 400 mm^3 by day 11 and day 15 post-inoculation (Fig. 3.25b). Tumors had to be excised due to the appearance of necrosis.

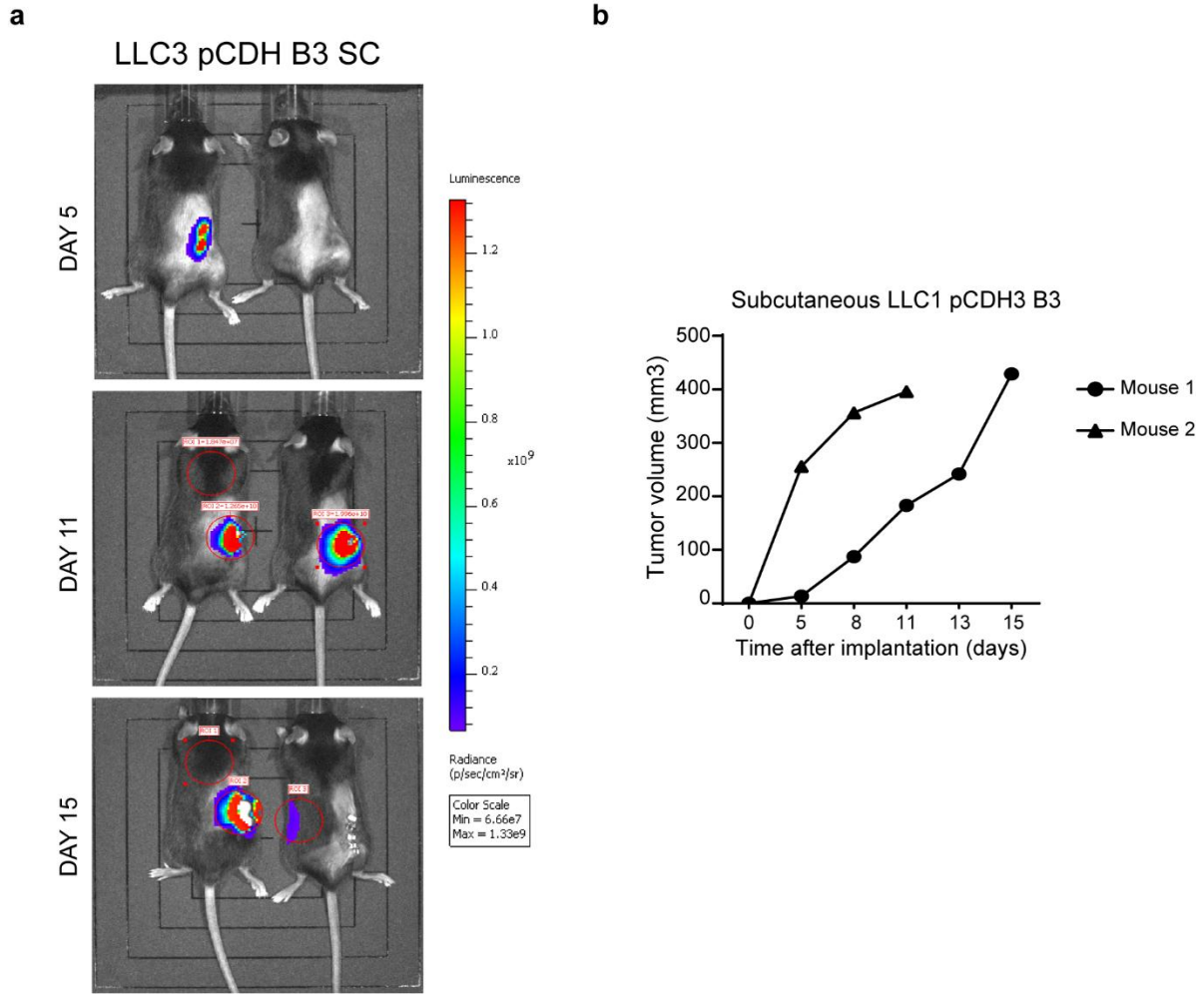

Figure 3.25. LLC1 pCDH B3 cells are tumorigenic. a. Bioluminescence images show LLC1 pCDH B3 tumor growth in subcutaneously injected C57Bl/6 mice. Relative levels of luminescence ranging from low (blue), to medium (green), to high (red). Injections were performed by Nuray Bögürcü-Seidel. **b.** Tumor growth analysis of the two mice shown in (**a**) was plotted against time in days. Mouse 1: left, Mouse 2: right.

Similarly, intravenous injection of LLC1 pCDH B3 cells resulted in rapid development of lung tumors (Fig. 3.26a). Mice had to be sacrificed at 14 and 20 days post-inoculation. This

was due to strong tumor-associated luminescence detected in the lungs, as an indication of a high tumor burden. Moreover, this was accompanied by early signs of clinical deterioration, including body weight loss and reduced overall condition. We also tested for the tumorigenic potential of LLC1 pCDH B3 / sLP mCherry B3 cells as well as their tumor microenvironment labelling potential, by injecting these cells intravenously into C57BL/6 mice. The sLPmCherry construct encodes a monomeric Cherry red fluorescent protein (mCherry) fused to a modified lipo-permeable Transactivator of Transcription (TATk) peptide, enabling the protein to be secreted by the labelling cells, and subsequently taken up by neighboring unlabeled cells. However, tumors that were initially growing, began to exhibit signs of immune-mediated rejection by day 18 post-inoculation (Fig. 3.26b). Despite this, we were able to harvest a tumor-bearing lung from one mouse, perform tissue digestion, and carry out FACS analysis (Fig. 3.26c,d). Viable cells were gated, and mCherry-positive populations were sorted. Cancer cells were identified as $GFP^{+}/mCherry^{+}$, whereas labeled stromal cells were detected as $GFP^{-}/mCherry^{+}$, compromising almost half of the $mCherry^{+}$ population (Fig. 3.26d), thus confirming effective labeling of the tumor microenvironment. LLC1 pCDH B3 / sLP mCherry B2 cells, transduced only twice with sLP mCherry, were also tested intravenously, but failed to establish tumors (not shown). Taken together, the pronounced immunogenicity of these engineered cells, prevented their use in further experiments, despite their successful labeling capabilities.

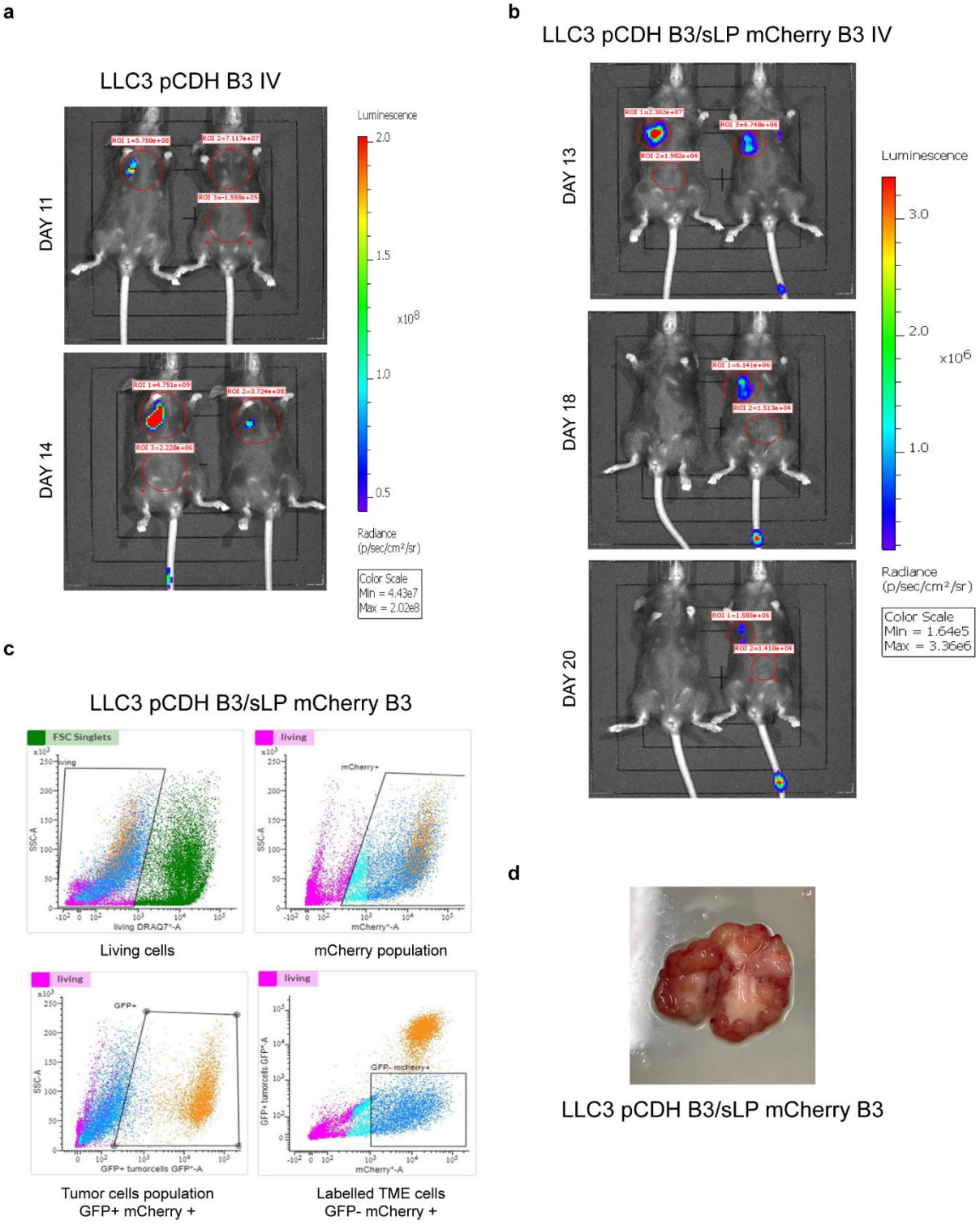

Figure 3.26. Tumor formation and microenvironment labeling using LLC1 cells. a,b. Bioluminescence imaging of lung tumors of intravenously injected LLC1 pCDH B3 cells (**a**) and LLC1 pCDH B3 / sLP mCherry B3 cells (**b**) in C57Bl/6 mice. Relative levels of luminescence ranging from low (blue), to medium (green), to high (yellow/red). Injections were performed by Nuray Bögürcü-Seidel. **c.** FACS sorting of GFP^+/$mCherry^+$ labeling cancer cells, and GFP^-/$mCherry^+$ stromal cells from (**b**). Tumor digestion, cell preparation and FACS analysis were done in collaboration with Nuray Bögürcü-Seidel, Sabine Gräf, and Nazli Salik. **d.** Representative image of the tumor-bearing lungs from (**b**).

3.14.Successive viral transductions render cells immunogenic

To investigate the impact of IDH1 depletion on tumor growth and metastasis in a lung cancer model, we injected control and IDH1 knockdown LLC1 pCDH B3 cells subcutaneously or intravenously in C57BL/6 mice, respectively. The cells were earlier confirmed for IDH1 knockdown efficiency and Snail induction at both the protein and mRNA levels (Fig. 3.7e). Similarly, LLC1 pCDH B3 / sLP mCherry B2/ pGIPZ B1 were also checked *in vitro* (Fig. 3.7f), but they were not used in mouse experiments due to the observed immunogenicity of LLC1 pCDH B3 / sLP mCherry B2 LLC1 cells. In the subcutaneous tumor model, we observed slower tumor growth compared to the previously shown growth of LLC1 pCDH B3 cells (Fig. 3.25). In addition, IDH1 knockdown tumors exhibited faster growth than control tumors at day 8 post-inoculation (Fig. 3.27a,b). However, shIDH1 tumors began to show signs of immune rejection shortly thereafter, with some control tumors also being rejected or exhibiting slower growth. Similarly, LLC1 pCDH B3 / pGIPZ B3 injected intravenously failed to grow in the lungs, with only one mouse per condition growing a barely detectable lung tumor (not shown). Likewise, in xenograft models of H2030 pCDH control and shIDH1 tumors, we noted tumor rejection after subcutaneous injection, and engraftment failure, when cells were introduced intravenously (data not shown). In conclusion, successive boosting transduction resulted in increased tumor immunogenicity and subsequent rejection. Thus, further optimization of cell labeling with reduced immunogenicity is required.

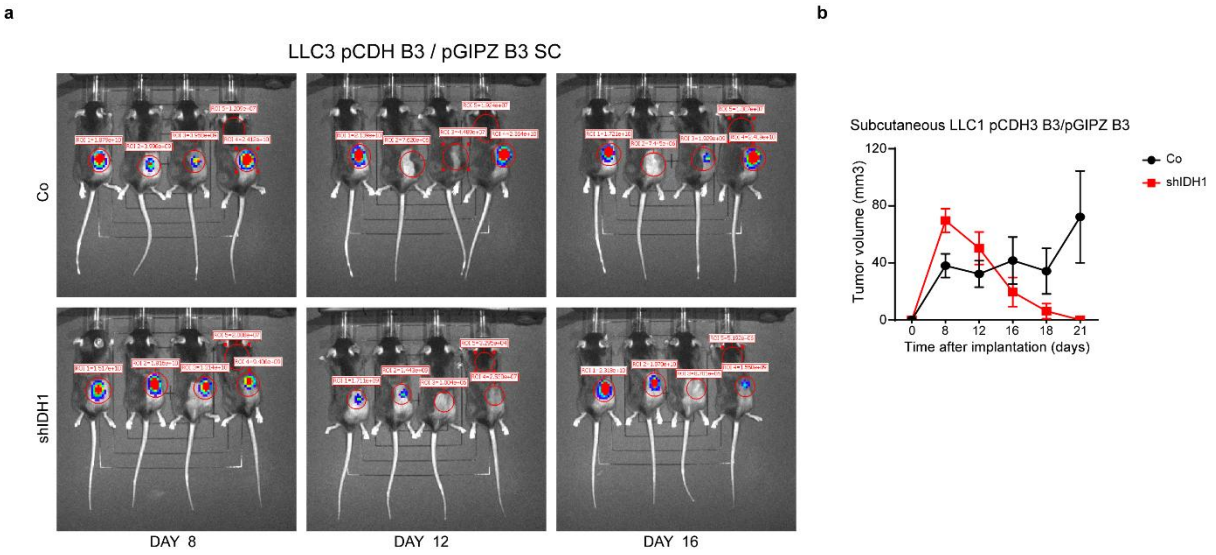

Figure 3.27. Enhanced reporter expression of tumor cells induces tumor immunogenicity *in vivo*. **a.** Representative bioluminescence images show tumor growth difference in LLC1 pCDH B3 /pGIPZ B3 co and shIDH1 cells, following subcutaneous cell injection in C57Bl/6 mice. Relative levels of luminescence ranging from low (blue), to medium (green), to high (red). Representative mice from control and shIDH1 groups at each time point are shown. **b.** Tumor growth analysis based on caliper measurements (starting number of mice was n=12 in co, and n=11 in shIDH1). Data are presented as means ± SEM.

4. Discussion

EMT and invasion are hallmarks of both primary and secondary brain malignancies. Indeed, glioblastoma along with brain metastases originating from breast and lung cancers are characterized by highly infiltrative and invasive phenotypes that confer profound resistance to conventional therapies (Fedele et al. 2019; Iser et al. 2017; Liaghat et al. 2024; Liang et al. 2025; Lu et al. 2025; Margarido et al. 2022; Seker-Polat et al. 2022). Mounting evidence demonstrates that metabolic reprogramming is interconnected with the onset of EMT and invasion (Drapela and Gomes 2021; Georgakopoulos-Soares et al. 2020; Jia et al. 2021). Thus, uncovering metabolic vulnerabilities that disrupt the early steps of metastasis may offer clinically relevant strategies for combating invasive cancers. In this context, the metabolite α-KG has emerged as an anti-tumorigenic molecule. It has been shown that disruption of α-KG homeostasis through IDH1 depletion enhances EMT induction and invasion (Bögürcü-Seidel 2018). However, the impact of α-KG supplementation on EMT, as well as the molecular mechanisms underlying this regulation, remain poorly understood. Therefore, in the present study, we aimed to deepen our understanding of the microenvironmental regulation of EMT and metabolism, investigate the inhibitory role of α-KG on EMT and invasiveness, dissect the mechanistic pathways mediating this regulation, and highlight its therapeutic potential.

4.1. The TGFβ–Snail axis is a shared driver of EMT in the investigated brain, lung and breast cancer models

EMT/PMT is defined as a combination of microenvironmental stimuli-induced signaling pathways, gene expression reprogramming, as well as phenotypic and behavioral changes (Lamouille et al. 2014; Yang et al. 2020), thereby its assessment and interpretation should take into consideration all of these aspects. Various microenvironmental cues and stress conditions can activate distinct EMT programs, among which TGFβ remains the most potent and well-characterized inducer. It was therefore selected as the primary stimulus in this study (Moustakas and Heldin 2016; Xu, Lamouille, and Derynck 2009).

It has been shown previously in our laboratory that Snail is upregulated upon IDH1 knockdown or knockout in human U87MG and G55 glioblastoma cell lines, as well as in MDA-MB-231 breast and A549 lung cancer cells, under hypoxic conditions or following TGFβ stimulation (Bögürcü-Seidel 2018). Thus, we sought to examine the TGFβ-mediated regulation of various EMT TFs, implicated in both PMT and EMT (Karsy et al. 2016; Lambert and Weinberg 2021; Yang et al. 2020), more broadly and systematically in parental, non-selected populations of the knockout and knockdown human cell lines and in LLC1 murine lung cancer

cells. Our results showed that SNAI1 (Snail) mRNA levels were strongly and consistently upregulated following TGFβ treatment in all cell lines tested (Fig. 3.1a,b,d, Fig. 3.2b). Snail upregulation was also visible at protein levels following TGFβ stimulation, as assessed by western blotting and immunofluorescence (Fig. 3.1c, Fig. 3.2a,c, Fig. 3.3a, Fig. 3.4b). Moreover, TGFβ treatment enhanced Snail protein nuclear retention (Fig. 3.3a). Stabilization of Snail protein could be due to the inhibition of GSK3β by TGFβ downstream signaling pathways (Z.-C. Liu et al. 2014; Zhang et al. 2006; Zhou et al. 2004), however GSK3β expression was not determined in this context. Our findings align with previously published studies highlighting TGFβ as a principal inducer of EMT, and Snail as a central EMT transcription factor upregulated across diverse tumor types. Indeed, TGFβ has been shown to induce transcriptional and translational upregulation of Snail in glioblastoma, as well as breast and lung adenocarcinomas (Han et al. 2015; Kaul, Risinger, and Mooberry 2019; Kim et al. 2020; R.-Y. Liu et al. 2014; Motizuki et al. 2024; Nozaki and Nishizuka 2021; Smith et al. 2009; Zhu et al. 2022).

Consistent with our findings, Snail protein and mRNA levels exhibited a rapid and pronounced induction within three to six hours of TGFβ exposure in LLC1 cells. Conversely, the induction of Snai2 (Slug), Zeb1, and Twist1 was markedly delayed, as it was evident only after 48 to 72 hours of TGFβ treatment (Fig. 3.1c,d). Rapid Snail induction following TGFβ or other stimulus has been previously shown, usually preceding and activating other EMT TFs (Baulida, Díaz, and Herreros 2019; Dave et al. 2011; Guaita et al. 2002; Sundararajan et al. 2020; Wu et al. 2017; Youssef et al. 2024). Although SNAI2 and ZEB1 showed increased expression in response to TGFβ in the bulk RNA-seq, similar to SNAI1 (Fig. 3.1a), their upregulation at RNA and protein levels was not uniformly observed across the tested human cell lines (Fig. 3.1d, Fig. 3.2b,c). In agreement with our findings, it has been reported that TGFβ-induced Slug expression is infrequent, compared to the robust TGFβ-mediated Snail upregulation (Saitoh 2023), and ZEB1 has been shown to be induced following TGFβ treatment, but not as often as Snail (Gregory et al. 2011; Joseph et al. 2014) .

In addition to the core EMT TFs, PRRX1 and FOXC1 were upregulated following TGFβ induction in U87MG cells (Fig. 3.1a). PRRX1 is markedly overexpressed in glioma samples compared to normal counterparts (Z. Chen et al. 2021; Sugiyama et al. 2015), and is linked to multiple cancer hallmarks, as its depletion inhibits glioma proliferation, invasion, stemness, and angiogenesis (Z. Chen et al. 2021; Sugiyama et al. 2015). Its expression is promoted through TGFβ-mediated inhibition of miR-106 expression, a negative regulator of PRRX1 mRNA levels (Zheng et al. 2015). Furthermore, PRRX1 acts downstream of Snail,

being associated with highly mesenchymal phenotype along with enhanced invasive and migratory capacities in diverse TGFβ-induced normal or malignant cells (Youssef et al. 2024). On the other hand, FOXC1 expression levels are upregulated in CRC and esophageal cancer, compared to normal tissues (Zhang et al. 2025; Zhu et al. 2017). Its depletion reduces migration and invasion of GBM and CRC cells (Cao et al. 2019; Zhang et al. 2025). Interestingly, FoxC1 has been shown to regulate SNAI1, TWIST1, and ZEB2 expression (Cao et al. 2019; Zhang et al. 2025; Zhu et al. 2017), and to be induced by TGFβ treatment (Hopkins, Coatham, and Berry 2017).

TGFβ treatment also impacted mesenchymal and epithelial markers, as it induced the expression and spatial reorganization of Vimentin in carcinoma cell lines, while reducing E-cadherin (CDH1) RNA and protein expression (Fig. 3.1d, Fig. 3.3d-g, Fig. 3.4), consistent with Snail's well-established function as CDH1 transcriptional repressor. Notably, Vimentin expression was previously reported to be unresponsive to TGFβ treatment in GBM cells in our laboratory (Goos 2015), therefore its protein levels and subcellular organization were not assessed in U87MG. More importantly, TGFβ significantly enhanced the invasive capacities of all cancer models as determined by a modified Boyden chamber assay (Fig. 3.5a,b,e). Our results align with previously published findings, which showed that TGFβ stimulation of A549 lung cancer cells results in upregulation of N-cadherin, Vimentin, and Fibronectin, while reducing E-cadherin expression (Kim et al. 2020). Moreover, TGFβ induction or overexpression of Snail enhances cell motility, migration, and invasion (Han et al. 2015; Kim et al. 2020; R.-Y. Liu et al. 2014; Myung et al. 2014; Nozaki and Nishizuka 2021).

In patient samples, elevated SNAI1 expression correlated with reduced overall survival across the three cancer types (Fig. 3.23c–e). Indeed, the clinical impact of SNAI1 is well-established, with previous reports demonstrating that high SNAI1 levels are invariably associated with poor patient outcomes in multiple cancer types (Chang et al. 2017; Shaojie Chen et al. 2021; W.-S. Liu et al. 2018; Moody et al. 2005; M. Xu et al. 2018; Zivotic et al. 2023).

4.2. α-KG-mediated suppression of EMT and invasion

Compared to the established role of TGFβ in EMT activation and invasion, less is known about the role of α-KG in regulating EMT TFs and EMT-related processes. Notably, Snail mRNA and protein levels were dramatically and consistently reduced upon α-KG supplementation, across the different cancer models (Fig. 3.2a-c, Fig. 3.3a, Fig. 3.4b), as shown by RT-qPCR, western blotting and immunofluorescence. Moreover, α-KG treatment reduced the expression of the mesenchymal marker Vimentin but minimally affected its cellular

reorganization as revealed by western blot, immunofluorescence, and FACS analyses in MDA-MB-231-VIM-RFP and A549-VIM-RFP cells as EMT models (Fig. 3.4). Conversely, α-KG treatment failed to rescue the levels of the epithelial marker E-cadherin, despite Snail inhibition (Fig. 3.3c-e). This observation could be attributed to the regulation of E-cadherin expression by other EMT TFs, which were not reduced by α-KG, or alternatively, to the insufficiency of α-KG concentration or duration of treatment. To our knowledge, no previous studies have reported a direct inhibitory effect of α-KG supplementation on EMT TFs expression, and specifically Snail levels. Earlier work has primarily focused on the consequences of the reduction of its intracellular level due to the inhibition of its regulating enzymes. For instance, reduced α-KG levels result in upregulation of ZEB1 and ZEB2, concomitant with a downregulation of E-cadherin (H. Sun et al. 2022), whereas its elevated levels suppress ZEB1 expression (Atlante et al. 2018). While these findings suggest a negative role of α-KG on the EMT program, a general negative impact on Snail and mechanistic insights remained largely unexplored until our study.

Moreover, we investigated the effect of α-KG on cancer cell invasion. In our Boyden chamber assays, α-KG supplementation not only reversed but also prevented TGFβ-induced invasiveness across all examined cancer cell lines (Fig. 3.5a,b), with the exception of 8 mM of α-KG in the prevention experiment (Fig. 3.5b). The lack of effect at this concentration may be attributed to Dm-α-KG-induced medium acidification (Parker et al. 2021), potentially due to insufficient pH adjustment of the α-KG containing medium. Extracellular acidification is known to promote invasion (Audero et al. 2023; de Bem Prunes et al. 2022; Bohloli et al. 2016; Han et al. 2013). Notably, even in the absence of TGFβ and any exogenous EMT inducer, α-KG reduced Snail expression levels and suppressed the invasive capacity of MDA-MB-231 parental, ni, and i10 cells (Fig. 3.5c,f). This is in line with α-KG's suppressive effect on migration and invasion in various cancer models, including osteosarcoma, breast carcinoma, liver cancer, renal cell carcinoma (RCC), and gastric cancer (Choi et al. 2025; Kaławaj et al. 2020; Liu et al. 2025; Tseng et al. 2018; Wu et al. 2023). It is also consistent with the finding that glutamine deficiency in CRC cells' growth medium, which limits intracellular α-KG availability, promotes their invasion ability (H. Sun et al. 2022).

These findings, however, appear to contrast with a recent study reporting α-KG as a promoter of migration and invasion in U87MG GBM cells (Shen et al. 2020). In that study, cells were exposed to lower concentrations of α-KG under adherent conditions and without prior TGFβ stimulation, a setup that differs significantly from ours (see Fig. 2.4). We reproduced their conditions and found no change in Snail protein levels following α-KG

treatment in 2D culture. Interestingly, Snail expression was modestly increased upon treatment with 2.5 mM α-KG under TSM suspension conditions. After pH adjustment, however, the effect was reversed. Conversly, in both adherent and suspension cultures, α-KG at 2.5 mM or higher consistently reduced TGFβ-induced Snail expression, even without prior pH adjustment (data not shown). Four key differences in experimental design likely account for the divergent observations. First, the nature of α-KG used in the study by X. Shen et al., was not specified (Shen et al. 2020). This is an essential point, as α-KG and its derivatives can exert markedly different cellular effects, as discussed in detail below in section 4.7 (Baracco et al. 2019; Parker et al. 2021). Second, it was not indicated whether the experiments by Shen et al. were performed with pH adjustment. In our system, pH calibration is critical because an acidic microenvironment, as created by the addition of Dm-α-KG, is well known to initially restrict tumor growth but subsequently enhance cancer cell invasion (Audero et al. 2023; de Bem Prunes et al. 2022; Bohloli et al. 2016; Han et al. 2013). Third, GBM cells were cultured in the Shen et al. study exclusively under adherent conditions. Numerous studies have shown that epithelial and GBM cells display substantial differences in transcriptome, metabolome, responsiveness and processing of stimuli, cellular morphology, and behavior depending on whether they are grown in adherent versus suspension conditions (Abbas et al. 2023; El Mokbel et al. 2024; Kapałczyńska et al. 2018; Peixoto et al. 2021). Finally, our experimental design frequently incorporated prior TGFβ treatment, which directly engages the EMT program and its metabolic rewiring, a key mechanistic axis absent in the setup by Shen and colleagues. Nevertheless, we found that α-KG also repressed Snail expression and invasion without prior TGFβ stimulation in MDA-MB-231 cells (Fig. 3.5c,f). Together, these observations underscore the importance of growth conditions and the combination of microenvironmental factors and metabolic changes in shaping distinct EMT responses, and highlight the need for proper reporting of reagents, including source and catalog numbers, as well as detailed methodological procedures such as pH adjustment to ensure reproducibility. Additional studies examining the context-specific effects of TGFβ and α-KG on transcriptional programs and invasive behavior under sphere conditions are warranted. Moreover, sphere cultures could be adapted for *ex vivo* invasiveness assays, using organotypic brain or lung slice models. To initiate this, we extended our investigations to establish 3D culture models of mouse LLC1 lung adenocarcinoma cells that can be used in syngeneic models and assessed their growth in suspension and invasiveness in a collagen invasion assay (Fig. 3.24a,b).

Certain oncometabolites can compete with α-KG and impair the activity of α-KGDDs, thus having opposite effects on EMT and invasion than α-KG. For instance, D-2-HG has been

demonstrated to enhance CRC cells migration and invasion, and increase the active mark H3K4me3 deposition at the ZEB1 promoter, thereby upregulating ZEB1 expression, along with Vimentin and Fibronectin (Colvin et al. 2016). Similarly, fumarate accumulation in FH-deficient renal cancer cells, leads to the induction of several EMT TFs and mesenchymal markers, primarily through inhibition of TET-mediated DNA demethylation of the antimetastatic miRNA-200 family (Sciacovelli et al. 2016). Furthermore, dysregulated succinate metabolism, either through SDH deficiency or exogenous succinate supplementation, is reported to induce EMT in ovarian and lung cancer cells. This is associated with the upregulation of Snail, Slug, and TWIST, the increased expression of mesenchymal markers such as Vimentin and N-cadherin, and the repression of E-cadherin (Aspuria et al. 2014; J.-Y. Wu et al. 2020).

In some contexts, the concentration range of α-KG used in our experiments also exerts anti-proliferative effects, reducing cell viability, proliferation, and growth (Lee et al. 2023; Liu et al. 2025; Raffel et al. 2017; Rzeski et al. 2012). Moreover, repeated Dm-α-KG dramatically reduces liver cancer cell's viability in a time- and dose-dependent manner (Choi et al. 2025). However, we have not observed any drastic effect of α-KG on proliferation or viability across the different cell types, except in U87MG, where cells proliferation but not viability was dramatically affected by α-KG supplementation (Fig. 3.6a,b). Yet, alternative proliferation and viability assays, such as BrdU incorporation, CellTiter-Blue®, or MTT assays, as well as colony formation assays, in addition to apoptosis assays, and cell cycle analysis could further supplement our investigations in future experiments.

4.3. α-KG as a therapeutic agent in cancer and beyond

α-KG showed robust inhibition of Snail expression and invasiveness across three tumor models in our *in vitro* settings. This highlights its potential relevance in a therapeutic context. Indeed, several *in vivo* studies have indicated anti-tumorigenic and anti-metastatic effects of α-KG. For instance, in subcutaneous xenograft mouse models of colon cancer, supplementation with Dm-α-KG, either intraperitoneally or orally in solution, significantly reduces tumor growth and volume. Similarly, in a spontaneous transgenic mouse model of CRC, intraperitoneal Dm-α-KG treatment decreases intestinal tumor burden (Tran et al. 2020). In a CRC cachexia model, α-KG not only mitigates body mass loss but also reduces tumor growth (Ruiz et al. 2023). Moreover, in an orthotopic TNBC model, intraperitoneal α-KG administration prevents lung and lymph node metastases in addition to reduction of primary tumor growth (Li et al. 2024; Tseng et al. 2018), with comparable effects observed in syngeneic lung and renal cell carcinoma models (L. Li et al. 2023; Matsumoto et al. 2009). Furthermore,

intratumoral injection of Dm-α-KG leads to a marked tumor regression in subcutaneously-transplanted diffuse large B-cell lymphoma cells (Cai et al. 2023). However, this delivery route is limited to accessible subcutaneous lesions, which renders it not beneficial in pre-clinical and clinical trials.

Accumulating evidence indicates that α-KG exerts anti-cancer effects through various mechanisms across different cancer types. These include inhibition of cellular proliferation and survival, as demonstrated earlier (Fu et al. 2015; Kaławaj et al. 2020), induction of apoptosis and ferroptosis (Cai et al. 2023; Kaławaj et al. 2020; Sica et al. 2019), mitigation of hypoxia-mediated HIF signaling and suppression of angiogenesis (Bögürcü-Seidel 2018; MacKenzie et al. 2007; Matsumoto et al. 2006), promotion of cellular differentiation (Morris et al. 2019; Pan et al. 2016), enhancement of oxidative stress (Choi et al. 2025), prevention of immune evasion and increased cytotoxic T cells infiltration (L. Li et al. 2023; Liu et al. 2023; Tan et al. 2023), and attenuation of cancer-associated cachexia (Ruiz et al. 2023).

Cancer cells in hybrid E/M states tend to display increased stemness, and therapeutic resistance (Jia et al. 2021; Sciacovelli and Frezza 2017). Interestingly, altered α-KG homeostasis has also been shown to inhibit stemness, and sensitize cancer cells to treatments, highlighting the tight interconnection between metabolic rewiring and EMT-associated stemness and treatment evasion. Indeed, previous findings from our laboratory demonstrated that low levels of α-KG enhance GBM cancer stem cell markers (Bögürcü-Seidel 2018). In accordance with these observations, diminished α-KG cellular levels result in increased stemness by inactivating α-KG–dependent histone and DNA demethylases, leading to hypermethylation of histones and DNA in melanoma, CRC, gliomas, acute myeloid leukemia, and PDAC (Lu et al. 2012; Morris et al. 2019; Pan et al. 2016; Raffel et al. 2017; Tran et al. 2020). Depending on the tumor type, and which demethylases are inhibited by low α-KG levels, this can increase either active or repressive histone marks, thereby activating stemness programs or repressing differentiation genes, respectively. Importantly, restoring α-KG homeostasis reverses molecular and cellular phenotypes associated with stemness. For instance, α-KG addition promotes DNA hypomethylation and activation of differentiation genes, while also driving drastic H3K4me3 hypomethylation on Wnt target genes, which are required for CRC development, thereby suppressing them (Tran et al. 2020). Similarly, in PDAC, accumulation of α-KG, achieved through restoration of wild-type p53 function or OGDH inhibition, increases 5hmC levels, thereby activating premalignant differentiation transcriptional programs (Morris et al. 2019). It is important to emphasize that α-KG effects are cell type- and context- dependent. Compared to cancer cells, supplementation of Dm-α-KG

maintains pluripotency in naive embryonic stem cells (Carey et al. 2015), whereas its addition induces differentiation in primed pluripotent stem cells (TeSlaa et al. 2016). Beyond stemness and differentiation, α-KG dysregulation is associated with DNA damage and therapy resistance in lung cancer, melanoma, and glioma (Lang et al. 2025; Pan et al. 2016; Sulkowski et al. 2017, 2020; Xiang et al. 2024). Oncometabolite accumulation, following metabolic enzyme inhibition or through direct supplementation, has been shown to impair homology-directed DNA repair, thereby sensitizing cancer cells to synthetic lethality (Lang et al. 2025; Sulkowski et al. 2017, 2020). In contrast, reduced glutamine availability has been associated with acquired resistance to BRAF-targeted therapy in melanoma cells (Pan et al. 2016).

In certain contexts, α-KG alone exerts minimal inhibitory effects on tumor cells *in vitro* or *in vivo*. However, when paired with targeted or conventional therapies, it improves treatment efficiency. Indeed, disodium α-KG induces synergistic growth inhibition when combined with BCAT1 genetic or pharmacological inhibition. Their administration by oral gavage suppresses tumor growth in IDH1 WT GBM patient-derived xenograft models (Zhang et al. 2022). Similarly, combining α-KG with targeted therapies significantly reduces cancer cells proliferation and viability *in vitro*, and tumor size and volume *in vivo*, compared to single treatments in both lung cancer and CRC (Sica et al. 2019; Xiang et al. 2024), with further potentiation upon radiotherapy in lung cancer (Xiang et al. 2024). Although previous studies have shown that α-KG alone can reduce cancer cell viability and tumor growth in TNBC, lung cancer, and renal cell carcinoma, its effects are amplified when combined with chemotherapeutic or immunotherapeutic agents (Li et al. 2024; L. Li et al. 2023; Matsumoto et al. 2009). Collectively, these findings highlight that α-KG could function within a synthetic lethality framework, where its metabolic and signaling effects selectively sensitize tumor cells to additional targeted, chemotherapeutic, radiotherapeutic, or immunotherapeutic interventions, while sparing normal cells.

Importantly, α-KG is a metabolite with pleiotropic activities and plays a role in multiple metabolic pathways. Thus, its use has been investigated across a range of physiological and pathological contexts, beyond oncology. Pre-clinical studies have demonstrated benefits in combating age-related morbidity (Asadi Shahmirzadi et al. 2020), extending lifespan (Asadi Shahmirzadi et al. 2020; Chin et al. 2014; Su et al. 2019), inhibiting autophagy (Baracco et al. 2019), and preventing muscle atrophy (Vaubourdolle et al. 1991). Further implications are reviewed in detail elsewhere (Bayliak and Lushchak 2021; Gyanwali et al. 2022; Harrison and Pierzynowski 2008; Meng et al. 2022; Wu et al. 2016). Interestingly, few reports have established a positive effect of α-KG dietary supplementation in humans, with improving

appetite, body weight, and overall quality of life, as well as reducing age-associated DNA methylation and morbidity in old individuals (Brocker et al. 1994; Demidenko et al. 2021). α-KG supplementation also accelerates wound healing (Cynober 1991; Donati et al. 1999), prevents muscle loss and increases protein synthesis (Demidenko et al. 2021; Donati et al. 1999; Wernerman et al. 1987; Wernerman, Hammarqvist, and Vinnars 1990), as well as preserves bone mass (Filip et al. 2007). Additionally, α-KG demonstrates therapeutic promise in liver, renal, and gastrointestinal disorders (Bayliak and Lushchak 2021; Gyanwali et al. 2022; Harrison and Pierzynowski 2008; Meng et al. 2022; Wu et al. 2016).

α-KG supplementation to cells, or in pre-clinical tumor models, regardless of the diverse administration routes consistently elevates cellular and intratumoral α-KG levels, (Baracco et al. 2019; Li et al. 2024; MacKenzie et al. 2007; Tran et al. 2020). Similarly, genetic perturbations of metabolic enzymes or tumor suppressors dramatically alters α-KG abundance in *in vitro* and *in vivo* settings (Gao et al. 2025; Kitazawa et al. 2017; Li et al. 2024; Morris et al. 2019; Shen et al. 2020; Shrimali et al. 2021; X. Wang et al. 2019). In animals, the used dosages are well tolerated, with no adverse effects on general health (Liu et al. 2023; Matsumoto et al. 2009; Zhang et al. 2022), and even prevent tumor-associated weight loss (Matsumoto et al. 2009; Ruiz et al. 2023; Tran et al. 2020), and prolong the survival of tumor-bearing mice (Liu et al. 2023; Sica et al. 2019). Similarly, clinical studies have confirmed the safety of α-KG as a dietary supplement and an anti-aging molecule, with minimal side effects reported (Gyanwali et al. 2022). Nevertheless, critical parameters, including the optimal route of administration, chemical form of α-KG, dosage, and treatment duration should be systematically defined to maximize reproducibility and efficiency.

As cancer is an age-related disease, and considering the dramatically reduced plasma levels of α-KG upon aging (Gyanwali et al. 2022; Harrison and Pierzynowski 2008), as well as intratumorally or in serum of cancer patients (Cai et al. 2023; L. Li et al. 2023; Liu et al. 2023; Pan et al. 2016), and the plethora of cellular pathways and functions that α-KG is regulating, our results and previous reports highlight an anti-tumorigenic and health promoting function of α-KG.

4.4. IDH1 depletion regulates EMT induction and invasive behavior

Given the role of α-KG supplementation in suppressing EMT and invasiveness, and considering that modulation of intracellular α-KG levels through its key metabolic enzymes, including α-KGDH (Atlante et al. 2018; Lu et al. 2019), GLUD1 (X. Wang et al. 2019) or IDH1 (Bögürcü-Seidel 2018), impacts these cellular phenotypes, we aimed to further characterize the effect of α-KG in IDH1-depleted cells. While oncogenic mutations in IDH1/2 genes have been

extensively characterized, the role of wild-type IDH1/2 levels remains to be further defined in tumor settings. Our results confirmed previous data from our laboratory, where IDH1 knockdown and subsequent reduced-α-KG intracellular levels (Bögürcü-Seidel 2018), markedly increased Snail protein and mRNA levels in the presence or absence of TGFβ stimulation, in U87MG glioblastoma cells (Fig. 3.7a). Moreover, IDH1 depletion enhanced the invasive capacity of these cells (Fig. 3.7b). To determine whether this also applies to other types of cancer, we extended our analysis to breast and lung cancer models. Remarkably, IDH1 knockdown resulted in Snail expression upregulation at both RNA and protein levels, in MDA-MB-231-VIM-RFP breast cancer cells, and GFP only- or GFP and mCherry-labelled LLC1 lung cancer cells (Fig. 3.7d-f). Snai1 but not Snai2 or Zeb1/2 mRNA levels were further induced following TGFβ treatment in IDH1-depleted LLC1 cells (Fig. 3.7f). This suggests that Snail is the only common EMT TF downstream of TGFβ and IDH1 axis (Fig. 3.1d, Fig. 3.7f). Interestingly, α-KG supplementation reversed IDH1 knockdown- and TGFβ-induced Snail expression (Fig. 3.7c). Furthermore, we have shown that inducible overexpression of IDH1 resulted in Snail, HIF-1α, and HIF-2α downregulation (Fig. 3.8). Collectively, these findings underscore a regulatory role of IDH1 WT in restraining EMT and invasion, likely via α-KG-dependent mechanisms.

Our findings are in agreement with earlier reports showing IDH1 downregulation in tumor tissue compared to adjacent normal samples, in osteosarcoma (Hu et al. 2014), renal cancer (Song Chen et al. 2021), and breast cancer (W.-S. Liu et al. 2018). In various experimental models of these tumors, IDH1 knockdown promotes cell growth, proliferation, colony formation, migration, and invasion, whereas its overexpression impairs these cellular phenotypes (Song Chen et al. 2021; Hu et al. 2014; W.-S. Liu et al. 2018). Moreover, IDH1-depleted cells exhibit a significantly faster tumor growth rate, with larger tumors (Song Chen et al. 2021; Hu et al. 2014), in addition to increased lung nodules in osteosarcoma and breast carcinoma metastasis model (Bögürcü-Seidel 2018; Hu et al. 2014). According to our literature search only one study shows so far a correlation between IDH1, Snail, EMT and invasiveness (W.-S. Liu et al. 2018). In this study, the expression levels of Snail, Slug, and TWIST proteins and mRNA are significantly induced upon IDH1 knockdown, whereas Vimentin levels remain unchanged. Moreover, Snail levels are consistently increased in different breast cancer lines representative of different molecular subtypes (W.-S. Liu et al. 2018). However, the mechanism by which IDH1 regulates EMT and the invasive phenotype, was not investigated in this study. The correlation between IDH expression and HIF-α stability, on the other hand, is well-established and mechanistically explained through the activity of PHDs as α-KGDDs (Song

Chen et al. 2021; Li et al. 2018, 2024; W.-S. Liu et al. 2018). It is important to note that HIF-α is known to directly regulate the SNAI1 gene (Gai et al. 2020; Hapke and Haake 2020; Luo et al. 2011; Saxena et al. 2020; Shen et al. 2024; Zhang et al. 2013) thereby providing a possible mechanistic link between IDH1-dependent regulation of Snail levels. The investigations of this link are discussed in detail in Sections 4.8 and 4.9.

In contrast to the discussed downregulation of IDH1 in different cancer settings, increased levels of IDH1 in ovarian (Dahl et al. 2019), and lung cancers (Tan et al. 2012), as well as melanoma (Zarei et al. 2022) have been reported. It has also been shown that higher levels of IDH1 are required for increased proliferation, survival, stemness, oxidative stress adaptation, proper mitochondrial functions, lipid biosynthesis, and migration, under both normal or nutrient limitation conditions (Atalay, Senturk, and Kayali 2023; Bergaggio and Piva 2019; Calvert et al. 2017; Dahl et al. 2019; Shen et al. 2020; Tan et al. 2012; Vaziri-Gohar et al. 2022; Zarei et al. 2022). Remarkably, genetic or pharmacological inactivation of IDH1 has also been found to diminish tumor growth *in vivo* (Calvert et al. 2017; Tan et al. 2012; Vaziri-Gohar et al. 2022; Zarei et al. 2022). It is worth noting that none of these studies examined EMT and invasion of IDH1-depleted cells. Overall, the observed tumor-promoting effects of IDH1 depletion or overexpression suggest that IDH1 and α-KG levels may have cancer cell (pheno)type-specific effects, warranting further investigation.

Our analyses of patient data revealed that lower IDH1 expression correlated with worse overall survival across all three tumor types examined (Fig. 3.a,b,d-g). Moreover, the combination of low IDH1 and high SNAI1 levels was associated with markedly poorer prognosis in both breast and lung cancers (Fig. 3.23f,g), underscoring the potential prognostic value of their combined assessment. These findings are consistent with one report in breast cancer (W.-S. Liu et al. 2018), in which low IDH1 and high Snail levels are significantly associated with poor disease-specific, disease-free, and overall survivals. In contrast, a significant association between high IDH1 expression and reduced overall or progression-free survival in ovarian cancer and melanoma is identified (Dahl et al., 2019; Zarei et al., 2022). In NSCLC, one study links IDH1-positive tumors to poorer clinical outcomes (Tan et al. 2012), whereas another finds no statistically significant correlation between IDH1 expression and patient survival (X. Zhang et al. 2021). The observed discrepancies in survival analyses may stem from the investigation of various tumor types and subtypes, the use of different patients' datasets, as well as the methodologies used to assess mRNA expression, such as microarray versus RNA sequencing. Moreover, analyses based on large tumor cell populations and bulk

genomics data may overlook the transient and context-dependent effects of IDH1 levels, underscoring the need for incorporating single-cell analyses.

As IDH1 dysregulation has been reported to impact primary and secondary tumor formation in breast, renal, and osteosarcoma cancer models (Bögürcü-Seidel 2018; Song Chen et al. 2021; Hu et al. 2014), and as mouse models are indispensable to functionally recapitulate the clinical course of a metastatic disease, we aimed to investigate IDH1 function on lung cancer growth and metastasis using syngeneic and xenograft models. Although LLC1 cells, which were transduced three times with a dual EGFP-luciferase construct successfully engrafted and grew macroscopic tumors subcutaneously, or in the lungs (Fig. 3.25, Fig. 3.26a), further transductions with sLP-mCherry or pGIPZ-shIDH1 constructs, while increasing detectability, rendered the tumors immunogenic (Fig. 3.26b, Fig. 3.27). Tumors either regressed after initial growth or failed to establish, when injected subcutaneously or intravenously, respectively. Consecutive rounds of lentiviral transductions with reduced vector doses is an established way of increasing transduction efficiency and expression of multiple integrated vectors at different genomic sites while maintaining reduced cytotoxicity (Donnelley et al. 2023; Sinn et al. 2008; Yu et al. 2011). However, despite the necessity of reporter genes and luciferase to non-invasively monitor tumor growth and metastasis, they are known to induce an immune response in immunocompetent mice (Grzelak et al. 2022; Schultheiß and Binder 2022). Intracellular selectable markers such as puromycin resistance via puromycin N-acetyltransferase expression also limit tumor growth (Dubrot et al. 2021; Stripecke et al. 1999). EGFP-expressing cells are also known to get rejected few days after transplantation in immunocompetent mice but not in nude mice, usually due to CD8+ T-cell response (Bhuniya, Pattarayan, and Yang 2022; Grzelak et al. 2022). Moreover, transplantation of low GFP-expressing cells or a few eGFP-expressing cells within a larger pool, escape the immune response, and are able to develop tumors, but still fail to metastasize (Gejman et al. 2018; Grzelak et al. 2022). Only in GFP-tolerant transgenic mice are cells able to successfully metastasize (Bhuniya et al. 2022; Grzelak et al. 2022). We also used H2030 human lung cancer cells as a xenograft model. Although these cells were not boosted with multiple rounds of lentiviral transduction, tumors either regressed after initial growth or stopped growing when transplanted subcutaneously, or failed to establish macroscopic tumor nodules in the lungs following tail vein cell injections (data not shown). This may stem from the low tumorigenic capacity of these cells. However, further testing is required to confirm this hypothesis. To circumvent the problem of immunogenicity, the use of mice that tolerate multiple reporter proteins (Bresser et al. 2020) or Cre-based removal of immunogens (Dubrot et al. 2021) could be considered in future experiments.

Since α-KG levels are shaped not only by cytosolic IDH1 but also by mitochondrial IDH2, we reviewed findings on IDH2 to better contextualize our results. IDH2 is highly expressed in lung as well as breast cancers (Li et al. 2018, 2024). However, IDH2 overexpression results in reduced α-KG levels and its depletion, in contrast to IDH1 depletion, leads to aberrant α-KG accumulation, increases oxidative stress, and promotes HIF-1α degradation. This impairs cell proliferation and viability *in vitro*, and tumor growth *in vivo* (Li et al. 2018, 2024). Indeed, The different IDH isoforms have overlapping but non-redundant functions in cellular metabolism (Alzial et al. 2022). It is suggested that IDH2 regulates the reversible reaction in the direction of reductive TCA cycle (Fig. 1.7) (Li et al. 2024). IDH2 knockdown also results in decreased Snail expression, as well as suppressed breast cancer cells migration, and invasion *in vitro*, and lung metastasis *in vivo* (Li et al. 2024).

4.5. α-KG homeostasis regulation under TGFβ signaling

In our experiments we have observed a downregulation of IDH1 mRNA and protein levels following TGFβ treatment (Fig. 3.7, Fig. 3.21a). However, no change was observed in the other IDH isoforms (Fig. 3.21b). In agreement with our observations, increasing concentrations of TGFβ have been shown to downregulate IDH1 protein levels in TGFβ-activated fibroblasts (Hou et al. 2017). This downregulation is dependent on canonical TGFB pathway, as depletion of Smad2, Smad3, or Smad4 fails to reduce IDH1 levels. Interestingly, a feedback loop between TGFβ and IDH1 is suggested, as reduced IDH1 levels lead to an increase in α-KG cellular levels. This could be due to context-dependent compensation by altered glutamine metabolism, although this possibility has not yet been explored. Accumulated α-KG downregulates the TGFBR protein inhibitor Cav1, by demethylating H3K4 on its promoter. In turn, the activated TGFBR promotes TGFβ signaling, which increases phosphorylation levels of Smad2 and Smad3. Interestingly, IDH1-depleted fibroblasts enhance melanoma cells proliferation *in vitro* and tumor growth *in vivo* (Hou et al. 2017). Moreover, U87MG cells transduced with mutant IDH1 exhibit a pronounced increase in Smad2 and Smad3 phosphorylation, along with elevated Smad4 expression, compared to their IDH1 WT counterparts (Gao et al. 2021). Thus, Gao and colleagues hypothesized that the growth-suppressive phenotype associated with IDH1 mutations could be exerted by downstream effectors of the TGFβ/Smad signaling pathway. In an independent observation, low IDH1 levels in breast cancer are attributed to inhibitory regulation by miRNAs (W.-S. Liu et al. 2018), where no direct connection to TGFβ signaling has been indicated. To date, the precise mechanism by which TGFβ regulates IDH1 remains unclear. We hypothesize it is mediated either at the transcriptional level via Smads or at the post-translational level through miRNAs. It is possible

that the effect of TGFβ on IDH1 and the feedback loop represent a general mechanism, but the impact on α-KG levels and on the cellular phenotype is context- and cell type-dependent.

TGFβ signaling is well known to enhance glycolysis in cancer cells (Rodríguez-García et al. 2017; Shen et al. 2023), which in turn promotes EMT and invasion (Liu and Chen 2022; Shen et al. 2023; Yalcin et al. 2017). However, its effects on OXPHOS and glutamine metabolism appear to be cell type– and context-dependent, with reports of both enhancement and repression (Hua et al. 2020; Jia et al. 2021; Liu and Chen 2022). To gain further insight into TGFβ-dependent, IDH1-compensatory or -independent regulation of α-KG levels, we set out to explore additional enzymes involved in α-KG homeostasis. A slight decrease in PSAT1 levels was detected in U87MG and A549 cells (Fig. 3.21c). However, PSAT1 has been demonstrated to be overexpressed in multiple tumor types, such as NSCLC (H. Li et al. 2023), renal cancer (Ye et al. 2024), ovarian cancer (Li et al. 2025), and uterine corpus endometrial carcinoma (Wang, Yue, and Yang 2023). Its high expression is associated with worse overall survival, and its knockdown impairs cell migration and invasiveness (H. Li et al. 2023; Li et al. 2025; Wang et al. 2023; Ye et al. 2024). We also found that GLUD1, the cytoplasmic isoform of glutamate dehydrogenase, was consistently downregulated across all three cancer cell lines following TGFβ treatment (Fig. 3.21c). GLUD1 has been reported to be either upregulated or downregulated in different cancer contexts. On one hand, GLUD1 expression has been reported to decrease during renal cancer progression, with reduced levels correlating with poorer survival and resistance to tyrosine kinase inhibitors. Notably, GLUD1 overexpression suppresses RCC cell proliferation, survival, and migration, in part by inhibiting PI3K-AKT-mTORC1 pathway activation (Lei Wang et al. 2022). On the other hand, it is mainly upregulated in gastric cancer, NSCLC, CRC, and cholangiocarcinoma, in which its genetic or pharmacological interference impairs cancer cells viability, migration and invasion, as well as tumor growth (Liu et al. 2015; Su et al. 2017; X. Wang et al. 2019; Qizhi Wang et al. 2022; Y.-J. Wu et al. 2019). Additionally, GLUD1 overexpression in CRC cells induces STAT3 phosphorylation, and increased expression of ZEB1 and Vimentin (Liu et al. 2015). Moreover, docetaxel-resistant NSCLC cells acquire glutamine addiction through GLUD1 upregulation, which elevates intracellular α-KG levels, leading to excessive ROS accumulation and subsequent Snail induction (Qizhi Wang et al. 2022). These results contrast with our observations on the anti-tumorigenic and health-promoting functions of α-KG. However, α-KG has been shown to exert context-dependent effects on ROS and Snail (Choi et al. 2025; Shen et al. 2020; Wu et al. 2023). Variations in α-KG metabolic routing, growth conditions, and therapeutic context, can explain these discrepancies. Notably, ROS accumulation itself can act

as a double-edged sword, either promoting or inhibiting tumor progression (Das, Suman, and Damodaran 2014; Jiang et al. 2017; Shagieva et al. 2017). Further investigations are required to better understand the crosstalk between TGFβ and α-KG producing enzymes, and its possible cellular and pathophysiological consequences.

4.6. Snail as a central mediator of EMT and invasion in IDH1-deficient cells

As previously highlighted, Snail's function as a master regulator of EMT and its response to IDH1 depletion, which distinguishes Snail from the other core EMT TFs, prompted us to further confirm its role in EMT and invasion in IDH1-deficient cells. Knockdown or knockout of Snail almost diminished its expression in these cells (Fig. 3.9b,d). Its short-hairpin- or RNP-mediated depletion also led to a substantial reduction in invasion (Fig. 3.9a,c). An incomplete depletion of Snail by sgRNA#1 resulted in a greater impairment in invasion compared to complete knockout by sgRNA#2 (Fig. 3.9c,d). This could indicate the activation of compensatory pro-invasive mechanisms in the complete knockout, which needs to be studied further. In line with our findings, Snail's role in mediating migration and invasion has been investigated in several studies. Transient or stable depletion of Snail results in extensive reduction of tumor cell migration and invasion, across various cancer models, including NSCLC (Jiang et al. 2019; Motizuki et al. 2024; Yang et al. 2017), ovarian cancer (Hojo et al. 2018), gastric cancer (Mishra et al. 2010), breast cancer (Lee, Park, and Oh 2020; Wu et al. 2009), and GBM (Goos 2015; Kühnöl et al. 2017; Mahabir et al. 2014; Myung et al. 2014). Moreover, Snail knockdown triggers E-cadherin and other cell adhesion molecule upregulation, concomitant with a reduction in mesenchymal and stem cell markers, such as N-cadherin, Vimentin, Nanog, CD133, and CD117, as well as MMPs expression (Hojo et al. 2018; Kühnöl et al. 2017; Mahabir et al. 2014; Wu et al. 2009; Yang et al. 2017; Zhou et al. 2014). Furthermore, Snail silencing impairs tumor growth (Goos 2015; Zhou et al. 2014), and metastatic burden (Hojo et al. 2018; Wu et al. 2009), *in vivo*. Conversely, overexpression of Snail has been associated with opposing phenotypes. It induces EMT in breast cancer and enhances anchorage-independent growth and migration and invasion *in vitro*, and results in larger tumors *in vivo* (Singh, Deshmukh, and Das 2021; Smith et al. 2014). Particularly, overexpression of Snail in luminal breast cancer cells confers migrative and invasive phenotypes comparable to the more aggressive and invasive TNBC cell lines (Singh et al. 2021). In contrast, overexpression of Snail has little effect on the migration or invasion of GBM cells (Kühnöl et al. 2017).

We also investigated the differential expression of potential downstream targets of Snail upon TGFβ treatment and modulation of intracellular α-KG levels. Analysis of our bulk RNA-

seq data highlighted known as well as new potential Snail targets, of which we were particularly interested in α-KG-responsive ones. We have observed an increase in MMP7, MMP13 and MMP15, upon both TGFβ stimulation and IDH1 depletion. Importantly, their expression levels were reduced following prolonged incubation with α-KG, mimicking Snail transcriptional regulation (Fig. 3.10a,b). Indeed, it has been demonstrated that MMP7 expression is elevated following ectopic overexpression of Snail (Miyoshi et al. 2004), supporting a potential regulatory relationship. This has been further confirmed by luciferase reporter assays, which demonstrates that Snail directly activates the MMP7 promoter, as transient knockdown of Snail results in reduced MMP7 reporter activity (Mishra et al. 2010). Likewise, Snail depletion results in reduced MMP13 expression, as well as its promoter activity (Ren et al. 2011; Singh et al. 2021). Particularly, deletion of Snail binding sites on MMP13 promoter sequence diminishes its activity, highlighting that MMP13 is a direct target of Snail TF (Singh et al. 2021). In contrast, Snail-dependent regulation of MMP15 is only reported in developmental growth of the heart cells, where Snail-induced mesenchymal transition, required for migration and invasion of both epicardial and endocardial cells, is mediated through MMP15 activity (Tao et al. 2011; Tao, Miller, and Lincoln 2013). To confirm this, we examined MMP7, and MMP15 RNA levels also by RT-qPCR. They were upregulated upon combined IDH1 depletion and TGFβ treatment, with MMP7 responding more to TGFβ and MMP15 responding to both IDH1 depletion and TGFβ in the single treatments. Importantly, they were robustly suppressed following 72 hours of α-KG treatment in IDH1 depleted and TGFβ treated cells (Fig. 3.10a,b). The absence of observable changes after 6 hours of α-KG treatment could be attributed to the delayed kinetics of Snail induction, as its upregulation in response to TGFβ stimulation typically required several hours in U87MG cells (Fig. 3.1a,b). Additionally, the suppressive effect of α-KG on Snail does not appear to be immediate or direct, suggesting that an extended exposure duration may be necessary to elicit a measurable response on its function as a TF.

When we examined MMP7 and MMP15 expression in parental cells, MMP7 showed some variations between the different cancer cells, while MMP15 was consistently upregulated following TGFβ, then reduced upon α-KG treatment (Fig. 3.10c), highlighting that their expression and regulation is cell type-dependent. Our findings and recent publications strongly highlight that TGFβ or IDH1 depletion-induced invasiveness may be driven at least partially by MMPs. MMP15 could be part of this process as a potential Snail downstream target, as suggested by its robust induction following TGFβ treatment and subsequent downregulation upon α-KG supplementation, which correlates well with the Snail expression pattern. Further experiments, examining its protein levels, as well as functional assays via its knockdown are

necessary to confirm this hypothesis. Although MMP-inhibitors have failed in the clinical trials (Cabral-Pacheco et al. 2020; Cox 2021; M. Li et al. 2023), multi-modal therapy including α-KG treatment in low IDH1 WT expressing cells could be interesting to test.

We also observed the downregulation of TGFβ- and IDH1 depletion-induced COL3A1, COL8A2, and COL14A1, following α-KG treatment (Fig. 3.10a). Interestingly, COL3A1 expression has been positively correlated with Snail, ZEB1, TWIST, Slug, and MMP7 (Cheng et al. 2021; Lautert-Dutra et al. 2024; Pepin et al. 2025; S. Wang et al. 2019). Knockdown of either COL3A1 or COL8A2 suppresses cell proliferation, invasion, and migration, whereas their overexpression enhances these processes, and results in increased expression of Snail, Vimentin, and N-cadherin, indicative of EMT induction in GBM, ovarian cancer, HCC, TNBC, and NSCLC (Cheng et al. 2021; Choi et al. 2025; Gao et al. 2018; Ren et al. 2024; W. Wang et al. 2013; F. Yang et al. 2022; Yang et al. 2025; Yin et al. 2021; Zhou et al. 2022). We have also observed an increase in COL14A1 mRNA levels following both IDH1 knockdown and TGFβ treatment in GBM cells (Fig. 3.10a-c), which was reduced upon 24 or 72 hours of α-KG treatment (Fig. 3.10a-c). However, it was barely expressed in carcinoma cells (Fig. 3.10c). As no prior correlation between COL14A1 and Snail has been reported, our results suggest a potential Snail-mediated COL14A1 regulation, although further validation is required to confirm this hypothesis. In addition, we propose a previously unrecognized role of COL14A1 in EMT downstream of TGFβ and IDH1 in GBM, which warrants further investigation in future experiments.

While we have identified potential downstream effectors of Snail that are negatively regulated upon α-KG treatment in IDH1-depleted TGFβ-stimulated cells, other targets that were not detected in the bulk RNA-seq analysis of a single cell line could also be involved in Snail-mediated EMT and negatively regulated by α-KG supplementation.

4.7. Snail regulation is exerted via multiple signaling pathways in IDH1-depleted cells

After identifying the α-KG-dependent role of IDH1 on Snail levels and the Snail-dependent regulatory mechanisms, we investigated the possible mechanisms by which α-KG might control the cellular level of the Snail protein. As demonstrated by Chin et al., octyl α-ketoglutarate (O-α-KG) can directly bind to the β subunit of ATP synthase (Fig. 1.9), thereby inhibiting its activity, particularly under nutrient-deprived conditions. This inhibition reduces ATP production, consequently impairing mTORC1 activity (Chin et al. 2014). Similar findings were obtained following treatment with oligomycin (Chin et al. 2014; Fu et al. 2015), an inhibitor of ATP synthase, which binds at the interface between the c8 ring and ATP6 in the F0 domain (Fig. 1.9) (Antoniel et al. 2014; Devenish et al. 2000; Hearne et al. 2020; Symersky et

al. 2012). α-KG supplementation has been since reported to lower ATP levels and the ATP/ADP ratio in diverse models, including human fibroblasts, human cancer cells, nematodes, Drosophila, and porcine oocytes (Baracco et al. 2019; Bodineau et al. 2021; Chin et al. 2014; Choi et al. 2025; Demianchuk et al. 2024; Su et al. 2019; Xiang et al. 2024; Z. Zhang et al. 2021). Notably, octyl derivatives of D-2-HG and L-2-HG have also been shown to inhibit ATP synthase and decrease ATP levels as well as ATP/ADP ratio (Fu et al. 2015). In line with the aforementioned findings, Dm-α-KG supplementation significantly reduced both ATP levels and the ATP/ADP ratio in U87MG cells in a concentration-dependent manner, to an extent comparable with oligomycin treatment (Fig. 3.11a,b). In IDH1-depleted and TGFβ-stimulated cells, α-KG also lowered ATP levels, and its combination with oligomycin further enhanced this reduction (Fig. 3.11c). This supports the notion that oligomycin and α-KG target different domains of ATP synthase (Antoniel et al. 2014; Chin et al. 2014; Devenish et al. 2000; Hearne et al. 2020; Symersky et al. 2012).

Based on the results of intensive research, it became clear that the metabolic pathways and biological effects of α-KG derivatives differ substantially (Baracco et al. 2019; Cynober et al. 1990; Hou et al. 2014; MacKenzie et al. 2007, 2007; Parker et al. 2021, 2021). In osteosarcoma cells, ATP levels decrease only after treatment with O-α-KG or trifluoromethylbenzyl α-KG (TFMB-α-KG), but not Dm-α-KG (Baracco et al. 2019), despite all derivatives comparably elevating intracellular α-KG levels (Baracco et al. 2019; Li et al. 2024). Conversely, in liver cancer cells, repeated Dm-α-KG treatment significantly reduces ATP levels to an extent comparable with starvation (Choi et al. 2025). Similarly, in breast cancer cells, treatment with Dm-α-KG significantly diminishes mitochondrial ATP production (Li et al. 2024). However, in the original report by Chin et al. (2014), all tested α-KG precursors significantly extend nematode lifespan and produce similar reductions in oxygen consumption rate (OCR) (Chin et al. 2014). α-KG is a weak hydrophilic acid with limited membrane permeability, which hinders its successful administration (Gyanwali et al. 2022). Thus, α-KG is administered to cells, animals, or humans, in the form of derivatives, such as methyl, octyl, ornithine, sodium, and calcium (Gyanwali et al. 2022; Zdzisińska et al. 2017). Once the esterified-precursors penetrate the cells, the esters are hydrolyzed by cytosolic esterases, whereas the base-derivatives are readily hydrolyzed once they pass the membrane esterases (Gyanwali et al. 2022; MacKenzie et al. 2007; Parker et al. 2021). Given that O-α-KG has been used in the key studies linking α-KG to ATP synthase inhibition and mTORC1 suppression, it would be interesting to test its effect compared to Dm-α-KG, which was used in our models.

The impact of α-KG and 2-HG on mTORC1 has been widely observed, with a strong reduction of phosphorylated forms of p70S6K and 4EBP1 upon treatment with α-KG or 2-HG (Chin et al. 2014; Choi et al. 2025; Fu et al. 2015). In agreement with these observations, α-KG-containing drinking water supplemented to mice for 6-12 months, diminishes mTOR activation in the ovary, kidney, and spleen (Z. Zhang et al. 2021). Our results supported these findings, in that α-KG treatment suppressed the activity of mTORC1 in all three cancer cell lines examined, as evidenced by reduced phosphorylation of p70S6K and/or 4EBP1. MDA-MB-231 and A549 cells showed inhibition of only 4EBP1, while U87MG cells exhibited suppression of both effectors (Fig. 3.12). These results suggest that α-KG-dependent modulation of mTORC1 represents a general mechanism, though the repressed effectors appear to depend on the cellular context (Fig. 3.12c).

The functional outcome of α-KG treatment on ATP and mTOR signaling appears to be highly context-dependent. Under nutrient-rich conditions, α-KG may enhance mTOR signaling pathway, promoting protein synthesis, proliferation, survival, and migration, among other cellular processes (Bodineau et al. 2021; Ge et al. 2018; Guo et al. 2016; Lampa et al. 2017; Shen et al. 2020; Wang et al. 2016; Żurek et al. 2019). Conversely, under metabolic stress or nutrient deprivation, as in our experimental setup, α-KG suppresses mTOR activity, triggers catabolic processes, autophagy and apoptosis, and inhibits cells growth and motility (Chin et al. 2014; Choi et al. 2025; Fu et al. 2015). Such variability likely reflects differences in experimental conditions, particularly medium composition. Our treatments were conducted under FBS starvation or in FBS-free TSM medium (Fig. 2.2, Fig. 2.9, Fig. 3.11, Fig. 3.12, Fig.3.13), whereas several reports do not specify serum deprivation. Additional evidence for conditional effects comes from a study by Xiang et al., who observed that α-KG alone does not reduce ATP level in NSCLC cells, but markedly lowers it when combined with CTPI2, a small-molecule inhibitor of the mitochondrial citrate transporter SLC25A1 (Xiang et al. 2024). Moreover, the type of model system used appears to influence the outcome of α-KG treatment. While the results are highly variable in cell culture models, *in vivo* studies more consistently demonstrate TOR-inhibitory effect of α-KG (Chin et al. 2014; Su et al. 2019; Z. Zhang et al. 2021). However, an exception was observed in aged mice, where dietary supplementation with calcium α-KG (Ca-α-KG) fails to alter mTORC1 activity across multiple organs (Asadi Shahmirzadi et al. 2020). These findings emphasize that the biological impact of α-KG is not only shaped by nutrient availability and culture conditions, but also by organismal context and physiological state.

In addition to ATP synthase inhibition, other mechanisms may also contribute to α-KG-mediated mTORC1 suppression. Recent studies propose that α-KG-induced mTOR inhibition is mediated by elevating ROS levels (Choi et al. 2025; Wu et al. 2023). This is in line with the observation that ATP5B knockdown alone does not substantially inhibit mTOR compared with α-KG treatment (Fu et al. 2015). These findings also imply that α-KG acts via parallel and not mutually exclusive mechanisms. Moreover, α-KG has also been shown to regulate mTOR upstream axes, by reducing PI3K mRNA expression without affecting MEK-ERK signaling (Su et al. 2019). We have not examined the mRNA levels of mTOR upstream regulators, yet we have observed in immunoblot analyses of TGFβ-stimulated A549 cells that AKT activity but not ERK was reduced following α-KG supplementation (Fig. 3.12c). Moreover, IDH1 knockdown enhanced AKT and ERK as well as P70S6K and 4EBP1 phosphorylation levels (Fig. 3.13a,b), contrasting with previous findings where IDH1 overexpression or α-KG treatment promotes PI3K-mTORC1 signaling (Ge et al. 2018; Shen et al. 2020). It is important to note that these observations, in contrast to our analyses, were made under nutrient-rich cell culture conditions.

Since ATP can stimulate mTOR either directly, or indirectly by inactivating AMPK, the mTOR upstream inhibitor (Amin et al. 2021; Battaglioni et al. 2022; Dennis et al. 2001; Gwinn et al. 2008; Inoki, Zhu, and Guan 2003; Kimura et al. 2003), we tested whether α-KG affects AMPK activation. Despite using several commercial antibodies in immunoblot experiments to measure total and active AMPK levels (see Table 2.1), we have not detected any remarkable changes following α-KG treatment (data not shown). Importantly, in the same experiments a strong and consistent decrease in ATP levels as well as mTORC1 activity was observed (Fig. 3.11a-c, 3.12a-c). Insufficient inhibition of ATP synthase could explain these findings, suggesting that higher concentrations or longer incubation with α-KG may be required to achieve greater inhibition of ATP synthase and activate AMPK. This interpretation aligns with previous findings demonstrating that, although low-dose α-KG or short-term exposure to 2-HG or α-KG effectively reduces ATP levels and suppresses mTORC1 activity, AMPK phosphorylation and activation requires higher concentrations of α-KG or prolonged exposure to 2-HG (Chin et al. 2014; Fu et al. 2015). Indeed, chronic *in vivo* supplementation of α-KG increases AMPK phosphorylation and activity in various organs (Z. Zhang et al. 2021). Notably, some reports have even suggested that α-KG increases the expression of AMPK subunits at both RNA and protein levels under environmental stress, leading to pronounced AMPK activation (He et al. 2017; Su et al. 2019), which could be explained by a feedback mechanism upon decreased ATP levels.

We observed increased mTORC1 activity upon TGFβ treatment in all parental cell lines as well as in IDH1-knockdown cells (Fig. 3.12a-c, Fig. 3.13a,b). Consistent with this, TGFβ is a well-established activator of the mTORC1 pathway, as it regularly activates PI3K-AKT or MEK-ERK, as part of its non-canonical signaling pathways (Deng et al. 2024; Ge et al. 2018; Lamouille and Derynck 2007; Massagué and Sheppard 2023; Song et al. 2018; Yeh et al. 2016). In our experiments, TGFβ stimulation also enhanced AKT and ERK phosphorylation in A549 (Fig. 3.12c), and IDH1-depleted U87MG cells (Fig. 3.13a). To determine which pathways are required for the Snail upregulation in IDH1-deficient cells, various inhibitors targeting key factors of the TGFβ-Snail axis have been employed (Fig. 3.13c). The results revealed that the TGFβ-PI3K-AKT-mTORC1 and ATP synthase-mTORC1 signaling axes, but not the TGFβ-MEK-ERK-mTORC1 signaling axis, are essential for Snail regulation in IDH1-depleted cells (Fig. 3.13a,b). In addition, increased Smad activity has also been detected previously in our laboratory in IDH1-knockdown cells with or without TGFβ stimulation by DLR assay (Bögürcü-Seidel 2018). This pathway could also contribute to mTOR regulation as Smad proteins are well-known regulators of mTOR, through suppression of DEPTOR (Das et al. 2013; Woodcock et al. 2019). These observations highlight that TGFβ- and IDH1-mediated Snail regulation can be exerted via multiple signaling pathways.

4.8. α-KG activates signaling pathways that converge on SNAI1

As the mTORC1 signaling pathway has been found to be an integral part of TGFβ as well as α-KG mediated regulation of Snail, we have investigated three established downstream targets of mTORC1, namely c-Myc, FoxK1, and FoxK2 (Chen et al. 2018; He et al. 2018; Nakatsumi et al. 2017; Sakaguchi et al. 2019; Stengel et al. 2022; West et al. 1998), which transcription factors have previously been shown to control Snail expression (X. Lin et al. 2017; Peng et al. 2016; Smith et al. 2009; Runze Wang et al. 2022; H. Xu et al. 2018; Zhai et al. 2018).

Our findings indicate that TGFβ-mediated activation of mTORC1 is accompanied by increased c-Myc and FoxK1 protein levels across multiple cancer cell lines, which were partially attenuated by α-KG supplementation (Fig. 3.13a-c). As c-Myc is an established 4-EBP1 target (Chen et al. 2018; Stengel et al. 2022; West et al. 1998; Yun et al. 2016), our results are consistent with the observed robust increase in 4-EBP1 activity upon IDH1 knockdown and TGFβ treatment, and its impairment following α-KG supplementation across the different cell lines (Fig. 3.12, Fig. 3.13). This is in alignment with published reports, highlighting reduced c-Myc protein levels following 4EBP1 knockdown (Yun et al. 2016), or after the pharmacological inhibition of PI3K (Stengel et al. 2022). Interestingly, c-Myc is upregulated following IDH1

overexpression and subsequent mTORC1 activation in U87MG (Shen et al. 2020), despite the variations in culture and treatment conditions as described earlier in section 4.2, these results highlight that c-Myc translation is regulated by mTORC1. Moreover, FoxK1 expression has been demonstrated to be upregulated upon TGFβ treatment in a time and dose dependent manner (Peng et al. 2016).

Interestingly, transient knockdown experiments revealed that c-Myc, but not FoxK1 or FoxK2, is critical for Snail upregulation in IDH1-depleted cells, at both mRNA and protein levels (Fig. 3.14a-c). The integral role of FoxK1 in EMT onset has been previously shown, as its transient knockdown decreases the levels of EMT markers, and inhibits migration and invasion in gastric cancer (Peng et al. 2016; Zhang et al. 2019). However, our data suggest that c-Myc, rather than FoxK1, functions as a central mediator linking mTORC1 signaling to Snail expression in the context of IDH1 deficiency, defining the IDH1-ATP synthase-mTORC1-c-Myc axis as a key regulatory pathway. Since the IDH1-PHD-HIF pathway has already been shown to partially regulate Snail levels (Bögürcü-Seidel 2018), we aimed to determine if these two signaling pathways cooperate in the control of Snail expression. Indeed, simultaneous knockdown of HIF-1α/2α and c-Myc resulted in a more pronounced reduction of Snail than either single knockdown (Fig. 3.15a-c). From this, we concluded that the α-KG-dependent IDH1-PHD-HIF and IDH1-ATP synthase-mTORC1-c-Myc signaling pathways converge on the SNAI1 gene and co-regulate Snail levels.

Despite repeated trials, we had technical difficulty in detecting TF binding on the SNAI1 promoter in MDA-MB-231 and U87MG cells using commercially available antibodies against c-Myc, HIF-1α, or HIF-1β in ChIP experiments (see Table 2.1). Thus, we mined publicly available ChIP-seq datasets of c-Myc or HIF-1α, HIF-2α, and HIF-1β (Fig. 3.19), which confirmed previous reports of their binding to the SNAI1 promoter (Gai et al. 2020; Luo et al. 2011; Smith et al. 2009; Runze Wang et al. 2022; Zhai et al. 2018; Zhang et al. 2013). Binding peaks overlapped with H3K4me3 and H3K27ac signals, indicating that the promoter regions, where these TFs are binding, are in an open and accessible chromatin conformation. Notably, analysis of HIF ChIP-seq data revealed the best detectability for HIF-2α, which was not assessed in our experiments and could be tested in future ones.

Utilizing a complementary approach to TF ChIP, we indirectly validated c-Myc and HIF binding by dual luciferase assays. We used two Snail promoter fragments, with one encompassing the TSS (Fig. 3.20a), a region enriched for c-Myc as well as Smad2-Smad3 binding as determined in ChIP experiments (Smith et al. 2009). Both TGFβ stimulation and hypoxia increased promoter activity, with further enhancement upon IDH1 knockdown (Fig.

3.20b,c,d). α-KG addition reduced SNAI1 promoter activity, which agreed with our RNA and protein analyses (Fig. 3.2b,c) and with histone modification ChIP-qPCR results (Fig. 3.18) that are discussed in Section 4.9. below. Finally, we have shown that c-Myc and HIF-1α/HIF-2α knockdown diminished TGFβ- or hypoxia-induced SNAI1 promoter activity (Fig. 3.20f,g). Collectively, these results established a positive role of TGFβ and hypoxia as EMT inducers, and c-Myc and HIF as key mediators of Snail transcriptional regulation.

4.9. α-KG could modulate Snail levels via intricate transcriptional and post-transcriptional mechanisms

Given that Snail levels were regulated following TGFβ stimulation, IDH1 depletion, and α-KG supplementation by TFs, it was important to determine whether and how epigenetic mechanisms, such as histone modifications, cooperate with c-Myc and HIFs. Considering that α-KG serves as a cofactor for a variety of epigenetic modifiers, including histone, DNA, and RNA demethylases (Losman et al. 2020), and that α-KG-mediated global changes in histone marks have been previously observed (Chung et al. 2020; Pan et al. 2016; TeSlaa et al. 2016; Tran et al. 2020; Xu et al. 2011), we first examined whether α-KG treatment induced global histone methylation changes. However no detectable variation was observed for either the active marks H3K4me3 and H3K36me3 (Chantalat et al. 2011; Xiao et al. 2021; Zhang, Cooper, and Brockdorff 2015), or the repressive mark H3K27me3 (Fig. 3.16), suggesting that the regulatory effect of α-KG on Snail expression is not related to widespread alterations in global histone methylation, but may involve site-specific histone modifications. Thus, we assessed active and repressive histone marks at several regions of SNAI1 promoter in MDA-MB-231 and U87MG IDH1-depleted cells following TGFβ and α-KG treatment (Fig. 3.17a). In MDA-MB-231 cells, TGFβ stimulation increased H3K27ac, a well-established activation mark, on the SNAI1 promoter (Fig. 3.17b). Similarly, both TGFβ stimulation and IDH1 depletion collaboratively increased H3K27ac and H3K4me3 in U87MG, consistent with transcriptional activation (Fig. 3.18a,b), and paralleling the observed gradual rise in Snail mRNA and protein levels (Fig. 3.1, Fig. 3.2). Conversely, α-KG supplementation reduced both active marks, indicative of transcriptional repression (Fig. 3.18a,b). Moreover, the repressive mark H3K27me3, diminished by TGFβ and/or IDH1 depletion, showed a partial restoration following α-KG supplementation, particularly at promoter regions containing HREs and E-boxes (Fig. 3.18b). Consistent with our findings, SNAI1 transcription is known to be regulated by various diverse epigenetic mechanisms (Baulida et al. 2019), including histone demethylation by α-KG dependent KDMs, which are frequently deregulated in cancer (Diao et

al. 2022; Gray et al. 2025; Hua et al. 2021; Tran, Dillingham, and Sridharan 2019; Yang et al. 2021). KDMs can function as either tumor suppressors or oncogenes, depending on their interacting binding partners, protein complexes, target gene, and cellular context (Gray et al. 2025). Although we did not examine other histone marks or directly interrogate different KDMs functions via genetic or pharmacological perturbation, several studies have documented KDM-mediated effects on SNAI1 promoter activity. For instance, KDM6A (UTX) and KDM6B, which remove H3K27me2 and H3K27me3 repressive marks, exert opposing functions on Snail expression in breast cancer cells, as well as migration and invasion. On one hand, KDM6A negatively regulates EMT through the transcriptional repression of Snail, ZEB1, and ZEB2, via recruitment of H3K4 demethylase LSD1 and formation of a repressive complex with histone deacetylase 1 (HDAC1) and DNA methyltransferase 1 (DNMT1), independent of its demethylase activity (Choi et al. 2015). On the other hand, TGFβ-induced KDM6B promotes Snail expression by removing H3K27me3 from the SNAI1 gene promoter (Ramadoss, Chen, and Wang 2012). Interestingly, in colon cancer, KDM6B knockdown is associated with increased Snail and ZEB1 expression (Pereira et al. 2011), although direct promoter regulation has not been demonstrated. Moreover, KDM8 (JMJD5) promotes EMT by demethylating H3K36me2 at the SNAI1 locus, and its overexpression promotes breast cancer cells invasiveness (Z. Zhao et al. 2015). Acetylation-dependent activation of SNAI1 has also been reported (Chang et al. 2017; Li et al. 2020; Sinha et al. 2024; Yao et al. 2020). Although KDM5 family members, which mediate H3K4me3 demethylation, have not been directly linked to SNAI1 regulation so far, some studies reported that KDM5 genetic or pharmacological inhibition is associated with aberrant Snail expression (Bamodu et al. 2016; Knyazev et al. 2023).

Beyond chromatin-dependent regulation, Snail levels can also be modulated post-transcriptionally. For instance, miRNAs, such as miR-34, miR-30, and miR-153 families, target Snail mRNA 3′-UTRs, promoting its degradation and inhibiting EMT (Baulida et al. 2019; Ye et al. 2015). TGFβ-mediated TET3 downregulation in ovarian cancer suppresses miR-30d expression, while TET3 overexpression reverses EMT through demethylation of miR-30d precursor gene (Ye et al. 2016). Additionally, the RNA demethylase FTO directly demethylates Snail mRNA, reducing its stability without affecting other EMT TFs. Its overexpression impairs EMT induction (M. Sun et al. 2022). Furthermore, FTO loss upregulates Snail, Slug, and ZEB1 expression, and induces EMT, through transcript stabilization of several factors of the WNT signaling cascade, across different cancer cell types, which mimics TGFβ-induced EMT

(Jeschke et al. 2021). These observations raise the possibility that other α-KG–dependent mechanisms may also contribute to Snail regulation.

4.10.Conclusion and outlook

The results presented in this work underscore the reciprocal link between EMT and metabolism and provide new insights into the mechanisms controlling EMT and tumor invasion in three different tumor models. On one hand, we highlighted the pivotal role of TGFβ and the hypoxic microenvironment in triggering Snail-orchestrated EMT and invasion in brain, lung and breast cancer cells. We also emphasized the indispensable function of Snail in mediating cancer cell invasiveness and suggested several Snail targets that may contribute to Snail-associated tumor invasion. Further experiments assessing the expression of these target genes following Snail knockdown, alongside functional assays, will be required to establish their roles. On the other hand, we provided evidence of the anti-tumorigenic effect of α-KG through the control of Snail expression and tumor cell invasion, a mechanism that may be impaired in cancer cells due to IDH1 downregulation or alternative mechanisms to reduce α-KG levels. It remains essential to investigate the impact of α-KG treatment on brain-metastatic breast and lung cancer cells, as well as on both primary tumor growth and metastatic spread following IDH1 depletion. Importantly, we provided detailed mechanistic insights into α-KG-mediated Snail regulation (Fig. 4.1). Our results support a model in which α-KG converges on Snail through two pathways, a previously uncharacterized mechanistic link via the ATP synthase-mTORC1-c-Myc pathway and the previously described PHD-HIF pathway (Bögürcü-Seidel 2018). Moreover, we demonstrated that the expression of Snail in IDH1-depleted cells is transcriptionally controlled by both c-Myc and HIF. To gain a more complete mechanistic understanding of their coordinated role, future studies should assess SNAI1 promoter activity following c-Myc and/or HIF overexpression, or after targeted mutation of HRE and E-box sites, coupled with functional assays, such as invasion. While a prior report suggested a correlation between IDH1 knockdown and Snail upregulation (W.-S. Liu et al. 2018), our study not only confirms this relationship across multiple tumor models, but more importantly dissects the mechanisms involved in the regulation between α-KG and Snail. Finally, we observed that TGFβ treatment reduced the expression of several α-KG regulating enzymes. To better understand the role of other α-KG regulating enzymes and transporters in maintaining α-KG cellular homeostasis, we have generated a CRISPR-sgRNA library targeting direct and indirect α-KG producing and consuming enzymes and multiple transporters for *in vivo* screening. Our aim is to identify metabolic factors that inhibit the growth of primary tumors and/or the

colonization of metastases, and which could be exploited in therapeutic interventions, possibly in combination with the administration of α-KG.

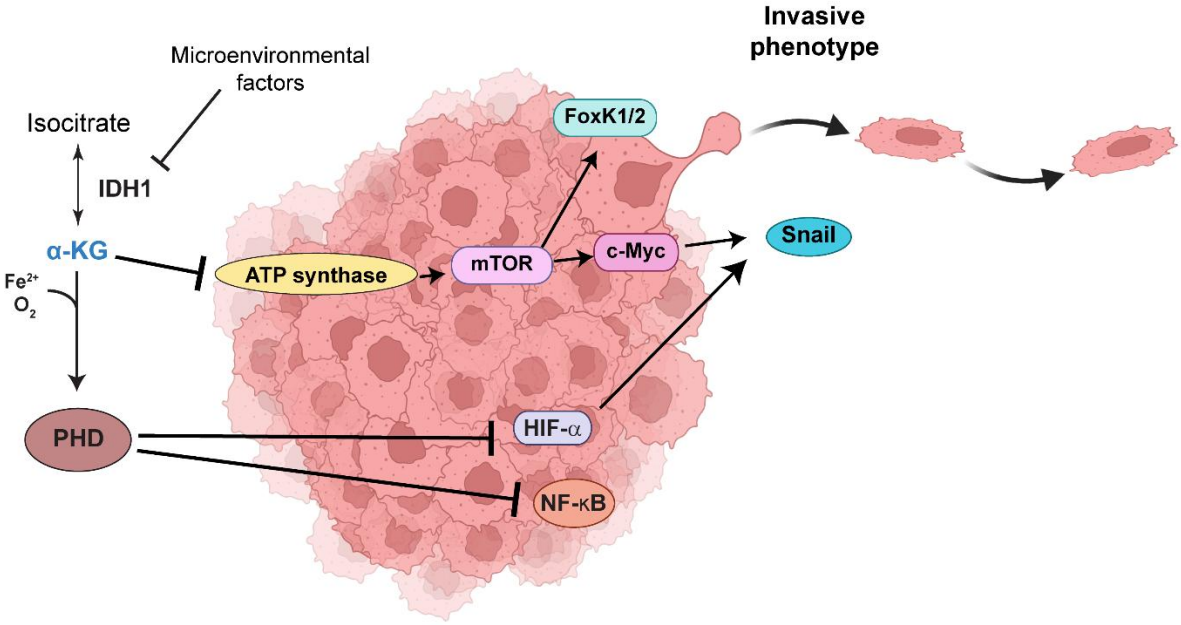

Figure 4.1. Graphical abstract of α-KG-mediated Snail regulation.

5. Summary

Metastasis, a defining hallmark of cancer, remains the leading cause of mortality among cancer patients. It is a multistep process in which tumor cells undergo epithelial-to-mesenchymal transition (EMT), invade surrounding tissues, disseminate through the circulation, evade immune surveillance, and colonize distant organs. EMT is induced by microenvironmental cues such as transforming growth factor β (TGFβ) and hypoxia, which activate transcription factors (TFs) including SNAI1/2, ZEB1/2, and TWIST1/2 that orchestrate EMT onset and enhance migratory and invasive capacities. EMT and invasion are particularly critical in primary and secondary brain malignancies. Glioblastoma (GBM), as well as brain metastases originating from lung and breast cancers, are characterized by highly aggressive tumor cells that exhibit profound resistance to conventional therapies. Current treatment options, including surgery, chemotherapy, radiotherapy, and targeted agents, yield only modest survival effects.

Metabolic rewiring is another hallmark of tumor progression, enabling cancer cells to sustain growth, adapt to adverse microenvironments, and fuel dissemination. Growing evidence points to a reciprocal crosstalk between metabolism and EMT, thus, identifying metabolic vulnerabilities that can disrupt the early steps of metastasis represents a promising strategy for the development of more effective therapies against invasive cancers. α-Ketoglutarate (α-KG), a pleiotropic metabolite, participates in cellular respiration, macromolecule biosynthesis, hypoxia regulation, and epigenetic modulation via the regulation of α-KG–dependent dioxygenases (α-KGDDs), and ATP synthase inhibition. While α-KG has been proposed to exert anti-tumorigenic and anti-aging functions, its mechanistic role in EMT regulation and invasion in GBM, breast, and lung cancers remains insufficiently defined.

In this study, we demonstrated that TGFβ treatment consistently upregulated Snail, but not other EMT TFs, thereby driving invasion in GBM, lung and breast carcinoma models. Supplementation with α-KG reduced Snail expression at RNA and protein levels, impaired EMT induction, and suppressed invasion, while leaving proliferation largely unaffected. To examine the impact of α-KG modulation on EMT regulation, we manipulated isocitrate dehydrogenase 1 (IDH1)-expression, a major source for α-KG in cells. While we detected highly elevated Snail levels and enhanced invasive phenotype following IHD1 depletion, IDH1 overexpression downregulated Snail and HIF-α levels. Importantly, Snail depletion abrogated the invasive phenotype of IDH1-deficient cells, confirming its essential role. We further identified MMPs and collagens as potential downstream mediators of Snail-driven invasion.

Mechanistically, α-KG regulated Snail expression on several levels. At the chromatin level, α-KG supplementation reduced active histone marks and modestly increased repressive marks on the SNAI1 promoter. On the signaling and transcriptional levels, α-KG inhibited the ATP synthase-mTORC1-c-Myc axis alongside the established PHD-HIF pathway, converging on Snail transcriptional repression. Consistently, knockdown of HIF-α and c-Myc counteracted the activating effect of IDH1 depletion on Snail promoter function under TGFβ or hypoxic stimulation. Using tumorsphere cultures, we validated the opposing effects of TGFβ and α-KG on tumor invasion. Additionally, we identified TGFβ as a regulator of enzymes controlling α-KG metabolism, possibly linking microenvironmental signaling to α-KG availability and suggesting a feedback loop between the tumor microenvironment and metabolic regulation of EMT. Finally, the prognostic impact of IDH1 and Snail was evaluated using statistical analyses of patient survival data. Low IDH1 and high Snail expression were significantly associated with poor overall survival in patients across GBM, breast, and lung cancers, underscoring the clinical relevance of our findings.

Taken together, our work identifies α-KG as an anti-tumorigenic metabolite that suppresses EMT and invasion across multiple tumor models by converging epigenetic and metabolic mechanisms on Snail regulation. Our findings reveal a previously unrecognized feedback link between microenvironmental signaling, metabolic rewiring, and transcriptional control of EMT. By delineating this IDH1-α-KG-Snail axis, the study identifies a metabolic vulnerability underlying EMT induction that could be therapeutically exploited to limit invasion and metastatic dissemination of primary and secondary brain tumors.

6. Zusammenfassung

Metastasierung, ein charakteristisches Merkmal von Krebs, stellt die führende Todesursache bei Krebspatienten dar. Es handelt sich um einen mehrstufigen Prozess, bei dem Tumorzellen eine epithelium-mesenchymale Transition (EMT) durchlaufen, in angrenzende Gewebe eindringen, über den Blutkreislauf disseminieren, der Immunabwehr entgehen und sich in entfernten Organen ansiedeln. EMT wird durch Signale der Mikroumgebung wie Transforming Growth Factor β (TGFβ) und Hypoxie induziert, welche Transkriptionsfaktoren (TFs) einschließlich SNAI1/2, ZEB1/2 und TWIST1/2 aktivieren, die den Beginn der EMT koordinieren und die Migrations- sowie Invasionsfähigkeit verstärken. EMT und Invasion sind besonders kritisch bei primären und sekundären bösartigen Hirntumoren. Glioblastome (GBM) sowie Hirnmetastasen aus Lungen- und Brustkrebs sind durch sehr aggressive Tumorzellen charakterisiert, die eine ausgeprägte Resistenz gegenüber konventionellen Therapien aufweisen. Aktuelle Behandlungsoptionen, einschließlich Chirurgie, Chemotherapie, Radiotherapie und zielgerichteten Wirkstoffen erzielen nur geringe Effekte hinsichtlich der Überlebensdauer.

Metabolische Umprogrammierung ist ein weiteres Kennzeichen der Tumorprogression und ermöglicht es Krebszellen, Wachstum aufrechtzuerhalten, sich an ungünstige Mikroumgebungen anzupassen und Dissemination zu fördern. Immer mehr Hinweise deuten auf eine reziproke Wechselwirkung zwischen dem Metabolismus und der EMT hin. Dementsprechend stellt die Identifizierung metabolischer Anfälligkeiten, die die frühen Schritte der Metastasierung aufhalten können, eine vielversprechende Strategie für die Entwicklung wirksamerer Therapien gegen invasive Tumoren dar. α-Ketoglutarat (α-KG), ein pleiotroper Metabolit, ist an Zellatmung, Makromolekülbiosynthese, Hypoxieregulation und epigenetischer Modulation über die Regulation α-KG–abhängiger Dioxygenasen (α-KGDDs) und die Hemmung der ATP-Synthase beteiligt. Obwohl α-KG anti-tumorigene und anti-aging Wirkungen zugeschrieben werden, ist seine mechanistische Rolle in der EMT-Regulation und Invasion bei GBM-, Brust- und Lungenkrebs noch nicht ausreichend geklärt.

In dieser Studie zeigten wir, dass die TGFβ-Behandlung Snail, jedoch keine anderen EMT-Transkriptionsfaktoren, konsistent hochregulierte und dadurch Invasion in GBM-, Lungen- und Brustkarzinommodellen vorantrieb. Die Supplementierung mit α-KG reduzierte die Snail-Expression auf RNA- und Proteinebene, beeinträchtigte die EMT-Induktion und unterdrückte die Invasion, während die Proliferation weitgehend unbeeinträchtigt blieb. Um den Einfluss der α-KG-Modulation auf die EMT-Regulation zu untersuchen, manipulierten wir die Expression

von Isocitratdehydrogenase 1 (IDH1), einer Hauptquelle für α-KG in Zellen. Während wir nach IDH1-Depletion stark erhöhte Snail-Spiegel und einen verstärkt invasiven Phänotyp beobachteten, senkte eine IDH1-Überexpression die Snail- und HIF-α-Level. Wichtig ist dabei, dass die Depletion von Snail den invasiven Phänotyp von IDH1-defizienten Zellen aufhob, was die wesentliche Rolle von Snail bestätigt. Zudem identifizierten wir MMPs und Kollagene als potenzielle nachgeschaltete Mediatoren der Snail-gesteuerten Invasion.

Mechanistisch regulierte α-KG die Snail-Expression auf mehreren Ebenen. Auf Chromatinebene reduzierte die α-KG-Supplementierung aktive Histonmarkierungen und erhöhte moderat repressive Markierungen am SNAI1-Promotor. Auf Signal- und Transkriptionsebene inhibierte α-KG die ATP-Synthase–mTORC1–c-Myc-Achse neben dem etablierten PHD-HIF-Signalweg und führte zu einer transkriptionellen Repression von Snail. Konsistent dazu wirkten Knockdowns von HIF-α und c-Myc dem aktivierenden Effekt der IDH1-Depletion auf die Snail-Promotoraktivität unter TGFβ- oder hypoxischer Stimulation entgegen. Unter Verwendung von Tumorsphärenkulturen validierten wir die gegensätzlichen Effekte von TGFβ und α-KG auf die Tumorinvasion. Darüber hinaus identifizierten wir TGFβ als Regulator von Enzymen des α-KG-Metabolismus, was möglicherweise eine Verbindung zwischen der Signalübertragung in der Mikroumgebung und der Verfügbarkeit von α-KG herstellt und auf ein Feedback zwischen der Tumormikroumgebung und metabolischer Regulation der EMT hindeutet. Abschließend wurde die prognostische Bedeutung von IDH1 und Snail anhand statistischer Analysen von Patientendaten bewertet. Niedrige IDH1- und hohe Snail-Expression waren signifikant mit einer schlechten Gesamtüberlebensrate bei Patienten mit GBM, Brust- und Lungenkrebs assoziiert und unterstreichen die klinische Relevanz unserer Ergebnisse.

Zusammenfassend identifiziert unsere Arbeit α-KG als antitumorigenen Metaboliten, der die EMT und Invasion in mehreren Tumormodellen durch die Konvergenz epigenetischer und metabolischer Mechanismen bei der Snail-Regulation hemmt. Unsere Ergebnisse deuten auf einen bisher unbekannten Feedback-Link zwischen Mikroumgebungssignalen, metabolischem Rewiring und Transkriptionskontrolle der EMT hin. Durch die Charakterisierung der IDH1–α-KG–Snail-Achse identifiziert diese Studie eine metabolische Verwundbarkeit der EMT-Induktion, die therapeutisch genutzt werden könnte, um Invasion und metastatische Dissemination primärer und sekundärer Hirntumoren zu begrenzen.

Abbreviations list

µg	microgram
µL	microliter
2-OG	2-Oxoglutarate
2-OGDDs	2-oxoglutarate-dependent dioxygenases
2-OGDH	2-oxoglutarate dehydrogenase
4EBP1	eIF4E binding protein 1
5caC	5-carboxylcytosine
5fC	5-formylcytosine
5hmC	5-hydroxylmethylcytosine
5mC	5-methyl Cytosine
6.8PL	6.8-kDa proteolipid
ALKBH5	alkB homolg 5
AMPK	AMP-activated protein kinase
APS	Ammonium persulfate
ARNT	aryl hydrocarbon nuclear translocator
ATP	adenosine triphosphate
BCAAs	branched-chain amino acids
BCAT	branched-chain aminotransferases
BCKAs	branched-chain-α-keto acids
BER	Base-Excision Repair
bHLH	basic helix-loop-helix
BLI	bioluminescence imaging
BR/HLH/LZ	basic-region /helix-loop-helix/leucine-zipper
BSA	Bovine serum albumin
Ca-α-KG	calcium α-KG
CBP	CREB-binding protein
ChIP-qPCR	chromatin immunoprecipitation quantitative polymerase chain reaction
CLDN	Claudins
co	control
CRC	colorectal cancer
crRNAs	Crispr RNAs

C_t	Cycle threshold
CTAD	C-terminal transactivating domain
CTCF	Corrected total cell fluorescence
CTNF	Corrected total nucleus fluorescence
D-2-HG	D-2-hydroxyglutarate
DAPI	4',6-diamidino-2-phenylindole
DAPIT	diabetes-associated protein in insulin-sensitive tissue
DEG	differentially expressed genes
DEPC	Diethylpyrocarbonate
DEPTOR	DEP-domain-containing mTOR-interacting protei
DLR	dual luciferase assay
DMEM	Dulbecco's Modified Eagle Medium
Dm-α-KG	dimethyl-alpha-ketoglutarate
DNAse I	Deoxyribonuclease I
DNMT1	DNA methyltransferase 1
Dor	Dorsomorphin
E/M	epithelial and mesenchymal
E-cad/E-cadherin	Epithelial cadherin
ECM	extracellular matrix
EGF	epidermal growth factor
EGFP	enhanced green fluorescent protein
EGLN	*egg laying defective nine*
EIF	eukaryotic initiation factor
EMP	Epithelial-mesenchymal-plasticity
EMT	Epithelial-mesenchymal-transition
ER	endoplasmic reticulum
ERK1/2	the extracellular-signal-regulated kinase 1/2
ETC	electron transport chain
FACS	Fluorescence-activated cell sorting
FAD	flavin adenine dinucleotide
FBS	Fetal Bovine Serum
Fe^{2+}	ferrous iron
FGF	fibroblast growth factor

FH	fumarate hydratase
FHA	forkhead-associated domain
FIH1	hydroxylase factor-inhibiting HIF
FKBP-12	FK506-binding protein 12
FOXC1	forkhead box C1
FoxK	Forkhead box K
FRB	FKBP12-rapamycin binding
FTO	fat mass and obesity-associated protein
g	Gram
GAP	GTPase-activating protein
GBM	glioblastoma
GDH	glutamate dehydrogenase
GEO	Gene Expression Omnibus
GLI1	Glioma-associated oncogene homolog 1
GLS	glutaminase
GLUD	glutamate dehydrogenase
GMT	glial-to-mesenchymal transition
GOT	glutamate oxaloacetate transaminases
GPT	glutamate pyruvate transaminases
gRNAs	guide RNAs
GSK-3β	glycogen synthase kinase 3 beta
H^+	hydrogen ions
HCC	hepatocellular carcinoma
HCl	Hydrochloric acid
HDAC1	histone deacetylase 1
HER2	human epidermal growth factor receptor 2
HIF	Hypoxia inducible factor
HRE	hypoxia response elements
i10	Invasive cells after 10 rounds of selection
IDH	isocitrate dehydrogenase
IF	Immunofluorescence
IGB	Integrated Genome Browser
IGFs	insulin-like growth factors

IKK	IκB kinase
IMM	inner mitochondrial membrane
IP	input
IVIS	*in vivo* imaging system
IκB	inhibitor of κB
JmjC	Jumonji C
KD	knockdown
KDMs	Lysine demethylases
KGM	α-ketoglutaramate
KM	Kaplan Meier
KO	Knockout
L	Liter
L-2-HG	L-2-hydroxyglutarate
LB	Luria-Bertani
LY	LY294002
m6A	N6-methyladenosine
MAPK	mitogen-activated protein kinase
mCherry	Cherry red fluorescent protein
MET	Mesenchymal-to-epithelial transition
mg	milligram
mL	milliliter
mLST8	mammalian lethal with sec-13 protein 8
mM	millimolar
mM	millimolar
MMPs	matrix metalloproteinases
mSIN1	mammalian stress-activated MAPK-interacting protein 1
MT-MMPs	Membrane-type MMPs
mTOR	Mechanistic/mammalian target of rapamycin
mTORC1	mTOR complex 1
mTORC2	mTOR complex 2
NaOH	Sodium hydroxide
NC	non-targeting control
N-cad/N-cadherin	Neural cadherin

NF-κB	nuclear factor kappa-light chain-enhancer of activated B cells
ng	nanogram
NGS	Normal goat serum
ni	non-invasive
NLS	nuclear localization signals
NSCLC	non-small cell lung cancer
NTAD	N-terminal transactivating domain
O_2	oxygen
OCLN	Occludin
OCR	oxygen consumption rate
ODDDs	oxygen-dependent degradation domain
OE	overexpression
OGC	oxoglutarate carrier
Oli	Oligomycin
ORF	open reading frame
OSCP	oligomycin sensitivity-conferring protein
OXPHOS	oxidative phosphorylation
O-α-KG	octyl α-ketoglutarate
P4H	prolyl 4-hydroxylases
P4HA	prolyl 4-hydroxylases alpha subunit
P4HB	prolyl 4-hydroxylases beta subunit
PAS	Per-Arnt-Sim
PDCD4	programmed cell death 4
PDK1	Phosphoinositide-dependent kinase 1
PFA	Paraformaldehyde
PHDs	prolyl hydroxylase domain-containing proteins
pHEMA	Poly-2-hydroxyethyl methacrylate
Pi	inorganic phosphate
PI3K	phosphatidylinositol 3-kinase
PIKK	phosphoinositide 3-kinase related kinase
PIP2	phosphatidylinositol-4,5-bisphosphate
PIP3	phosphatidylinositol-3,4,5-triphosphate
PLOD	procollagen-lysine 2-oxyglutarate 5-dioxygenase

PMT	Proneural-mesenchymal-transition
POR	pLenti6-ODD-RLuc
PRAS40	proline-rich AKT substrate 40 kDa
PRC2	Polycomb repressive complex 2
PROTOR-1	protein observed with Rictor-1
PRRX1	paired-related homebox 1
PSAT	phosphoserine aminotransferase
psi	pounds per square inch
pVHL	von Hippel-Lindau protein
RAGs	RAS-related GTP-binding proteins
Rap	Rapamycin
RAPTOR	regulatory-associated protein of mTOR
RCC	renal cell carcinoma
RFP	red fluorescent protein
RICTOR	rapamycin-insensitive companion of mTOR
RLU	relative luciferase units
RNP	Ribonucleoprotein
RNS	Reactive nitrogen species
ROI	Regions of interest
ROS	Reactive oxygen species
RPMI	Roswell Park Memorial Institute
rps6	Ribosomal protein S6
RSK1	p90 ribosomal S6 kinase 1
RT	Room temperature
RTKs	Receptor tyrosine kinases
RT-qPCR	Reverse transcription quantitative polymerase chain reaction
rtTA	Reverse tetracycline-controlled transactivator
S6K1	Ribosomal protein S6 kinase 1
SB	SB431542
SD	Standard deviation
SDH	Succinate dehydrogenase
SDS-PAGE	Sodium-Dodecyl-Sulfate-PolyAcrylamide Gel Electrophoresis
SEM	Standard error of means

TATk	Transactivator of Transcription
TBC1D7	TBC1 domain family member 7
TC	Tissue culture
TCA	Tricarboxylic acid
TCGA	The Cancer Genome Atlas
TDG	Thymine-DNA glycosylase
TEMED	Tetramethylenediamine
TET	Ten–eleven translocation
TF	Transcription factor
TFMB-α-KG	Trifluoromethylbenzyl α-KG
TGFβ	Transforming growth factor beta
TNBC	Triple negative breast cancer
TNFα	Tumor necrosis factor alpha
TRE	Tetracycline response element
TSC	Tuberous sclerosis complex
TSM	Tumorsphere medium
TSS	Transcription start site
TU	Transducing unit
U0	U0126
UTRs	Untranslated regions
V	Voltage
VDAC	Voltage-dependent anion channels
Vim	Vimentin
WB	Western blotting
WT	Wild-type
α-KG	α-ketoglutarate
α-KGDDs	α-Ketoglutarate dependent dioxygenases
α-KGDH	α-KG dehydrogenase

Index of figures and tables

Figure Index

Figure 1.1. Schematic illustration of the hallmarks of cancer. 10
Figure 1.2. Overview of the metastatic cascade. Schematic showing the essential steps of metastasis. 12
Figure 1.3. Overview of molecular and phenotypic changes during EMT. 15
Figure 1.4. Overview of the TGFβ canonical and non-canonical signaling pathways regulating EMT core TFs. 18
Figure 1.5. Overview of the HIF signaling pathway. 20
Figure 1.6. Overview of Snail target genes. 25
Figure 1.7. Overview of the enzymes and transporters governing α-KG homeostasis. 30
Figure 1.8. Overview of α-KG pleiotropic activities and a schematic of α-KGDDs reactions and subfamilies. 32
Figure 1.9. The impact of IDH1 knockdown on EMT, invasion, tumor growth, and metastasis. 34
Figure 1.10. Overview of ATP synthase structure and α-KG and oligomycin target sites. 39
Figure 1.11. Overview of mTORC1 and mTORC2 structure. 40
Figure 1.12. Overview of mTORC1 upstream and downstream signaling pathways from TGFβ receptors and RTKs to Snail gene regulation. 42
Figure 2.1. Experimental setups for TGFβ time course analyses. 72
Figure 2.2. Experimental setups for the analyses of combined TGFβ / α-KG treatments. 73
Figure 2.3. Experimental setups for the analyses of combined TGFβ / inhibitor treatments 74
Figure 2.4. Experimental setups for the analyses of IDH1 overexpression. 74
Figure 2.5. Experimental setups for dual luciferase assays. 79
Figure 2.6. Experimental setups for dual luciferase assay including siRNA treatments. 80
Figure 2.7. Experimental setups for the pre-treatment with TGFβ and / or α-KG prior to modified Boyden chamber invasion assay. 84
Figure 2.8. Experimental setup to detect the effect of α-KG treatment on cell proliferation and viability. 85
Figure 2.9. Experimental setups for ATP/ADP and ATP assays. 86
Figure 2.10. Experimental setups for the treatments of cells subjected to RNA-seq analyses. 89
Figure 2.11. Experimental setups for immunofluorescence analyses of Snail. 92
Figure 2.12. Experimental setups for immunofluorescence analysis of Vimentin. 93
Figure 2.13. Experimental setups for immunofluorescence analysis of E-cadherin. 94
Figure 2.14. Experimental setups for ChIP-qPCR analyses. 97

Figure 3.1.TGFβ stimulation increases Snail level in different cancer cell types. 105
Figure 3.2. α-KG treatment reduces TGFβ-induced EMT induction. 107
Figure 3.3. Immunofluorescence analyses of α-KG-mediated suppression of TGFβ-induced EMT. 109
Figure 3.4. Flow cytometry analyses of α-KG-mediated suppression of TGFβ-induced EMT. 110
Figure 3.5. α-KG attenuates tumor cell invasion. 112
Figure 3.6. α-KG has minor effect on cell proliferation and no remarkable impact on viability. 113
Figure 3.7. IDH1 depletion induces the EMT TF Snail and invasion. 115
Figure 3.8. IDH1-induced overexpression reduces EMT induction. 116
Figure 3.9. Snail knockdown mitigates IDH1 loss-induced invasion. 117
Figure 3.10. α-KG inhibits Snail transcriptional regulation and suppresses EMT program. 118
Figure 3.11. α-KG reduces ATP levels and the ATP/ADP ratio. 120
Figure 3.12. α-KG simultaneously reduces Snail levels, ATP synthase-mTORC1 activity and c-Myc levels. 121
Figure 3.13. Snail regulation is mediated through two pathways converging on mTORC1. 123
Figure 3.14. α-KG controls Snail levels partially through c-Myc. 123
Figure 3.15. α-KG suppresses Snail levels through converging pathways. 124
Figure 3.16. α-KG supplementation does not affect global pattern of histone modification. 124
Figure 3.17. TGFβ-induced chromatin regulation the SNAI1 gene promoter. 125
Figure 3.18. α-KG regulates Snail at promoter level. 126
Figure 3.19. c-Myc and HIFs bind to the Snail promoter. 127
Figure 3.20. The Snail promoter is regulated by IDH1 depletion, TGFβ, and hypoxia. 129
Figure 3.21. TGFβ downregulates IDH1 expression. 130
Figure 3.22. TGFβ controls α-KG-regulating enzymes. 131
Figure 3.23. Low IDH1 and high SNAI1 expression levels are associated with worse survival. 132
Figure 3.24. LLC1 cells are growing and invading in tumorsphere culture. 133
Figure 3.25. LLC1 pCDH B3 cells are tumorigenic. 134
Figure 3.26. Tumor formation and microenvironment labeling using LLC1 cells. 136
Figure 3.27. Enhanced reporter expression of tumor cells induces tumor immunogenicity *in vivo*. . 137
Figure 4.1. Graphical abstract of α-KG-mediated Snail regulation. 163

List of Tables

Table 2.1. Primary antibodies 48
Table 2.2. Secondary antibodies 50
Table 2.3. Antibiotics used for selection of bacterial cells 51
Table 2.4. Antibiotics used for selection of mammalian cells 51
Table 2.5. Inhibitors used and their targets 52
Table 2.6. List of RT-qPCR primers used in this study 53
Table 2.7. ChIP-qPCR primers list used in this study 55
Table 2.8. PCR primers used to amplify and clone part of the human SNAI1 promoter 56
Table 2.9. Crispr RNAs (crRNAs) and guide RNAs (gRNAs) purchased from IDT 58
Table 2.10. Commercial components from IDT 58
Table 2.11. Stable knockdown (KD) through shRNAs, knockout (KO) using RNP system, or overexpression (OE) cell lines generated by lentivirus transduction or transfection and subsequent selection 60
Table 2.12. Restriction digestion enzymes used for molecular cloning 63
Table 2.13. Growth factors used in cell culture 63
Table 2.14. Medium, buffers, and reagents purchased ready-to-use 64
Table 2.15. Kits and reagents used for RNA and genomic and plasmid DNA isolation and analysis 66
Table 2.16. Reagents used in various steps of protein analysis via western blot 68
Table 2.17. Reagents used in various steps of protein analysis via immunofluorescence 69
Table 2.18. Final single siRNA concentration used in reverse siRNA transient transfection 81
Table 2.19. Standard RT-qPCR amplification program using SYBR green 87
Table 2.20. Standard ChIP-qPCR amplification program using SYBR green 97
Table 2.21. Amplification program for SNAI1 promoter 98

References

Abbas, Zaid Nsaif, Ali Z. Al-Saffar, Saba Mahdi Jasim, and Ghassan M. Sulaiman. 2023. "Comparative Analysis between 2D and 3D Colorectal Cancer Culture Models for Insights into Cellular Morphological and Transcriptomic Variations." *Scientific Reports* 13(1):18380. doi:10.1038/s41598-023-45144-w.

Abla, Houda, Manuela Sollazzo, Giuseppe Gasparre, Luisa Iommarini, and Anna Maria Porcelli. 2020. "The Multifaceted Contribution of α-Ketoglutarate to Tumor Progression: An Opportunity to Exploit?" *Seminars in Cell & Developmental Biology* 98:26–33. doi:10.1016/j.semcdb.2019.05.031.

Achrol, Achal Singh, Robert C. Rennert, Carey Anders, Riccardo Soffietti, Manmeet S. Ahluwalia, Lakshmi Nayak, Solange Peters, Nils D. Arvold, Griffith R. Harsh, Patricia S. Steeg, and Steven D. Chang. 2019. "Brain Metastases." *Nature Reviews. Disease Primers* 5(1):5. doi:10.1038/s41572-018-0055-y.

Aftab, Saira, and Abdul Rauf Shakoori. 2022. "Glucose Deprivation Promotes Cancer Cell Invasion by Varied Expression of EMT Structural Proteins and Regulatory Molecules in MDA-MB-231 Triple-Negative Breast Cancer Cells." *Critical Reviews in Eukaryotic Gene Expression* 33(1):53–66. doi:10.1615/CritRevEukaryotGeneExpr.2022044483.

Aizer, Ayal A., Nayan Lamba, Manmeet S. Ahluwalia, Kenneth Aldape, Adrienne Boire, Priscilla K. Brastianos, Paul D. Brown, D. Ross Camidge, Veronica L. Chiang, Michael A. Davies, Leland S. Hu, Raymond Y. Huang, Timothy Kaufmann, Priya Kumthekar, Keng Lam, Eudocia Q. Lee, Nancy U. Lin, Minesh Mehta, Michael Parsons, David A. Reardon, Jason Sheehan, Riccardo Soffietti, Hussein Tawbi, Michael Weller, and Patrick Y. Wen. 2022. "Brain Metastases: A Society for Neuro-Oncology (SNO) Consensus Review on Current Management and Future Directions." *Neuro-Oncology* 24(10):1613–46. doi:10.1093/neuonc/noac118.

Ala-Aho, Risto, Nina Johansson, Andrew H. Baker, and Veli-Matti Kähäri. 2002. "Expression of Collagenase-3 (MMP-13) Enhances Invasion of Human Fibrosarcoma HT-1080 Cells." *International Journal of Cancer* 97(3):283–89. doi:10.1002/ijc.1619.

Ali, Eunus S., Kangkana Mitra, Shamima Akter, Sarker Ramproshad, Banani Mondal, Ishaq N. Khan, Muhammad Torequl Islam, Javad Sharifi-Rad, Daniela Calina, and William C. Cho. 2022. "Recent Advances and Limitations of mTOR Inhibitors in the Treatment of Cancer." *Cancer Cell International* 22(1):284. doi:10.1186/s12935-022-02706-8.

Alzial, Gabriel, Ophelie Renoult, François Paris, Catherine Gratas, Anne Clavreul, and Claire Pecqueur. 2022. "Wild-Type Isocitrate Dehydrogenase under the Spotlight in Glioblastoma." *Oncogene* 41(5):613–21. doi:10.1038/s41388-021-02056-1.

Amin, Anubhav G., Seung Won Jeong, John L. Gillick, Tolga Sursal, Raj Murali, Chirag D. Gandhi, and Meena Jhanwar-Uniyal. 2021. "Targeting the mTOR Pathway Using Novel ATP-competitive Inhibitors, Torin1, Torin2 and XL388, in the Treatment of Glioblastoma." *International Journal of Oncology* 59(4):83. doi:10.3892/ijo.2021.5263.

Antoniel, Manuela, Valentina Giorgio, Federico Fogolari, Gary D. Glick, Paolo Bernardi, and Giovanna Lippe. 2014. “The Oligomycin-Sensitivity Conferring Protein of Mitochondrial ATP Synthase: Emerging New Roles in Mitochondrial Pathophysiology.” *International Journal of Molecular Sciences* 15(5):7513–36. doi:10.3390/ijms15057513.

Asadi Shahmirzadi, Azar, Daniel Edgar, Chen-Yu Liao, Yueh-Mei Hsu, Mark Lucanic, Arash Asadi Shahmirzadi, Christopher D. Wiley, Garbo Gan, Dong Eun Kim, Herbert G. Kasler, Chisaka Kuehnemann, Brian Kaplowitz, Dipa Bhaumik, Rebeccah R. Riley, Brian K. Kennedy, and Gordon J. Lithgow. 2020. “Alpha-Ketoglutarate, an Endogenous Metabolite, Extends Lifespan and Compresses Morbidity in Aging Mice.” *Cell Metabolism* 32(3):447-456.e6. doi:10.1016/j.cmet.2020.08.004.

Aspuria, Paul-Joseph P., Sophia Y. Lunt, Leif Väremo, Laurent Vergnes, Maricel Gozo, Jessica A. Beach, Brenda Salumbides, Karen Reue, W. Ruprecht Wiedemeyer, Jens Nielsen, Beth Y. Karlan, and Sandra Orsulic. 2014. “Succinate Dehydrogenase Inhibition Leads to Epithelial-Mesenchymal Transition and Reprogrammed Carbon Metabolism.” *Cancer & Metabolism* 2:21. doi:10.1186/2049-3002-2-21.

Atalay, Esra Bulut, Serif Senturk, and Hulya Ayar Kayali. 2023. “Wild-Type IDH1 Knockout Leads to G0/G1 Arrest, Impairs Cancer Cell Proliferation, Altering Glycolysis, and the TCA Cycle in Colon Cancer.” *Biochemical Genetics* 61(4):1470–86. doi:10.1007/s10528-022-10325-1.

Atlante, Sandra, Alessia Visintin, Elisabetta Marini, Matteo Savoia, Chiara Dianzani, Marta Giorgis, Duran Sürün, Federica Maione, Frank Schnütgen, Antonella Farsetti, Andreas M. Zeiher, Massimo Bertinaria, Enrico Giraudo, Francesco Spallotta, Chiara Cencioni, and Carlo Gaetano. 2018. “α-Ketoglutarate Dehydrogenase Inhibition Counteracts Breast Cancer-Associated Lung Metastasis.” *Cell Death & Disease* 9(7):756. doi:10.1038/s41419-018-0802-8.

Audero, Madelaine Magalì, Tiago Miguel Amaral Carvalho, Federico Alessandro Ruffinatti, Thorsten Loeck, Maya Yassine, Giorgia Chinigò, Antoine Folcher, Valerio Farfariello, Samuele Amadori, Chiara Vaghi, Albrecht Schwab, Stephan J. Reshkin, Rosa Angela Cardone, Natalia Prevarskaya, and Alessandra Fiorio Pla. 2023. “Acidic Growth Conditions Promote Epithelial-to-Mesenchymal Transition to Select More Aggressive PDAC Cell Phenotypes In Vitro.” *Cancers* 15(9). doi:10.3390/cancers15092572.

Babaei, Ghader, Shiva Gholizadeh-Ghaleh Aziz, and Nasrin Zare Zavieyh Jaghi. 2021. “EMT, Cancer Stem Cells and Autophagy; The Three Main Axes of Metastasis.” *Biomedicine & Pharmacotherapy = Biomedecine & Pharmacotherapie* 133:110909. doi:10.1016/j.biopha.2020.110909.

Baksh, Sanjeethan C., and Lydia W. S. Finley. 2021. “Metabolic Coordination of Cell Fate by α-Ketoglutarate-Dependent Dioxygenases.” *Trends in Cell Biology* 31(1):24–36. doi:10.1016/j.tcb.2020.09.010.

Bamodu, Oluwaseun Adebayo, Wen-Chien Huang, Wei-Hwa Lee, Alexander Wu, Liang Shun Wang, Michael Hsiao, Chi-Tai Yeh, and Tsu-Yi Chao. 2016. “Aberrant KDM5B Expression Promotes Aggressive Breast Cancer through MALAT1 Overexpression and Downregulation of Hsa-miR-448.” *BMC Cancer* 16:160. doi:10.1186/s12885-016-2108-5.

Baracco, Elisa Elena, Francesca Castoldi, Sylvère Durand, David P. Enot, Jelena Tadic, Katharina Kainz, Frank Madeo, Alexis Chery, Valentina Izzo, Maria Chiara Maiuri, Federico Pietrocola, and Guido Kroemer. 2019. "α-Ketoglutarate Inhibits Autophagy." *Aging* 11(11):3418–31. doi:10.18632/aging.102001.

Battaglioni, Stefania, Don Benjamin, Matthias Wälchli, Timm Maier, and Michael N. Hall. 2022. "mTOR Substrate Phosphorylation in Growth Control." *Cell* 185(11):1814–36. doi:10.1016/j.cell.2022.04.013.

Baulida, Josep, Víctor M. Díaz, and Antonio García de Herreros. 2019. "Snail1: A Transcriptional Factor Controlled at Multiple Levels." *Journal of Clinical Medicine* 8(6). doi:10.3390/jcm8060757.

Bayliak, Maria M., and Volodymyr I. Lushchak. 2021. "Pleiotropic Effects of Alpha-Ketoglutarate as a Potential Anti-Ageing Agent." *Ageing Research Reviews* 66:101237. doi:10.1016/j.arr.2020.101237.

de Bem Prunes, Bianca, Júlia Silveira Nunes, Viviane Palmeira da Silva, Natalia Koerich Laureano, Douglas Rodrigues Gonçalves, Ian Santana Machado, Silvia Barbosa, Marcelo Lazzaron Lamers, Pantelis Varvaki Rados, Ina Kurth, Jochen Hess, Adriana Jou, and Fernanda Visioli. 2022. "The Role of Tumor Acidification in Aggressiveness, Cell Dissemination and Treatment Resistance of Oral Squamous Cell Carcinoma." *Life Sciences* 288:120163. doi:10.1016/j.lfs.2021.120163.

van den Bent, Martin J., Marjolein Geurts, Pim J. French, Marion Smits, David Capper, Jacoline E. C. Bromberg, and Susan M. Chang. 2023. "Primary Brain Tumours in Adults." *Lancet (London, England)* 402(10412):1564–79. doi:10.1016/S0140-6736(23)01054-1.

Bergaggio, Elisa, and Roberto Piva. 2019. "Wild-Type IDH Enzymes as Actionable Targets for Cancer Therapy." *Cancers* 11(4). doi:10.3390/cancers11040563.

Bergers, Gabriele, and Sarah-Maria Fendt. 2021. "The Metabolism of Cancer Cells during Metastasis." *Nature Reviews. Cancer* 21(3):162–80. doi:10.1038/s41568-020-00320-2.

Bhuniya, Avishek, Dhamotharan Pattarayan, and Da Yang. 2022. "Lentiviral Vector Transduction Provides Nonspecific Immunogenicity for Syngeneic Tumor Models." *Molecular Carcinogenesis* 61(12):1073–81. doi:10.1002/mc.23467.

Blaheta, Roman A., Jiaoyan Han, Elsie Oppermann, Wolf Otto Bechstein, Katrin Burkhard, Axel Haferkamp, Michael A. Rieger, and Patrizia Malkomes. 2025. "Transglutaminase 2 Promotes Epithelial-to-Mesenchymal Transition by Regulating the Expression of Matrix Metalloproteinase 7 in Colorectal Cancer Cells via the MEK/ERK Signaling Pathway." *Biochimica et Biophysica Acta. Molecular Basis of Disease* 1871(1):167538. doi:10.1016/j.bbadis.2024.167538.

Bodineau, Clément, Mercedes Tomé, Sarah Courtois, Ana S. H. Costa, Marco Sciacovelli, Benoit Rousseau, Elodie Richard, Pierre Vacher, Carlos Parejo-Pérez, Emilie Bessede, Christine Varon, Pierre Soubeyran, Christian Frezza, Piedad Del Socorro Murdoch, Victor H. Villar, and Raúl V. Durán. 2021. "Two Parallel Pathways Connect

Glutamine Metabolism and mTORC1 Activity to Regulate Glutamoptosis." *Nature Communications* 12(1):4814. doi:10.1038/s41467-021-25079-4.

Bögürcü-Seidel, Nuray. 2018. "Regulatory Mechanisms of Tumor Initiation, Growth and Invasion: The Function of Isocitrate Dehydrogenase 1, Acidosis and ephrinB2." Doctoral dissertation, Justus Liebig University.

Bohloli, Mahbobeh, Amir Atashi, Masoud Soleimani, Saeid Kaviani, and Azadeh Anbarlou. 2016. "Investigating Effects of Acidic pH on Proliferation, Invasion and Drug-Induced Apoptosis in Lymphoblastic Leukemia." *Cancer Microenvironment : Official Journal of the International Cancer Microenvironment Society* 9(2–3):119–26. doi:10.1007/s12307-016-0187-0.

Bowman, Christopher John, Donald E. Ayer, and Brian David Dynlacht. 2014. "Foxk Proteins Repress the Initiation of Starvation-Induced Atrophy and Autophagy Programs." *Nature Cell Biology* 16(12):1202–14. doi:10.1038/ncb3062.

Bowman, Robert L., Qianghu Wang, Angel Carro, Roel G. W. Verhaak, and Massimo Squatrito. 2017. "GlioVis Data Portal for Visualization and Analysis of Brain Tumor Expression Datasets." *Neuro-Oncology* 19(1):139–41. doi:10.1093/neuonc/now247.

Brabletz, Simone, Harald Schuhwerk, Thomas Brabletz, and Marc P. Stemmler. 2021. "Dynamic EMT: A Multi-Tool for Tumor Progression." *The EMBO Journal* 40(18):e108647. doi:10.15252/embj.2021108647.

Brabletz, T., A. Jung, S. Reu, M. Porzner, F. Hlubek, L. A. Kunz-Schughart, R. Knuechel, and T. Kirchner. 2001. "Variable Beta-Catenin Expression in Colorectal Cancers Indicates Tumor Progression Driven by the Tumor Environment." *Proceedings of the National Academy of Sciences of the United States of America* 98(18):10356–61. doi:10.1073/pnas.171610498.

Bray, Julie K., Meelad M. Dawlaty, Amit Verma, and Anirban Maitra. 2021. "Roles and Regulations of TET Enzymes in Solid Tumors." *Trends in Cancer* 7(7):635–46. doi:10.1016/j.trecan.2020.12.011.

Brenner, Alex W., and Akash J. Patel. 2022. "Review of Current Principles of the Diagnosis and Management of Brain Metastases." *Frontiers in Oncology* 12:857622. doi:10.3389/fonc.2022.857622.

Bresser, Kaspar, Feline E. Dijkgraaf, Colin E. J. Pritchard, Ivo J. Huijbers, Ji-Ying Song, Jan C. Rohr, Ferenc A. Scheeren, and Ton N. Schumacher. 2020. "A Mouse Model That Is Immunologically Tolerant to Reporter and Modifier Proteins." *Communications Biology* 3(1):273. doi:10.1038/s42003-020-0979-0.

Brocker, P., B. Vellas, J. L. Albarede, and T. Poynard. 1994. "A Two-Centre, Randomized, Double-Blind Trial of Ornithine Oxoglutarate in 194 Elderly, Ambulatory, Convalescent Subjects." *Age and Ageing* 23(4):303–6. doi:10.1093/ageing/23.4.303.

Brunner, Julia S., and Lydia W. S. Finley. 2023. "Metabolic Determinants of Tumour Initiation." *Nature Reviews. Endocrinology* 19(3):134–50. doi:10.1038/s41574-022-00773-5.

Cabral-Pacheco, Griselda A., Idalia Garza-Veloz, Claudia Castruita-De la Rosa, Jesús M. Ramirez-Acuña, Braulio A. Perez-Romero, Jesús F. Guerrero-Rodriguez, Nadia Martinez-Avila, and Margarita L. Martinez-Fierro. 2020. "The Roles of Matrix Metalloproteinases and Their Inhibitors in Human Diseases." *International Journal of Molecular Sciences* 21(24). doi:10.3390/ijms21249739.

Cai, Yiqing, Liemei Lv, Tiange Lu, Mengfei Ding, Zhuoya Yu, Xiaomin Chen, Xiangxiang Zhou, and Xin Wang. 2023. "α-KG Inhibits Tumor Growth of Diffuse Large B-Cell Lymphoma by Inducing ROS and TP53-Mediated Ferroptosis." *Cell Death Discovery* 9(1):182. doi:10.1038/s41420-023-01475-1.

Calvert, Andrea E., Alexandra Chalastanis, Yongfei Wu, Lisa A. Hurley, Fotini M. Kouri, Yingtao Bi, Maureen Kachman, Jasmine L. May, Elizabeth Bartom, Youjia Hua, Rama K. Mishra, Gary E. Schiltz, Oleksii Dubrovskyi, Andrew P. Mazar, Marcus E. Peter, Hongwu Zheng, C. David James, Charles F. Burant, Navdeep S. Chandel, Ramana V. Davuluri, Craig Horbinski, and Alexander H. Stegh. 2017. "Cancer-Associated IDH1 Promotes Growth and Resistance to Targeted Therapies in the Absence of Mutation." *Cell Reports* 19(9):1858–73. doi:10.1016/j.celrep.2017.05.014.

Cano, Amparo, and M. Angela Nieto. 2016. "Snail Transcription Factors." Pp. 1–6 in *Encyclopedia of Cancer*, edited by M. Schwab. Berlin, Heidelberg: Springer Berlin Heidelberg.

Cao, Qinchen, Xinxin Wang, Yonggang Shi, Mingzhi Zhang, Jing Yang, Meilian Dong, Yin Mi, Zhigang Zhang, Ke Liu, Li Jiang, Na Wang, and Ping Wang. 2019. "FOXC1 Silencing Inhibits the Epithelial-to-mesenchymal Transition of Glioma Cells: Involvement of B-catenin Signaling." *Molecular Medicine Reports* 19(1):251–61. doi:10.3892/mmr.2018.9650.

Carey, Bryce W., Lydia W. S. Finley, Justin R. Cross, C. David Allis, and Craig B. Thompson. 2015. "Intracellular α-Ketoglutarate Maintains the Pluripotency of Embryonic Stem Cells." *Nature* 518(7539):413–16. doi:10.1038/nature13981.

Casalino, Laura, and Pasquale Verde. 2020. "Multifaceted Roles of DNA Methylation in Neoplastic Transformation, from Tumor Suppressors to EMT and Metastasis." *Genes* 11(8). doi:10.3390/genes11080922.

Chaffer, Christine L., Beatriz P. San Juan, Elgene Lim, and Robert A. Weinberg. 2016. "EMT, Cell Plasticity and Metastasis." *Cancer Metastasis Reviews* 35(4):645–54. doi:10.1007/s10555-016-9648-7.

Chang, Ming-Min, Su-Zhen Wu, Shang-Hsun Yang, Chia-Ching Wu, Chia-Yih Wang, and Bu-Miin Huang. 2021. "FGF9/FGFR1 Promotes Cell Proliferation, Epithelial-Mesenchymal Transition, M2 Macrophage Infiltration and Liver Metastasis of Lung Cancer." *Translational Oncology* 14(11):101208. doi:10.1016/j.tranon.2021.101208.

Chang, Rui, Yinjie Zhang, Peng Zhang, and Qinghua Zhou. 2017. "Snail Acetylation by Histone Acetyltransferase P300 in Lung Cancer." *Thoracic Cancer* 8(3):131–37. doi:10.1111/1759-7714.12408.

Chantalat, Sophie, Arnaud Depaux, Patrick Héry, Sophie Barral, Jean-Yves Thuret, Stefan Dimitrov, and Matthieu Gérard. 2011. "Histone H3 Trimethylation at Lysine 36 Is

Associated with Constitutive and Facultative Heterochromatin." *Genome Research* 21(9):1426–37. doi:10.1101/gr.118091.110.

Chen, Hong-Chen. 2005. "Boyden Chamber Assay." *Methods in Molecular Biology (Clifton, N.J.)* 294:15–22. doi:10.1385/1-59259-860-9:015.

Chen, Hui, Hudan Liu, and Guoliang Qing. 2018. "Targeting Oncogenic Myc as a Strategy for Cancer Treatment." *Signal Transduction and Targeted Therapy* 3:5. doi:10.1038/s41392-018-0008-7.

Chen, Shaojie, Feifei Huang, Chong He, Jiajia Li, Shangxiang Chen, Yaqing Li, Yinting Chen, Guoda Lian, and Kaihong Huang. 2021. "Peripheral Blood Monocytes Predict Clinical Prognosis and Support Tumor Invasiveness through NF-κB-Dependent Upregulation of Snail in Pancreatic Cancer." *Translational Cancer Research* 10(11):4773–85. doi:10.21037/tcr-21-980.

Chen, Shu, Simin Jiang, Fen Hu, Yongjian Xu, Tao Wang, and Qi Mei. 2017. "Foxk2 Inhibits Non-Small Cell Lung Cancer Epithelial-Mesenchymal Transition and Proliferation through the Repression of Different Key Target Genes." *Oncology Reports* 37(4):2335–47. doi:10.3892/or.2017.5461.

Chen, Song, Yejinpeng Wang, Yaoyi Xiong, Tianchen Peng, Mengxin Lu, Lian Zhang, and Zhongqiang Guo. 2021. "Wild-Type IDH1 Inhibits the Tumor Growth through Degrading HIF-α in Renal Cell Carcinoma." *International Journal of Biological Sciences* 17(5):1250–62. doi:10.7150/ijbs.54401.

Chen, Xingchen, Pengkai Sun, Yan Liu, Senlin Shen, Tengfei Ma, and Jianping Ding. 2022. "Structures of a Constitutively Active Mutant of Human IDH3 Reveal New Insights into the Mechanisms of Allosteric Activation and the Catalytic Reaction." *The Journal of Biological Chemistry* 298(12):102695. doi:10.1016/j.jbc.2022.102695.

Chen, Yuping, Jinhuan Wu, Guang Liang, Guohe Geng, Fei Zhao, Ping Yin, Somaira Nowsheen, Chengming Wu, Yunhui Li, Lei Li, Wootae Kim, Qin Zhou, Jinzhou Huang, Jiaqi Liu, Chao Zhang, Guijie Guo, Min Deng, Xinyi Tu, Xiumei Gao, Zhongmin Liu, Yihan Chen, Zhenkun Lou, Kuntian Luo, and Jian Yuan. 2020. "CHK2-FOXK Axis Promotes Transcriptional Control of Autophagy Programs." *Science Advances* 6(1):eaax5819. doi:10.1126/sciadv.aax5819.

Chen, Zetao, Yihong Chen, Yan Li, Weidong Lian, Kehong Zheng, Yuxuan Zhang, Yujie Zhang, Chuang Lin, Chaoqun Liu, Fei Sun, Xinlin Sun, Jihui Wang, Liang Zhao, and Yiquan Ke. 2021. "Prrx1 Promotes Stemness and Angiogenesis via Activating TGF-β/Smad Pathway and Upregulating Proangiogenic Factors in Glioma." *Cell Death & Disease* 12(6):615. doi:10.1038/s41419-021-03882-7.

Chen, Zhou, Fangfang Han, Yan Du, Huaqing Shi, and Wence Zhou. 2023. "Hypoxic Microenvironment in Cancer: Molecular Mechanisms and Therapeutic Interventions." *Signal Transduction and Targeted Therapy* 8(1):70. doi:10.1038/s41392-023-01332-8.

Cheng, Yali. 2022. "miR-135b-5p Targets SIRT1 to Inhibit Deacetylation of c-JUN and Increase MMP7 Expression to Promote Migration and Invasion of Nasopharyngeal Carcinoma Cells." *Molecular Biotechnology* 64(6):693–701. doi:10.1007/s12033-022-00457-5.

Cheng, Ying-Xin, Lin Xiao, Yan-Li Yang, Xiao-Dong Liu, Xiu-Rong Zhou, Zhen-Fu Bu, Pei-Cheng Cao, and Dao-Kui Wang. 2021. "Collagen Type VIII Alpha 2 Chain (COL8A2), an Important Component of the Basement Membrane of the Corneal Endothelium, Facilitates the Malignant Development of Glioblastoma Cells via Inducing EMT." *Journal of Bioenergetics and Biomembranes* 53(1):49–59. doi:10.1007/s10863-020-09865-1.

Chin, Randall M., Xudong Fu, Melody Y. Pai, Laurent Vergnes, Heejun Hwang, Gang Deng, Simon Diep, Brett Lomenick, Vijaykumar S. Meli, Gabriela C. Monsalve, Eileen Hu, Stephen A. Whelan, Jennifer X. Wang, Gwanghyun Jung, Gregory M. Solis, Farbod Fazlollahi, Chitrada Kaweeteerawat, Austin Quach, Mahta Nili, Abby S. Krall, Hilary A. Godwin, Helena R. Chang, Kym F. Faull, Feng Guo, Meisheng Jiang, Sunia A. Trauger, Alan Saghatelian, Daniel Braas, Heather R. Christofk, Catherine F. Clarke, Michael A. Teitell, Michael Petrascheck, Karen Reue, Michael E. Jung, Alison R. Frand, and Jing Huang. 2014. "The Metabolite α-Ketoglutarate Extends Lifespan by Inhibiting ATP Synthase and TOR." *Nature* 510(7505):397–401. doi:10.1038/nature13264.

Choi, Hee-Joo, Ji-Hye Park, Mikyung Park, Hee-Young Won, Hyeong-Seok Joo, Chang Hoon Lee, Jeong-Yeon Lee, and Gu Kong. 2015. "UTX Inhibits EMT-Induced Breast CSC Properties by Epigenetic Repression of EMT Genes in Cooperation with LSD1 and HDAC1." *EMBO Reports* 16(10):1288–98. doi:10.15252/embr.201540244.

Choi, Sung Kyung, Myoung Jun Kim, and Jueng Soo You. 2025. "αKG-Induced Oxidative Stress and mTOR Inhibition as a Therapeutic Strategy for Liver Cancer." *Medical Oncology (Northwood, London, England)* 42(4):105. doi:10.1007/s12032-025-02653-0.

Chung, Chan, Stefan R. Sweha, Drew Pratt, Benita Tamrazi, Pooja Panwalkar, Adam Banda, Jill Bayliss, Debra Hawes, Fusheng Yang, Ho-Joon Lee, Mengrou Shan, Marcin Cieslik, Tingting Qin, Christian K. Werner, Daniel R. Wahl, Costas A. Lyssiotis, Zhiguo Bian, J. Brad Shotwell, Viveka Nand Yadav, Carl Koschmann, Arul M. Chinnaiyan, Stefan Blüml, Alexander R. Judkins, and Sriram Venneti. 2020. "Integrated Metabolic and Epigenomic Reprograming by H3K27M Mutations in Diffuse Intrinsic Pontine Gliomas." *Cancer Cell* 38(3):334-349.e9. doi:10.1016/j.ccell.2020.07.008.

Cockman, Matthew E., Kerstin Lippl, Ya-Min Tian, Hamish B. Pegg, William D. Jnr Figg, Martine I. Abboud, Raphael Heilig, Roman Fischer, Johanna Myllyharju, Christopher J. Schofield, and Peter J. Ratcliffe. 2019. "Lack of Activity of Recombinant HIF Prolyl Hydroxylases (PHDs) on Reported Non-HIF Substrates." *eLife* 8. doi:10.7554/eLife.46490.

Colvin, Hugh, Naohiro Nishida, Masamitsu Konno, Naotsugu Haraguchi, Hidekazu Takahashi, Junichi Nishimura, Taishi Hata, Koichi Kawamoto, Ayumu Asai, Kenta Tsunekuni, Jun Koseki, Tsunekazu Mizushima, Taroh Satoh, Yuichiro Doki, Masaki Mori, and Hideshi Ishii. 2016. "Oncometabolite D-2-Hydroxyglurate Directly Induces Epithelial-Mesenchymal Transition and Is Associated with Distant Metastasis in Colorectal Cancer." *Scientific Reports* 6:36289. doi:10.1038/srep36289.

Conza, Giusy Di, Chin-Hsien Tsai, and Ping-Chih Ho. 2019. “Fifty Shades of α-Ketoglutarate on Cellular Programming.” *Molecular Cell* 76(1):1–3. doi:https://doi.org/10.1016/j.molcel.2019.09.002.

Cox, Thomas R. 2021. “The Matrix in Cancer.” *Nature Reviews. Cancer* 21(4):217–38. doi:10.1038/s41568-020-00329-7.

Cummins, Eoin P., Edurne Berra, Katrina M. Comerford, Amandine Ginouves, Kathleen T. Fitzgerald, Fergal Seeballuck, Catherine Godson, Jens E. Nielsen, Paul Moynagh, Jacques Pouyssegur, and Cormac T. Taylor. 2006. “Prolyl Hydroxylase-1 Negatively Regulates IkappaB Kinase-Beta, Giving Insight into Hypoxia-Induced NFkappaB Activity.” *Proceedings of the National Academy of Sciences of the United States of America* 103(48):18154–59. doi:10.1073/pnas.0602235103.

Cynober, L. 1991. “Ornithine Alpha-Ketoglutarate in Nutritional Support.” *Nutrition (Burbank, Los Angeles County, Calif.)* 7(5):313–22.

Cynober, L., C. Coudray-Lucas, J. P. de Bandt, J. Guéchot, C. Aussel, M. Salvucci, and J. Giboudeau. 1990. “Action of Ornithine Alpha-Ketoglutarate, Ornithine Hydrochloride, and Calcium Alpha-Ketoglutarate on Plasma Amino Acid and Hormonal Patterns in Healthy Subjects.” *Journal of the American College of Nutrition* 9(1):2–12. doi:10.1080/07315724.1990.10720343.

Dahl, Erika S., Raquel Buj, Kelly E. Leon, Jordan M. Newell, Yuka Imamura, Benjamin G. Bitler, Nathaniel W. Snyder, and Katherine M. Aird. 2019. “Targeting IDH1 as a Prosenescent Therapy in High-Grade Serous Ovarian Cancer.” *Molecular Cancer Research : MCR* 17(8):1710–20. doi:10.1158/1541-7786.MCR-18-1233.

Das, Falguni, Nandini Ghosh-Choudhury, Amit Bera, Nirmalya Dey, Hanna E. Abboud, Balakuntalam S. Kasinath, and Goutam Ghosh Choudhury. 2013. “Transforming Growth Factor β Integrates Smad 3 to Mechanistic Target of Rapamycin Complexes to Arrest Deptor Abundance for Glomerular Mesangial Cell Hypertrophy.” *The Journal of Biological Chemistry* 288(11):7756–68. doi:10.1074/jbc.M113.455782.

Das, Trinath P., Suman Suman, and Chendil Damodaran. 2014. “Induction of Reactive Oxygen Species Generation Inhibits Epithelial-Mesenchymal Transition and Promotes Growth Arrest in Prostate Cancer Cells.” *Molecular Carcinogenesis* 53(7):537–47. doi:10.1002/mc.22014.

Dave, Natàlia, Sandra Guaita-Esteruelas, Susana Gutarra, Àlex Frias, Manuel Beltran, Sandra Peiró, and Antonio García de Herreros. 2011. “Functional Cooperation between Snail1 and Twist in the Regulation of ZEB1 Expression during Epithelial to Mesenchymal Transition.” *The Journal of Biological Chemistry* 286(14):12024–32. doi:10.1074/jbc.M110.168625.

Debnath, Pallabi, Rohit Singh Huirem, Paloma Dutta, and Santanu Palchaudhuri. 2022. “Epithelial-Mesenchymal Transition and Its Transcription Factors.” *Bioscience Reports* 42(1). doi:10.1042/BSR20211754.

Demianchuk, Oleh, Maria Lylyk, Vitalii Balatskiy, Dmytro Gospodaryov, and Maria Bayliak. 2024. “Alpha-Ketoglutarate Supplementation in Long-Lived Drosophila

Melanogaster: Impact on Lifespan and Metabolic Responses." *Archives of Insect Biochemistry and Physiology* 116(1):e22116. doi:10.1002/arch.22116.

Demidenko, Oleksandr, Diogo Barardo, Valery Budovskii, Robb Finnemore, Francis R. Palmer, Brian K. Kennedy, and Yelena V. Budovskaya. 2021. "Rejuvant®, a Potential Life-Extending Compound Formulation with Alpha-Ketoglutarate and Vitamins, Conferred an Average 8 Year Reduction in Biological Aging, after an Average of 7 Months of Use, in the TruAge DNA Methylation Test." *Aging* 13(22):24485–99. doi:10.18632/aging.203736.

Deng, Ziqin, Tao Fan, Chu Xiao, He Tian, Yujia Zheng, Chunxiang Li, and Jie He. 2024. "TGF-β Signaling in Health, Disease, and Therapeutics." *Signal Transduction and Targeted Therapy* 9(1):61. doi:10.1038/s41392-024-01764-w.

Dengler, Veronica L., Matthew Galbraith, and Joaquín M. Espinosa. 2014. "Transcriptional Regulation by Hypoxia Inducible Factors." *Critical Reviews in Biochemistry and Molecular Biology* 49(1):1–15. doi:10.3109/10409238.2013.838205.

Dennis, P. B., A. Jaeschke, M. Saitoh, B. Fowler, S. C. Kozma, and G. Thomas. 2001. "Mammalian TOR: A Homeostatic ATP Sensor." *Science (New York, N.Y.)* 294(5544):1102–5. doi:10.1126/science.1063518.

Depner, C., H. Zum Buttel, N. Böğürcü, A. M. Cuesta, M. R. Aburto, S. Seidel, F. Finkelmeier, F. Foss, J. Hofmann, K. Kaulich, S. Barbus, M. Segarra, G. Reifenberger, B. K. Garvalov, T. Acker, and A. Acker-Palmer. 2016. "EphrinB2 Repression through ZEB2 Mediates Tumour Invasion and Anti-Angiogenic Resistance." *Nature Communications* 7:12329. doi:10.1038/ncomms12329.

Derynck, Rik, Baby Periyanayaki Muthusamy, and Koy Y. Saeteurn. 2014. "Signaling Pathway Cooperation in TGF-β-Induced Epithelial-Mesenchymal Transition." *Current Opinion in Cell Biology* 31:56–66. doi:10.1016/j.ceb.2014.09.001.

Devenish, R. J., M. Prescott, G. M. Boyle, and P. Nagley. 2000. "The Oligomycin Axis of Mitochondrial ATP Synthase: OSCP and the Proton Channel." *Journal of Bioenergetics and Biomembranes* 32(5):507–15. doi:10.1023/a:1005621125812.

Dhanasekaran, Renumathy, Anja Deutzmann, Wadie D. Mahauad-Fernandez, Aida S. Hansen, Arvin M. Gouw, and Dean W. Felsher. 2022. "The MYC Oncogene - the Grand Orchestrator of Cancer Growth and Immune Evasion." *Nature Reviews. Clinical Oncology* 19(1):23–36. doi:10.1038/s41571-021-00549-2.

Diao, Wenfei, Jiabin Zheng, Yong Li, Junjiang Wang, and Songhui Xu. 2022. "Targeting Histone Demethylases as a Potential Cancer Therapy (Review)." *International Journal of Oncology* 61(3):103. doi:10.3892/ijo.2022.5393.

Dillekås, Hanna, Michael S. Rogers, and Oddbjørn Straume. 2019. "Are 90% of Deaths from Cancer Caused by Metastases?" *Cancer Medicine* 8(12):5574–76. doi:10.1002/cam4.2474.

Donati, L., F. Ziegler, G. Pongelli, and M. S. Signorini. 1999. "Nutritional and Clinical Efficacy of Ornithine Alpha-Ketoglutarate in Severe Burn Patients." *Clinical Nutrition (Edinburgh, Scotland)* 18(5):307–11. doi:10.1054/clnu.1999.0040.

Dong, Bo, and Yadi Wu. 2021. “Epigenetic Regulation and Post-Translational Modifications of SNAI1 in Cancer Metastasis.” *International Journal of Molecular Sciences* 22(20). doi:10.3390/ijms222011062.

Dongre, Anushka, and Robert A. Weinberg. 2019. “New Insights into the Mechanisms of Epithelial-Mesenchymal Transition and Implications for Cancer.” *Nature Reviews. Molecular Cell Biology* 20(2):69–84. doi:10.1038/s41580-018-0080-4.

Donnelley, Martin, Patricia Cmielewski, Emma Knight, Chantelle Carpentieri, Alexandra McCarron, Nathan Rout-Pitt, David Parsons, and Nigel Farrow. 2023. “Repeat or Single-Dose Lentiviral Vector Administration to Mouse Lungs? It’s All about the Timing.” *Gene Therapy* 30(9):698–705. doi:10.1038/s41434-023-00403-3.

Drapela, Stanislav, and Ana P. Gomes. 2021. “Metabolic Requirements of the Metastatic Cascade.” *Current Opinion in Systems Biology* 28:100381. doi:10.1016/j.coisb.2021.100381.

Du, Feng, Chenyang Qiao, Xiaowei Li, Zhangqian Chen, Hao Liu, Shengda Wu, Sijun Hu, Zhaoyan Qiu, Meirui Qian, Dean Tian, Kaichun Wu, Daiming Fan, Yongzhan Nie, and Limin Xia. 2019. “Forkhead Box K2 Promotes Human Colorectal Cancer Metastasis by Upregulating ZEB1 and EGFR.” *Theranostics* 9(13):3879–3902. doi:10.7150/thno.31716.

Dubrot, Juan, Sarah Kate Lane-Reticker, Emily A. Kessler, Austin Ayer, Gargi Mishra, Clara H. Wolfe, Margaret D. Zimmer, Peter P. Du, Animesh Mahapatra, Kyle M. Ockerman, Thomas G. R. Davis, Ian C. Kohnle, Hans W. Pope, Peter M. Allen, Kira E. Olander, Arvin Iracheta-Vellve, John G. Doench, W. Nicholas Haining, Kathleen B. Yates, and Robert T. Manguso. 2021. “In Vivo Screens Using a Selective CRISPR Antigen Removal Lentiviral Vector System Reveal Immune Dependencies in Renal Cell Carcinoma.” *Immunity* 54(3):571-585.e6. doi:10.1016/j.immuni.2021.01.001.

Eckschlager, Tomas, Ales Vicha, and Daniela Frolikova. 2025. “Lysine Demethylases and Cancer.” *Pathology, Research and Practice* 271:156011. doi:10.1016/j.prp.2025.156011.

El Mokbel, Naya, Alicia A. Goyeneche, Rewati Prakash, Benjamin N. Forgie, Farah H. Abdalbari, Xing Zeng, Basile Tessier-Cloutier, Shuk On Annie Leung, and Carlos M. Telleria. 2024. “Comparison of Two-Dimensional and Three-Dimensional Culture Systems and Their Responses to Chemotherapy in Cells Representing Disease Progression of High-Grade Serous Ovarian Cancer.” *Biochemistry and Biophysics Reports* 40:101838. doi:10.1016/j.bbrep.2024.101838.

Elia, Ilaria, Matteo Rossi, Steve Stegen, Dorien Broekaert, Ginevra Doglioni, Marit van Gorsel, Ruben Boon, Carmen Escalona-Noguero, Sophie Torrekens, Catherine Verfaillie, Erik Verbeken, Geert Carmeliet, and Sarah-Maria Fendt. 2019. “Breast Cancer Cells Rely on Environmental Pyruvate to Shape the Metastatic Niche.” *Nature* 568(7750):117–21. doi:10.1038/s41586-019-0977-x.

Enkhbaatar, Zanabazar, Minoru Terashima, Dulamsuren Oktyabri, Shoichiro Tange, Akihiko Ishimura, Seiji Yano, and Takeshi Suzuki. 2013. “KDM5B Histone Demethylase Controls Epithelial-Mesenchymal Transition of Cancer Cells by Regulating the

Expression of the microRNA-200 Family." *Cell Cycle (Georgetown, Tex.)* 12(13):2100–2112. doi:10.4161/cc.25142.

Fan, Peng, Naidong Zhang, Eleonora Candi, Massimiliano Agostini, Mauro Piacentini, Yufang Shi, Yuhui Huang, and Gerry Melino. 2023. "Alleviating Hypoxia to Improve Cancer Immunotherapy." *Oncogene* 42(49):3591–3604. doi:10.1038/s41388-023-02869-2.

Fang, Min, Jingping Yuan, Chunwei Peng, and Yan Li. 2014. "Collagen as a Double-Edged Sword in Tumor Progression." *Tumour Biology : The Journal of the International Society for Oncodevelopmental Biology and Medicine* 35(4):2871–82. doi:10.1007/s13277-013-1511-7.

Fares, Jawad, Mohamad Y. Fares, Hussein H. Khachfe, Hamza A. Salhab, and Youssef Fares. 2020. "Molecular Principles of Metastasis: A Hallmark of Cancer Revisited." *Signal Transduction and Targeted Therapy* 5(1):28. doi:10.1038/s41392-020-0134-x.

Fedele, Monica, Laura Cerchia, Silvia Pegoraro, Riccardo Sgarra, and Guidalberto Manfioletti. 2019. "Proneural-Mesenchymal Transition: Phenotypic Plasticity to Acquire Multitherapy Resistance in Glioblastoma." *International Journal of Molecular Sciences* 20(11). doi:10.3390/ijms20112746.

Fendt, Sarah-Maria. 2024. "100 Years of the Warburg Effect: A Cancer Metabolism Endeavor." *Cell* 187(15):3824–28. doi:10.1016/j.cell.2024.06.026.

Fidler, I. J. 1990. "Critical Factors in the Biology of Human Cancer Metastasis: Twenty-Eighth G.H.A. Clowes Memorial Award Lecture." *Cancer Research* 50(19):6130–38.

Fidler, Isaiah J. 2003. "The Pathogenesis of Cancer Metastasis: The 'seed and Soil' Hypothesis Revisited." *Nature Reviews. Cancer* 3(6):453–58. doi:10.1038/nrc1098.

Filip, Rafał S., Stefan G. Pierzynowski, Birger Lindegard, Jan Wernerman, Agnieszka Haratym-Maj, and Małgorzata Podgurniak. 2007. "Alpha-Ketoglutarate Decreases Serum Levels of C-Terminal Cross-Linking Telopeptide of Type I Collagen (CTX) in Postmenopausal Women with Osteopenia: Six-Month Study." *International Journal for Vitamin and Nutrition Research. Internationale Zeitschrift Fur Vitamin- Und Ernahrungsforschung. Journal International de Vitaminologie et de Nutrition* 77(2):89–97. doi:10.1024/0300-9831.77.2.89.

Fiorini, Giorgia, and Christopher J. Schofield. 2024. "Biochemistry of the Hypoxia-Inducible Factor Hydroxylases." *Current Opinion in Chemical Biology* 79:102428. doi:10.1016/j.cbpa.2024.102428.

Fu, Chenkun, Lina Chen, Yiju Cheng, Wenting Yang, Honglan Zhu, Xiao Wu, and Banruo Cai. 2023. "Identification of Immune Biomarkers Associated with Basement Membranes in Idiopathic Pulmonary Fibrosis and Their Pan-Cancer Analysis." *Frontiers in Genetics* 14:1114601. doi:10.3389/fgene.2023.1114601.

Fu, Xudong, Randall M. Chin, Laurent Vergnes, Heejun Hwang, Gang Deng, Yanpeng Xing, Melody Y. Pai, Sichen Li, Lisa Ta, Farbod Fazlollahi, Chuo Chen, Robert M. Prins, Michael A. Teitell, David A. Nathanson, Albert Lai, Kym F. Faull, Meisheng Jiang, Steven G. Clarke, Timothy F. Cloughesy, Thomas G. Graeber, Daniel Braas, Heather

R. Christofk, Michael E. Jung, Karen Reue, and Jing Huang. 2015. “2-Hydroxyglutarate Inhibits ATP Synthase and mTOR Signaling.” *Cell Metabolism* 22(3):508–15. doi:10.1016/j.cmet.2015.06.009.

Fujita, Naoyuki, David L. Jaye, Masahiro Kajita, Cissy Geigerman, Carlos S. Moreno, and Paul A. Wade. 2003. “MTA3, a Mi-2/NuRD Complex Subunit, Regulates an Invasive Growth Pathway in Breast Cancer.” *Cell* 113(2):207–19. doi:10.1016/s0092-8674(03)00234-4.

Gaete, Diana, Diego Rodriguez, Deepika Watts, Sundary Sormendi, Triantafyllos Chavakis, and Ben Wielockx. 2021. “HIF-Prolyl Hydroxylase Domain Proteins (PHDs) in Cancer-Potential Targets for Anti-Tumor Therapy?” *Cancers* 13(5). doi:10.3390/cancers13050988.

Gai, Xiaohong, Peng Zhou, Meng Xu, Zhikui Liu, Xin Zheng, and Qingguang Liu. 2020. “Hyperactivation of IL-6/STAT3 Pathway Leaded to the Poor Prognosis of Post-TACE HCCs by HIF-1α/SNAI1 Axis-Induced Epithelial to Mesenchymal Transition.” *Journal of Cancer* 11(3):570–82. doi:10.7150/jca.35631.

Gao, Ge, Yong Shi, Han-Xiang Deng, and Dimitri Krainc. 2025. “Dysregulation of Mitochondrial α-Ketoglutarate Dehydrogenase Leads to Elevated Lipid Peroxidation in CHCHD2-Linked Parkinson’s Disease Models.” *Nature Communications* 16(1):1982. doi:10.1038/s41467-025-57142-9.

Gao, Yongying, Yanwei Wu, Ningmei Zhang, Hongmei Yuan, Fei Wang, Hui Xu, Jiaxiang Yu, Jie Ma, Shaozhang Hou, and Xiangmei Cao. 2021. “IDH1 Gene Mutation Activates Smad Signaling Molecules to Regulate the Expression Levels of Cell Cycle and Biological Rhythm Genes in Human Glioma U87-MG Cells.” *Molecular Medicine Reports* 23(5):354. doi:10.3892/mmr.2021.11993.

Gao, Yuan-Feng, Xiao-Yuan Mao, Tao Zhu, Chen-Xue Mao, Zhi-Xiong Liu, Zhi-Bin Wang, Ling Li, Xi Li, Ji-Ye Yin, Wei Zhang, Hong-Hao Zhou, and Zhao-Qian Liu. 2016. “COL3A1 and SNAP91: Novel Glioblastoma Markers with Diagnostic and Prognostic Value.” *Oncotarget* 7(43):70494–503. doi:10.18632/oncotarget.12038.

Gao, Yuan-Feng, Tao Zhu, Juan Chen, Lin Liu, and Rong Ouyang. 2018. “Knockdown of Collagen α-1(III) Inhibits Glioma Cell Proliferation and Migration and Is Regulated by miR128-3p.” *Oncology Letters* 16(2):1917–23. doi:10.3892/ol.2018.8830.

Ge, Jing, Huachun Cui, Na Xie, Sami Banerjee, Sijia Guo, Shubham Dubey, Stephen Barnes, and Gang Liu. 2018. “Glutaminolysis Promotes Collagen Translation and Stability via α-Ketoglutarate-Mediated mTOR Activation and Proline Hydroxylation.” *American Journal of Respiratory Cell and Molecular Biology* 58(3):378–90. doi:10.1165/rcmb.2017-0238OC.

Gejman, Ron S., Aaron Y. Chang, Heather F. Jones, Krysta DiKun, Abraham Ari Hakimi, Andrea Schietinger, and David A. Scheinberg. 2018. “Rejection of Immunogenic Tumor Clones Is Limited by Clonal Fraction.” *eLife* 7. doi:10.7554/eLife.41090.

Georgakopoulos-Soares, Ilias, Dionysios V. Chartoumpekis, Venetsana Kyriazopoulou, and Apostolos Zaravinos. 2020. “EMT Factors and Metabolic Pathways in Cancer.” *Frontiers in Oncology* 10:499. doi:10.3389/fonc.2020.00499.

Gilkes, Daniele M., Gregg L. Semenza, and Denis Wirtz. 2014. “Hypoxia and the Extracellular Matrix: Drivers of Tumour Metastasis.” *Nature Reviews. Cancer* 14(6):430–39. doi:10.1038/nrc3726.

Gonzalez, David M., and Damian Medici. 2014. “Signaling Mechanisms of the Epithelial-Mesenchymal Transition.” *Science Signaling* 7(344):re8. doi:10.1126/scisignal.2005189.

Goos, Sarah. 2015. “The Role of Snail and Slug in Invasion and Cancer Stem Cell Maintenance in Glioblastoma Multiforme.” Doctoral dissertation, Justus Liebig University.

Gray, Zach H., Madison A. Honer, Pooja Ghatalia, Yang Shi, and Johnathan R. Whetstine. 2025. “20 Years of Histone Lysine Demethylases: From Discovery to the Clinic and Beyond.” *Cell* 188(7):1747–83. doi:10.1016/j.cell.2025.02.023.

Gregory, Philip A., Cameron P. Bracken, Eric Smith, Andrew G. Bert, Josephine A. Wright, Suraya Roslan, Melanie Morris, Leila Wyatt, Gelareh Farshid, Yat-Yuen Lim, Geoffrey J. Lindeman, M. Frances Shannon, Paul A. Drew, Yeesim Khew-Goodall, and Gregory J. Goodall. 2011. “An Autocrine TGF-Beta/ZEB/miR-200 Signaling Network Regulates Establishment and Maintenance of Epithelial-Mesenchymal Transition.” *Molecular Biology of the Cell* 22(10):1686–98. doi:10.1091/mbc.E11-02-0103.

Grzelak, Candice A., Erica T. Goddard, Emma E. Lederer, Kamya Rajaram, Jinxiang Dai, Ryann E. Shor, Andrea R. Lim, Jeanna Kim, Slobodan Beronja, Alister P. W. Funnell, and Cyrus M. Ghajar. 2022. “Elimination of Fluorescent Protein Immunogenicity Permits Modeling of Metastasis in Immune-Competent Settings.” *Cancer Cell* 40(1):1–2. doi:10.1016/j.ccell.2021.11.004.

Guaita, Sandra, Isabel Puig, Clara Franci, Marta Garrido, David Dominguez, Eduard Batlle, Elena Sancho, Shoukat Dedhar, Antonio Garcia De Herreros, and Josep Baulida. 2002. “Snail Induction of Epithelial to Mesenchymal Transition in Tumor Cells Is Accompanied by MUC1 Repression and ZEB1 Expression.” *The Journal of Biological Chemistry* 277(42):39209–16. doi:10.1074/jbc.M206400200.

Guo, Lijing, Shihua Chen, Liping Ou, Shangmei Li, Zhen-Nan Ye, and Hua-Feng Liu. 2022. “Disrupted Alpha-Ketoglutarate Homeostasis: Understanding Kidney Diseases from the View of Metabolism and Beyond.” *Diabetes, Metabolic Syndrome and Obesity : Targets and Therapy* 15:1961–74. doi:10.2147/DMSO.S369090.

Guo, Lili, Bo Zhou, Zhengqing Liu, Ying Xu, Hao Lu, Meng Xia, Ensong Guo, Wanying Shan, Gang Chen, and Changyu Wang. 2016. “Blockage of Glutaminolysis Enhances the Sensitivity of Ovarian Cancer Cells to PI3K/mTOR Inhibition Involvement of STAT3 Signaling.” *Tumour Biology : The Journal of the International Society for Oncodevelopmental Biology and Medicine* 37(8):11007–15. doi:10.1007/s13277-016-4984-3.

Gwinn, Dana M., David B. Shackelford, Daniel F. Egan, Maria M. Mihaylova, Annabelle Mery, Debbie S. Vasquez, Benjamin E. Turk, and Reuben J. Shaw. 2008. “AMPK Phosphorylation of Raptor Mediates a Metabolic Checkpoint.” *Molecular Cell* 30(2):214–26. doi:10.1016/j.molcel.2008.03.003.

Gyanwali, Bibek, Zi Xiang Lim, Janjira Soh, Clarissa Lim, Shou Ping Guan, Jorming Goh, Andrea B. Maier, and Brian K. Kennedy. 2022. “Alpha-Ketoglutarate Dietary Supplementation to Improve Health in Humans.” *Trends in Endocrinology and Metabolism: TEM* 33(2):136–46. doi:10.1016/j.tem.2021.11.003.

Győrffy, Balázs. 2024. “Integrated Analysis of Public Datasets for the Discovery and Validation of Survival-Associated Genes in Solid Tumors.” *Innovation (Cambridge (Mass.))* 5(3):100625. doi:10.1016/j.xinn.2024.100625.

Haerinck, Jef, Steven Goossens, and Geert Berx. 2023. “The Epithelial-Mesenchymal Plasticity Landscape: Principles of Design and Mechanisms of Regulation.” *Nature Reviews. Genetics* 24(9):590–609. doi:10.1038/s41576-023-00601-0.

Hamel, W., M. Westphal, and H. M. Shepard. 1993. “Loss in Expression of the Retinoblastoma Gene Product in Human Gliomas Is Associated with Advanced Disease.” *Journal of Neuro-Oncology* 16(2):159–65. doi:10.1007/BF01324703.

Han, Dan, Gang Wu, Chan Chang, Fang Zhu, Yin Xiao, Qiuhui Li, Tao Zhang, and Liling Zhang. 2015. “Disulfiram Inhibits TGF-β-Induced Epithelial-Mesenchymal Transition and Stem-like Features in Breast Cancer via ERK/NF-κB/Snail Pathway.” *Oncotarget* 6(38):40907–19. doi:10.18632/oncotarget.5723.

Han, Tianyu, De Kang, Daokun Ji, Xiaoyu Wang, Weihua Zhan, Minggui Fu, Hong-Bo Xin, and Jian-Bin Wang. 2013. “How Does Cancer Cell Metabolism Affect Tumor Migration and Invasion?” *Cell Adhesion & Migration* 7(5):395–403. doi:10.4161/cam.26345.

Hanahan, D., and R. A. Weinberg. 2000. “The Hallmarks of Cancer.” *Cell* 100(1):57–70. doi:10.1016/s0092-8674(00)81683-9.

Hanahan, Douglas. 2022. “Hallmarks of Cancer: New Dimensions.” *Cancer Discovery* 12(1):31–46. doi:10.1158/2159-8290.CD-21-1059.

Hanahan, Douglas, and Robert A. Weinberg. 2011. “Hallmarks of Cancer: The next Generation.” *Cell* 144(5):646–74. doi:10.1016/j.cell.2011.02.013.

Hao, Yang, David Baker, and Peter Ten Dijke. 2019. “TGF-β-Mediated Epithelial-Mesenchymal Transition and Cancer Metastasis.” *International Journal of Molecular Sciences* 20(11). doi:10.3390/ijms20112767.

Hapke, Robert Y., and Scott M. Haake. 2020. “Hypoxia-Induced Epithelial to Mesenchymal Transition in Cancer.” *Cancer Letters* 487:10–20. doi:10.1016/j.canlet.2020.05.012.

Harrison, A. P., and S. G. Pierzynowski. 2008. “Biological Effects of 2-Oxoglutarate with Particular Emphasis on the Regulation of Protein, Mineral and Lipid Absorption/Metabolism, Muscle Performance, Kidney Function, Bone Formation and Cancerogenesis, All Viewed from a Healthy Ageing Perspective State of the Art-- Review Article.” *Journal of Physiology and Pharmacology : An Official Journal of the Polish Physiological Society* 59 Suppl 1:91–106.

He, Liuqin, Niu Huang, Huan Li, Junquan Tian, Xihong Zhou, Tiejun Li, Kang Yao, Guoyao Wu, and Yulong Yin. 2017. “AMPK/α-Ketoglutarate Axis Regulates Intestinal Water

and Ion Homeostasis in Young Pigs." *Journal of Agricultural and Food Chemistry* 65(11):2287–98. doi:10.1021/acs.jafc.7b00324.

He, Long, Ana P. Gomes, Xin Wang, Sang Oh Yoon, Gina Lee, Michal J. Nagiec, Sungyun Cho, Andre Chavez, Tasnia Islam, Yonghao Yu, John M. Asara, Bo Yeon Kim, and John Blenis. 2018. "mTORC1 Promotes Metabolic Reprogramming by the Suppression of GSK3-Dependent Foxk1 Phosphorylation." *Molecular Cell* 70(5):949-960.e4. doi:10.1016/j.molcel.2018.04.024.

Hearne, Abby, Haotong Chen, Anna Monarchino, and Jeffrey S. Wiseman. 2020. "Oligomycin-Induced Proton Uncoupling." *Toxicology in Vitro : An International Journal Published in Association with BIBRA* 67:104907. doi:10.1016/j.tiv.2020.104907.

Ho, Hsin-Yu, Mu-Kuan Chen, Chia-Chieh Lin, Yu-Sheng Lo, Yi-Ching Chuang, and Ming-Ju Hsieh. 2023. "Epiberberine Suppresses the Metastasis of Head and Neck Squamous Cell Carcinoma Cells by Regulating the MMP-13 and JNK Pathway." *Journal of Cellular and Molecular Medicine* 27(23):3796–3804. doi:10.1111/jcmm.17954.

Hojo, N., A. L. Huisken, H. Wang, E. Chirshev, N. S. Kim, S. M. Nguyen, H. Campos, C. A. Glackin, Y. J. Ioffe, and J. J. Unternaehrer. 2018. "Snail Knockdown Reverses Stemness and Inhibits Tumour Growth in Ovarian Cancer." *Scientific Reports* 8(1):8704. doi:10.1038/s41598-018-27021-z.

Hopkins, Alex, Mackenzie L. Coatham, and Fred B. Berry. 2017. "FOXC1 Regulates FGFR1 Isoform Switching to Promote Invasion Following TGFβ-Induced EMT." *Molecular Cancer Research : MCR* 15(10):1341–53. doi:10.1158/1541-7786.MCR-17-0185.

Hou, Peifeng, Ching-Ying Kuo, Chun-Ting Cheng, Jing-Ping Liou, David K. Ann, and Qiang Chen. 2014. "Intermediary Metabolite Precursor Dimethyl-2-Ketoglutarate Stabilizes Hypoxia-Inducible Factor-1α by Inhibiting Prolyl-4-Hydroxylase PHD2." *PloS One* 9(11):e113865. doi:10.1371/journal.pone.0113865.

Hou, Xiaodan, Jieying Zhang, Yongbin Wang, Wujun Xiong, and Jun Mi. 2017. "TGFBR-IDH1-Cav1 Axis Promotes TGF-β Signalling in Cancer-Associated Fibroblast." *Oncotarget* 8(48):83962–74. doi:10.18632/oncotarget.20861.

Hu, Xiang, Yang Liu, Chunxia Qin, Zhenyu Pan, Jun Luo, Aixi Yu, and Zhen Cheng. 2014. "Up-Regulated Isocitrate Dehydrogenase 1 Suppresses Proliferation, Migration and Invasion in Osteosarcoma: In Vitro and in Vivo." *Cancer Letters* 346(1):114–21. doi:10.1016/j.canlet.2013.12.020.

Hua, Chunyan, Jiaqing Chen, Shuting Li, Jianan Zhou, Jiahong Fu, Weijian Sun, and Wenqian Wang. 2021. "KDM6 Demethylases and Their Roles in Human Cancers." *Frontiers in Oncology* 11:779918. doi:10.3389/fonc.2021.779918.

Hua, Wan, Peter Ten Dijke, Sarantos Kostidis, Martin Giera, and Marten Hornsveld. 2020. "TGFβ-Induced Metabolic Reprogramming during Epithelial-to-Mesenchymal Transition in Cancer." *Cellular and Molecular Life Sciences : CMLS* 77(11):2103–23. doi:10.1007/s00018-019-03398-6.

Huang, Hai, Ying Han, Zhijun Chen, Xin Pan, Putao Yuan, Xiangde Zhao, Hongfang Zhu, Jiying Wang, Xuewu Sun, and Peihua Shi. 2020. "ML264 Inhibits Osteosarcoma Growth and Metastasis via Inhibition of JAK2/STAT3 and WNT/β-Catenin Signalling Pathways." *Journal of Cellular and Molecular Medicine* 24(10):5652–64. doi:10.1111/jcmm.15226.

Huang, Jiacheng, Lele Zhang, Dalong Wan, Lin Zhou, Shusen Zheng, Shengzhang Lin, and Yiting Qiao. 2021. "Extracellular Matrix and Its Therapeutic Potential for Cancer Treatment." *Signal Transduction and Targeted Therapy* 6(1):153. doi:10.1038/s41392-021-00544-0.

Huang, Jia-Yuan, Kai Zhang, Dong-Qin Chen, Jing Chen, Bing Feng, Haizhu Song, Yitian Chen, Ziman Zhu, Lei Lu, Wei De, Rui Wang, and Long-Bang Chen. 2015. "MicroRNA-451: Epithelial-Mesenchymal Transition Inhibitor and Prognostic Biomarker of Hepatocelluar Carcinoma." *Oncotarget* 6(21):18613–30. doi:10.18632/oncotarget.4317.

Huang, Yanqing, Daniel Lin, and Cullen M. Taniguchi. 2017. "Hypoxia Inducible Factor (HIF) in the Tumor Microenvironment: Friend or Foe?" *Science China. Life Sciences* 60(10):1114–24. doi:10.1007/s11427-017-9178-y.

Huang, Yuhe, Weiqi Hong, and Xiawei Wei. 2022. "The Molecular Mechanisms and Therapeutic Strategies of EMT in Tumor Progression and Metastasis." *Journal of Hematology & Oncology* 15(1):129. doi:10.1186/s13045-022-01347-8.

Inoki, Ken, Tianqing Zhu, and Kun-Liang Guan. 2003. "TSC2 Mediates Cellular Energy Response to Control Cell Growth and Survival." *Cell* 115(5):577–90. doi:10.1016/s0092-8674(03)00929-2.

Inoue, Akihiro, Hisaaki Takahashi, Hironobu Harada, Shohei Kohno, Shiro Ohue, Kana Kobayashi, Hajime Yano, Junya Tanaka, and Takanori Ohnishi. 2010. "Cancer Stem-like Cells of Glioblastoma Characteristically Express MMP-13 and Display Highly Invasive Activity." *International Journal of Oncology* 37(5):1121–31. doi:10.3892/ijo_00000764.

Intlekofer, Andrew M., Raymond G. Dematteo, Sriram Venneti, Lydia W. S. Finley, Chao Lu, Alexander R. Judkins, Ariën S. Rustenburg, Patrick B. Grinaway, John D. Chodera, Justin R. Cross, and Craig B. Thompson. 2015. "Hypoxia Induces Production of L-2-Hydroxyglutarate." *Cell Metabolism* 22(2):304–11. doi:10.1016/j.cmet.2015.06.023.

Iser, Isabele C., Mariana B. Pereira, Guido Lenz, and Márcia R. Wink. 2017. "The Epithelial-to-Mesenchymal Transition-Like Process in Glioblastoma: An Updated Systematic Review and In Silico Investigation." *Medicinal Research Reviews* 37(2):271–313. doi:10.1002/med.21408.

Islam, Mohammad Mainul, Manisha Nautiyal, R. Max Wynn, James A. Mobley, David T. Chuang, and Susan M. Hutson. 2010. "Branched-Chain Amino Acid Metabolon: Interaction of Glutamate Dehydrogenase with the Mitochondrial Branched-Chain Aminotransferase (BCATm)." *The Journal of Biological Chemistry* 285(1):265–76. doi:10.1074/jbc.M109.048777.

Iwadate, Yasuo. 2016. “Epithelial-Mesenchymal Transition in Glioblastoma Progression.” *Oncology Letters* 11(3):1615–20. doi:10.3892/ol.2016.4113.

Jeschke, Jana, Evelyne Collignon, Clémence Al Wardi, Mohammad Krayem, Martin Bizet, Yan Jia, Soizic Garaud, Zéna Wimana, Emilie Calonne, Bouchra Hassabi, Renato Morandini, Rachel Deplus, Pascale Putmans, Gaurav Dube, Nitesh Kumar Singh, Alexander Koch, Kateryna Shostak, Lara Rizzotto, Robert L. Ross, Christine Desmedt, Yacine Bareche, Françoise Rothé, Jacqueline Lehmann-Che, Martine Duterque-Coquillaud, Xavier Leroy, Gerben Menschaert, Luis Teixeira, Mingzhou Guo, Patrick A. Limbach, Pierre Close, Alain Chariot, Eleonora Leucci, Ghanem Ghanem, Bi-Feng Yuan, Karen Willard-Gallo, Christos Sotiriou, Jean-Christophe Marine, and François Fuks. 2021. “Downregulation of the FTO m(6)A RNA Demethylase Promotes EMT-Mediated Progression of Epithelial Tumors and Sensitivity to Wnt Inhibitors.” *Nature Cancer* 2(6):611–28. doi:10.1038/s43018-021-00223-7.

Jia, Dongya, Jun Hyoung Park, Harsimran Kaur, Kwang Hwa Jung, Sukjin Yang, Shubham Tripathi, Madeline Galbraith, Youyuan Deng, Mohit Kumar Jolly, Benny Abraham Kaipparettu, José N. Onuchic, and Herbert Levine. 2021. “Towards Decoding the Coupled Decision-Making of Metabolism and Epithelial-to-Mesenchymal Transition in Cancer.” *British Journal of Cancer* 124(12):1902–11. doi:10.1038/s41416-021-01385-y.

Jia, You Chao, Jian Yi Wang, Yu Ying Liu, Bin Li, Hui Guo, and Ai Min Zang. 2019. “LncRNA MAFG-AS1 Facilitates the Migration and Invasion of NSCLC Cell via Sponging miR-339-5p from MMP15.” *Cell Biology International* 43(4):384–93. doi:10.1002/cbin.11092.

Jiang, Jingwen, Kui Wang, Yan Chen, Haining Chen, Edouard C. Nice, and Canhua Huang. 2017. “Redox Regulation in Tumor Cell Epithelial-Mesenchymal Transition: Molecular Basis and Therapeutic Strategy.” *Signal Transduction and Targeted Therapy* 2:17036. doi:10.1038/sigtrans.2017.36.

Jiang, Kanqiu, Ting Zhao, Mingjing Shen, Fuquan Zhang, Shanzhou Duan, Zhe Lei, and Yongbing Chen. 2019. “MiR-940 Inhibits TGF-β-Induced Epithelial-Mesenchymal Transition and Cell Invasion by Targeting Snail in Non-Small Cell Lung Cancer.” *Journal of Cancer* 10(12):2735–44. doi:10.7150/jca.31800.

Jiang, Mingxia, Huapan Fang, and Huayu Tian. 2025. “Metabolism of Cancer Cells and Immune Cells in the Initiation, Progression, and Metastasis of Cancer.” *Theranostics* 15(1):155–88. doi:10.7150/thno.103376.

Jiang, Yue, Fangfang Chen, Xunshan Ren, Yu Yang, Jiajun Luo, Jingwen Yuan, Jingping Yuan, and Qiang Tong. 2022. “RNA-Binding Protein COL14A1, TNS1, NUSAP1 and YWHAE Are Valid Biomarkers to Predict Peritoneal Metastasis in Gastric Cancer.” *Frontiers in Oncology* 12:830688. doi:10.3389/fonc.2022.830688.

Jolly, Mohit Kumar, Kathryn E. Ware, Shivee Gilja, Jason A. Somarelli, and Herbert Levine. 2017. “EMT and MET: Necessary or Permissive for Metastasis?” *Molecular Oncology* 11(7):755–69. doi:10.1002/1878-0261.12083.

Joseph, J. V., S. Conroy, T. Tomar, E. Eggens-Meijer, K. Bhat, S. Copray, A. M. E. Walenkamp, E. Boddeke, V. Balasubramanyian, M. Wagemakers, W. F. A. den Dunnen, and F. A. E. Kruyt. 2014. "TGF-β Is an Inducer of ZEB1-Dependent Mesenchymal Transdifferentiation in Glioblastoma That Is Associated with Tumor Invasion." *Cell Death & Disease* 5(10):e1443. doi:10.1038/cddis.2014.395.

Kaławaj, Katarzyna, Adrianna Sławińska-Brych, Magdalena Mizerska-Kowalska, Aleksandra Żurek, Agnieszka Bojarska-Junak, Martyna Kandefer-Szerszeń, and Barbara Zdzisińska. 2020. "Alpha Ketoglutarate Exerts In Vitro Anti-Osteosarcoma Effects through Inhibition of Cell Proliferation, Induction of Apoptosis via the JNK and Caspase 9-Dependent Mechanism, and Suppression of TGF-β and VEGF Production and Metastatic Potential of Cells." *International Journal of Molecular Sciences* 21(24). doi:10.3390/ijms21249406.

Kapałczyńska, Marta, Tomasz Kolenda, Weronika Przybyła, Maria Zajączkowska, Anna Teresiak, Violetta Filas, Matthew Ibbs, Renata Bliźniak, Łukasz Łuczewski, and Katarzyna Lamperska. 2018. "2D and 3D Cell Cultures - a Comparison of Different Types of Cancer Cell Cultures." *Archives of Medical Science : AMS* 14(4):910–19. doi:10.5114/aoms.2016.63743.

Karsy, Michael, Jian Guan, Randy Jensen, L. Eric Huang, and Howard Colman. 2016. "The Impact of Hypoxia and Mesenchymal Transition on Glioblastoma Pathogenesis and Cancer Stem Cells Regulation." *World Neurosurgery* 88:222–36. doi:10.1016/j.wneu.2015.12.032.

Kaul, Roma, April L. Risinger, and Susan L. Mooberry. 2019. "Eribulin Rapidly Inhibits TGF-β-Induced Snail Expression and Can Induce Slug Expression in a Smad4-Dependent Manner." *British Journal of Cancer* 121(7):611–21. doi:10.1038/s41416-019-0556-9.

Khalili-Tanha, Ghazaleh, Evette S. Radisky, Derek C. Radisky, and Alireza Shoari. 2025. "Matrix Metalloproteinase-Driven Epithelial-Mesenchymal Transition: Implications in Health and Disease." *Journal of Translational Medicine* 23(1):436. doi:10.1186/s12967-025-06447-w.

Khan, Imran, and Patricia S. Steeg. 2022. "Keeping Brain Metastases Dormant." *Nature Cancer* 3(1):3–5. doi:10.1038/s43018-021-00321-6.

Kim, Bit Na, Dong Hyuck Ahn, Nahyeon Kang, Chang Dong Yeo, Young Kyoon Kim, Kyo Young Lee, Tae-Jung Kim, Sug Hyung Lee, Mi Sun Park, Hyeon Woo Yim, Jong Y. Park, Chan Kwon Park, and Seung Joon Kim. 2020. "TGF-β Induced EMT and Stemness Characteristics Are Associated with Epigenetic Regulation in Lung Cancer." *Scientific Reports* 10(1):10597. doi:10.1038/s41598-020-67325-7.

Kimura, Naoki, Chiharu Tokunaga, Sushila Dalal, Christine Richardson, Ken-ichi Yoshino, Kenta Hara, Bruce E. Kemp, Lee A. Witters, Osamu Mimura, and Kazuyoshi Yonezawa. 2003. "A Possible Linkage between AMP-Activated Protein Kinase (AMPK) and Mammalian Target of Rapamycin (mTOR) Signalling Pathway." *Genes to Cells : Devoted to Molecular & Cellular Mechanisms* 8(1):65–79. doi:10.1046/j.1365-2443.2003.00615.x.

Kitazawa, Satoshi, Shunsuke Ebara, Ayumi Ando, Yuji Baba, Yoshinori Satomi, Tomoyoshi Soga, and Takahito Hara. 2017. “Succinate Dehydrogenase B-Deficient Cancer Cells Are Highly Sensitive to Bromodomain and Extra-Terminal Inhibitors.” *Oncotarget* 8(17):28922–38. doi:10.18632/oncotarget.15959.

Knyazev, E. N., R. S. Kalinin, V. A. Abrikosova, Yu A. Mokrushina, and S. A. Tonevitskaya. 2023. “KDM5 Family Demethylase Inhibitor KDOAM-25 Reduces Entry of SARS-CoV-2 Pseudotyped Viral Particles into Cells.” *Bulletin of Experimental Biology and Medicine* 175(1):150–56. doi:10.1007/s10517-023-05827-w.

Kodama, Manabu, Kiyotaka Oshikawa, Hideyuki Shimizu, Susumu Yoshioka, Masatomo Takahashi, Yoshihiro Izumi, Takeshi Bamba, Chisa Tateishi, Takeshi Tomonaga, Masaki Matsumoto, and Keiichi I. Nakayama. 2020. “A Shift in Glutamine Nitrogen Metabolism Contributes to the Malignant Progression of Cancer.” *Nature Communications* 11(1):1320. doi:10.1038/s41467-020-15136-9.

Kong, Jian, Qingyun Zhang, Xuefeng Liang, and Wenbing Sun. 2020. “FOXK2 Downregulation Suppresses EMT in Hepatocellular Carcinoma.” *Open Medicine (Warsaw, Poland)* 15(1):702–8. doi:10.1515/med-2020-0129.

Krieg, Sarah, Sara Isabel Fernandes, Constantinos Kolliopoulos, Ming Liu, and Sarah-Maria Fendt. 2024. “Metabolic Signaling in Cancer Metastasis.” *Cancer Discovery* 14(6):934–52. doi:10.1158/2159-8290.CD-24-0174.

Kubelt, Carolin, Kirsten Hattermann, Susanne Sebens, H. Maximilian Mehdorn, and Janka Held-Feindt. 2015. “Epithelial-to-Mesenchymal Transition in Paired Human Primary and Recurrent Glioblastomas.” *International Journal of Oncology* 46(6):2515–25. doi:10.3892/ijo.2015.2944.

Kühnöl, Caspar D., Carina Würfel, Martin S. Staege, and Christof Kramm. 2017. “Snail Homolog 1 Is Involved in Epithelial-Mesenchymal Transition-like Processes in Human Glioblastoma Cells.” *Oncology Letters* 13(5):3882–88. doi:10.3892/ol.2017.5875.

Kuiper, Caroline, and Margreet C. M. Vissers. 2014. “Ascorbate as a Co-Factor for Fe- and 2-Oxoglutarate Dependent Dioxygenases: Physiological Activity in Tumor Growth and Progression.” *Frontiers in Oncology* 4:359. doi:10.3389/fonc.2014.00359.

Kumar, Vinod, Zachary A. Yochum, Princey Devadassan, Eric H. B. Huang, Ethan Miller, Roja Baruwal, Purva H. Rumde, Autumn L. GaitherDavis, Laura P. Stabile, and Timothy F. Burns. 2024. “TWIST1 Is a Critical Downstream Target of the HGF/MET Pathway and Is Required for MET Driven Acquired Resistance in Oncogene Driven Lung Cancer.” *Oncogene* 43(19):1431–44. doi:10.1038/s41388-024-02987-5.

Lai, Yuezheng, Yuying Zhang, Shan Zhou, Jinxu Xu, Zhanqiang Du, Ziyan Feng, Long Yu, Ziqing Zhao, Weiwei Wang, Yanting Tang, Xiuna Yang, Luke W. Guddat, Fengjiang Liu, Yan Gao, Zihe Rao, and Hongri Gong. 2023. “Structure of the Human ATP Synthase.” *Molecular Cell* 83(12):2137-2147.e4. doi:10.1016/j.molcel.2023.04.029.

Lambert, Arthur W., and Robert A. Weinberg. 2021. “Linking EMT Programmes to Normal and Neoplastic Epithelial Stem Cells.” *Nature Reviews. Cancer* 21(5):325–38. doi:10.1038/s41568-021-00332-6.

Lamouille, Samy, and Rik Derynck. 2007. “Cell Size and Invasion in TGF-Beta-Induced Epithelial to Mesenchymal Transition Is Regulated by Activation of the mTOR Pathway.” *The Journal of Cell Biology* 178(3):437–51. doi:10.1083/jcb.200611146.

Lamouille, Samy, Jian Xu, and Rik Derynck. 2014. “Molecular Mechanisms of Epithelial-Mesenchymal Transition.” *Nature Reviews. Molecular Cell Biology* 15(3):178–96. doi:10.1038/nrm3758.

Lampa, Michael, Heike Arlt, Timothy He, Beatriz Ospina, Jason Reeves, Bailin Zhang, Joshua Murtie, Gejing Deng, Claude Barberis, Dietmar Hoffmann, Hong Cheng, Jack Pollard, Christopher Winter, Victoria Richon, Carlos Garcia-Escheverria, Francisco Adrian, Dmitri Wiederschain, and Lakshmi Srinivasan. 2017. “Glutaminase Is Essential for the Growth of Triple-Negative Breast Cancer Cells with a Deregulated Glutamine Metabolism Pathway and Its Suppression Synergizes with mTOR Inhibition.” *PloS One* 12(9):e0185092. doi:10.1371/journal.pone.0185092.

Lang, Fengchao, Karambir Kaur, Haiqing Fu, Javeria Zaheer, Diego Luis Ribeiro, Mirit I. Aladjem, and Chunzhang Yang. 2025. “D-2-Hydroxyglutarate Impairs DNA Repair through Epigenetic Reprogramming.” *Nature Communications* 16(1):1431. doi:10.1038/s41467-025-56781-2.

Langhans, Julia, Lukas Schneele, Nancy Trenkler, Hélène von Bandemer, Lisa Nonnenmacher, Georg Karpel-Massler, Markus D. Siegelin, Shaoxia Zhou, Marc-Eric Halatsch, Klaus-Michael Debatin, and Mike-Andrew Westhoff. 2017. “The Effects of PI3K-Mediated Signalling on Glioblastoma Cell Behaviour.” *Oncogenesis* 6(11):398. doi:10.1038/s41389-017-0004-8.

Laplante, Mathieu, and David M. Sabatini. 2013. “Regulation of mTORC1 and Its Impact on Gene Expression at a Glance.” *Journal of Cell Science* 126(Pt 8):1713–19. doi:10.1242/jcs.125773.

Lapointe, Sarah, Arie Perry, and Nicholas A. Butowski. 2018. “Primary Brain Tumours in Adults.” *Lancet (London, England)* 392(10145):432–46. doi:10.1016/S0140-6736(18)30990-5.

Lautert-Dutra, William, Camila Morais Melo, Luiz Paulo Chaves, Francisco Cesar Sousa, Cheryl Crozier, Dan Dion, Filipe S. Avante, Fabiano Pinto Saggioro, Rodolfo Borges Dos Reis, Leticia Fröhlich Archangelo, Jane Bayani, and Jeremy A. Squire. 2024. “Investigating the Role of SNAI1 and ZEB1 Expression in Prostate Cancer Progression and Immune Modulation of the Tumor Microenvironment.” *Cancers* 16(8). doi:10.3390/cancers16081480.

Lebrun, Jean-Jacques. 2012. “The Dual Role of TGFβ in Human Cancer: From Tumor Suppression to Cancer Metastasis.” *ISRN Molecular Biology* 2012:381428. doi:10.5402/2012/381428.

Lee, Kyubin, Sohyeong Yun, Jisu Park, Seokchan Lee, Angel M. Carcaboso, Sun-Ju Yi, and Kyunghwan Kim. 2023. “Dimethyl Alpha-Ketoglutarate Inhibits Proliferation in Diffuse Intrinsic Pontine Glioma by Reprogramming Epigenetic and Transcriptional Networks.” *Biochemical and Biophysical Research Communications* 677:6–12. doi:10.1016/j.bbrc.2023.07.050.

Lee, Young-Ju, Jung-Hwan Park, and Sang-Muk Oh. 2020. “Activation of NF-κB by TOPK Upregulates Snail/Slug Expression in TGF-B1 Signaling to Induce Epithelial-Mesenchymal Transition and Invasion of Breast Cancer Cells.” *Biochemical and Biophysical Research Communications* 530(1):122–29. doi:10.1016/j.bbrc.2020.07.015.

Legendre, F., A. MacLean, V. P. Appanna, and V. D. Appanna. 2020. “Biochemical Pathways to α-Ketoglutarate, a Multi-Faceted Metabolite.” *World Journal of Microbiology & Biotechnology* 36(8):123. doi:10.1007/s11274-020-02900-8.

Lewis, Caroline A., Seth J. Parker, Brian P. Fiske, Douglas McCloskey, Dan Y. Gui, Courtney R. Green, Natalie I. Vokes, Adam M. Feist, Matthew G. Vander Heiden, and Christian M. Metallo. 2014. “Tracing Compartmentalized NADPH Metabolism in the Cytosol and Mitochondria of Mammalian Cells.” *Molecular Cell* 55(2):253–63. doi:10.1016/j.molcel.2014.05.008.

Li, H., G. Y. Zhang, C. H. Pan, X. Y. Zhang, and X. Y. Su. 2019. “LncRNA MAFG-AS1 Promotes the Aggressiveness of Breast Carcinoma through Regulating miR-339-5p/MMP15.” *European Review for Medical and Pharmacological Sciences* 23(7):2838–46. doi:10.26355/eurrev_201904_17561.

Li, Hong-Mei, Yan-Ran Bi, Yang Li, Rong Fu, Wen-Cong Lv, Nan Jiang, Ying Xu, Bo-Xue Ren, Ya-Dong Chen, Hui Xie, Shui Wang, Tao Lu, and Zhao-Qiu Wu. 2020. “A Potent CBP/P300-Snail Interaction Inhibitor Suppresses Tumor Growth and Metastasis in Wild-Type P53-Expressing Cancer.” *Science Advances* 6(17):eaaw8500. doi:10.1126/sciadv.aaw8500.

Li, Hongmu, Chun Wu, Wuguang Chang, Leqi Zhong, Wuyou Gao, Mingyue Zeng, Zhesheng Wen, Shijuan Mai, and Youfang Chen. 2023. “Overexpression of PSAT1 Is Correlated with Poor Prognosis and Immune Infiltration in Non-Small Cell Lung Cancer.” *Frontiers in Bioscience (Landmark Edition)* 28(10):243. doi:10.31083/j.fbl2810243.

Li, Jiangjiang, Ya He, Zheqiong Tan, Jingchen Lu, Liling Li, Xin Song, Feng Shi, Longlong Xie, Shuo You, Xiangjian Luo, Namei Li, Yueshuo Li, Xiaolan Liu, Min Tang, Xinxian Weng, Wei Yi, Jia Fan, Jian Zhou, Gao Qiang, ShuangJian Qiu, Weizhong Wu, Ann M. Bode, and Ya Cao. 2018. “Wild-Type IDH2 Promotes the Warburg Effect and Tumor Growth through HIF1α in Lung Cancer.” *Theranostics* 8(15):4050–61. doi:10.7150/thno.21524.

Li, Jiang-Jiang, Tiantian Yu, Peiting Zeng, Jingyu Tian, Panpan Liu, Shuang Qiao, Shijun Wen, Yumin Hu, Qiao Liu, Wenhua Lu, Hui Zhang, and Peng Huang. 2024. “Wild-Type IDH2 Is a Therapeutic Target for Triple-Negative Breast Cancer.” *Nature Communications* 15(1):3445. doi:10.1038/s41467-024-47536-6.

Li, Le, Xing Zeng, Zheng Chao, Jing Luo, Wei Guan, Qiang Zhang, Yue Ge, Yanan Wang, Zezhong Xiong, Sheng Ma, Qiang Zhou, Junbiao Zhang, Jihua Tian, David Horne, Bertram Yuh, Zhiquan Hu, Gong-Hong Wei, Baojun Wang, Xu Zhang, Peixiang Lan, and Zhihua Wang. 2023. “Targeting Alpha-Ketoglutarate Disruption Overcomes Immunoevasion and Improves PD-1 Blockade Immunotherapy in Renal Cell Carcinoma.” *Advanced Science (Weinheim, Baden-Wurttemberg, Germany)* 10(27):e2301975. doi:10.1002/advs.202301975.

Li, Meng, Tingting Yan, Yanqiu Cai, Yingyuan Wei, and Qiqi Xie. 2023. “Expression of Matrix Metalloproteinases and Their Association with Clinical Characteristics of Solid Tumors.” *Gene* 850:146927. doi:10.1016/j.gene.2022.146927.

Li, Mingzhe, Xin Bu, Bolei Cai, Ping Liang, Kai Li, Xuan Qu, and Liangliang Shen. 2019. “Biological Role of Metabolic Reprogramming of Cancer Cells during Epithelial-mesenchymal Transition (Review).” *Oncology Reports* 41(2):727–41. doi:10.3892/or.2018.6882.

Li, Ting, Christopher Copeland, and Anne Le. 2021. “Glutamine Metabolism in Cancer.” *Advances in Experimental Medicine and Biology* 1311:17–38. doi:10.1007/978-3-030-65768-0_2.

Li, Xiao, Shuang Wang, Xin Nie, Yuexin Hu, Ouxuan Liu, Yuxuan Wang, and Bei Lin. 2025. “PSAT1 Regulated by STAT4 Enhances the Proliferation, Invasion and Migration of Ovarian Cancer Cells via the PI3K/AKT Pathway.” *International Journal of Molecular Medicine* 55(6):88. doi:10.3892/ijmm.2025.5529.

Li, Yangchan, Rui Su, Xiaolan Deng, Yong Chen, and Jianjun Chen. 2022. “FTO in Cancer: Functions, Molecular Mechanisms, and Therapeutic Implications.” *Trends in Cancer* 8(7):598–614. doi:10.1016/j.trecan.2022.02.010.

Liaghat, Mahsa, Saeid Ferdousmakan, Seyedeh Haniyeh Mortazavi, Sheida Yahyazadeh, Asrin Irani, Sara Banihashemi, Fatemeh Sadat Seyedi Asl, Abdullatif Akbari, Farnoosh Farzam, Fatemeh Aziziyan, Maryam Bakhtiyari, Mohammad Javad Arghavani, Hamidreza Zalpoor, and Mohsen Nabi-Afjadi. 2024. “The Impact of Epithelial-Mesenchymal Transition (EMT) Induced by Metabolic Processes and Intracellular Signaling Pathways on Chemo-Resistance, Metastasis, and Recurrence in Solid Tumors.” *Cell Communication and Signaling : CCS* 22(1):575. doi:10.1186/s12964-024-01957-4.

Liang, Zhuming, Yanan Mo, Yujiao Zhang, Yanjing Yu, and Yinan Ji. 2025. “Molecular Mechanisms and Signaling Pathways Related to Brain Metastasis in Breast Cancer.” *Frontiers in Pharmacology* 16:1585668. doi:10.3389/fphar.2025.1585668.

Lin, Aifen, Hui-Hui Xu, Dan-Ping Xu, Xia Zhang, Qing Wang, and Wei-Hua Yan. 2013. “Multiple Steps of HLA-G in Ovarian Carcinoma Metastasis: Alter NK Cytotoxicity and Induce Matrix Metalloproteinase-15 (MMP-15) Expression.” *Human Immunology* 74(4):439–46. doi:10.1016/j.humimm.2012.11.021.

Lin, Mei-Fang, Yu-Feng Yang, Zhen-Peng Peng, Mei-Fang Zhang, Jin-Yu Liang, Wei Chen, Xu-Hui Liu, and Yan-Ling Zheng. 2017. “FOXK2, Regulted by miR-1271-5p, Promotes Cell Growth and Indicates Unfavorable Prognosis in Hepatocellular Carcinoma.” *The International Journal of Biochemistry & Cell Biology* 88:155–61. doi:10.1016/j.biocel.2017.05.019.

Lin, Xian, Ran Sun, Xiulan Zhao, Dongwang Zhu, Xueming Zhao, Qiang Gu, Xueyi Dong, Danfang Zhang, Yanhui Zhang, Yanlei Li, and Baocun Sun. 2017. “C-Myc Overexpression Drives Melanoma Metastasis by Promoting Vasculogenic Mimicry via c-Myc/Snail/Bax Signaling.” *Journal of Molecular Medicine (Berlin, Germany)* 95(1):53–67. doi:10.1007/s00109-016-1452-x.

Lin, Ying-Chao, Jia-Ching Lin, Chao-Ming Hung, Yeh Chen, Liang-Chih Liu, Tin-Chang Chang, Jung-Yie Kao, Chi-Tang Ho, and Tzong-Der Way. 2014. "Osthole Inhibits Insulin-like Growth Factor-1-Induced Epithelial to Mesenchymal Transition via the Inhibition of PI3K/Akt Signaling Pathway in Human Brain Cancer Cells." *Journal of Agricultural and Food Chemistry* 62(22):5061–71. doi:10.1021/jf501047g.

Liu, Fangyuan, Xuemeng Sun, Yun Zeng, Xiangyun Meng, Rongrong Zhang, Liya Su, and Gang Liu. 2025. "Integrative Machine Learning Reveals the Biological Function and Prognostic Significance of α-Ketoglutarate in Gastric Cancer." *Oncology Letters* 30(2):392. doi:10.3892/ol.2025.15138.

Liu, Gaojie, Jie Zhu, Menglei Yu, Canfeng Cai, Yu Zhou, Min Yu, Zhiqiang Fu, Yuanfeng Gong, Bin Yang, Yingru Li, Quanbo Zhou, Qin Lin, Huilin Ye, Liangtao Ye, Xiaohui Zhao, Zhihua Li, Rufu Chen, Fanghai Han, Chaoming Tang, and Bing Zeng. 2015. "Glutamate Dehydrogenase Is a Novel Prognostic Marker and Predicts Metastases in Colorectal Cancer Patients." *Journal of Translational Medicine* 13:144. doi:10.1186/s12967-015-0500-6.

Liu, Grace Y., and David M. Sabatini. 2020. "mTOR at the Nexus of Nutrition, Growth, Ageing and Disease." *Nature Reviews. Molecular Cell Biology* 21(4):183–203. doi:10.1038/s41580-019-0199-y.

Liu, Huidong, and Ye-Guang Chen. 2022. "The Interplay Between TGF-β Signaling and Cell Metabolism." *Frontiers in Cell and Developmental Biology* 10:846723. doi:10.3389/fcell.2022.846723.

Liu, Nian, Jianglin Zhang, Mingjie Yan, Lihui Chen, Jie Wu, Qian Tao, Bei Yan, Xiang Chen, and Cong Peng. 2023. "Supplementation with α-Ketoglutarate Improved the Efficacy of Anti-PD1 Melanoma Treatment through Epigenetic Modulation of PD-L1." *Cell Death & Disease* 14(2):170. doi:10.1038/s41419-023-05692-5.

Liu, Reng-Yun, Yuanyuan Zeng, Zhe Lei, Longqiang Wang, Haiping Yang, Zeyi Liu, Jun Zhao, and Hong-Tao Zhang. 2014. "JAK/STAT3 Signaling Is Required for TGF-β-Induced Epithelial-Mesenchymal Transition in Lung Cancer Cells." *International Journal of Oncology* 44(5):1643–51. doi:10.3892/ijo.2014.2310.

Liu, Shaojuan, Liuqin He, and Kang Yao. 2018. "The Antioxidative Function of Alpha-Ketoglutarate and Its Applications." *BioMed Research International* 2018:3408467. doi:10.1155/2018/3408467.

Liu, Wen-Shan, Shih-Hsuan Chan, Hong-Tai Chang, Guan-Cheng Li, Ya-Ting Tu, Hui-Hwa Tseng, Ting-Ying Fu, Hui-Yu Chang, Huei-Han Liou, Luo-Ping Ger, and Kuo-Wang Tsai. 2018. "Isocitrate Dehydrogenase 1-Snail Axis Dysfunction Significantly Correlates with Breast Cancer Prognosis and Regulates Cell Invasion Ability." *Breast Cancer Research : BCR* 20(1):25. doi:10.1186/s13058-018-0953-7.

Liu, Xi, Xiaodong Wei, Wei Niu, Dong Wang, Bo Wang, and Hao Zhuang. 2018. "Downregulation of FOXK2 Is Associated with Poor Prognosis in Patients with Gastric Cancer." *Molecular Medicine Reports* 18(5):4356–64. doi:10.3892/mmr.2018.9466.

Liu, Zong-Cai, Hong-Sheng Wang, Ge Zhang, Hao Liu, Xiao-Hui Chen, Fan Zhang, Dan-Yang Chen, Shao-Hui Cai, and Jun Du. 2014. "AKT/GSK-3β Regulates Stability and Transcription of Snail Which Is Crucial for bFGF-Induced Epithelial-Mesenchymal Transition of Prostate Cancer Cells." *Biochimica et Biophysica Acta* 1840(10):3096–3105. doi:10.1016/j.bbagen.2014.07.018.

Livak, K. J., and T. D. Schmittgen. 2001. "Analysis of Relative Gene Expression Data Using Real-Time Quantitative PCR and the 2(-Delta Delta C(T)) Method." *Methods (San Diego, Calif.)* 25(4):402–8. doi:10.1006/meth.2001.1262.

Lo Buglio, Gabriele, Alessandra Lo Cicero, Simona Campora, and Giulio Ghersi. 2024. "The Multifaced Role of Collagen in Cancer Development and Progression." *International Journal of Molecular Sciences* 25(24). doi:10.3390/ijms252413523.

Losman, Julie-Aurore, Peppi Koivunen, and William G. Jr Kaelin. 2020. "2-Oxoglutarate-Dependent Dioxygenases in Cancer." *Nature Reviews. Cancer* 20(12):710–26. doi:10.1038/s41568-020-00303-3.

LOWRY, O. H., N. J. ROSEBROUGH, A. L. FARR, and R. J. RANDALL. 1951. "Protein Measurement with the Folin Phenol Reagent." *The Journal of Biological Chemistry* 193(1):265–75.

Lu, Chao, Patrick S. Ward, Gurpreet S. Kapoor, Dan Rohle, Sevin Turcan, Omar Abdel-Wahab, Christopher R. Edwards, Raya Khanin, Maria E. Figueroa, Ari Melnick, Kathryn E. Wellen, Donald M. O'Rourke, Shelley L. Berger, Timothy A. Chan, Ross L. Levine, Ingo K. Mellinghoff, and Craig B. Thompson. 2012. "IDH Mutation Impairs Histone Demethylation and Results in a Block to Cell Differentiation." *Nature* 483(7390):474–78. doi:10.1038/nature10860.

Lu, Wei, and Yibin Kang. 2019. "Epithelial-Mesenchymal Plasticity in Cancer Progression and Metastasis." *Developmental Cell* 49(3):361–74. doi:10.1016/j.devcel.2019.04.010.

Lu, Xin, Nan Wu, Wanli Yang, Jia Sun, Kemin Yan, and Jing Wu. 2019. "OGDH Promotes the Progression of Gastric Cancer by Regulating Mitochondrial Bioenergetics and Wnt/β-Catenin Signal Pathway." *OncoTargets and Therapy* 12:7489–7500. doi:10.2147/OTT.S208848.

Lu, Yu, Yunhang Huang, Chenyan Zhu, Zhidan Li, Bin Zhang, Hui Sheng, Haotai Li, Xixi Liu, Zhongwen Xu, Yi Wen, Jing Zhang, and Liguo Zhang. 2025. "Cancer Brain Metastasis: Molecular Mechanisms and Therapeutic Strategies." *Molecular Biomedicine* 6(1):12. doi:10.1186/s43556-025-00251-0.

Luo, Daochun, Jinxia Wang, Jeff Li, and Martin Post. 2011. "Mouse Snail Is a Target Gene for HIF." *Molecular Cancer Research : MCR* 9(2):234–45. doi:10.1158/1541-7786.MCR-10-0214.

Ma, Yu-Shui, Zhi-Jun Wu, Rui-Zhen Bai, Hua Dong, Bing-Xue Xie, Xiao-Hong Wu, Xiao-Sheng Hang, Ai-Ning Liu, Xiao-Hui Jiang, Gao-Ren Wang, Jun-Jian Jiang, Wen-Huan Xu, Xiao-Ping Chen, Guang-Hong Tan, Da Fu, Ji-Bin Liu, and Quan Liu. 2018. "DRR1 Promotes Glioblastoma Cell Invasion and Epithelial-Mesenchymal Transition via Regulating AKT Activation." *Cancer Letters* 423:86–94. doi:10.1016/j.canlet.2018.03.015.

MacKenzie, Elaine D., Mary A. Selak, Daniel A. Tennant, Lloyd J. Payne, Stuart Crosby, Casper M. Frederiksen, David G. Watson, and Eyal Gottlieb. 2007. "Cell-Permeating Alpha-Ketoglutarate Derivatives Alleviate Pseudohypoxia in Succinate Dehydrogenase-Deficient Cells." *Molecular and Cellular Biology* 27(9):3282–89. doi:10.1128/MCB.01927-06.

Mahabir, Roshan, Mishie Tanino, Aiman Elmansuri, Lei Wang, Taichi Kimura, Tamio Itoh, Yusuke Ohba, Hiroshi Nishihara, Hiroki Shirato, Masumi Tsuda, and Shinya Tanaka. 2014. "Sustained Elevation of Snail Promotes Glial-Mesenchymal Transition after Irradiation in Malignant Glioma." *Neuro-Oncology* 16(5):671–85. doi:10.1093/neuonc/not239.

Majc, Bernarda, Tilen Sever, Miki Zarić, Barbara Breznik, Boris Turk, and Tamara T. Lah. 2020. "Epithelial-to-Mesenchymal Transition as the Driver of Changing Carcinoma and Glioblastoma Microenvironment." *Biochimica et Biophysica Acta. Molecular Cell Research* 1867(10):118782. doi:10.1016/j.bbamcr.2020.118782.

Mani, Kyle, Daxuan Deng, Christine Lin, Ming Wang, Melinda L. Hsu, and Nicholas G. Zaorsky. 2024. "Causes of Death among People Living with Metastatic Cancer." *Nature Communications* 15(1):1519. doi:10.1038/s41467-024-45307-x.

Margarido, Andreia S., Rebeca Uceda-Castro, Kerstin Hahn, Roebi de Bruijn, Lennart Kester, Ingrid Hofland, Jeroen Lohuis, Danielle Seinstra, Annegien Broeks, Jos Jonkers, Marike L. D. Broekman, Pieter Wesseling, Claire Vennin, Miguel Vizoso, and Jacco van Rheenen. 2022. "Epithelial-to-Mesenchymal Transition Drives Invasiveness of Breast Cancer Brain Metastases." *Cancers* 14(13). doi:10.3390/cancers14133115.

Massagué, Joan, and Dean Sheppard. 2023. "TGF-β Signaling in Health and Disease." *Cell* 186(19):4007–37. doi:10.1016/j.cell.2023.07.036.

Matsumoto, Ken, Shigehiko Imagawa, Naoshi Obara, Norio Suzuki, Satoru Takahashi, Toshiro Nagasawa, and Masayuki Yamamoto. 2006. "2-Oxoglutarate Downregulates Expression of Vascular Endothelial Growth Factor and Erythropoietin through Decreasing Hypoxia-Inducible Factor-1alpha and Inhibits Angiogenesis." *Journal of Cellular Physiology* 209(2):333–40. doi:10.1002/jcp.20733.

Matsumoto, Ken, Naoshi Obara, Masatsugu Ema, Masaki Horie, Ayano Naka, Satoru Takahashi, and Shigehiko Imagawa. 2009. "Antitumor Effects of 2-Oxoglutarate through Inhibition of Angiogenesis in a Murine Tumor Model." *Cancer Science* 100(9):1639–47. doi:10.1111/j.1349-7006.2009.01249.x.

McFaline-Figueroa, J. Ricardo, and Eudocia Q. Lee. 2018. "Brain Tumors." *The American Journal of Medicine* 131(8):874–82. doi:10.1016/j.amjmed.2017.12.039.

McKinnon, Chris, Meera Nandhabalan, Scott A. Murray, and Puneet Plaha. 2021. "Glioblastoma: Clinical Presentation, Diagnosis, and Management." *BMJ (Clinical Research Ed.)* 374:n1560. doi:10.1136/bmj.n1560.

Mendoza, Michelle C., E. Emrah Er, and John Blenis. 2011. "The Ras-ERK and PI3K-mTOR Pathways: Cross-Talk and Compensation." *Trends in Biochemical Sciences* 36(6):320–28. doi:10.1016/j.tibs.2011.03.006.

Meng, Xingqi, Huiqing Liu, Lixuan Peng, Weiguo He, and Suyun Li. 2022. “Potential Clinical Applications of Alpha-ketoglutaric Acid in Diseases (Review).” *Molecular Medicine Reports* 25(5):151. doi:10.3892/mmr.2022.12667.

Mishra, Prajna, Subramanian Senthivinayagam, Ajay Rana, and Basabi Rana. 2010. “Glycogen Synthase Kinase-3beta Regulates Snail and Beta-Catenin during Gastrin-Induced Migration of Gastric Cancer Cells.” *Journal of Molecular Signaling* 5:9. doi:10.1186/1750-2187-5-9.

Miyoshi, A., Y. Kitajima, K. Sumi, K. Sato, A. Hagiwara, Y. Koga, and K. Miyazaki. 2004. “Snail and SIP1 Increase Cancer Invasion by Upregulating MMP Family in Hepatocellular Carcinoma Cells.” *British Journal of Cancer* 90(6):1265–73. doi:10.1038/sj.bjc.6601685.

Moghbeli, Meysam. 2024. “PI3K/AKT Pathway as a Pivotal Regulator of Epithelial-Mesenchymal Transition in Lung Tumor Cells.” *Cancer Cell International* 24(1):165. doi:10.1186/s12935-024-03357-7.

Moody, Susan E., Denise Perez, Tien-chi Pan, Christopher J. Sarkisian, Carla P. Portocarrero, Christopher J. Sterner, Kathleen L. Notorfrancesco, Robert D. Cardiff, and Lewis A. Chodosh. 2005. “The Transcriptional Repressor Snail Promotes Mammary Tumor Recurrence.” *Cancer Cell* 8(3):197–209. doi:10.1016/j.ccr.2005.07.009.

Morris, John P. 4th, Jossie J. Yashinskie, Richard Koche, Rohit Chandwani, Sha Tian, Chi-Chao Chen, Timour Baslan, Zoran S. Marinkovic, Francisco J. Sánchez-Rivera, Steven D. Leach, Carlos Carmona-Fontaine, Craig B. Thompson, Lydia W. S. Finley, and Scott W. Lowe. 2019. “α-Ketoglutarate Links P53 to Cell Fate during Tumour Suppression.” *Nature* 573(7775):595–99. doi:10.1038/s41586-019-1577-5.

Morris, M. R., C. Ricketts, D. Gentle, M. Abdulrahman, N. Clarke, M. Brown, T. Kishida, M. Yao, F. Latif, and E. R. Maher. 2010. “Identification of Candidate Tumour Suppressor Genes Frequently Methylated in Renal Cell Carcinoma.” *Oncogene* 29(14):2104–17. doi:10.1038/onc.2009.493.

Mossmann, Dirk, Sujin Park, and Michael N. Hall. 2018. “mTOR Signalling and Cellular Metabolism Are Mutual Determinants in Cancer.” *Nature Reviews. Cancer* 18(12):744–57. doi:10.1038/s41568-018-0074-8.

Motizuki, Mitsuyoshi, Takashi Yokoyama, Masao Saitoh, and Keiji Miyazawa. 2024. “The Snail Signaling Branch Downstream of the TGF-β/Smad3 Pathway Mediates Rho Activation and Subsequent Stress Fiber Formation.” *The Journal of Biological Chemistry* 300(1):105580. doi:10.1016/j.jbc.2023.105580.

Moustakas, Aristidis, and Carl-Henrik Heldin. 2016. “Mechanisms of TGFβ-Induced Epithelial-Mesenchymal Transition.” *Journal of Clinical Medicine* 5(7). doi:10.3390/jcm5070063.

Murphy, Michael P. 2009. “How Mitochondria Produce Reactive Oxygen Species.” *The Biochemical Journal* 417(1):1–13. doi:10.1042/BJ20081386.

Muz, Barbara, Pilar de la Puente, Feda Azab, and Abdel Kareem Azab. 2015. “The Role of Hypoxia in Cancer Progression, Angiogenesis, Metastasis, and Resistance to Therapy.” *Hypoxia (Auckland, N.Z.)* 3:83–92. doi:10.2147/HP.S93413.

Myung, Jae Kyung, Seung Ah Choi, Seung-Ki Kim, Kyu-Chang Wang, and Sung-Hye Park. 2014. “Snail Plays an Oncogenic Role in Glioblastoma by Promoting Epithelial Mesenchymal Transition.” *International Journal of Clinical and Experimental Pathology* 7(5):1977–87.

Nakatsumi, Hirokazu, Masaki Matsumoto, and Keiichi I. Nakayama. 2017. “Noncanonical Pathway for Regulation of CCL2 Expression by an mTORC1-FOXK1 Axis Promotes Recruitment of Tumor-Associated Macrophages.” *Cell Reports* 21(9):2471–86. doi:10.1016/j.celrep.2017.11.014.

Nesci, Salvatore, Fabiana Trombetti, Cristina Algieri, and Alessandra Pagliarani. 2019. “A Therapeutic Role for the F(1)F(O)-ATP Synthase.” *SLAS Discovery : Advancing Life Sciences R & D* 24(9):893–903. doi:10.1177/2472555219860448.

Nestal de Moraes, Gabriela, Luciana da Torre Carneiro, Raquel Ciuvalschi Maia, Eric Wing-Fai Lam, and Andrew David Sharrocks. 2019. “FOXK2 Transcription Factor and Its Emerging Roles in Cancer.” *Cancers* 11(3). doi:10.3390/cancers11030393.

Nieto, M. Angela. 2002. “The Snail Superfamily of Zinc-Finger Transcription Factors.” *Nature Reviews Molecular Cell Biology* 3(3):155–66. doi:10.1038/nrm757.

Nieto, M. Angela, Ruby Yun-Ju Huang, Rebecca A. Jackson, and Jean Paul Thiery. 2016. “EMT: 2016.” *Cell* 166(1):21–45. doi:10.1016/j.cell.2016.06.028.

Niland, Stephan, Andrea Ximena Riscanevo, and Johannes Andreas Eble. 2021. “Matrix Metalloproteinases Shape the Tumor Microenvironment in Cancer Progression.” *International Journal of Molecular Sciences* 23(1). doi:10.3390/ijms23010146.

Nozaki, Misa, and Makoto Nishizuka. 2021. “Repression of RhoJ Expression Promotes TGF-β-Mediated EMT in Human Non-Small-Cell Lung Cancer A549cells.” *Biochemical and Biophysical Research Communications* 566:94–100. doi:10.1016/j.bbrc.2021.06.004.

Oizel, Kristell, Cynthia Chauvin, Lisa Oliver, Catherine Gratas, Fanny Geraldo, Ulrich Jarry, Emmanuel Scotet, Marion Rabe, Marie-Clotilde Alves-Guerra, Raluca Teusan, Fabien Gautier, Delphine Loussouarn, Vincent Compan, Jean-Claude Martinou, François M. Vallette, and Claire Pecqueur. 2017. “Efficient Mitochondrial Glutamine Targeting Prevails Over Glioblastoma Metabolic Plasticity.” *Clinical Cancer Research : An Official Journal of the American Association for Cancer Research* 23(20):6292–6304. doi:10.1158/1078-0432.CCR-16-3102.

Oliver, Kathryn M., Cormac T. Taylor, and Eoin P. Cummins. 2009. “Hypoxia. Regulation of NFkappaB Signalling during Inflammation: The Role of Hydroxylases.” *Arthritis Research & Therapy* 11(1):215. doi:10.1186/ar2575.

Ombrato, Luigi, Emma Nolan, Ivana Kurelac, Antranik Mavousian, Victoria Louise Bridgeman, Ivonne Heinze, Probir Chakravarty, Stuart Horswell, Estela Gonzalez-Gualda, Giulia Matacchione, Anne Weston, Joanna Kirkpatrick, Ehab Husain, Valerie

Speirs, Lucy Collinson, Alessandro Ori, Joo-Hyeon Lee, and Ilaria Malanchi. 2019. "Metastatic-Niche Labelling Reveals Parenchymal Cells with Stem Features." *Nature* 572(7771):603–8. doi:10.1038/s41586-019-1487-6.

Pan, Min, Michael A. Reid, Xazmin H. Lowman, Rajan P. Kulkarni, Thai Q. Tran, Xiaojing Liu, Ying Yang, Jenny E. Hernandez-Davies, Kimberly K. Rosales, Haiqing Li, Willy Hugo, Chunying Song, Xiangdong Xu, Dustin E. Schones, David K. Ann, Viviana Gradinaru, Roger S. Lo, Jason W. Locasale, and Mei Kong. 2016. "Regional Glutamine Deficiency in Tumours Promotes Dedifferentiation through Inhibition of Histone Demethylation." *Nature Cell Biology* 18(10):1090–1101. doi:10.1038/ncb3410.

Panwar, Vivek, Aishwarya Singh, Manini Bhatt, Rajiv K. Tonk, Shavkatjon Azizov, Agha Saquib Raza, Shinjinee Sengupta, Deepak Kumar, and Manoj Garg. 2023. "Multifaceted Role of mTOR (Mammalian Target of Rapamycin) Signaling Pathway in Human Health and Disease." *Signal Transduction and Targeted Therapy* 8(1):375. doi:10.1038/s41392-023-01608-z.

Parker, Seth J., Joel Encarnación-Rosado, Kate E. R. Hollinshead, David M. Hollinshead, Leonard J. Ash, Juan A. K. Rossi, Elaine Y. Lin, Albert S. W. Sohn, Mark R. Philips, Drew R. Jones, and Alec C. Kimmelman. 2021. "Spontaneous Hydrolysis and Spurious Metabolic Properties of α-Ketoglutarate Esters." *Nature Communications* 12(1):4905. doi:10.1038/s41467-021-25228-9.

Pavlova, Natalya N., Jiajun Zhu, and Craig B. Thompson. 2022. "The Hallmarks of Cancer Metabolism: Still Emerging." *Cell Metabolism* 34(3):355–77. doi:10.1016/j.cmet.2022.01.007.

Peiró, Sandra, Maria Escrivà, Isabel Puig, Maria José Barberà, Natàlia Dave, Nicolás Herranz, Maria Jesús Larriba, Minna Takkunen, Clara Francí, Alberto Muñoz, Ismo Virtanen, Josep Baulida, and Antonio García de Herreros. 2006. "Snail1 Transcriptional Repressor Binds to Its Own Promoter and Controls Its Expression." *Nucleic Acids Research* 34(7):2077–84. doi:10.1093/nar/gkl141.

Peixoto, Joana, Sudha Janaki-Raman, Lisa Schlicker, Werner Schmitz, Susanne Walz, Alina M. Winkelkotte, Christel Herold-Mende, Paula Soares, Almut Schulze, and Jorge Lima. 2021. "Integrated Metabolomics and Transcriptomics Analysis of Monolayer and Neurospheres from Established Glioblastoma Cell Lines." *Cancers* 13(6). doi:10.3390/cancers13061327.

Peng, Ying, Pei Zhang, Xiaoting Huang, Qingqing Yan, Meiyan Wu, Ruyi Xie, Yao Wu, Mengnan Zhang, Qingzhen Nan, Jinjun Zhao, Aimin Li, Jing Xiong, Yuexin Ren, Yang Bai, Ye Chen, Side Liu, and Jide Wang. 2016. "Direct Regulation of FOXK1 by C-Jun Promotes Proliferation, Invasion and Metastasis in Gastric Cancer Cells." *Cell Death & Disease* 7(11):e2480. doi:10.1038/cddis.2016.225.

Pepin, Sarah Kym, Alain Zgheib, Marie-Eve Roy, and Borhane Annabi. 2025. "Quercetin Targets TGFβ-Primed Human MDA-MB-231 Triple-Negative Breast Cancer Cells, Linking Epithelial-Mesenchymal Transition to Cell Senescence and Fibrosis." *Molecular Biology Reports* 52(1):725. doi:10.1007/s11033-025-10828-1.

Pereira, Fábio, Antonio Barbáchano, Javier Silva, Félix Bonilla, Moray J. Campbell, Alberto Muñoz, and María Jesús Larriba. 2011. "KDM6B/JMJD3 Histone Demethylase Is Induced by Vitamin D and Modulates Its Effects in Colon Cancer Cells." *Human Molecular Genetics* 20(23):4655–65. doi:10.1093/hmg/ddr399.

Pérez-González, Andrea, Kevin Bévant, and Cédric Blanpain. 2023. "Cancer Cell Plasticity during Tumor Progression, Metastasis and Response to Therapy." *Nature Cancer* 4(8):1063–82. doi:10.1038/s43018-023-00595-y.

Pisal, R. V., H. Hrebíková, J. Chvátalová, D. Kunke, S. Filip, and J. Mokrý. 2016. "Detection of Mycoplasma Contamination Directly from Culture Supernatant Using Polymerase Chain Reaction." *Folia Biologica* 62(5):203–6. doi:10.14712/fb2016062050203.

Pouyan, Ashkan, Masoud Ghorbanlo, Masoud Eslami, Majid Jahanshahi, Ehsan Ziaei, Ali Salami, Khatere Mokhtari, Koorosh Shahpasand, Najma Farahani, Tohid Emami Meybodi, Maliheh Entezari, Afshin Taheriazam, Kiavash Hushmandi, and Mehrdad Hashemi. 2025. "Glioblastoma Multiforme: Insights into Pathogenesis, Key Signaling Pathways, and Therapeutic Strategies." *Molecular Cancer* 24(1):58. doi:10.1186/s12943-025-02267-0.

Qu, Jianwei, Haimeng Yan, Yifan Hou, Wen Cao, Yang Liu, Enfan Zhang, Jingsong He, and Zhen Cai. 2022. "RNA Demethylase ALKBH5 in Cancer: From Mechanisms to Therapeutic Potential." *Journal of Hematology & Oncology* 15(1):8. doi:10.1186/s13045-022-01224-4.

Raffel, Simon, Mattia Falcone, Niclas Kneisel, Jenny Hansson, Wei Wang, Christoph Lutz, Lars Bullinger, Gernot Poschet, Yannic Nonnenmacher, Andrea Barnert, Carsten Bahr, Petra Zeisberger, Adriana Przybylla, Markus Sohn, Martje Tönjes, Ayelet Erez, Lital Adler, Patrizia Jensen, Claudia Scholl, Stefan Fröhling, Sibylle Cocciardi, Patrick Wuchter, Christian Thiede, Anne Flörcken, Jörg Westermann, Gerhard Ehninger, Peter Lichter, Karsten Hiller, Rüdiger Hell, Carl Herrmann, Anthony D. Ho, Jeroen Krijgsveld, Bernhard Radlwimmer, and Andreas Trumpp. 2017. "BCAT1 Restricts αKG Levels in AML Stem Cells Leading to IDHmut-like DNA Hypermethylation." *Nature* 551(7680):384–88. doi:10.1038/nature24294.

Ramadoss, Sivakumar, Xiaohong Chen, and Cun-Yu Wang. 2012. "Histone Demethylase KDM6B Promotes Epithelial-Mesenchymal Transition." *The Journal of Biological Chemistry* 287(53):44508–17. doi:10.1074/jbc.M112.424903.

Ren, Dayong, Yasuhiro Minami, and Michiru Nishita. 2011. "Critical Role of Wnt5a-Ror2 Signaling in Motility and Invasiveness of Carcinoma Cells Following Snail-Mediated Epithelial-Mesenchymal Transition." *Genes to Cells : Devoted to Molecular & Cellular Mechanisms* 16(3):304–15. doi:10.1111/j.1365-2443.2011.01487.x.

Ren, Jiankun, Songwei Zhao, and Junyu Lai. 2024. "Role and Mechanism of COL3A1 in Regulating the Growth, Metastasis, and Drug Sensitivity in Cisplatin-Resistant Non-Small Cell Lung Cancer Cells." *Cancer Biology & Therapy* 25(1):2328382. doi:10.1080/15384047.2024.2328382.

Rodríguez-García, Ana, Paula Samsó, Pere Fontova, Helga Simon-Molas, Anna Manzano, Esther Castaño, Jose Luis Rosa, Ubaldo Martinez-Outshoorn, Francesc Ventura, Àurea Navarro-Sabaté, and Ramon Bartrons. 2017. "TGF-B1 Targets Smad, P38

MAPK, and PI3K/Akt Signaling Pathways to Induce PFKFB3 Gene Expression and Glycolysis in Glioblastoma Cells." *The FEBS Journal* 284(20):3437–54. doi:10.1111/febs.14201.

Ruiz, Bryan I., Xazmin H. Lowman, Ying Yang, Qi Fan, Tianhong Wang, Hongmei Wu, Eric A. Hanse, and Mei Kong. 2023. "Alpha-Ketoglutarate Regulates Tnfrsf12a/Fn14 Expression via Histone Modification and Prevents Cancer-Induced Cachexia." *Genes* 14(9). doi:10.3390/genes14091818.

Rzeski, Wojciech, Katarzyna Walczak, Małgorzata Juszczak, Ewa Langner, Piotr Pożarowski, Martyna Kandefer-Szerszeń, and Stefan G. Pierzynowski. 2012. "Alpha-Ketoglutarate (AKG) Inhibits Proliferation of Colon Adenocarcinoma Cells in Normoxic Conditions." *Scandinavian Journal of Gastroenterology* 47(5):565–71. doi:10.3109/00365521.2012.660539.

Safran, Michal, William Y. Kim, Fionnuala O'Connell, Lee Flippin, Volkmar Günzler, James W. Horner, Ronald A. Depinho, and William G. Jr Kaelin. 2006. "Mouse Model for Noninvasive Imaging of HIF Prolyl Hydroxylase Activity: Assessment of an Oral Agent That Stimulates Erythropoietin Production." *Proceedings of the National Academy of Sciences of the United States of America* 103(1):105–10. doi:10.1073/pnas.0509459103.

Saita, Ei-ichiro, Toshiharu Suzuki, Kazuhiko Jr Kinosita, and Masasuke Yoshida. 2015. "Simple Mechanism Whereby the F1-ATPase Motor Rotates with near-Perfect Chemomechanical Energy Conversion." *Proceedings of the National Academy of Sciences of the United States of America* 112(31):9626–31. doi:10.1073/pnas.1422885112.

Saitoh, Masao. 2023. "Transcriptional Regulation of EMT Transcription Factors in Cancer." *Seminars in Cancer Biology* 97:21–29. doi:10.1016/j.semcancer.2023.10.001.

Sakaguchi, Masaji, Weikang Cai, Chih-Hao Wang, Carly T. Cederquist, Marcos Damasio, Erica P. Homan, Thiago Batista, Alfred K. Ramirez, Manoj K. Gupta, Martin Steger, Nicolai J. Wewer Albrechtsen, Shailendra Kumar Singh, Eiichi Araki, Matthias Mann, Sven Enerbäck, and C. Ronald Kahn. 2019. "FoxK1 and FoxK2 in Insulin Regulation of Cellular and Mitochondrial Metabolism." *Nature Communications* 10(1):1582. doi:10.1038/s41467-019-09418-0.

Salminen, Antero, Anu Kauppinen, and Kai Kaarniranta. 2015. "2-Oxoglutarate-Dependent Dioxygenases Are Sensors of Energy Metabolism, Oxygen Availability, and Iron Homeostasis: Potential Role in the Regulation of Aging Process." *Cellular and Molecular Life Sciences : CMLS* 72(20):3897–3914. doi:10.1007/s00018-015-1978-z.

Sandhöfer, N., K. H. Metzeler, M. Rothenberg, T. Herold, S. Tiedt, V. Groiß, M. Carlet, G. Walter, T. Hinrichsen, O. Wachter, M. Grunert, S. Schneider, M. Subklewe, A. Dufour, S. Fröhling, H. G. Klein, W. Hiddemann, I. Jeremias, and K. Spiekermann. 2015. "Dual PI3K/mTOR Inhibition Shows Antileukemic Activity in MLL-Rearranged Acute Myeloid Leukemia." *Leukemia* 29(4):828–38. doi:10.1038/leu.2014.305.

Saxena, Kritika, Mohit Kumar Jolly, and Kuppusamy Balamurugan. 2020. “Hypoxia, Partial EMT and Collective Migration: Emerging Culprits in Metastasis.” *Translational Oncology* 13(11):100845. doi:10.1016/j.tranon.2020.100845.

Saxton, Robert A., and David M. Sabatini. 2017. “mTOR Signaling in Growth, Metabolism, and Disease.” *Cell* 168(6):960–76. doi:10.1016/j.cell.2017.02.004.

Schaff, Lauren R., and Ingo K. Mellinghoff. 2023. “Glioblastoma and Other Primary Brain Malignancies in Adults: A Review.” *JAMA* 329(7):574–87. doi:10.1001/jama.2023.0023.

Scholz, Carsten C., and Cormac T. Taylor. 2013. “Hydroxylase-Dependent Regulation of the NF-κB Pathway.” *Biological Chemistry* 394(4):479–93. doi:10.1515/hsz-2012-0338.

Schultheiß, Christoph, and Mascha Binder. 2022. “Overcoming Unintended Immunogenicity in Immunocompetent Mouse Models of Metastasis: The Case of GFP.” *Signal Transduction and Targeted Therapy* 7(1):68. doi:10.1038/s41392-022-00929-9.

Schwager, Samantha C., Jenna A. Mosier, Reethi S. Padmanabhan, Addison White, Qinzhe Xing, Lauren A. Hapach, Paul V. Taufalele, Ismael Ortiz, and Cynthia A. Reinhart-King. 2022. “Link between Glucose Metabolism and Epithelial-to-Mesenchymal Transition Drives Triple-Negative Breast Cancer Migratory Heterogeneity.” *iScience* 25(10):105190. doi:10.1016/j.isci.2022.105190.

Sciacovelli, Marco, and Christian Frezza. 2017. “Metabolic Reprogramming and Epithelial-to-Mesenchymal Transition in Cancer.” *The FEBS Journal* 284(19):3132–44. doi:10.1111/febs.14090.

Sciacovelli, Marco, Emanuel Gonçalves, Timothy Isaac Johnson, Vincent Roberto Zecchini, Ana Sofia Henriques da Costa, Edoardo Gaude, Alizee Vercauteren Drubbel, Sebastian Julian Theobald, Sandra Riekje Abbo, Maxine Gia Binh Tran, Vinothini Rajeeve, Simone Cardaci, Sarah Foster, Haiyang Yun, Pedro Cutillas, Anne Warren, Vincent Gnanapragasam, Eyal Gottlieb, Kristian Franze, Brian Huntly, Eamonn Richard Maher, Patrick Henry Maxwell, Julio Saez-Rodriguez, and Christian Frezza. 2016. “Fumarate Is an Epigenetic Modifier That Elicits Epithelial-to-Mesenchymal Transition.” *Nature* 537(7621):544–47. doi:10.1038/nature19353.

Seker-Polat, Fidan, Nareg Pinarbasi Degirmenci, Ihsan Solaroglu, and Tugba Bagci-Onder. 2022. “Tumor Cell Infiltration into the Brain in Glioblastoma: From Mechanisms to Clinical Perspectives.” *Cancers* 14(2). doi:10.3390/cancers14020443.

Seoane, Joan, and Roger R. Gomis. 2017. “TGF-β Family Signaling in Tumor Suppression and Cancer Progression.” *Cold Spring Harbor Perspectives in Biology* 9(12). doi:10.1101/cshperspect.a022277.

Shagieva, Galina, Lidiya Domnina, Olga Makarevich, Boris Chernyak, Vladimir Skulachev, and Vera Dugina. 2017. “Depletion of Mitochondrial Reactive Oxygen Species Downregulates Epithelial-to-Mesenchymal Transition in Cervical Cancer Cells.” *Oncotarget* 8(3):4901–13. doi:10.18632/oncotarget.13612.

Shan, Lin, Xing Zhou, Xinhua Liu, Yue Wang, Dongxue Su, Yongqiang Hou, Na Yu, Chao Yang, Beibei Liu, Jie Gao, Yang Duan, Jianguo Yang, Wanjin Li, Jing Liang, Luyang

Sun, Kexin Chen, Chenghao Xuan, Lei Shi, Yan Wang, and Yongfeng Shang. 2016. "FOXK2 Elicits Massive Transcription Repression and Suppresses the Hypoxic Response and Breast Cancer Carcinogenesis." *Cancer Cell* 30(5):708–22. doi:10.1016/j.ccell.2016.09.010.

Shen, Chengquan, Jing Liu, Wei Jiao, Xuezhou Zhang, Xinzhao Zhao, Xuecheng Yang, and Yonghua Wang. 2023. "A Feed-Forward Loop Based on Aerobic Glycolysis and TGF-β between Tumor-Associated Macrophages and Bladder Cancer Cells Promoted Malignant Progression and Immune Escape." *Journal of Cancer Research and Clinical Oncology* 149(14):12867–80. doi:10.1007/s00432-023-05164-5.

Shen, Xiaopeng, Shen Wu, Jingyi Zhang, Meng Li, Feng Xu, Ao Wang, Yang Lei, and Guoping Zhu. 2020. "Wild-type IDH1 Affects Cell Migration by Modulating the PI3K/AKT/mTOR Pathway in Primary Glioblastoma Cells." *Molecular Medicine Reports* 22(3):1949–57. doi:10.3892/mmr.2020.11250.

Shen, Zhongjun, Na Yu, Yanfeng Zhang, Mingbo Jia, Ying Sun, Yao Li, and Liyan Zhao. 2024. "The Potential Roles of HIF-1α in Epithelial-Mesenchymal Transition and Ferroptosis in Tumor Cells." *Cellular Signalling* 122:111345. doi:10.1016/j.cellsig.2024.111345.

Shin, Kum-Joo, Estelle A. Wall, Joelle R. Zavzavadjian, Leah A. Santat, Jamie Liu, Jong-Ik Hwang, Robert Rebres, Tamara Roach, William Seaman, Melvin I. Simon, and Iain D. C. Fraser. 2006. "A Single Lentiviral Vector Platform for microRNA-Based Conditional RNA Interference and Coordinated Transgene Expression." *Proceedings of the National Academy of Sciences of the United States of America* 103(37):13759–64. doi:10.1073/pnas.0606179103.

Shrimali, Nishith M., Sakshi Agarwal, Simrandeep Kaur, Sulagna Bhattacharya, Sankar Bhattacharyya, Josef T. Prchal, and Prasenjit Guchhait. 2021. "α-Ketoglutarate Inhibits Thrombosis and Inflammation by Prolyl Hydroxylase-2 Mediated Inactivation of Phospho-Akt." *EBioMedicine* 73:103672. doi:10.1016/j.ebiom.2021.103672.

Shu, Mincong, Yuhan Liu, and Jianbin Wang. 2025. "Protein Post-Translational Modifications in Serine Synthetic Pathway: Functions and Molecular Mechanisms." *Cell Communication and Signaling : CCS* 23(1):311. doi:10.1186/s12964-025-02327-4.

Sica, Valentina, Jose Manuel Bravo-San Pedro, Valentina Izzo, Jonathan Pol, Sandra Pierredon, David Enot, Sylvère Durand, Noélie Bossut, Alexis Chery, Sylvie Souquere, Gerard Pierron, Evangelia Vartholomaiou, Naoufal Zamzami, Thierry Soussi, Allan Sauvat, Laura Mondragón, Oliver Kepp, Lorenzo Galluzzi, Jean-Claude Martinou, Holger Hess-Stumpp, Karl Ziegelbauer, Guido Kroemer, and Maria Chiara Maiuri. 2019. "Lethal Poisoning of Cancer Cells by Respiratory Chain Inhibition plus Dimethyl α-Ketoglutarate." *Cell Reports* 27(3):820-834.e9. doi:10.1016/j.celrep.2019.03.058.

Singh, Digvijay, Rohit K. Deshmukh, and Amitava Das. 2021. "SNAI1-Mediated Transcriptional Regulation of Epithelial-to-Mesenchymal Transition Genes in Breast Cancer Stem Cells." *Cellular Signalling* 87:110151. doi:10.1016/j.cellsig.2021.110151.

Sinha, Abhipsa, Krishan Kumar Saini, Aakash Chandramouli, Kiran Tripathi, Muqtada Ali Khan, Saumya Ranjan Satrusal, Ayushi Verma, Biswajit Mandal, Priyanka Rai, Sanjeev Meena, Mushtaq Ahmad Nengroo, Manish Pratap Singh, Namratha Shashi Bhushan, Madavan Vasudevan, Atin Singhai, Kulranjan Singh, Anand Kumar Mishra, Siddhesh S. Kamat, and Dipak Datta. 2024. "ACSL4-Mediated H3K9 and H3K27 Hyperacetylation Upregulates SNAIL to Drive TNBC Metastasis." *Proceedings of the National Academy of Sciences of the United States of America* 121(52):e2408049121. doi:10.1073/pnas.2408049121.

Sinn, Patrick L., Ariadna C. Arias, Kim A. Brogden, and Paul B. Jr McCray. 2008. "Lentivirus Vector Can Be Readministered to Nasal Epithelia without Blocking Immune Responses." *Journal of Virology* 82(21):10684–92. doi:10.1128/JVI.00227-08.

Sizemore, Steven T., and Ruth A. Keri. 2012. "The Forkhead Box Transcription Factor FOXC1 Promotes Breast Cancer Invasion by Inducing Matrix Metalloprotease 7 (MMP7) Expression." *The Journal of Biological Chemistry* 287(29):24631–40. doi:10.1074/jbc.M112.375865.

Smith, A. P., A. Verrecchia, G. Fagà, M. Doni, D. Perna, F. Martinato, E. Guccione, and B. Amati. 2009. "A Positive Role for Myc in TGFbeta-Induced Snail Transcription and Epithelial-to-Mesenchymal Transition." *Oncogene* 28(3):422–30. doi:10.1038/onc.2008.395.

Smith, Bethany N., Liza J. Burton, Veronica Henderson, Diandra D. Randle, Derrick J. Morton, Basil A. Smith, Latonia Taliaferro-Smith, Peri Nagappan, Clayton Yates, Majd Zayzafoon, Leland W. K. Chung, and Valerie A. Odero-Marah. 2014. "Snail Promotes Epithelial Mesenchymal Transition in Breast Cancer Cells in Part via Activation of Nuclear ERK2." *PloS One* 9(8):e104987. doi:10.1371/journal.pone.0104987.

Smith-Díaz, Carlos C., Andrew B. Das, Tomasz P. Jurkowski, Timothy A. Hore, and Margreet C. M. Vissers. 2025. "Exploring the Ascorbate Requirement of the 2-Oxoglutarate-Dependent Dioxygenases." *Journal of Medicinal Chemistry* 68(3):2219–37. doi:10.1021/acs.jmedchem.4c02342.

Song, Yang, Yong Chen, Yunqian Li, Xiaoyan Lyu, Jiayue Cui, Ye Cheng, Liyan Zhao, and Gang Zhao. 2018. "Metformin Inhibits TGF-B1-Induced Epithelial-to-Mesenchymal Transition-like Process and Stem-like Properties in GBM via AKT/mTOR/ZEB1 Pathway." *Oncotarget* 9(6):7023–35. doi:10.18632/oncotarget.23317.

Springer, Michael, Zeynep Aydin Burakgazi, Anastasiia Domukhovska, Ben Nafchi, Michael C. Beary, Arielle Acquisto, Juliette Acquisto, Vladyslav Komarov, Madison Jensen, Brandon Gulledge, Maksym Poplavskyi, Md Gias Uddin, Gamal Rayan, and Shoshanna N. Zucker. 2025. "HIF-1α-Mediated Disruption of Cellular Junctions: The Impact of Hypoxia on the Tumor Microenvironment and Invasion." *International Journal of Molecular Sciences* 26(11). doi:10.3390/ijms26115101.

Stengel, Sven, Kevin R. Petrie, Yordan Sbirkov, Clara Stanko, Faezeh Ghazvini Zadegan, Veronica Gil, Rafał Skopek, Paweł Kamiński, Łukasz Szymański, Annamaria Brioli, Arthur Zelent, and Tino Schenk. 2022. "Suppression of MYC by PI3K/AKT/mTOR Pathway Inhibition in Combination with All-Trans Retinoic Acid Treatment for

Therapeutic Gain in Acute Myeloid Leukaemia." *British Journal of Haematology* 198(2):338–48. doi:10.1111/bjh.18187.

Stripecke, R., M. Carmen Villacres, D. Skelton, N. Satake, S. Halene, and D. Kohn. 1999. "Immune Response to Green Fluorescent Protein: Implications for Gene Therapy." *Gene Therapy* 6(7):1305–12. doi:10.1038/sj.gt.3300951.

Struys, Eduard A. 2013. "2-Hydroxyglutarate Is Not a Metabolite; D-2-Hydroxyglutarate and L-2-Hydroxyglutarate Are!" *Proceedings of the National Academy of Sciences of the United States of America* 110(51):E4939. doi:10.1073/pnas.1318777110.

Su, Yuan, Tao Wang, Nan Wu, Diyan Li, Xiaolan Fan, Zhongxian Xu, Shailendra Kumar Mishra, and Mingyao Yang. 2019. "Alpha-Ketoglutarate Extends Drosophila Lifespan by Inhibiting mTOR and Activating AMPK." *Aging* 11(12):4183–97. doi:10.18632/aging.102045.

Su, Zheng, Gaojie Liu, Tingfeng Fang, Ketao Zhang, Shanglin Yang, Huayao Zhang, Yang Wang, Zejian Lv, and Jianping Liu. 2017. "Expression and Prognostic Value of Glutamate Dehydrogenase in Extrahepatic Cholangiocarcinoma Patients." *American Journal of Translational Research* 9(5):2106–18.

Sugiyama, Mai, Hitoki Hasegawa, Satoko Ito, Kazuya Sugiyama, Masao Maeda, Kosuke Aoki, Toshihiko Wakabayashi, Michinari Hamaguchi, Atsushi Natsume, and Takeshi Senga. 2015. "Paired Related Homeobox 1 Is Associated with the Invasive Properties of Glioblastoma Cells." *Oncology Reports* 33(3):1123–30. doi:10.3892/or.2014.3681.

Suh, John H., Rupesh Kotecha, Samuel T. Chao, Manmeet S. Ahluwalia, Arjun Sahgal, and Eric L. Chang. 2020. "Current Approaches to the Management of Brain Metastases." *Nature Reviews. Clinical Oncology* 17(5):279–99. doi:10.1038/s41571-019-0320-3.

Sulkowski, Parker L., Christopher D. Corso, Nathaniel D. Robinson, Susan E. Scanlon, Karin R. Purshouse, Hanwen Bai, Yanfeng Liu, Ranjini K. Sundaram, Denise C. Hegan, Nathan R. Fons, Gregory A. Breuer, Yuanbin Song, Ketu Mishra-Gorur, Henk M. De Feyter, Robin A. de Graaf, Yulia V. Surovtseva, Maureen Kachman, Stephanie Halene, Murat Günel, Peter M. Glazer, and Ranjit S. Bindra. 2017. "2-Hydroxyglutarate Produced by Neomorphic IDH Mutations Suppresses Homologous Recombination and Induces PARP Inhibitor Sensitivity." *Science Translational Medicine* 9(375). doi:10.1126/scitranslmed.aal2463.

Sulkowski, Parker L., Sebastian Oeck, Jonathan Dow, Nicholas G. Economos, Lily Mirfakhraie, Yanfeng Liu, Katelyn Noronha, Xun Bao, Jing Li, Brian M. Shuch, Megan C. King, Ranjit S. Bindra, and Peter M. Glazer. 2020. "Oncometabolites Suppress DNA Repair by Disrupting Local Chromatin Signalling." *Nature* 582(7813):586–91. doi:10.1038/s41586-020-2363-0.

Sun, Hongyan, Chuan Zhang, Yang Zheng, Chenlu Liu, Xue Wang, and Xianling Cong. 2022. "Glutamine Deficiency Promotes Recurrence and Metastasis in Colorectal Cancer through Enhancing Epithelial-Mesenchymal Transition." *Journal of Translational Medicine* 20(1):330. doi:10.1186/s12967-022-03523-3.

Sun, Meige, Xiaocui Zhang, Fangfang Bi, Dandan Wang, Xin Zhou, Xiao Li, and Qing Yang. 2022. “FTO Inhibits Epithelial Ovarian Cancer Progression by Destabilising SNAI1 mRNA through IGF2BP2.” *Cancers* 14(21). doi:10.3390/cancers14215218.

Sun, Pengkai, Yan Liu, Tengfei Ma, and Jianping Ding. 2020. “Structure and Allosteric Regulation of Human NAD-Dependent Isocitrate Dehydrogenase.” *Cell Discovery* 6(1):94. doi:10.1038/s41421-020-00220-7.

Sun, Zhonghui, Yunyi Guo, Danlu Zhang, Guolong Zhang, Ying Zhang, and Xiuli Wang. 2022. “FABP7 Inhibits Proliferation and Invasion Abilities of Cutaneous Squamous Cell Carcinoma Cells via the Notch Signaling Pathway.” *Oncology Letters* 24(2):254. doi:10.3892/ol.2022.13374.

Sundararajan, Vignesh, Ming Tan, Tuan Zea Tan, Qing You Pang, Jieru Ye, Vin Yee Chung, and Ruby Yun-Ju Huang. 2020. “SNAI1-Driven Sequential EMT Changes Attributed by Selective Chromatin Enrichment of RAD21 and GRHL2.” *Cancers* 12(5). doi:10.3390/cancers12051140.

Symersky, Jindrich, Daniel Osowski, D. Eric Walters, and David M. Mueller. 2012. “Oligomycin Frames a Common Drug-Binding Site in the ATP Synthase.” *Proceedings of the National Academy of Sciences of the United States of America* 109(35):13961–65. doi:10.1073/pnas.1207912109.

Tan, Fengwei, Ying Jiang, Nan Sun, Zhaoli Chen, Yongzhuang Lv, Kang Shao, Ning Li, Bin Qiu, Yibo Gao, Baozhong Li, Xiaogang Tan, Fang Zhou, Zhen Wang, Dapeng Ding, Jiwen Wang, Jian Sun, Jie Hang, Susheng Shi, Xiaoli Feng, Fuchu He, and Jie He. 2012. “Identification of Isocitrate Dehydrogenase 1 as a Potential Diagnostic and Prognostic Biomarker for Non-Small Cell Lung Cancer by Proteomic Analysis.” *Molecular & Cellular Proteomics : MCP* 11(2):M111.008821. doi:10.1074/mcp.M111.008821.

Tan, Hongpei, Jiahao Liu, Jing Huang, Yanan Li, Qiongxuan Xie, Yuqian Dong, Ze Mi, Xiaoqian Ma, and Pengfei Rong. 2023. “Ketoglutaric Acid Can Reprogram the Immunophenotype of Triple-Negative Breast Cancer after Radiotherapy and Improve the Therapeutic Effect of Anti-PD-L1.” *Journal of Translational Medicine* 21(1):462. doi:10.1186/s12967-023-04312-2.

Tao, Ge, Agata K. Levay, Thomas Gridley, and Joy Lincoln. 2011. “Mmp15 Is a Direct Target of Snai1 during Endothelial to Mesenchymal Transformation and Endocardial Cushion Development.” *Developmental Biology* 359(2):209–21. doi:10.1016/j.ydbio.2011.08.022.

Tao, Ge, Lindsey J. Miller, and Joy Lincoln. 2013. “Snai1 Is Important for Avian Epicardial Cell Transformation and Motility.” *Developmental Dynamics : An Official Publication of the American Association of Anatomists* 242(6):699–708. doi:10.1002/dvdy.23967.

TeSlaa, Tara, Andrea C. Chaikovsky, Inna Lipchina, Sandra L. Escobar, Konrad Hochedlinger, Jing Huang, Thomas G. Graeber, Daniel Braas, and Michael A. Teitell. 2016. “α-Ketoglutarate Accelerates the Initial Differentiation of Primed Human Pluripotent Stem Cells.” *Cell Metabolism* 24(3):485–93. doi:10.1016/j.cmet.2016.07.002.

Thiery, Jean Paul. 2002. “Epithelial-Mesenchymal Transitions in Tumour Progression.” *Nature Reviews. Cancer* 2(6):442–54. doi:10.1038/nrc822.

Thompson, Erik W., Andrew D. Redfern, Simone Brabletz, Geert Berx, Veenoo Agarwal, Karuna Ganesh, Ruby Y. Huang, Dana Ishay-Ronen, Pierre Savagner, Guojun Sheng, Marc P. Stemmler, and Thomas Brabletz. 2025. “EMT and Cancer: What Clinicians Should Know.” *Nature Reviews. Clinical Oncology*. doi:10.1038/s41571-025-01058-2.

Tran, Khoa A., Caleb M. Dillingham, and Rupa Sridharan. 2019. “The Role of α-Ketoglutarate-Dependent Proteins in Pluripotency Acquisition and Maintenance.” *The Journal of Biological Chemistry* 294(14):5408–19. doi:10.1074/jbc.TM118.000831.

Tran, Thai Q., Eric A. Hanse, Amber N. Habowski, Haiqing Li, Mari B. Ishak Gabra, Ying Yang, Xazmin H. Lowman, Amelia M. Ooi, Shu Y. Liao, Robert A. Edwards, Marian L. Waterman, and Mei Kong. 2020. “α-Ketoglutarate Attenuates Wnt Signaling and Drives Differentiation in Colorectal Cancer.” *Nature Cancer* 1(3):345–58. doi:10.1038/s43018-020-0035-5.

Trejo-Solis, Cristina, Daniela Silva-Adaya, Norma Serrano-García, Roxana Magaña-Maldonado, Dolores Jimenez-Farfan, Elizabeth Ferreira-Guerrero, Arturo Cruz-Salgado, and Rosa Angelica Castillo-Rodriguez. 2023. “Role of Glycolytic and Glutamine Metabolism Reprogramming on the Proliferation, Invasion, and Apoptosis Resistance through Modulation of Signaling Pathways in Glioblastoma.” *International Journal of Molecular Sciences* 24(24). doi:10.3390/ijms242417633.

Tretter, Laszlo, and Vera Adam-Vizi. 2004. “Generation of Reactive Oxygen Species in the Reaction Catalyzed by Alpha-Ketoglutarate Dehydrogenase.” *The Journal of Neuroscience : The Official Journal of the Society for Neuroscience* 24(36):7771–78. doi:10.1523/JNEUROSCI.1842-04.2004.

Tseng, Chien-Wei, Wen-Hung Kuo, Shih-Hsuan Chan, Hong-Lin Chan, King-Jen Chang, and Lu-Hai Wang. 2018. “Transketolase Regulates the Metabolic Switch to Control Breast Cancer Cell Metastasis via the α-Ketoglutarate Signaling Pathway.” *Cancer Research* 78(11):2799–2812. doi:10.1158/0008-5472.CAN-17-2906.

Uddin, Md Nazim, and Xiaosheng Wang. 2022. “Identification of Key Tumor Stroma-Associated Transcriptional Signatures Correlated with Survival Prognosis and Tumor Progression in Breast Cancer.” *Breast Cancer (Tokyo, Japan)* 29(3):541–61. doi:10.1007/s12282-022-01332-6.

Uphoff, Cord C., and Hans G. Drexler. 2004. “Detecting Mycoplasma Contamination in Cell Cultures by Polymerase Chain Reaction.” *Methods in Molecular Medicine* 88:319–26. doi:10.1385/1-59259-406-9:319.

Uphoff, Cord C., and Hans G. Drexler. 2014. “Detection of Mycoplasma Contamination in Cell Cultures.” *Current Protocols in Molecular Biology* 106:28.4.1-28.4.14. doi:10.1002/0471142727.mb2804s106.

Vaubourdolle, M., C. Coudray-Lucas, A. Jardel, F. Ziegler, O. G. Ekindjian, and L. Cynober. 1991. “Action of Enterally Administered Ornithine Alpha-Ketoglutarate on Protein

Breakdown in Skeletal Muscle and Liver of the Burned Rat." *JPEN. Journal of Parenteral and Enteral Nutrition* 15(5):517–20. doi:10.1177/0148607191015005517.

Vaziri-Gohar, Ali, Joel Cassel, Farheen S. Mohammed, Mehrdad Zarei, Jonathan J. Hue, Omid Hajihassani, Hallie J. Graor, Yellamelli V. V. Srikanth, Saadia A. Karim, Ata Abbas, Erin Prendergast, Vanessa Chen, Erryk S. Katayama, Katerina Dukleska, Imran Khokhar, Anthony Andren, Li Zhang, Chunying Wu, Bernadette Erokwu, Chris A. Flask, Mahsa Zarei, Rui Wang, Luke D. Rothermel, Andrea M. P. Romani, Jessica Bowers, Robert Getts, Curtis Tatsuoka, Jennifer P. Morton, Ilya Bederman, Henri Brunengraber, Costas A. Lyssiotis, Joseph M. Salvino, Jonathan R. Brody, and Jordan M. Winter. 2022. "Limited Nutrient Availability in the Tumor Microenvironment Renders Pancreatic Tumors Sensitive to Allosteric IDH1 Inhibitors." *Nature Cancer* 3(7):852–65. doi:10.1038/s43018-022-00393-y.

Verhaak, Roel G. W., Katherine A. Hoadley, Elizabeth Purdom, Victoria Wang, Yuan Qi, Matthew D. Wilkerson, C. Ryan Miller, Li Ding, Todd Golub, Jill P. Mesirov, Gabriele Alexe, Michael Lawrence, Michael O'Kelly, Pablo Tamayo, Barbara A. Weir, Stacey Gabriel, Wendy Winckler, Supriya Gupta, Lakshmi Jakkula, Heidi S. Feiler, J. Graeme Hodgson, C. David James, Jann N. Sarkaria, Cameron Brennan, Ari Kahn, Paul T. Spellman, Richard K. Wilson, Terence P. Speed, Joe W. Gray, Matthew Meyerson, Gad Getz, Charles M. Perou, and D. Neil Hayes. 2010. "Integrated Genomic Analysis Identifies Clinically Relevant Subtypes of Glioblastoma Characterized by Abnormalities in PDGFRA, IDH1, EGFR, and NF1." *Cancer Cell* 17(1):98–110. doi:10.1016/j.ccr.2009.12.020.

Villarejo, Ana, Alvaro Cortés-Cabrera, Patricia Molina-Ortíz, Francisco Portillo, and Amparo Cano. 2014. "Differential Role of Snail1 and Snail2 Zinc Fingers in E-Cadherin Repression and Epithelial to Mesenchymal Transition." *The Journal of Biological Chemistry* 289(2):930–41. doi:10.1074/jbc.M113.528026.

Vlasov, Alexey V., Stepan D. Osipov, Nikolay A. Bondarev, Vladimir N. Uversky, Valentin I. Borshchevskiy, Mikhail F. Yanyushin, Ilya V. Manukhov, Andrey V. Rogachev, Anastasiia D. Vlasova, Nikolay S. Ilyinsky, Alexandr I. Kuklin, Norbert A. Dencher, and Valentin I. Gordeliy. 2022. "ATP Synthase F(O)F(1) Structure, Function, and Structure-Based Drug Design." *Cellular and Molecular Life Sciences : CMLS* 79(3):179. doi:10.1007/s00018-022-04153-0.

Wang, Bo, XueBin Zhang, Wei Wang, ZhiZhong Zhu, Fan Tang, Dong Wang, Xi Liu, Hao Zhuang, and XiaoLing Yan. 2018. "Forkhead Box K2 Inhibits the Proliferation, Migration, and Invasion of Human Glioma Cells and Predicts a Favorable Prognosis." *OncoTargets and Therapy* 11:1067–75. doi:10.2147/OTT.S157126.

Wang, J. R., X. H. Li, X. J. Gao, S. C. An, H. Liu, J. Liang, K. Zhang, Z. Liu, J. Wang, Z. Chen, and W. Sun. 2013. "Expression of MMP-13 Is Associated with Invasion and Metastasis of Papillary Thyroid Carcinoma." *European Review for Medical and Pharmacological Sciences* 17(4):427–35.

Wang, Jun, Yunming Li, Jian Wang, Congyang Li, Ke Yu, and Qingsong Wang. 2012. "Increased Expression of Matrix Metalloproteinase-13 in Glioma Is Associated with Poor Overall Survival of Patients." *Medical Oncology (Northwood, London, England)* 29(4):2432–37. doi:10.1007/s12032-012-0181-4.

Wang, Lei, Zhiyu Fang, Peixiang Gao, and Junfang Zheng. 2022. “GLUD1 Suppresses Renal Tumorigenesis and Development via Inhibiting PI3K/Akt/mTOR Pathway.” *Frontiers in Oncology* 12:975517. doi:10.3389/fonc.2022.975517.

Wang, Lei, Dan Yi, Yongqing Hou, Binying Ding, Kang Li, Baocheng Li, Huiling Zhu, Yulan Liu, and Guoyao Wu. 2016. “Dietary Supplementation with α-Ketoglutarate Activates mTOR Signaling and Enhances Energy Status in Skeletal Muscle of Lipopolysaccharide-Challenged Piglets.” *The Journal of Nutrition* 146(8):1514–20. doi:10.3945/jn.116.236000.

Wang, Lihuai, Yinhui Sun, Zhongcong Guo, and Hua Liu. 2022. “COL3A1 Overexpression Associates with Poor Prognosis and Cisplatin Resistance in Lung Cancer.” *Balkan Medical Journal* 39(6):393–400. doi:10.4274/balkanmedj.galenos.2022.2022-6-16.

Wang, Min, Song Yue, and Zhu Yang. 2023. “Downregulation of PSAT1 Inhibits Cell Proliferation and Migration in Uterine Corpus Endometrial Carcinoma.” *Scientific Reports* 13(1):4081. doi:10.1038/s41598-023-31325-0.

Wang, Qianghu, Baoli Hu, Xin Hu, Hoon Kim, Massimo Squatrito, Lisa Scarpace, Ana C. deCarvalho, Sali Lyu, Pengping Li, Yan Li, Floris Barthel, Hee Jin Cho, Yu-Hsi Lin, Nikunj Satani, Emmanuel Martinez-Ledesma, Siyuan Zheng, Edward Chang, Charles-Etienne Gabriel Sauvé, Adriana Olar, Zheng D. Lan, Gaetano Finocchiaro, Joanna J. Phillips, Mitchel S. Berger, Konrad R. Gabrusiewicz, Guocan Wang, Eskil Eskilsson, Jian Hu, Tom Mikkelsen, Ronald A. DePinho, Florian Muller, Amy B. Heimberger, Erik P. Sulman, Do-Hyun Nam, and Roel G. W. Verhaak. 2017. “Tumor Evolution of Glioma-Intrinsic Gene Expression Subtypes Associates with Immunological Changes in the Microenvironment.” *Cancer Cell* 32(1):42-56.e6. doi:10.1016/j.ccell.2017.06.003.

Wang, Qizhi, Ming Wu, Haobin Li, Xin Rao, Luyao Ao, Huan Wang, Lan Yao, Xinyu Wang, Xiaodan Hong, Jun Wang, Jiye Aa, Minjie Sun, Guangji Wang, Jiali Liu, and Fang Zhou. 2022. “Therapeutic Targeting of Glutamate Dehydrogenase 1 That Links Metabolic Reprogramming and Snail-Mediated Epithelial-Mesenchymal Transition in Drug-Resistant Lung Cancer.” *Pharmacological Research* 185:106490. doi:10.1016/j.phrs.2022.106490.

Wang, Runze, Cuixiu Peng, Junying Song, Yanan Hua, Qinglan Wu, Lin Deng, Yi Cao, Jinyu Zhang, Li Zhang, Li Wu, and Lin Hou. 2022. “Downregulated RRS1 Inhibits Invasion and Metastasis of BT549 through RPL11-c-Myc-SNAIL Axis.” *International Journal of Oncology* 60(3):33. doi:10.3892/ijo.2022.5323.

Wang, Shang, Li Zhong, Yin Li, Desheng Xiao, Ruhua Zhang, Dan Liao, Dongming Lv, Xin Wang, Juanfei Wang, Xianbiao Xie, Jing Chen, Yuanzhong Wu, and Tiebang Kang. 2019. “Up-Regulation of PCOLCE by TWIST1 Promotes Metastasis in Osteosarcoma.” *Theranostics* 9(15):4342–53. doi:10.7150/thno.34090.

Wang, Wen, Gang Xu, Cui-Ling Ding, Lan-Juan Zhao, Ping Zhao, Hao Ren, and Zhong-Tian Qi. 2013. “All-Trans Retinoic Acid Protects Hepatocellular Carcinoma Cells against Serum-Starvation-Induced Cell Death by Upregulating Collagen 8A2.” *The FEBS Journal* 280(5):1308–19. doi:10.1111/febs.12122.

Wang, Xiongjun, Ruilong Liu, Xiujuan Qu, Hua Yu, Huiying Chu, Yajuan Zhang, Wencheng Zhu, Xueyuan Wu, Hong Gao, Bangbao Tao, Wenfeng Li, Ji Liang, Guohui Li, and Weiwei Yang. 2019. "α-Ketoglutarate-Activated NF-κB Signaling Promotes Compensatory Glucose Uptake and Brain Tumor Development." *Molecular Cell* 76(1):148-162.e7. doi:10.1016/j.molcel.2019.07.007.

Wang, Yizhuo, Liping Zhang, Na Wei, Yue Sun, Weiyun Pan, and Yan Chen. 2020. "Silencing LINC00482 Inhibits Tumor-Associated Inflammation and Angiogenesis through down-Regulation of MMP-15 via FOXA1 in Bladder Cancer." *Aging* 13(2):2264–78. doi:10.18632/aging.202247.

Wang, Zhaojun, Xinling Liu, Zhanju Wang, and Zhenbo Hu. 2022. "FOXK2 Transcription Factor and Its Roles in Tumorigenesis (Review)." *Oncology Letters* 24(6):461. doi:10.3892/ol.2022.13581.

Wencong, Ma, Wang Jinghan, Yu Yong, Ao Jianyang, Li Bin, Cheng Qingbao, Liu Chen, and Jiang Xiaoqing. 2020. "FOXK1 Promotes Proliferation and Metastasis of Gallbladder Cancer by Activating AKT/mTOR Signaling Pathway." *Frontiers in Oncology* 10:545. doi:10.3389/fonc.2020.00545.

Wernerman, J., F. Hammarqvist, A. von der Decken, and E. Vinnars. 1987. "Ornithine-Alpha-Ketoglutarate Improves Skeletal Muscle Protein Synthesis as Assessed by Ribosome Analysis and Nitrogen Use after Surgery." *Annals of Surgery* 206(5):674–78. doi:10.1097/00000658-198711000-00020.

Wernerman, J., F. Hammarqvist, and E. Vinnars. 1990. "Alpha-Ketoglutarate and Postoperative Muscle Catabolism." *Lancet (London, England)* 335(8691):701–3. doi:10.1016/0140-6736(90)90811-i.

West, M. J., M. Stoneley, and A. E. Willis. 1998. "Translational Induction of the C-Myc Oncogene via Activation of the FRAP/TOR Signalling Pathway." *Oncogene* 17(6):769–80. doi:10.1038/sj.onc.1201990.

Williams, Elizabeth D., Dingcheng Gao, Andrew Redfern, and Erik W. Thompson. 2019. "Controversies around Epithelial-Mesenchymal Plasticity in Cancer Metastasis." *Nature Reviews. Cancer* 19(12):716–32. doi:10.1038/s41568-019-0213-x.

Winkler, Juliane, Abisola Abisoye-Ogunniyan, Kevin J. Metcalf, and Zena Werb. 2020. "Concepts of Extracellular Matrix Remodelling in Tumour Progression and Metastasis." *Nature Communications* 11(1):5120. doi:10.1038/s41467-020-18794-x.

Woodcock, Hannah V., Jessica D. Eley, Delphine Guillotin, Manuela Platé, Carmel B. Nanthakumar, Matteo Martufi, Simon Peace, Gerard Joberty, Daniel Poeckel, Robert B. Good, Adam R. Taylor, Nico Zinn, Matthew Redding, Ellen J. Forty, Robert E. Hynds, Charles Swanton, Morten Karsdal, Toby M. Maher, Andrew Fisher, Giovanna Bergamini, Richard P. Marshall, Andy D. Blanchard, Paul F. Mercer, and Rachel C. Chambers. 2019. "The mTORC1/4E-BP1 Axis Represents a Critical Signaling Node during Fibrogenesis." *Nature Communications* 10(1):6. doi:10.1038/s41467-018-07858-8.

Wu, Fan, Xuexia Xie, Guoliang Li, Dongping Bao, Haomin Li, Guohao Wu, Yiqi Lai, Yaping Xing, Peng Ouyang, Guo Chen, Zhifeng Wang, and Caiyong Lai. 2023. "AKG

Induces Cell Apoptosis by Inducing Reactive Oxygen Species-Mediated Endoplasmic Reticulum Stress and by Suppressing PI3K/AKT/mTOR-Mediated Autophagy in Renal Cell Carcinoma." *Environmental Toxicology* 38(1):17–27. doi:10.1002/tox.23658.

Wu, Jing-Yiing, Tsai-Wang Huang, Yi-Ting Hsieh, Yi-Fu Wang, Chia-Chien Yen, Guan-Lin Lee, Chang-Ching Yeh, Yi-Jen Peng, Ya-Yi Kuo, Hsiu-Ting Wen, Hui-Chen Lin, Cheng-Wen Hsiao, Kenneth K. Wu, Hsing-Jien Kung, Yu-Juei Hsu, and Cheng-Chin Kuo. 2020. "Cancer-Derived Succinate Promotes Macrophage Polarization and Cancer Metastasis via Succinate Receptor." *Molecular Cell* 77(2):213-227.e5. doi:10.1016/j.molcel.2019.10.023.

Wu, Min-Hua, Pei-Ru Wu, Yi-Hsien Hsieh, Chia-Liang Lin, Chung-Jung Liu, and Tsung-Ho Ying. 2020. "Silencing PROK2 Inhibits Invasion of Human Cervical Cancer Cells by Targeting MMP15 Expression." *International Journal of Molecular Sciences* 21(17). doi:10.3390/ijms21176391.

Wu, Nan, Mingyao Yang, Uma Gaur, Huailiang Xu, Yongfang Yao, and Diyan Li. 2016. "Alpha-Ketoglutarate: Physiological Functions and Applications." *Biomolecules & Therapeutics* 24(1):1–8. doi:10.4062/biomolther.2015.078.

Wu, Wen-Sheng, Ren-In You, Chuan-Chu Cheng, Ming-Che Lee, Teng-Yi Lin, and Chi-Tan Hu. 2017. "Snail Collaborates with EGR-1 and SP-1 to Directly Activate Transcription of MMP 9 and ZEB1." *Scientific Reports* 7(1):17753. doi:10.1038/s41598-017-18101-7.

Wu, Yadi, Jiong Deng, Piotr G. Rychahou, Suimin Qiu, B. Mark Evers, and Binhua P. Zhou. 2009. "Stabilization of Snail by NF-kappaB Is Required for Inflammation-Induced Cell Migration and Invasion." *Cancer Cell* 15(5):416–28. doi:10.1016/j.ccr.2009.03.016.

Wu, Yingjie, Shan Pan, Jun Leng, Tian Xie, Muhammad Jamal, Qian Yin, Jingyuan Li, Chunjiang He, Xin Dong, Liang Shao, and Qiuping Zhang. 2019. "The Prognostic Value of Matrix Metalloproteinase-7 and Matrix Metalloproteinase-15 in Acute Myeloid Leukemia." *Journal of Cellular Biochemistry* 120(6):10613–24. doi:10.1002/jcb.28351.

Wu, You-Jun, Zi-Long Hu, Shi-Dong Hu, Yu-Xuan Li, Xiao-Wei Xing, Yu Yang, and Xiao-Hui Du. 2019. "Glutamate Dehydrogenase Inhibits Tumor Growth in Gastric Cancer through the Notch Signaling Pathway." *Cancer Biomarkers : Section A of Disease Markers* 26(3):303–12. doi:10.3233/CBM-190022.

Xia, Pu. 2025. "The Significance of Epithelial–mesenchymal Transition (EMT) in the Initiation, Plasticity, and Treatment of Glioblastoma." *Genes & Diseases* 101711. doi:10.1016/j.gendis.2025.101711.

Xiang, Kexu, Mikhail Kunin, Safa Larafa, Maike Busch, Nicole Dünker, Verena Jendrossek, and Johann Matschke. 2024. "α-Ketoglutarate Supplementation and NAD+ Modulation Enhance Metabolic Rewiring and Radiosensitization in SLC25A1 Inhibited Cancer Cells." *Cell Death Discovery* 10(1):27. doi:10.1038/s41420-024-01805-x.

Xiao, Chu, Tao Fan, He Tian, Yujia Zheng, Zheng Zhou, Shuofeng Li, Chunxiang Li, and Jie He. 2021. “H3K36 Trimethylation-Mediated Biological Functions in Cancer.” *Clinical Epigenetics* 13(1):199. doi:10.1186/s13148-021-01187-2.

Xu, Can, Pengyu Hou, Xiang Li, Menglin Xiao, Ziqi Zhang, Ziru Li, Jianglong Xu, Guoming Liu, Yanli Tan, and Chuan Fang. 2024. “Comprehensive Understanding of Glioblastoma Molecular Phenotypes: Classification, Characteristics, and Transition.” *Cancer Biology & Medicine* 21(5):363–81. doi:10.20892/j.issn.2095-3941.2023.0510.

Xu, Can, Jin Yang, Huan Xiong, Xiaoteng Cui, Yuhao Zhang, Mingjun Gao, Lei He, Qiuyue Fang, Changxi Han, Wei Liu, Yangyang Wang, Jin Zhang, Ying Yuan, Zhaomu Zeng, and Ruxiang Xu. 2025. “Machine Learning and Multi-Omics Analysis Reveal Key Regulators of Proneural-Mesenchymal Transition in Glioblastoma.” *Scientific Reports* 15(1):19731. doi:10.1038/s41598-025-04862-z.

Xu, Haitao, Shulan Huang, Xiaonan Zhu, Wangcheng Zhang, and Xiangyang Zhang. 2018. “FOXK1 Promotes Glioblastoma Proliferation and Metastasis through Activation of Snail Transcription.” *Experimental and Therapeutic Medicine* 15(3):3108–16. doi:10.3892/etm.2018.5732.

Xu, Jian, Samy Lamouille, and Rik Derynck. 2009. “TGF-β-Induced Epithelial to Mesenchymal Transition.” *Cell Research* 19(2):156–72. doi:10.1038/cr.2009.5.

Xu, Mingjie, Jiangfeng Li, Xiao Wang, Shuai Meng, Jiaying Shen, Song Wang, Xin Xu, Bo Xie, Ben Liu, and Liping Xie. 2018. “MiR-22 Suppresses Epithelial-Mesenchymal Transition in Bladder Cancer by Inhibiting Snail and MAPK1/Slug/Vimentin Feedback Loop.” *Cell Death & Disease* 9(2):209. doi:10.1038/s41419-017-0206-1.

Xu, Wei, Hui Yang, Ying Liu, Ying Yang, Ping Wang, Se-Hee Kim, Shinsuke Ito, Chen Yang, Pu Wang, Meng-Tao Xiao, Li-xia Liu, Wen-qing Jiang, Jing Liu, Jin-ye Zhang, Bin Wang, Stephen Frye, Yi Zhang, Yan-hui Xu, Qun-ying Lei, Kun-Liang Guan, Shi-min Zhao, and Yue Xiong. 2011. “Oncometabolite 2-Hydroxyglutarate Is a Competitive Inhibitor of α-Ketoglutarate-Dependent Dioxygenases.” *Cancer Cell* 19(1):17–30. doi:10.1016/j.ccr.2010.12.014.

Yalcin, Abdullah, Tugba H. Solakoglu, Selahattin C. Ozcan, Saime Guzel, Sabire Peker, Serap Celikler, Basak D. Balaban, Elif Sevinc, Yunus Gurpinar, and Jason A. Chesney. 2017. “6-Phosphofructo-2-Kinase/Fructose 2,6-Bisphosphatase-3 Is Required for Transforming Growth Factor B1-Enhanced Invasion of Panc1 Cells in Vitro.” *Biochemical and Biophysical Research Communications* 484(3):687–93. doi:10.1016/j.bbrc.2017.01.178.

Yang, Fan, Ling Lin, Xiaohua Li, Ronglan Wen, and Xin Zhang. 2022. “Silencing of COL3A1 Represses Proliferation, Migration, Invasion, and Immune Escape of Triple Negative Breast Cancer Cells via down-Regulating PD-L1 Expression.” *Cell Biology International* 46(11):1959–69. doi:10.1002/cbin.11875.

Yang, Guan-Jun, Ming-Hui Zhu, Xin-Jiang Lu, Yan-Jun Liu, Jian-Fei Lu, Chung-Hang Leung, Dik-Lung Ma, and Jiong Chen. 2021. “The Emerging Role of KDM5A in Human Cancer.” *Journal of Hematology & Oncology* 14(1):30. doi:10.1186/s13045-021-01041-1.

Yang, Hong Wei, Lata G. Menon, Peter M. Black, Rona S. Carroll, and Mark D. Johnson. 2010. “SNAI2/Slug Promotes Growth and Invasion in Human Gliomas.” *BMC Cancer* 10:301. doi:10.1186/1471-2407-10-301.

Yang, Jing, Parker Antin, Geert Berx, Cédric Blanpain, Thomas Brabletz, Marianne Bronner, Kyra Campbell, Amparo Cano, Jordi Casanova, Gerhard Christofori, Shoukat Dedhar, Rik Derynck, Heide L. Ford, Jonas Fuxe, Antonio García de Herreros, Gregory J. Goodall, Anna-Katerina Hadjantonakis, Ruby Y. J. Huang, Chaya Kalcheim, Raghu Kalluri, Yibin Kang, Yeesim Khew-Goodall, Herbert Levine, Jinsong Liu, Gregory D. Longmore, Sendurai A. Mani, Joan Massagué, Roberto Mayor, David McClay, Keith E. Mostov, Donald F. Newgreen, M. Angela Nieto, Alain Puisieux, Raymond Runyan, Pierre Savagner, Ben Stanger, Marc P. Stemmler, Yoshiko Takahashi, Masatoshi Takeichi, Eric Theveneau, Jean Paul Thiery, Erik W. Thompson, Robert A. Weinberg, Elizabeth D. Williams, Jianhua Xing, Binhua P. Zhou, and Guojun Sheng. 2020. “Guidelines and Definitions for Research on Epithelial-Mesenchymal Transition.” *Nature Reviews. Molecular Cell Biology* 21(6):341–52. doi:10.1038/s41580-020-0237-9.

Yang, Jing, Rongxia He, Xiaoling Zhang, Xing Wang, Min Liu, Xiaolong Liu, and Yulan Li. 2025. “KLC3 Activates PI3K/AKT Signaling and Promotes Ovarian Cancer Cell Proliferation and Migration through COL3A1.” *Oncology Reports* 53(6):67. doi:10.3892/or.2025.8900.

Yang, Miaomiao, Yanming Lu, Weilan Piao, and Hua Jin. 2022. “The Translational Regulation in mTOR Pathway.” *Biomolecules* 12(6). doi:10.3390/biom12060802.

Yang, Xueying, Mengmeng Han, Haibo Han, Bingjing Wang, Sheng Li, Zhiqian Zhang, and Wei Zhao. 2017. “Silencing Snail Suppresses Tumor Cell Proliferation and Invasion by Reversing Epithelial-to-Mesenchymal Transition and Arresting G2/M Phase in Non-Small Cell Lung Cancer.” *International Journal of Oncology* 50(4):1251–60. doi:10.3892/ijo.2017.3888.

Yao, Guorong, Kaiyue Zhao, Kaikai Bao, and Jing Li. 2022. “Radiation Increases COL1A1, COL3A1, and COL1A2 Expression in Breast Cancer.” *Open Medicine (Warsaw, Poland)* 17(1):329–40. doi:10.1515/med-2022-0436.

Yao, Lv, Linying Jiang, Fuxing Zhang, Minghua Li, Bo Yang, Fangting Zhang, and Xiaoqiang Guo. 2020. “Acetate Promotes SNAI1 Expression by ACSS2-Mediated Histone Acetylation under Glucose Limitation in Renal Cell Carcinoma Cell.” *Bioscience Reports* 40(6). doi:10.1042/BSR20200382.

Yastrebova, M. A., A. I. Khamidullina, V. V. Tatarskiy, and A. M. Scherbakov. 2021. “Snail-Family Proteins: Role in Carcinogenesis and Prospects for Antitumor Therapy.” *Acta Naturae* 13(1):76–90. doi:10.32607/actanaturae.11062.

Ye, Jiali, Xing Huang, Shuo Tian, Jichen Wang, Hanfeng Wang, Huayi Feng, Xupeng Zhao, Shouqing Cao, Yundong Xuan, Xiubin Li, Xin Ma, Yan Huang, and Xu Zhang. 2024. “Upregulation of Serine Metabolism Enzyme PSAT1 Predicts Poor Prognosis and Promotes Proliferation, Metastasis and Drug Resistance of Clear Cell Renal Cell Carcinoma.” *Experimental Cell Research* 437(1):113977. doi:10.1016/j.yexcr.2024.113977.

Ye, Zhongxue, Jie Li, Xi Han, Huilian Hou, He Chen, Xia Zheng, Jiaojiao Lu, Lijie Wang, Wei Chen, Xu Li, and Le Zhao. 2016. “TET3 Inhibits TGF-B1-Induced Epithelial-Mesenchymal Transition by Demethylating miR-30d Precursor Gene in Ovarian Cancer Cells.” *Journal of Experimental & Clinical Cancer Research : CR* 35:72. doi:10.1186/s13046-016-0350-y.

Ye, Zhongxue, Le Zhao, Jie Li, Wei Chen, and Xu Li. 2015. “miR-30d Blocked Transforming Growth Factor B1-Induced Epithelial-Mesenchymal Transition by Targeting Snail in Ovarian Cancer Cells.” *International Journal of Gynecological Cancer : Official Journal of the International Gynecological Cancer Society* 25(9):1574–81. doi:10.1097/IGC.0000000000000546.

Yeh, Yen-Hsiu, Shih-Wei Wang, Yen-Cheng Yeh, Ho-Fu Hsiao, and Tsai-Kun Li. 2016. “Rhapontigenin Inhibits TGF-β-Mediated Epithelial-mesenchymal Transition via the PI3K/AKT/mTOR Pathway and Is Not Associated with HIF-1α Degradation.” *Oncology Reports* 35(5):2887–95. doi:10.3892/or.2016.4664.

Yin, Wen, Hecheng Zhu, Jun Tan, Zhaoqi Xin, Quanwei Zhou, Yudong Cao, Zhaoping Wu, Lei Wang, Ming Zhao, Xingjun Jiang, Caiping Ren, and Guihua Tang. 2021. “Identification of Collagen Genes Related to Immune Infiltration and Epithelial-Mesenchymal Transition in Glioma.” *Cancer Cell International* 21(1):276. doi:10.1186/s12935-021-01982-0.

Youssef, Khalil Kass, Nitin Narwade, Aida Arcas, Angel Marquez-Galera, Raúl Jiménez-Castaño, Cristina Lopez-Blau, Hassan Fazilaty, David García-Gutierrez, Amparo Cano, Joan Galcerán, Gema Moreno-Bueno, Jose P. Lopez-Atalaya, and M. Angela Nieto. 2024. “Two Distinct Epithelial-to-Mesenchymal Transition Programs Control Invasion and Inflammation in Segregated Tumor Cell Populations.” *Nature Cancer* 5(11):1660–80. doi:10.1038/s43018-024-00839-5.

Youssef, Khalil Kass, and M. Angela Nieto. 2024. “Epithelial-Mesenchymal Transition in Tissue Repair and Degeneration.” *Nature Reviews. Molecular Cell Biology* 25(9):720–39. doi:10.1038/s41580-024-00733-z.

Yu, Hongwei, Greg Fischer, Guangfu Jia, Jakob Reiser, Frank Park, and Quinn H. Hogan. 2011. “Lentiviral Gene Transfer into the Dorsal Root Ganglion of Adult Rats.” *Molecular Pain* 7:63. doi:10.1186/1744-8069-7-63.

Yu, Mengchao, Jie Lun, Hongwei Zhang, Lei Zhu, Gang Zhang, and Jing Fang. 2021. “The Non-Canonical Functions of HIF Prolyl Hydroxylases and Their Dual Roles in Cancer.” *The International Journal of Biochemistry & Cell Biology* 135:105982. doi:10.1016/j.biocel.2021.105982.

Yu, Mujun, Haozhen Yu, Nan Mu, Yishi Wang, Heng Ma, and Lu Yu. 2022. “The Function of FoxK Transcription Factors in Diseases.” *Frontiers in Physiology* 13:928625. doi:10.3389/fphys.2022.928625.

Yun, Seongseok, Nicole D. Vincelette, Katherine L. B. Knorr, Luciana L. Almada, Paula A. Schneider, Kevin L. Peterson, Karen S. Flatten, Haiming Dai, Keith W. Pratz, Allan D. Hess, B. Douglas Smith, Judith E. Karp, Andrea E. Wahner Hendrickson, Martin E. Fernandez-Zapico, and Scott H. Kaufmann. 2016. “4EBP1/c-MYC/PUMA and NF-κB/EGR1/BIM Pathways Underlie Cytotoxicity of mTOR Dual Inhibitors in

Malignant Lymphoid Cells." *Blood* 127(22):2711–22. doi:10.1182/blood-2015-02-629485.

Zacapala-Gómez, A. E., M. A. Mendoza-Catalán, V. Antonio-Véjar, H. Jiménez-Wences, J. Ortíz-Ortíz, P. A. Ávila-López, C. J. Baños-Hernández, and E. G. Salmerón-Bárcenas. 2024. "TET Enzymes and 5hmC Epigenetic Mark: New Key Players in Carcinogenesis and Progression in Gynecological Cancers." *European Review for Medical and Pharmacological Sciences* 28(3):1123–34. doi:10.26355/eurrev_202402_35349.

Zaccara, Sara, Ryan J. Ries, and Samie R. Jaffrey. 2019. "Reading, Writing and Erasing mRNA Methylation." *Nature Reviews. Molecular Cell Biology* 20(10):608–24. doi:10.1038/s41580-019-0168-5.

Zarei, Mehrdad, Omid Hajihassani, Jonathan J. Hue, Hallie J. Graor, Alexander W. Loftus, Moeez Rathore, Ali Vaziri-Gohar, John M. Asara, Jordan M. Winter, and Luke D. Rothermel. 2022. "Wild-Type IDH1 Inhibition Enhances Chemotherapy Response in Melanoma." *Journal of Experimental & Clinical Cancer Research : CR* 41(1):283. doi:10.1186/s13046-022-02489-w.

Zdzisińska, Barbara, Aleksandra Żurek, and Martyna Kandefer-Szerszeń. 2017. "Alpha-Ketoglutarate as a Molecule with Pleiotropic Activity: Well-Known and Novel Possibilities of Therapeutic Use." *Archivum Immunologiae et Therapiae Experimentalis* 65(1):21–36. doi:10.1007/s00005-016-0406-x.

Zeng, Junli, Ping Zhan, Guannan Wu, Wen Yang, Wenjun Liang, Tangfeng Lv, and Yong Song. 2015. "Prognostic Value of Twist in Lung Cancer: Systematic Review and Meta-Analysis." *Translational Lung Cancer Research* 4(3):236–41. doi:10.3978/j.issn.2218-6751.2015.04.06.

Zhai, Duanyang, Chunhui Cui, Lang Xie, Lianxu Cai, and Jinlong Yu. 2018. "Sterol Regulatory Element-Binding Protein 1 Cooperates with c-Myc to Promote Epithelial-Mesenchymal Transition in Colorectal Cancer." *Oncology Letters* 15(4):5959–65. doi:10.3892/ol.2018.8058.

Zhang, Bo, Hui Peng, Mi Zhou, Lei Bao, Chenliang Wang, Feng Cai, Hongxia Zhang, Jennifer E. Wang, Yanling Niu, Yan Chen, Yijie Wang, Kimmo J. Hatanpaa, John A. Copland, Ralph J. DeBerardinis, Yingfei Wang, and Weibo Luo. 2022. "Targeting BCAT1 Combined with α-Ketoglutarate Triggers Metabolic Synthetic Lethality in Glioblastoma." *Cancer Research* 82(13):2388–2402. doi:10.1158/0008-5472.CAN-21-3868.

Zhang, Haoran, Jinlin Nie, Zhen Bao, Yangdong Shi, Jin Gong, and Hailiang Li. 2025. "FOXC1 Promotes EMT and Colorectal Cancer Progression by Attracting M2 Macrophages via the TGF-β/Smad2/3/Snail Pathway." *Cellular Signalling* 130:111680. doi:10.1016/j.cellsig.2025.111680.

Zhang, Hui H., Alex I. Lipovsky, Christian C. Dibble, Mustafa Sahin, and Brendan D. Manning. 2006. "S6K1 Regulates GSK3 under Conditions of mTOR-Dependent Feedback Inhibition of Akt." *Molecular Cell* 24(2):185–97. doi:10.1016/j.molcel.2006.09.019.

Zhang, Hui, Xiaosheng Wu, Yizhi Xiao, Liqing Wu, Ying Peng, Weimei Tang, Guangnan Liu, Yong Sun, Jing Wang, Huiqiong Zhu, Mengwei Liu, Wenjing Zhang, Weiyu Dai, Ping Jiang, Aimin Li, Guoxin Li, Li Xiang, Side Liu, and Jide Wang. 2019. "Coexpression of FOXK1 and Vimentin Promotes EMT, Migration, and Invasion in Gastric Cancer Cells." *Journal of Molecular Medicine (Berlin, Germany)* 97(2):163–76. doi:10.1007/s00109-018-1720-z.

Zhang, J., J. Luo, J. Ni, L. Tang, H. P. Zhang, L. Zhang, J. F. Xu, and D. Zheng. 2014. "MMP-7 Is Upregulated by COX-2 and Promotes Proliferation and Invasion of Lung Adenocarcinoma Cells." *European Journal of Histochemistry : EJH* 58(1):2262. doi:10.4081/ejh.2014.2262.

Zhang, Lin, Gang Huang, Xiaowu Li, Yujun Zhang, Yan Jiang, Junjie Shen, Jia Liu, Qingliang Wang, Jin Zhu, Xiaobin Feng, Jiahong Dong, and Cheng Qian. 2013. "Hypoxia Induces Epithelial-Mesenchymal Transition via Activation of SNAI1 by Hypoxia-Inducible Factor -1α in Hepatocellular Carcinoma." *BMC Cancer* 13:108. doi:10.1186/1471-2407-13-108.

Zhang, Q., S. Liu, K. R. Parajuli, W. Zhang, K. Zhang, Z. Mo, J. Liu, Z. Chen, S. Yang, A. R. Wang, L. Myers, and Z. You. 2017. "Interleukin-17 Promotes Prostate Cancer via MMP7-Induced Epithelial-to-Mesenchymal Transition." *Oncogene* 36(5):687–99. doi:10.1038/onc.2016.240.

Zhang, Shao-Wei, Nan Zhang, and Na Wang. 2020. "Role of COL3A1 and POSTN on Pathologic Stages of Esophageal Cancer." *Technology in Cancer Research & Treatment* 19:1533033820977489. doi:10.1177/1533033820977489.

Zhang, Tianyi, Sarah Cooper, and Neil Brockdorff. 2015. "The Interplay of Histone Modifications - Writers That Read." *EMBO Reports* 16(11):1467–81. doi:10.15252/embr.201540945.

Zhang, Xintong, Shang Ma, Yan Chen, Yanjun Yin, Wanqiu Bai, Jinjing Tan, and Guangli Shi. 2021. "The Isocitrate Dehydrogenase 1 Is a Potential Prognostic Indicator for Non-Small Cell Lung Cancer Patients." *The International Journal of Biological Markers* 36(4):27–35. doi:10.1177/17246008211052571.

Zhang, Zhenzhen, Changjiu He, Yu Gao, Lu Zhang, Yukun Song, Tianqi Zhu, Kuanfeng Zhu, Dongying Lv, Jing Wang, Xiuzhi Tian, Teng Ma, Pengyun Ji, Wei Cui, and Guoshi Liu. 2021. "α-Ketoglutarate Delays Age-Related Fertility Decline in Mammals." *Aging Cell* 20(2):e13291. doi:10.1111/acel.13291.

Zhao, Ru-Zhou, Shuai Jiang, Lin Zhang, and Zhi-Bin Yu. 2019. "Mitochondrial Electron Transport Chain, ROS Generation and Uncoupling (Review)." *International Journal of Molecular Medicine* 44(1):3–15. doi:10.3892/ijmm.2019.4188.

Zhao, Xiulan, Baocun Sun, Yanlei Li, Yanrong Liu, Danfang Zhang, Xudong Wang, Qiang Gu, Jianmin Zhao, Xueyi Dong, Zhiyong Liu, and Na Che. 2015. "Dual Effects of Collagenase-3 on Melanoma: Metastasis Promotion and Disruption of Vasculogenic Mimicry." *Oncotarget* 6(11):8890–99. doi:10.18632/oncotarget.3189.

Zhao, Zhihua, Chuntao Sun, Fengqi Li, Jiankui Han, Xanjun Li, and Zhenguo Song. 2015. "Overexpression of Histone Demethylase JMJD5 Promotes Metastasis and Indicates a

Poor Prognosis in Breast Cancer." *International Journal of Clinical and Experimental Pathology* 8(9):10325–34.

Zheng, Lin, Yuqin Zhang, Shuimiao Lin, Aimin Sun, Runze Chen, Yi Ding, and Yanqing Ding. 2015. "Down-Regualtion of miR-106b Induces Epithelial-Mesenchymal Transition but Suppresses Metastatic Colonization by Targeting Prrx1 in Colorectal Cancer." *International Journal of Clinical and Experimental Pathology* 8(9):10534–44.

Zheng, Sen, Huita Wu, Fei Wang, Jie Lv, Jing Lu, Qinliang Fang, Fuqiang Wang, Yuyan Lu, Sheng Zhang, Yaping Xu, Qing Bao, Chengrong Xie, and Zhenyu Yin. 2019. "The Oncoprotein HBXIP Facilitates Metastasis of Hepatocellular Carcinoma Cells by Activation of MMP15 Expression." *Cancer Management and Research* 11:4529–40. doi:10.2147/CMAR.S198783.

Zheng, Shaoquan, Lu Yang, Yutian Zou, Jie-Ying Liang, Peng Liu, Guanfeng Gao, Anli Yang, Hailin Tang, and Xiaoming Xie. 2020. "Long Non-Coding RNA HUMT Hypomethylation Promotes Lymphangiogenesis and Metastasis via Activating FOXK1 Transcription in Triple-Negative Breast Cancer." *Journal of Hematology & Oncology* 13(1):17. doi:10.1186/s13045-020-00852-y.

Zhou, Binhua P., Jiong Deng, Weiya Xia, Jihong Xu, Yan M. Li, Mehmet Gunduz, and Mien-Chie Hung. 2004. "Dual Regulation of Snail by GSK-3beta-Mediated Phosphorylation in Control of Epithelial-Mesenchymal Transition." *Nature Cell Biology* 6(10):931–40. doi:10.1038/ncb1173.

Zhou, Jianfeng, Yushang Yang, Hanlu Zhang, Siyuan Luan, Xin Xiao, Xiaokun Li, Pinhao Fang, Qixin Shang, Longqi Chen, Xiaoxi Zeng, and Yong Yuan. 2022. "Overexpressed COL3A1 Has Prognostic Value in Human Esophageal Squamous Cell Carcinoma and Promotes the Aggressiveness of Esophageal Squamous Cell Carcinoma by Activating the NF-κB Pathway." *Biochemical and Biophysical Research Communications* 613:193–200. doi:10.1016/j.bbrc.2022.05.029.

Zhou, Wei, Ran Lv, Weilin Qi, Di Wu, Yunyun Xu, Wei Liu, Yiping Mou, and Liewei Wang. 2014. "Snail Contributes to the Maintenance of Stem Cell-like Phenotype Cells in Human Pancreatic Cancer." *PloS One* 9(1):e87409. doi:10.1371/journal.pone.0087409.

Zhu, Guang-hui, Chen Huang, Zheng-zhong Feng, Xiu-hong Lv, and Zheng-jun Qiu. 2013. "Hypoxia-Induced Snail Expression through Transcriptional Regulation by HIF-1α in Pancreatic Cancer Cells." *Digestive Diseases and Sciences* 58(12):3503–15. doi:10.1007/s10620-013-2841-4.

Zhu, Mingwei, Jiamei Niu, Jian Jiang, Tianxiu Dong, Yaodong Chen, Xiuhua Yang, and Pengfei Liu. 2022. "Chelerythrine Inhibits the Progression of Glioblastoma by Suppressing the TGFB1-ERK1/2/Smad2/3-Snail/ZEB1 Signaling Pathway." *Life Sciences* 293:120358. doi:10.1016/j.lfs.2022.120358.

Zhu, Xiaoming, Li Wei, Yangqiu Bai, Sen Wu, and Shuangyin Han. 2017. "FoxC1 Promotes Epithelial-Mesenchymal Transition through PBX1 Dependent Transactivation of ZEB2 in Esophageal Cancer." *American Journal of Cancer Research* 7(8):1642–53.

Zivotic, Maja, Sanjin Kovacevic, Gorana Nikolic, Ana Mioljevic, Isidora Filipovic, Marija Djordjevic, Vladimir Jovicic, Nikola Topalovic, Kristina Ilic, Sanja Radojevic Skodric, Dusko Dundjerovic, and Jelena Nesovic Ostojic. 2023. "SLUG and SNAIL as Potential Immunohistochemical Biomarkers for Renal Cancer Staging and Survival." *International Journal of Molecular Sciences* 24(15). doi:10.3390/ijms241512245.

Zoncu, Roberto, Alejo Efeyan, and David M. Sabatini. 2011. "mTOR: From Growth Signal Integration to Cancer, Diabetes and Ageing." *Nature Reviews. Molecular Cell Biology* 12(1):21–35. doi:10.1038/nrm3025.

Zuo, Wenli, Keshu Zhou, Mei Deng, Quande Lin, Qingsong Yin, Chunlei Zhang, Jian Zhou, and Yongping Song. 2020. "LINC00963 Facilitates Acute Myeloid Leukemia Development by Modulating miR-608/MMP-15." *Aging* 12(19):18970–81. doi:10.18632/aging.103252.

Żurek, Aleksandra, Magdalena Mizerska-Kowalska, Adrianna Sławińska-Brych, Katarzyna Kaławaj, Agnieszka Bojarska-Junak, Martyna Kandefer-Szerszeń, and Barbara Zdzisińska. 2019. "Alpha Ketoglutarate Exerts a Pro-Osteogenic Effect in Osteoblast Cell Lines through Activation of JNK and mTOR/S6K1/S6 Signaling Pathways." *Toxicology and Applied Pharmacology* 374:53–64. doi:10.1016/j.taap.2019.04.024.

Acknowledgments

I couldn't have reached this goal without the help and support of many incredible people in my life. I would like to take this opportunity to sincerely thank them.

First, I extend my deepest gratitude to my supervisor, Professor Till Acker, for giving me the opportunity to work on this exciting subject and for his continuous guidance and support.

I am also profoundly grateful to our research laboratory head, Professor Attila Nemeth, not only for his academic support but, more importantly, for his kind, humane, and understanding nature.

I would like to thank Professor Thorsten Stiewe for his interest in my work and for accepting the supervision of this dissertation.

I am also deeply thankful to Nuray for her supervision, and insightful critiques throughout my research journey.

This dissertation would not have been possible without the generous financial support from Loewe Schwerpunkt: iCANx.

I am grateful to Professor Amparo Acker-Palmer for granting me access to her animal facility in Frankfurt and for allowing me to work there. My sincere thanks also go to Dr. Monika Fischer and Dr. Bettina Kirchmaier for their constant support during my time in Frankfurt.

Moreover, I am thankful to the International Giessen Graduate Centre for the Life Sciences (GGL) for its role in shaping my scientific development. In particular, I would like to thank Professor Dr. Eveline Baumgart-Vogt and Dr. Lorna Lück for the enriching soft skills courses, annual conferences, and so much more.

I am also grateful to my former and present colleagues from the Institute of Neuropathology—Sabine, Sascha, Angelina, Annika, Carmen, Zoe, Abdelrahman, Lili, Weam, Anna, Isabel, and Yasmine—as well as colleagues in ForMed, including Dr. Ahmed Hussain, Marwah, Anette, and Sahar. Thank you for your friendship, encouragement, and shared laughter.

I would also like to thank Professor Hani Harb for his guidance in troubleshooting ChIP experiments.

I wish to express my deepest gratitude to the love of my life, my soulmate, Nour. You have endured everything with me throughout this journey. You kept me going, lifted me during the hardest times, and were always my safe place and home. You listened to my complaints, wiped my tears, and hugged me through every painful moment. Your endless support and understanding, especially during the most demanding phases of this research period, have been my anchor.

To my family and friends, in Egypt and in Germany, thank you for your love, support, and prayers. Your presence in my life, and knowing that I have you to lean on, means the world to me. Special thanks to Mama, Abeer, Uncle Ahmed, Tante Jailan, Engy, Ahmed, Sarah, Youssef, Zein, Rayan, Papa, Amr, Khalto Ekram, Salma, Asma, Shaimaa, and Hesham.

To Hamza, Hania, Layla, and Hedi, you may never fully understand my scientific journey or why I chose to leave home, but I hope one day you will be proud.

To Gedo and Teita, my grandparents, I miss you every single day. I know you would be proud of who I have become. May you rest in peace.

To Teita Thoraya, who passed away when I was ten years old, after a battle with breast cancer, you were my first inspiration to learn more about cancer. Because of you, I discovered my passion. I dedicate this work to you.

To Dr. Asma Amleh, my first mentor and forever second mother, thank you for believing in me and for your unwavering support. Your guidance will always be remembered and cherished.

Finally, to my cats, Sokar, Loza, and Freska, thank you for cheering me up, even online. I love you.